

Technical Report Documentation Page

| | | | | | |
|---|--|--------------------------------|--|---|--|
| 1. Report No. FHWA/TX-10/0-5574-1 | | 2. Government Accession No. | | 3. Recipient's Catalog No. | |
| 4. Title and Subtitle Guidance for Erection and Construction of Curved I-Girder Bridges | | | | 5. Report Date October 2009; Revised May 2010 | |
| | | | | 6. Performing Organization Code | |
| 7. Author(s) Jason Stith, Andrew Schuh, Jamie Farris, Brian Petruzzi, Todd Helwig, Eric Williamson, Karl Frank, Michael Engelhardt, Hyeong Jun Kim | | | | 8. Performing Organization Report No. 0-5574-1 | |
| 9. Performing Organization Name and Address Center for Transportation Research The University of Texas at Austin 1616 Guadalupe, Suite 4.202 Austin, TX 78701-1255 | | | | 10. Work Unit No. (TRAIS) | |
| | | | | 11. Contract or Grant No. 0-5574 | |
| 12. Sponsoring Agency Name and Address Texas Department of Transportation Research and Technology Implementation Office P.O. Box 5080 Austin, TX 78763-5080 | | | | 13. Type of Report and Period Covered Technical Report September 2006–August 2009 | |
| | | | | 14. Sponsoring Agency Code | |
| 15. Supplementary Notes Project performed in cooperation with the Texas Department of Transportation and the Federal Highway Administration. | | | | | |
| 16. Abstract <p>This report summarizes the methods, results, and recommendations from a research investigation on the behavior of horizontally curved girders during construction. The primary focus of the study is the behavior during early stages of construction when little or no bracing is provided. Girder behavior during placement of the concrete bridge deck was also considered. Research on the bridge behavior during early stages of construction provides valuable insight into the accuracy of past practices and is necessary to formulate safe construction procedures during girder erection and construction. In this research project all phases of girder erection and deck placement were investigated. The goal for the project was to provide a set of design guidelines that provide safe yet economical erected steel plate girders. The necessity of shore towers or holding cranes were also considered in the study.</p> <p>The research study included: 1) Field monitoring of curved girders during lifting, erection, and concrete slab construction; 2) Surveys of erectors to determine common erection practices; 3) Parametric finite element modeling of girders during lifting as well as partially erected bridges; 4) The derivation of analytical expressions for predicting the behavior of curved I-girders during lifting; 5) Development and verification of a macro-enabled spreadsheet design tool (UT Lift) to calculate curved girder behavior during lifting; and 6) Development and verification of a PC-based three-dimensional finite element program (UT Bridge) for analyzing steel bridges during construction.</p> <p>This report provides a description of the entire body of research that was conducted and pertinent to understanding the basis for the design guidelines that were developed. The data from the field results were used to validate the finite element model used in the parametric studies and to compare to the PC-based finite element program developed in the project. The information provides guidance on critical issues that bridge engineers face when designing curved steel plate I-girders.</p> | | | | | |
| 17. Key Words I-Girder, Curved Bridge, Lifting, Erection, Construction | | | 18. Distribution Statement No restrictions. This document is available to the public through the National Technical Information Service, Springfield, Virginia 22161; www.ntis.gov. | | |
| 19. Security Classif. (of report) Unclassified | 20. Security Classif. (of this page) Unclassified | 21. No. of pages 240 | | 22. Price | |



Guidance for Erection and Construction of Curved I-Girder Bridges

Jason Stith
Andrew Schuh
Jamie Farris
Brian Petruzzi
Todd Helwig
Eric Williamson
Karl Frank
Michael Engelhardt
Hyeong Jun Kim

| | |
|-----------------------|---|
| CTR Technical Report: | 0-5574-1 |
| Report Date: | October 2009; May 2010 |
| Project: | 0-5574 |
| Project Title: | Curved Plate Girder Design for Safe and Economical Construction |
| Sponsoring Agency: | Texas Department of Transportation |
| Performing Agency: | Center for Transportation Research at The University of Texas at Austin |

Project performed in cooperation with the Texas Department of Transportation and the Federal Highway Administration.

Center for Transportation Research
The University of Texas at Austin
1616 Guadalupe, Ste. 4.202
Austin, TX 78701-1255

www.utexas.edu/research/ctr

Copyright (c) 2010
Center for Transportation Research
The University of Texas at Austin

All rights reserved
Printed in the United States of America

Disclaimers

Author's Disclaimer: The contents of this report reflect the views of the authors, who are responsible for the facts and the accuracy of the data presented herein. The contents do not necessarily reflect the official view or policies of the Federal Highway Administration or the Texas Department of Transportation (TxDOT). This report does not constitute a standard, specification, or regulation.

Patent Disclaimer: There was no invention or discovery conceived or first actually reduced to practice in the course of or under this contract, including any art, method, process, machine manufacture, design or composition of matter, or any new useful improvement thereof, or any variety of plant, which is or may be patentable under the patent laws of the United States of America or any foreign country.

Notice: The United States Government and the State of Texas do not endorse products or manufacturers. If trade or manufacturers' names appear herein, it is solely because they are considered essential to the object of this report.

Engineering Disclaimer

NOT INTENDED FOR CONSTRUCTION, BIDDING, OR PERMIT PURPOSES.

Project Engineer: Dr. Todd A. Helwig
Professional Engineer License State and Number: Texas #94280
P. E. Designation: Research Supervisor

Acknowledgments

The authors would like to thank the TxDOT Project Director, Amy Eskridge, and the other members of the project monitoring committee for their assistance and direction including David Hohmann, John Holt, Dingyi Yang, and Duncan Stewart of TxDOT and Charles Stone of Stone Structural Engineering. Several individuals were instrumental in the coordination and completion of the field work including Pat Bachman, Greg Jenkins, and Chris Tanner of HDR Inc., Andrew Reid and Joe Mace of Lone Star Infrastructures, Harold Maier and Hirschfeld Industries Inc., and Choctaw Erectors Inc. The authors would also like to acknowledge Bill McEleney from NSBA for many of the survey contributor's contact information and the contributors of all the questionnaire participants as well as the feedback provided by Dave Sinsheimer and Brian Medcalf of Kiewit Engineering Company on UT Lift.

Products

The research discussed in this report produced two analysis tools: UT Lift and UT Bridge. UT Lift is an Excel-based spreadsheet discussed in Chapter 4. The spreadsheet provides critical information necessary for an engineer to evaluate the deformational behavior and safety of a girder during the stage when no bracing is present. UT Bridge is a PC-based three-dimensional finite element analysis software discussed in Chapter 6. The software performs either a linear elastic or an eigenvalue buckling analysis of a straight or curved I-girder bridge during the erection and concrete deck placement.

Table of Contents

| | |
|---|-----------|
| Chapter 1. Introduction..... | 1 |
| 1.1 Motivation..... | 1 |
| 1.2 Issues and Challenges of Curved I-Girders..... | 2 |
| 1.2.1 Interaction of Bending and Torsional Stress..... | 2 |
| 1.2.2 Geometric Instability | 3 |
| 1.2.3 Background on I-Girder Stability: Lateral-Torsional Buckling..... | 3 |
| 1.2.4 Background on I-Girder Stability: Eigenvalue Buckling Analysis..... | 6 |
| 1.3 Scope of Project | 7 |
| 1.4 Report Overview..... | 9 |
| Chapter 2. Literature Review | 11 |
| 2.1 Introduction..... | 11 |
| 2.2 Development of Guide Specifications for Horizontally Curved Highway Bridges | 11 |
| 2.2.1 Consortium of University Research Teams (CURT)..... | 11 |
| 2.2.2 Curved Steel Bridge Research Project (CSBRP)..... | 12 |
| 2.3 Curved Girders during Lifting | 12 |
| 2.4 Full Scale and Field Tests..... | 13 |
| 2.5 Computational Efforts..... | 18 |
| 2.6 State of Practice (Code Requirements)..... | 23 |
| Chapter 3. Field Tests..... | 27 |
| 3.1 Introduction..... | 27 |
| 3.2 Data Acquisition system | 27 |
| 3.3 SH 130/US 71 Bridge Instrumentation | 27 |
| 3.4 Hirschfeld Lift Test Instrumentation | 31 |
| 3.5 Data Reduction Technique..... | 32 |
| 3.5.1 Bending and Warping Stress Interaction | 33 |
| 3.5.2 Bending and Warping Stress Isolation..... | 33 |
| 3.6 Description and Results of SH 130/US 71 Bridge Erection | 34 |
| 3.6.1 SH 130/US 71 Direct Connector Erection | 34 |
| 3.6.2 SH 130/US 71 Girder Erection Results | 35 |
| 3.6.3 SH 130/US 71 Girder Erection Conclusions | 39 |
| 3.7 Description and Results of the Hirschfeld Lift Tests..... | 40 |
| 3.7.1 Girder Supports | 40 |
| 3.7.2 Girder Lifting | 41 |
| 3.7.3 Test Procedure | 41 |
| 3.7.4 Hirschfeld 16C4 Lift Tests Results..... | 42 |
| 3.7.5 Hirschfeld 14C2 Lift Test Results | 47 |
| 3.7.6 Hirschfeld Lift Tests Conclusions | 49 |
| 3.8 Description and Results from SH 130/US 71 Concrete Placement..... | 50 |
| 3.8.1 Introduction..... | 50 |
| 3.8.2 SH 130/US 71 Direct Connector Concrete Placement | 50 |
| 3.8.3 Summary of Results for Girders 3 and 4 | 54 |

| | |
|--|------------|
| 3.8.4 Cross Frames X1 and X2 | 59 |
| 3.8.5 Vertical Deflection Results | 60 |
| 3.8.6 Horizontal Thermal Expansion Results | 64 |
| 3.8.7 SH 130/US 71 Concrete Placement Summary | 67 |
| 3.9 Field Test Conclusions..... | 68 |
| Chapter 4. Lifting of Curved I-Girders | 69 |
| 4.1 Introduction..... | 69 |
| 4.2 Erection Practices for Lifting of Horizontally Curved I-Girders..... | 69 |
| 4.2.1 Introduction..... | 69 |
| 4.2.2 Question 1: Typical Lifting Scenario..... | 69 |
| 4.2.3 Question 2: Spreader Beams | 74 |
| 4.2.4 Question 3: Cranes | 76 |
| 4.2.5 Question 4: Girder Tilt..... | 77 |
| 4.2.6 Question 5: Determining Lifting Points..... | 79 |
| 4.2.7 Question 6: Problems or Concerns | 80 |
| 4.3 Buckling of Curved I-Girders during Lifting | 82 |
| 4.3.1 Introduction..... | 82 |
| 4.3.2 Parametric Finite Element Model | 82 |
| 4.3.3 Eigenvalue Buckling..... | 86 |
| 4.3.4 Eigenvalue Buckling Analysis Conclusions | 96 |
| 4.3.5 Geometric Nonlinear Buckling | 97 |
| 4.4 Curved I-Girder Deformation Behavior during Lifting..... | 101 |
| 4.4.1 Introduction..... | 101 |
| 4.4.2 Rigid Body Rotation | 102 |
| 4.4.3 Cross Sectional Twist | 111 |
| 4.4.4 Using L/b_f Ratios | 119 |
| 4.5 UT Lift Spreadsheet..... | 120 |
| 4.5.1 Introduction and Purpose | 120 |
| 4.5.2 Girder Input Sheet..... | 121 |
| 4.5.3 C.G. & Ideal Lift Sheet..... | 126 |
| 4.5.4 Calculated Behavior Sheet..... | 127 |
| 4.5.5 Girder Deformations and Torsional Diagrams | 130 |
| 4.5.6 Verification of UT Lift..... | 132 |
| 4.6 Conclusion | 135 |
| Chapter 5. Partially Constructed Bridges | 137 |
| 5.1 Introduction..... | 137 |
| 5.2 Common Practices | 139 |
| 5.2.1 Shore Towers and Holding Cranes | 139 |
| 5.3 Parametric Approach | 142 |
| 5.3.1 Parameters Considered..... | 142 |
| 5.3.2 Parameter Definitions | 143 |
| 5.4 Parametric Results | 145 |
| 5.4.1 Shore Tower Location Results..... | 145 |
| 5.4.2 Holding Crane Location Results..... | 148 |
| 5.4.3 Holding Crane Lifting Load Results..... | 149 |
| 5.5 Load Height Effects | 153 |

| | |
|---|------------|
| 5.5.1 Shore Towers | 153 |
| 5.5.2 Holding Cranes | 156 |
| 5.5.3 Linear-Elastic Comparison | 158 |
| 5.6 Critical Stages during Construction | 160 |
| 5.7 Conclusion | 161 |
| Chapter 6. UT Bridge Program | 163 |
| 6.1 General Information | 163 |
| 6.1.1 Pre-Processor | 163 |
| 6.1.2 Processor: | 164 |
| 6.1.3 Post-Processor | 164 |
| 6.2 Preprocessor | 164 |
| 6.3 UT Bridge Finite Element Computational Programming | 173 |
| 6.3.1 Finite Element Analysis | 173 |
| 6.3.2 Node Numbering | 175 |
| 6.3.3 Element Elastic Stiffness Formulations | 177 |
| 6.3.4 Element Geometric Stiffness Formulations: | 184 |
| 6.3.5 Solvers | 187 |
| 6.3.6 Post-Processing within UT Bridge | 187 |
| 6.4 Post –Processor, UT Viewer | 191 |
| 6.5 Verifications | 193 |
| 6.6 UT Bridge Conclusions | 201 |
| Chapter 7. Design Guidelines | 203 |
| 7.1 Purpose | 203 |
| 7.2 Cross Sectional Proportioning | 203 |
| 7.3 Lifting of Curved I-Girders | 204 |
| 7.3.1 Lifting Options | 204 |
| 7.3.2 Strength Limit State | 205 |
| 7.3.3 Serviceability Limit State | 205 |
| 7.3.4 Stability of Girder during Lifting | 205 |
| 7.3.5 UT Lift | 207 |
| 7.3.6 Recommendations | 207 |
| 7.4 Partially Constructed Bridges | 207 |
| 7.4.1 Critical Stages of Bridge Constructions | 207 |
| 7.4.2 Shore Towers | 208 |
| 7.4.3 Holding Cranes | 208 |
| 7.4.4 UT Bridge | 209 |
| 7.4.5 Recommendations | 210 |
| 7.5 Erection and Construction Calculation Recommendations | 210 |
| Drawings | 210 |
| Calculations | 211 |
| Appendix A. Curved I-Girder Erection Questionnaire | 213 |
| Appendix B. Bibliography | 215 |

List of Figures

| | |
|--|----|
| Figure 1.1: Early Stages of Curved I-Girder Bridge Construction | 1 |
| Figure 1.2: Girder Staged (a), Cross Frames Attached (b), Girder Erection (c)..... | 2 |
| Figure 1.3: Lateral-Torsional Buckling Mode for a Curved I-Girder Bridge during Construction..... | 4 |
| Figure 1.4: Single Crane I-Girder Erection..... | 7 |
| Figure 1.5: SH 130/US 71 Unit 3 Deck Placement | 8 |
| Figure 1.6: Instrumentation of SH 130/US 71 Bridge | 9 |
| Figure 1.7: Curved I-Girder Bridges Constructed with a Shore Tower and a Holding Crane | 10 |
| Figure 2.1: Mast's Equilibrium of Beam in Tilted Position (1989)..... | 13 |
| Figure 2.2: Plan View of Test Frame at FHWA Turner-Fairbanks Structures Laboratory (Hartmann 2005)..... | 15 |
| Figure 2.3: Test Frame at FHWA Turner-Fairbanks Structures Laboratory (Hartmann 2005) | 17 |
| Figure 2.4: Plan View of Bridge Studied by Bell (2004) | 18 |
| Figure 2.5: Plan and Isometric Bridge Modeled by Chavel (2008)..... | 22 |
| Figure 3.1: Bridge 88 Location (Google Maps 2009)..... | 28 |
| Figure 3.2: Typical Roadway Cross Section..... | 29 |
| Figure 3.3: Unit 6 Bridge Framing Plan & Girder Elevations w/ Gage Locations..... | 30 |
| Figure 3.4: X1 and X2 Elevation with Gage Locations..... | 31 |
| Figure 3.5: Hirschfeld Girder Elevations w/ Gage and Tilt Sensor Locations | 32 |
| Figure 3.6: Curved I-Girder Flange Stress Distributions..... | 33 |
| Figure 3.7: Bending and Warping Stress Isolation | 34 |
| Figure 3.8: Spreader Bar and Lift Clamp Apparatus | 34 |
| Figure 3.9: Erection Timeline for Girder 4 & 3..... | 35 |
| Figure 3.10: Girder 4 Timber Support Locations w/ Gaged Sections | 36 |
| Figure 3.11: Girder 4 Stress Change at Section C Top Flange..... | 37 |
| Figure 3.12: Dunnage Used for Girder Support..... | 40 |
| Figure 3.13: Wood Supports | 41 |
| Figure 3.14: MI-JACK Travelift Provided By Hirschfeld Steel and Lift Clamp Apparatus | 41 |
| Figure 3.15: Test Timeline for 16C4 & 14C2..... | 42 |
| Figure 3.16: 16C4 Rotation Changes for Support Location S1 | 43 |
| Figure 3.17: 16C4 Rotation Changes for Support Location S2 | 43 |
| Figure 3.18: 16C4 Bending Stress Change at Section C for Support Location S1..... | 44 |
| Figure 3.19: 16C4 Warping Stress Change at Section C for Support Location S1 | 44 |
| Figure 3.20: 16C4 Bending Stress Change at Section C for Support Location S2..... | 45 |
| Figure 3.21: 16C4 Warping Stress Change at Section C for Support Location S2 | 45 |

| | |
|---|----|
| Figure 3.22: Bridge 88 Unit 3 Concrete Deck Placement | 51 |
| Figure 3.23: Concrete Deck Placement at beginning of pour | 52 |
| Figure 3.24: Transverse Screed used in deck construction | 52 |
| Figure 3.25: Bridge 88 Unit 3 Concrete Deck Placement Timeline | 53 |
| Figure 3.26: Girder 3 Bending Stress Change at Section C | 55 |
| Figure 3.27: Girder 3 Warping Stress Change at Section C | 55 |
| Figure 3.28: Girder 4 Bending Stress Change at Section C | 57 |
| Figure 3.29: Girder 4 Warping Stress Change at Section C | 57 |
| Figure 3.30: Cross Frame X2 Axial Force | 60 |
| Figure 3.31: Vertical Deflection Readings at Mid Span 14 | 62 |
| Figure 3.32: Vertical Deflection Reading Locations | 62 |
| Figure 3.33: Wax Trace Box for Measuring Bearing Movements | 64 |
| Figure 3.34: Wax Thermal Expansion Device Measurement | 67 |
| Figure 3.35: Wax Device attached to Bent 14 | 67 |
| Figure 4.1: Air Splice | 70 |
| Figure 4.2: Shore Tower Supporting Curved Girders | 70 |
| Figure 4.3: Shore Tower Beam Supporting I-Girders | 71 |
| Figure 4.4: Ground Spliced Curved I-Girders | 73 |
| Figure 4.5: Spreader Beam Connected to I-Girder | 74 |
| Figure 4.6: Crane Lifting Curved I-Girder | 76 |
| Figure 4.7: Effect of Eccentricity on Curved I-Girder Tilt (Schuh, 2008) | 77 |
| Figure 4.8: Girder Segment Ends Connected at Splice | 78 |
| Figure 4.9: Lifting Curved I-Girder Segment | 79 |
| Figure 4.10: Girder Parameter Definitions | 83 |
| Figure 4.11: ANSYS Model of a Curved I-Girder during lifting | 84 |
| Figure 4.12: Close-up of the ANSYS Model of a Curved I-Girder during lifting | 85 |
| Figure 4.13: Actual I-Girder Lifted during Field Test | 85 |
| Figure 4.14: Effect of Lift Location and Radius of Curvature on the Eigenvalue | 87 |
| Figure 4.15: Effect of Lift Location and L/D on the Eigenvalue | 87 |
| Figure 4.16: Effect of Lift Location and b_f/D on the Eigenvalue | 88 |
| Figure 4.17: Curved Girder Buckled Shapes for $L/d = 10$, $b/d = .25$, $R = 500$ ft | 89 |
| Figure 4.18: Cb vs. a/L for Given Radius of Curvatures | 90 |
| Figure 4.19: Cb vs. a/L for Given Span to Depth Ratio | 91 |
| Figure 4.20: Effect of Lift Location and L/D on the Eigenvalue | 92 |
| Figure 4.21: Effect of Lift Location and b_f/D on the Eigenvalue | 92 |
| Figure 4.22: λ vs. L_{Lift} (Section 1=Section 2 = 60') | 93 |
| Figure 4.23: λ vs. Average a/L (Section 1=Section 2 = 60') | 94 |
| Figure 4.24: Cb vs. a/L for Given Radius of Curvatures (Symmetric Lift) | 95 |

| | |
|--|-----|
| Figure 4.25: C_b vs. a/L for Given Radius of Curvatures (Unsymmetric Lift)..... | 95 |
| Figure 4.26: Effect of Radius of Curvature on the Eigenvalue..... | 97 |
| Figure 4.27: Flange Lateral Displacement for Girder with $a/L = 0.2$ $b_f/D = 0.25$ $R = \text{Str.}$ | 99 |
| Figure 4.28: Flange Lateral Displacement for Girder with $a/L = 0.25$ $b_f/D = 0.25$ $R = \text{Str.}$ | 99 |
| Figure 4.29: Flange Lateral Displacement for Girder with $a/L = 0.2$ $b_f/D = 0.25$ $R = 500'$ | 100 |
| Figure 4.30: Flange Lateral Displacement for Girder with $a/L = 0.25$ $b_f/D = 0.25$ $R = 500'$ | 100 |
| Figure 4.31: Plan View Schematic of Curved and Straight Girder Center of Gravity (Schuh 2008)..... | 102 |
| Figure 4.32: Lifting of a Horizontally Curved Steel I-Girder with 1 Crane & 2 Lift Clamps | 103 |
| Figure 4.33: Variable Definition for C.G..... | 104 |
| Figure 4.34: C.G. Location | 104 |
| Figure 4.35: Schematic of Method used to Obtain Radial Distance to C.G. | 105 |
| Figure 4.36: Possible Lines of Support that Intersect the C.G..... | 106 |
| Figure 4.37: Zero Rotation/Equal Force Lift Location | 107 |
| Figure 4.38: Spreader Bar used by a Single Crane Lifting a Girder..... | 108 |
| Figure 4.39: Predicted Rotation and Lift Reactions..... | 108 |
| Figure 4.40: Approximating the Height of the Axis of Rotation (Schuh 2008) | 109 |
| Figure 4.41: Schematic of the Rigid Body Rotation..... | 110 |
| Figure 4.42: Torsion Induced Stress | 111 |
| Figure 4.43: Basic Idea for Calculating Torsion Diagram..... | 113 |
| Figure 4.44: Shear Center of a Plate Girder..... | 114 |
| Figure 4.45: Center of Gravity Eccentricity and Shear Center Eccentricity..... | 115 |
| Figure 4.46: Torsion Diagram for $L_{\text{Lift}}/L = 0.2$ | 116 |
| Figure 4.47: Torsion Diagram for $L_{\text{Lift}}/L = 0.211$ | 116 |
| Figure 4.48: Torsion Diagram for $L_{\text{Lift}}/L = 0.238$ | 117 |
| Figure 4.49: Torsion Diagram for $L_{\text{Lift}}/L = 0.25$ | 117 |
| Figure 4.50: Serviceability Limit State [$b_f/D = 1/6$; $R = 1,800$ ft] | 119 |
| Figure 4.51: Serviceability Limit State [$b_f/D = 1/4$; $R = 500$ ft] | 120 |
| Figure 4.52: Lifting of a Horizontally Curved Steel I-Girder with 1 Crane & 2 Lift Clamps | 121 |
| Figure 4.53: Screen Shot of UT Lift Girder Geometric Input | 123 |
| Figure 4.54: Screen Shot of UT Lift Girder Cross Frame Input..... | 124 |
| Figure 4.55: Plate Dimensions..... | 125 |
| Figure 4.56: Options of Cross Frame Location | 126 |
| Figure 4.57: Screen Shot of UT Lift C.G. & Ideal Lift Output | 127 |
| Figure 4.58: Definition of the Height to Axis of Rotation..... | 128 |
| Figure 4.59: Screen Shot of UT Lift Calculated Behavior Input..... | 129 |
| Figure 4.60: Screen Shot of UT Lift Calculated Behavior Output | 130 |

| | |
|---|-----|
| Figure 4.61: Screen Shot of UT Lift Graphical Output | 131 |
| Figure 4.62: UT Lift Validation Graph 1 | 132 |
| Figure 4.63: UT Lift Validation Graph 2..... | 133 |
| Figure 4.64: UT Lift Validation Graph 3 | 133 |
| Figure 4.65: UT Lift Validation Graph 4..... | 134 |
| Figure 5.1: Bending Stresses for a Girder being held by a Holding Crane | 137 |
| Figure 5.2: Warping Stresses for a Girder being held by a Holding Crane | 138 |
| Figure 5.3: Picture showing a shore tower under a partially constructed bridge [Right: KWH Constructors – William Bennett Bridge]..... | 140 |
| Figure 5.4: Picture showing a shore tower with common rotational restraint on top flange..... | 141 |
| Figure 5.5: Pictures showing a holding crane and its attachment to the top flange of the girder | 142 |
| Figure 5.6: Shore Tower Geometric Parametric Definitions | 143 |
| Figure 5.7: Temporary Support Location Parameter Definitions | 144 |
| Figure 5.8: Top Flange Lateral Support Options Considered..... | 144 |
| Figure 5.9: Location of Maximum Positive Moment; Simple Span with Cantilever on One Side..... | 146 |
| Figure 5.10: Vertical Reactions for Various Locations along a Girder | 147 |
| Figure 5.11: Geometry used in Figure 5.12 | 147 |
| Figure 5.12: Top Flange Vertical Displacements for Various Shore Tower Positions [Linear Geometry] | 148 |
| Figure 5.13: Geometry used for Figure 5.14..... | 149 |
| Figure 5.14: Top Flange Vertical Displacements for Various Holding Crane Locations [Linear Geometry] | 149 |
| Figure 5.15: Geometry used for Figure 5.16..... | 150 |
| Figure 5.16: Vertical Deflections for Varying Crane Loads..... | 150 |
| Figure 5.17: Geometry Used for Figure 5.18, 5.19, and 5.20 | 151 |
| Figure 5.18: Optimal load (36.5 kips) and close to optimal location (80 feet)..... | 152 |
| Figure 5.19: Not optimal load (40 kips) and close to optimal location (80 feet)..... | 152 |
| Figure 5.20: Optimal load (37.6 kips) and not optimal location (100 feet) | 153 |
| Figure 5.21: Disturbing Force Caused by a Lack of Bracing on the Top Flange | 154 |
| Figure 5.22: Geometry for Figure 5.23 | 154 |
| Figure 5.23: Linear and Non-Linear Displacements Along a Girder for a Girder with a Disturbing Force | 155 |
| Figure 5.24: Tipping Restraint Schematics..... | 156 |
| Figure 5.25: Restoring Force Caused by lack of Bracing in Top Flange | 157 |
| Figure 5.26: Geometry for Figure 5.27..... | 157 |
| Figure 5.27: Linear and Non-Linear Displacements Along a Girder for a Girder with a Restoring Force | 158 |
| Figure 5.28: Linear Elastic Comparison – Bottom Flange Loading, Disturbing Force..... | 159 |

| | |
|---|-----|
| Figure 5.29: Linear Elastic Comparison – Top Flange Loading, Restoring Force..... | 159 |
| Figure 5.30: Single Girder Segment Lifted for a Particular Cross Section | 160 |
| Figure 5.31: One, Two, Three, and Four Girder Erected Systems—Temporary Support at 80' | 161 |
| Figure 6.1: Flow Chart of UT Bridge | 163 |
| Figure 6.2: Typical Bridge Cross Section Looking Ahead Station | 165 |
| Figure 6.3: Sign Convention for Curved Bridges | 165 |
| Figure 6.4: Skew Angle Sign Convention | 166 |
| Figure 6.5: Typical X-Type Cross Frame | 167 |
| Figure 6.6: Bridge Erection Sequence with Associated UT Bridge Model..... | 168 |
| Figure 6.7: Bridge Erection Sequence with Associated UT Bridge Model..... | 168 |
| Figure 6.8: Bridge Erection Sequence with Associated UT Bridge Model..... | 169 |
| Figure 6.9: Deformation Pattern for Shear Studs in Concrete Deck (Topkaya 2002)..... | 170 |
| Figure 6.10: Schematic View of Push-out Test (Topkaya 2002)..... | 170 |
| Figure 6.11: Picture of Push-out Test Setup (Topkaya 2002) | 170 |
| Figure 6.12: Typical Load Displacement Graph (4 hr Concrete) (Topkaya 2002) | 171 |
| Figure 6.13: Coarse Mesh Density..... | 172 |
| Figure 6.14: Normal Mesh Density | 172 |
| Figure 6.15: Fine Mesh Density..... | 173 |
| Figure 6.16: Finite Element Idealization | 174 |
| Figure 6.17: Schematic of the Node Numbering Used in UT Bridge..... | 175 |
| Figure 6.18: Skewed Bridge Nodal Cross Section Schematic..... | 176 |
| Figure 6.19: Nine-Node Shell Element Schematic..... | 178 |
| Figure 6.20: Schematic of Bridge Shell Elements | 178 |
| Figure 6.21: Figure 6.1: Natural Coordinate System and Lagrangian Shape Functions | 179 |
| Figure 6.22: Cross Frame Schematic | 181 |
| Figure 6.23: Schematic Effect of Composite Action..... | 183 |
| Figure 6.24: Extrapolation from 3 x 3 "Gauss Element" (e') to 9-Noded Shell Element | 188 |
| Figure 6.25: 18 Gauss Points of the 3 x 3 x 2 Integration | 190 |
| Figure 6.26: Through Thickness Stress Variation | 190 |
| Figure 6.27: UT Viewer Screen Shot of a Bridge..... | 192 |
| Figure 6.28: Screen Shot of UT Bridge XY Plot..... | 193 |
| Figure 6.29: UT Bridge Field Data Comparison for Girder 3 (a) and Girder 4 (b)..... | 194 |
| Figure 6.30: UT Bridge Field Data Comparison for Girder 3 (a) and Girder 4 (b)..... | 194 |
| Figure 6.31: Girder 3 UT Bridge Comparison to Field Data and Commercial Programs | 195 |
| Figure 6.32: Girder 4 UT Bridge Comparison to Field Data and Commercial Programs | 196 |
| Figure 6.33: Girder 1 Comparison for Steel Dead Load Only..... | 197 |
| Figure 6.34: Girder 2 Comparison for Steel Dead Load Only..... | 197 |

| | |
|---|-----|
| Figure 6.35: Girder 3 Comparison for Steel Dead Load Only..... | 198 |
| Figure 6.36: Girder 4 Comparison for Steel Dead Load Only..... | 198 |
| Figure 6.37: Girder 5 Comparison for Steel Dead Load Only..... | 199 |
| Figure 6.38: Girder 1 Comparison for Steel and Concrete Slab Loading..... | 199 |
| Figure 6.39: Girder 2 Comparison for Steel and Concrete Slab Loading..... | 200 |
| Figure 6.40: Girder 3 Comparison for Steel and Concrete Slab Loading..... | 200 |
| Figure 6.41: Girder 4 Comparison for Steel and Concrete Slab Loading..... | 201 |
| Figure 6.42: Girder 5 Comparison for Steel and Concrete Slab Loading..... | 201 |

List of Tables

| | |
|---|-----|
| Table 2.1: Plate Girder Dimension for Erection Test (Linzell et al. 2004) | 16 |
| Table 2.2: Girder Plate Dimension Range (Bell, 2004)..... | 18 |
| Table 2.3: Geometric Summary (Bell, 2004)..... | 18 |
| Table 3.1: Girder 4 Stress Change Summary..... | 38 |
| Table 3.2: Girder 3 Stress Change Summary..... | 39 |
| Table 3.3: 16C4 Rotation Change Summary | 46 |
| Table 3.4: 16C4 Stress Change Summary | 47 |
| Table 3.5: 14C2 Rotation Change Summary | 48 |
| Table 3.6: 14C2 Stress Change Summary | 49 |
| Table 3.7: Girder 3 Flange Stress Change Summary..... | 56 |
| Table 3.8: Girder 3 Web Stress Change Summary | 56 |
| Table 3.9: Girder 4 Flange Stress Change Summary..... | 58 |
| Table 3.10: Girder 4 Web Stress Change Summary | 58 |
| Table 3.11: Cross Frame X2 Axial Force Summary..... | 60 |
| Table 3.12: Vertical Deflection Readings Along Girder 3 | 63 |
| Table 3.13: Vertical Deflection Readings Along Girder 4 | 63 |
| Table 3.14: Bridge 88, Unit 3 Girders 1 and 4 Lengths..... | 66 |
| Table 3.15: Summary of Thermal Movement on Unit 3 | 66 |
| Table 4.1: Single Girder Segment Reported Lengths | 72 |
| Table 4.2: Pre-spliced Girder Segment Reported Lengths | 73 |
| Table 4.3: Reported Spreader Beam Lengths | 75 |
| Table 4.4: Reported Typical Rotation Tolerances | 79 |
| Table 4.5: Topics of Question 6 Responses..... | 80 |
| Table 4.6: Eigenvalue Parametric Study Variables | 83 |
| Table 6.1: Push-out Test Results (Topkaya 2002)..... | 171 |
| Table 6.2: Natural Coordinates and Gauss Element Coordinates of 9-Node Shell Element..... | 189 |

Chapter 1. Introduction

1.1 Motivation

Horizontally curved steel I-girder highway bridges are often used throughout the state of Texas when the necessary geometry or surrounding terrain require long spans and curved roadway geometry. Unlike simply supported prestressed concrete beams, curved steel girders are usually continuous over supports and spliced near inflection points. The steel I-girders and cross frames that make up a curved bridge often behave as a single unit. The critical phases for stability of the steel girders often occur during girder erection and early stages of construction when the braces are not fully installed such as shown in Figure 1.1. Curved I-girders are subjected to various loading and support conditions throughout the different stages of construction. These critical early stages often dictate the proportions of the steel section and therefore have a significant impact on overall girder economy.



Figure 1.1: Early Stages of Curved I-Girder Bridge Construction

Preferred practices for Texas Department of Transportation (TxDOT) steel bridges recommend girder proportions that are conservative with respect to the American Association of State Highway and Transportation Officials (AASHTO) minimum requirements; however, the State of Texas also has a good record with respect to safety of the girders during erection and construction. Many of the TxDOT-preferred practices are based upon past experience without research justification. An accurate evaluation of the construction sequence of curved steel I-girders requires in-depth knowledge about stability, phasing, support conditions, composite action, and concrete curing time and temperature. The nature of the curved bridge geometry causes torsion on the girders that can result in significant shear and warping stresses in the girder cross-sections that add to the bending stresses. The interaction between warping and bending stresses complicates the design and the erection process for curved bridges. In the early 1990s,

approximately a quarter of the steel bridges being constructed in the United States were curved (Structural Stability Research Council (SSRC) 1991), a statistic that further highlights the need for adequate guidelines for curved girder during the construction phase. The Guide to Stability Design Criteria for Metal Structures (Galambos, 1998) states “the behavior of the curved steel girders is one of the least understood structural form and one of the few remaining unexplored frontiers of structural research.” The least understood behavior is the early stages of bridge construction when the girders are being erected (as shown in Figure 1.2).



Figure 1.2: Girder Staged (a), Cross Frames Attached (b), Girder Erection (c)

This report summarizes the methods, results, and recommendations from a research investigation on the behavior of horizontally curved girders during construction. The primary focus of the study is the behavior during early stages of construction when little or no bracing is provided. Girder behavior during placement of the concrete bridge deck was also considered. Research on the bridge behavior during early stages of construction provides valuable insight into the accuracy of past practices and is necessary to formulate safe construction procedures during girder erection and construction.

1.2 Issues and Challenges of Curved I-Girders

1.2.1 Interaction of Bending and Torsional Stress

The interaction between bending and torsional stresses presents a unique challenge to the analysis of curved I-girders. The torsional stiffness of I-shaped girders can be divided into two components: 1) the St. Venant stiffness, and 2) the warping stiffness. The St. Venant stiffness is not sensitive to the support boundary conditions or the girder span. The warping term, on the other hand, is sensitive to the boundary conditions and girder span, and is often referred to as the *non-uniform torsional stiffness*. Due to the presence of cross frames that reduce the unbraced length of the girders, the warping stiffness of I-shaped sections often dominate the total torsional stiffness compared to the St. Venant stiffness in the fully erected bridge. During girder erection when limited bracing is present, the warping stiffness is often significantly reduced and torsional stresses may become relatively large. The torsionally-induced warping stresses in horizontally curved girders can often equal or exceed the girder's bending stresses. This report presents results from field tests where both bending and warping stresses were monitored.

1.2.2 Geometric Instability

Another challenge presented by curved I-girders is their geometry. The curvature creates a geometrically unstable situation where a single girder's tendency is to tip over or rotate. This geometric instability occurs as an attempt to satisfy static equilibrium, because the center of gravity of a curved girder is eccentric to the girder centerline. As a result, when curved girders are staged prior to erection or once a single girder is erected into place, additional supports or bracing are often required. Typically, a minimum of three support locations is necessary to satisfy equilibrium.

1.2.3 Background on I-Girder Stability: Lateral-Torsional Buckling

The stability of curved girders during construction is a cause for concern especially when the bridge is only partially braced. Structural stability should not be confused with the geometric stability that may result from insufficient points of support for the curved girder that was alluded to earlier. Structural stability involves the capacity of the bridge to prevent buckling of the girders due to the applied loads. While girders are susceptible to both local and global buckling modes, during early stages of construction global buckling modes often control due to the limited availability of bracing. Local buckling includes both local web and flange type buckling that result from slender components within a member. This can be prevented by providing adequate slenderness ratios or stiffeners. Global buckling is challenging to predict and for bridge girders with a primarily bending moment applied, lateral-torsional buckling is the typically the dominant buckling mode. Lateral-torsional buckling of a girder occurs when a critical moment is reached, causing both a translation and twisting of the girder section. Figure 1.3 illustrates a global lateral torsional buckling mode for a curved I-girder bridge during construction.



Figure 1.3: Lateral-Torsional Buckling Mode for a Curved I-Girder Bridge during Construction

The critical moment required to induce lateral-torsional buckling of a straight beam can be calculated using the expression shown in Eq. (1.1) (Timoshenko 1961).

$$M_o = \frac{\pi}{L_b} \sqrt{EI_y GJ + E^2 I_y C_w \left(\frac{\pi^2}{L_b^2} \right)} \quad (1.1)$$

Where:

L_b = Unbraced length of girder (in)

E = Modulus of elasticity (ksi)

I_y = Weak axis moment of inertia (in⁴)

G = Shear modulus (ksi)

J = Torsional constant (in⁴) = $\sum \frac{bt^3}{3}$

C_w = Warping constant (in⁶) = $\frac{I_y h^2}{4}$

h = Distance between flange centroids (in)

Equation (1.1) and other solutions for lateral-torsional buckling moment provided by most design specifications were derived for the case of uniform moment acting along the length of the beam. The American Association of State Highway and Transportation Officials (AASHTO) *LRFD Bridge Design Specifications* (AASHTO 2007) uses an equation for the lateral-torsional buckling resistance of the compression flange given in AASHTO Section 6.10.8.2.3.

Equation (1.1) is applicable for the beams subjected to uniform moment loading. Although solutions can be derived for cases with variable moment along the beam length, most specifications make use of a moment modification factor, C_b , to account for moment gradient. The C_b factor is directly applied to the uniform moment solution as shown below in (1.2). For the purposes of this document, M_o is taken as the buckling moment given by the Timoshenko solution given by (1.1). Moment gradient factors have been tabulated for common cases and can also be found using expressions in design specifications, provided the girder boundary conditions are satisfied.

$$M_{cr} = C_b M_o \quad (1.2)$$

Where:

C_b = Adjustment factor derived computationally
 M_o = Critical buckling moment for uniform moment

The C_b factor can also be determined from a finite element analysis (FEA) on a beam with specific support and load conditions using (1.3). The moment M_{cr} is the maximum moment along the beam length determined from a finite element analysis on the beam with the desired support and loading conditions. The moment M_o represents the buckling capacity for uniform moment loading on a beam and can be determined either from a FEA analysis with constant bending moment or from (1.1).

$$C_b = \frac{M_{cr}}{M_o} \quad (1.3)$$

Where:

M_{cr} = Critical buckling moment determined analytically
 M_o = Critical buckling moment for uniform moment

A number of expressions have been presented for calculating the C_b factor to account for different load cases or support conditions. Accounting for moment gradient along a girder's unbraced length is a typical use for the adjustment factor. The American Institute of Steel Construction (AISC) *Load and Resistance Factor Design* (LRFD) specification (*Load* 13th 2005) has incorporated the expression for C_b given in (1.4). The *AASHTO-LRFD Bridge Design Specifications* (AASHTO 2007) uses an equation for C_b to account for moment gradient given in AASHTO Section 6.10.8.2.3.

$$C_b = \frac{12.5M_{max}}{2.5M_{max} + 3M_A + 4M_B + 3M_C} \quad (1.4)$$

Where:

M_{max} = Maximum moment along L_b
 M_A = Moment at $.25L_b$
 M_B = Moment at $.5L_b$
 M_C = Moment at $.75L_b$

The AISC and AASHTO equations for C_b are suitable for adjusting a critical buckling moment to account for moment gradient between points braced against twist or lateral movement of the compression flange. However, little guidance has been provided on how to evaluate the lateral-torsional buckling capacity of a curved I-girder during lifting when suitable bracing is not present to resist girder twist. One of the goals of this study was to develop a simple method of evaluating the stability of girder segments during lifting.

Using the expression given in (1.3) above, one of the ways M_{cr} can be determined is from an eigenvalue buckling analysis on the curved girder to find the eigenvalue associated with the applied loads, most often the self-weight, and the maximum moment under the given loading from a static analysis. The relationship is shown in (1.5).

$$M_{cr} = \lambda M_{max} \quad (1.5)$$

Where:

$$\begin{aligned} \lambda &= \text{Eigenvalue obtained from buckling analysis} \\ M_{max} &= \text{Maximum moment from static analysis} \end{aligned}$$

1.2.4 Background on I-Girder Stability: Eigenvalue Buckling Analysis

A simple method of determining the buckling capacity of a girder is with an eigenvalue buckling analysis that predicts the theoretical elastic buckling capacity of an ideal structure. The eigenvalue (λ) represents the scale factor that should be multiplied to the applied load to determine the critical buckling load. Because the behavior of the girder during lifting and early stages of erection was one of the primary stages of interest in this study, the applied load in most cases of this research was the self weight of the girder. In addition to a finite element program developed as part of this project, the analysis on the study was primarily conducted on ANSYS (2009). The user-defined parametric language that is available in ANSYS was employed to develop a batch input file that could be used to model a wide variety of systems. Several parameters were studied to determine their affect on the eigenvalue buckling capacity of straight and curved I-girders.

The typical linear elastic structural analysis assumes that the stiffness of the structure is independent of the forces in the members. As the force approaches the buckling load however, the member will “soften” and the stiffness will decrease. The eigenvalue problem takes the following generalized form:

$$[K + \lambda K_g] \Delta = \lambda P \quad (1.6)$$

Where:

$$\begin{aligned} K &= \text{Elastic stiffness matrix} \\ K_g &= \text{Geometric stiffness matrix} \\ \lambda &= \text{Eigenvalue} \\ P &= \text{Applied loads} \end{aligned}$$

K_g is a function of the member forces. Buckling will occur when an incremental load dP results in an infinitely large displacement, mathematically this occurs when the matrix $[K + \lambda K_g]$ is singular, which leads to the following generalized eigenproblem:

$$Kx = -\lambda K_g x \quad (1.7)$$

Where:

λ = Eigenvalue: factor of safety against buckling
 x = Eigenmode: buckled shape

Implicit in the linear eigenvalue analysis is the assumption that displacements prior to buckling remain infinitesimal. This assumption will not be valid for cases in which significant displacements occur prior to buckling, such as in the case of highly curved girders. To properly model the structural behavior in those circumstances, a large-displacement nonlinear analysis should be performed. For horizontally curved I-girders the curvature is similar to an initial imperfection that results in significant deflection once load is applied. This nonlinearity prevents the girder from reaching the predicted eigenvalue buckling capacity. This type of analysis can be computationally expensive and for many problems the eigenvalue buckling can give an acceptable indication of the stability of the bridge system. In curved girders, the eigenvalue is still useful because it provides an upper limit to the capacity of the girder system.

1.3 Scope of Project

The research for this report was funded by the Texas Department of Transportation for project 0-5574 which was entitled, *Curved Plate Girder Design for Safe and Economical Construction*. As mentioned in the previous section, the study focuses on the behavior during early stages of construction to assist in justifying some of TxDOT's curved steel I-girder design practices during erection and construction and proposing new design guidelines where necessary. Most bridge designers analyze the girder system using software based upon a grid-analysis to predict how the behavior of the fully erected bridge. Because of the simplifying assumptions, programs based upon a grid analysis have limited capabilities for providing accurate solutions during the early construction stages of girder erection and slab construction. Because of increased material costs, many engineers are designing curved I-girders with flange widths at the extreme limits of the AASHTO requirements. The decreased flange widths lead to very slender girders. Therefore, the lateral flexibility of slender girders can lead to dangerous stability problems before the bridge is fully braced and the slab is constructed (Figure 1.4).



Figure 1.4: Single Crane I-Girder Erection

In this research project all phases of girder erection and deck placement were investigated. The goal for the project was to provide a set of design guidelines that provide safe yet economical erected steel plate girders. The necessity of shore towers or holding cranes were also considered in the study.

The research study included:

- Field monitoring of curved girders during lifting, erection (Figure 1.4) and concrete slab construction (Figure 1.5);
- Surveys of erectors to determine common erection practices;
- Parametric finite element modeling during lifting and partially constructed bridges;
- The derivation of the equation necessary to predict the behavior of curved I-girders during lifting;
- Development and verification of a macro-enabled spreadsheet design tool to calculate curved girder behavior during lifting, UT Lift: and
- Development and verification of a PC-based three dimensional finite element program for analyzing steel bridges during construction, UT Bridge.

This report provides a description of the entire body of research that was conducted and pertinent to understanding the basis for the design guidelines is presented. The data from the field results were used to validate the finite element model used in the parametric studies and to compare to the PC-based finite element program developed in this project. The information provides guidance on critical issues that bridge engineers face when designing curved steel plate I-girders.

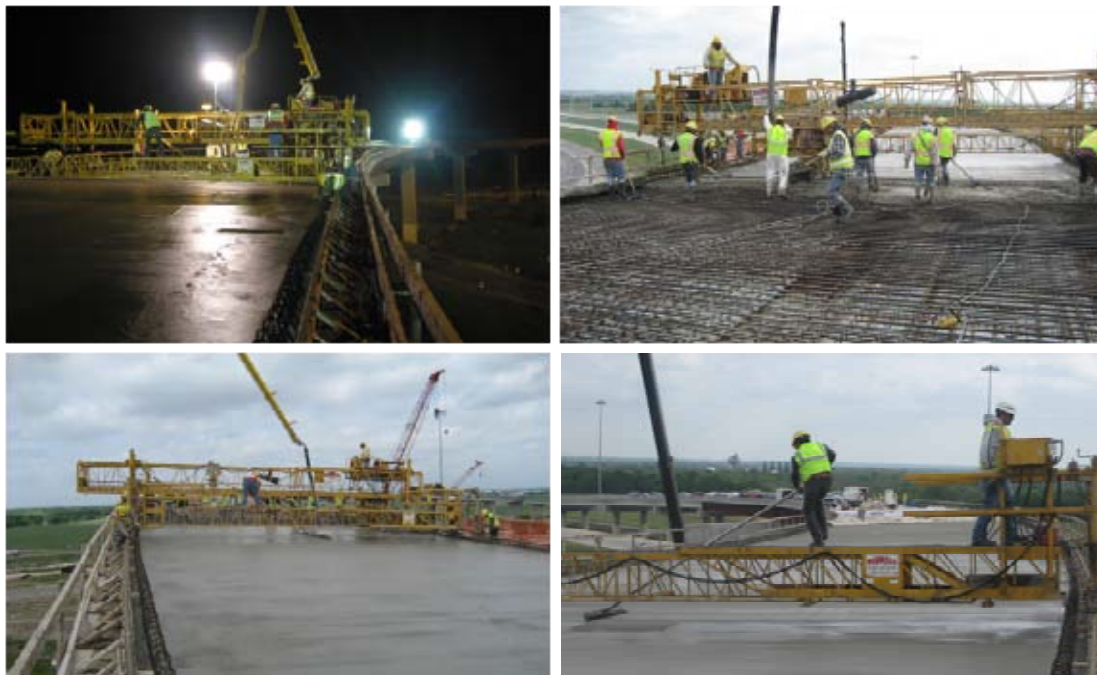


Figure 1.5: SH 130/US 71 Unit 3 Deck Placement

1.4 Report Overview

The report has been divided into seven chapters. Following this introductory chapter, a summary of previous curved I-girder research projects and field work pertaining to the behavior of curved I-girders during critical construction stages is presented in Chapter 2.

A discussion of the instrumentation along with data from the field monitoring of a bridge on SH 130 located in Austin, Texas (Figure 1.6) is then provided in Chapter 3. The bridge was monitored to determine the behavior of two curved I-girders and two cross frames during the erection and concrete slab placement stage of construction. The data includes strain gage readings from the girders and the cross-frames as well as the vertical deflection readings during deck placement. The thermal expansion of this bridge was also measured and reported. An additional test performed at the Hirschfeld Steel Fabrication Plant in San Angelo, Texas is also described and results provided.



Figure 1.6: Instrumentation of SH 130/US 71 Bridge

An overview of research methods and findings on the lifting of curved girders is provided in Chapter 4. This includes the summary of the response from the questionnaire created to survey various curved steel I-girder erection contractors, inspectors, and engineers. The questionnaire centers around the common practices for lifting curved I-girders, including spreader beam length, number of cranes, lift points, shore towers, and length of girder segments lifted (Figure 1.4). The results of multiple parametric studies utilizing both eigenvalue buckling and full nonlinear three dimensional finite element analysis of the lateral-torsional buckling of prismatic and nonprismatic curved I-girders during lifting are presented. The buckling analysis was performed using the finite element program, ANSYS 11.0 (2007). Chapter 4 also presents the derivation of equations that predict the girder deformations during lifting. These equations are implemented into an Excel spreadsheet called UT Lift. The spreadsheet provides a design tool for engineers to

accurately predict the lifting behavior of curved I-girders. The spreadsheet approach and validation is provided using both ANSYS nonlinear analyses and the field data.

A summary of the parametric work completed on the partially constructed bridge is given in Chapter 5. Partially constructed bridges do not have full bracing present and the validated models were used to perform both linear elastic and full geometric nonlinear analyses. The two most common methods to provide the necessary stability are holding cranes and shore towers as shown in Figure 1.7. Parametric studies investigated the optimum use of both holding cranes and shore towers. A set of guidelines and recommendations are provided as conclusions from the work.



Figure 1.7: Curved I-Girder Bridges Constructed with a Shore Tower and a Holding Crane

Chapter 6 is dedicated to the PC-based three dimensional finite element program, UT Bridge, that was developed as part of this project. The program is designed to analyze both curved and straight bridges during erection and concrete deck placement. The program includes a graphical user interface (GUI) with a pre- and post-processor to allow easy use for design engineers when conducting analyses during the most critical stages for bridge stability. The basics of the program are provided as well as validation using field data and validated finite element models. Finally, a summary of the report along with a list of design recommendations for the safe and economical erection and construction of curved steel I-girder bridges is given in Chapter 7.

Chapter 2. Literature Review

2.1 Introduction

This chapter provides an overview of past research on the behavior of curved girders. The first investigation into the behavior of curved beams was published by Barre De Saint Venant (1843). Numerous other studies and works have obviously been conducted since then, but interest in the United States did not begin in earnest until 1969 when an organized research effort began. A few syntheses of the research on curved steel girder have been conducted with more references than presented in this chapter, including (McManus et al. 1969), Zureick et al. (1994), which presented findings from pre-1993, and Yoo and Choi, which synthesized the research from 1993-2000 (2000).

2.2 Development of Guide Specifications for Horizontally Curved Highway Bridges

2.2.1 Consortium of University Research Teams (CURT)

In 1969, the United States Federal Highway Administration (FHWA) managed the first major study into the behavior of curved steel highway bridges funded by 25 states when it formed the Consortium of University Research Teams (CURT). The participating institutions were Carnegie Mellon University, the University of Pennsylvania, the University of Rhode Island, and Syracuse University.

The CURT project was focused on laboratory scale tests conducted mostly at Carnegie Mellon, as well as theoretical and analytical work conducted at the other universities. The results of I-girder bridge scale tests are documented by Mozer and Culver (1970) and Mozer et al. (1971, 1973). Some of the first analytical models for curved bridges were validated with tests that examined the interaction between bracing members and adjacent girder line by Brennan (1970, 1971, and 1974). McManus utilized some of the test results to validate the theoretical work to predict the behavior of doubly symmetric curved I-girders in bending (1971). Nasir studied the local buckling behavior of curved girder flanges (1970). A few studies on the stability of web panels were conducted as well (Brogan 1974; Culver et al. 1972, 1973). Another stability related study concentrated on the local buckling of the compression flange of curved I-girders in both the elastic and inelastic range (Culver and Frampton 1970; Culver and Nasir 1971). The CURT project did not explicitly study the behavior of curved steel bridge erection, but did investigate the behavior before and after the deck was placed (Brennan 1970).

The major result of the CURT project was the development of recommendations for an allowable stress design (ASD) specifications for curved bridges (Culver 1972; CURT 1975). This was looked at by AASHTO Committee on Flexural Members as well as additional scale test conducted at the University of Maryland (Kuo and Heins 1971) (Heins 1972) and analytical work at the University of California Berkeley (Mondkar and Powell 1974). The committee proposed a guide specification that was approved in 1976. Then the American Iron and Steel Institute (AISI) sponsored a research project to add load factor design (LFD) to the guide specification recommendation by converting the CURT ASD format to LFD (Stegmann and Galambos 1976). This resulted in the first edition of the Guide Specifications for Horizontally Curved Highway Bridges (AASHTO 1980). Then after eight interim revisions the second edition of the Guide Specs came out (AASHTO 1993).

2.2.2 Curved Steel Bridge Research Project (CSBRP)

Research in the area of curved girders continued through the 1980s (Yoo and Carbine 1985) (Yoo and Littrell 1986) (Schelling et al. 1989) and especially overseas in Japan. The Japanese conducted test to support the Hanshin Expressway Corporation's *Guidelines for the Design of Horizontally Curved Girder Bridges*. The literature is in Japanese, but has been reviewed by Zureick et al. (1994) and includes work on many areas such as the effects of transverse stiffeners (Nakai et al. 1985) and longitudinal stiffeners (Nakai et al. 1986) just to name a few. However, the next significant increase in the understanding of curved girders was not advanced until the early 1990s when the Structural Stability Research Council (SSRC) recommended areas of need for further research (SSRC 1991). This initiated the FHWA to fund the Curved Steel Bridge Research Project (CSBRP) in 1992. The projects goals included compiling a synthesis of all the previous research on the topic (Zureick et al. 1994) and addressing weaknesses in the CURT research project, specifically the lack of full-scale and field tests with realistic boundary conditions. This work lasted over ten years and greatly improved the understanding of curved bridge behavior. The results were formulated into the first Load and Resistant Factor Design (LRFD) provisions and then incorporated into the later editions of AASHTO. This includes the Guide Specifications for Horizontally Curved Steel Girder Highway Bridges 2003 (AASHTO 2003), which has been incorporated into the AASHTO LRFD Bridge Specifications 4th Edition 2007 (AASHTO 2007). Many of the projects and findings referenced in the following sections are a product of CSBRP either directly or indirectly.

2.3 Curved Girders during Lifting

Very little research into the lifting of horizontally curved I-girders has been preformed. Although the topic of lifting stability has been identified as important (NCHRP 2005), prior to this research project little guidance can be found. In the concrete area, Robert Mast (1989) worked on the lateral stability of long prestressed concrete beams during lifting. Within the article Mast identifies the roll axis as the line defined by the lifting points and a roll angle as the rotation of the girder about the roll axis. Due to initial imperfections in the beam and the misplacement of lifting loops the "straight" prestressed concrete beam will have an initial imperfection that results in the girder center of gravity located at an eccentricity to the roll axis. This results in the girder rotating to a new roll angle that produces a weak axis bending from the girder self weight, which increases the eccentricity of the center of gravity. This results in the girder either finding equilibrium or failing due to lack of elastic lateral stiffness. The other identified failure mode was a roll angle that exceeded a maximum permissible angle. Both failure modes are undesirable according to Mast and he provided two equations for determining the factor of safety for each possibility.

$$FS = \frac{y_r}{\bar{z}_o} \left(1 - \frac{\theta_i}{\theta_{max}} \right) \quad (2.1)$$

$$FS = \frac{\theta_{max}}{\theta_i} \left(1 - \frac{\bar{z}_o}{y_r} \right) \quad (2.2)$$

Where:

y_r = The height of the roll axis above the C.G. of the beam
 \bar{z}_o = The theoretical lateral deflection of the C.G. of the beam,
computed with the full dead weight applied laterally

θ_{max} = Maximum permissible tilt angle of the beam
 θ_i = The initial roll angle of the rigid beam
 $\{e_i/y_r \text{ or exactly } \tan(e_i/y_r)\}$
 e_i = The initial lateral eccentricity of the C.G. of the beam
 with respect to the roll axis

Figure 2.1 is a schematic drawing of the equilibrium of a beam in the tilted position provided by mast, with labels for both the roll axis and the roll angle. This idea of a roll angle or rigid body rotation is very important for the lifting of curved girders. This research project extended this idea to curved girder steel I-girders and additionally included the derivations for calculating cross sectional twist to the lateral deformation and the rigid body rotation that can be calculated from statics.

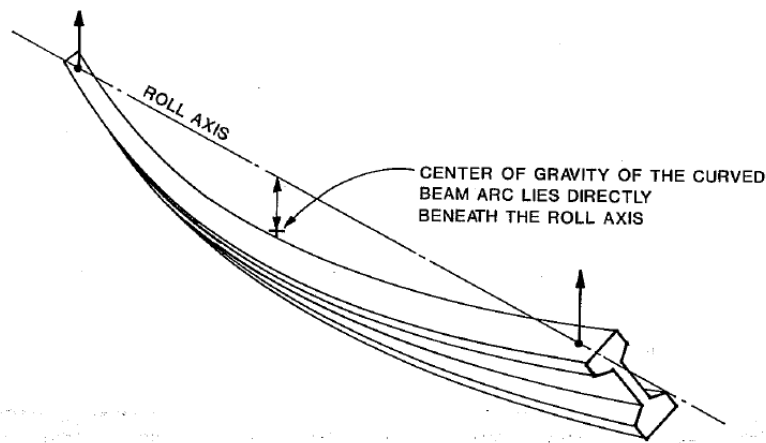


Fig. 1a. PERSPECTIVE OF A BEAM FREE TO ROLL AND DEFLECT LATERALLY

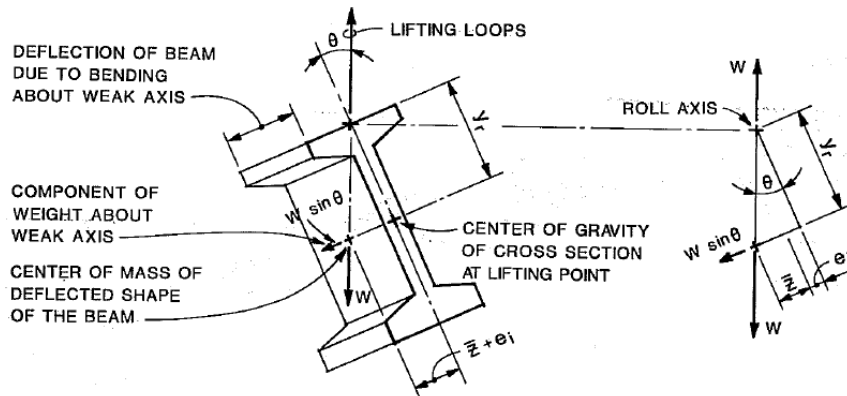


Fig. 1b. END VIEW

Fig. 1c. EQUILIBRIUM DIAGRAM

Figure 2.1: Mast's Equilibrium of Beam in Tilted Position (1989)

2.4 Full Scale and Field Tests

Full scale or field tests have served as an integral part of the understanding of curved I-girder behavior and an area of weakness within the research field according to SSRC (1991), but size, expense, and natural elements make successful field tests difficult to perform and rare in the

literature. One of the first attempts to monitor curved I-girders during early stages of construction was by Beal and Kissane in New York in 1971(a) when the Hulls Falls Bridge was instrumented. This bridge was a 4-girder 123 ft. simple span bridge with a 477.86 ft. radius of curvature. Dead load and static live load measurements were taken to determine the stress and deflection in the girders. To ensure that the instrumentation was not damaged, data was not collected until after the erection. However, data was collected during the deck placement and subsequent live load testing. Even with the precautions, the collected data was sparse due to damaged or malfunctioning instrumentations. The problems included strain gages damaged by the construction process, inadequate waterproofing, poor bonding of the gage cement, and high humidity. The diaphragm gages suffered from the same problems with many damaged during the construction or recording sporadic data. The results determined from the limited data were that the stresses were less than the computed values, but the measured deflections exceeded the computed values and deemed the analysis unconservative.

Shortly thereafter Beal and Kissane attempted a second instrumentation (1971b) of the Huyck Stream Bridge. This time another 4-girder simple span bridge with a span length of 95 ft. and 162 ft. radius of curvature was instrumented with 132 strain gages. While many of the strain gages were damaged or failed to work properly, the number was significantly less than their first attempt. They were able to conclude that the planar grid method of analysis available at that time was sufficient to predict the vertical bending and deflection. However, the model did not have the ability to predict the lateral bending stresses in the flange and several of the flange gages measured values above the allowable stress. It was recommended that methods should be developed that could account for these stresses.

In their third attempt Beal and Kissane (1972) instrumented an exit ramp bridge that consisted of a 5-girder symmetric two span system with span lengths of 200 ft. and a 266 ft. radius of curvature. A planar grid method was used for the analysis and instrumentation of one of the two spans was completed with 160 gages. Again several gages malfunctioned, but the instrumentation showed a large absolute value difference in the stresses between the inside and outside edge of the bottom flanges representing significant lateral bending and/or warping torsion. Many of the diaphragm gages worked for this test and the ones that did not were averaged with the remaining data. It was shown that during the static live load tests the diaphragms experience no significant load with stresses within the instrument noise. The conclusions of this test were similar to the second test and showed the lateral bending played a significant role in the stress distribution of the girder and was not captured with the planar grid method. They also concluded that the negative moment region of the bridge appeared to have the highest stresses and should control the bridge design.

In 1996 Galambos et al. instrumented a two span curved I-girder bridge with a skewed substructure. The MNDOT bridge No. 27998 had a centerline radius of curvature of 286 ft. and span lengths of approximately 146 ft. and 150 ft. The bridge had different depth girders ranging from 50 in. for the interior (inside of curve) girder to 72 in. for the exterior (outside of curve) girder. Sixty vibrating wire strain gages were used on both the girders and diaphragms of the superstructure. The gages were installed in the fabrication plant where a baseline reading could be recorded. Another baseline reading was taken in the field before the girders were lifted off the ground with the baseline readings differing by only 2-3%. Readings were taken throughout the erection process and concrete placement. Static tests with live load were then conducted on the completed structure. Deflection readings were taken with a survey level. Additionally, a planar grid method computer program was developed and compared to the measured results.

Conclusions from the comparison showed a qualitative match with some quantitative matches. During the first construction stage, the measured data showed little correlation with the model. This was attributed to low level of girder self weight stress and the relatively large fit-up stresses. Once the concrete deck was placed the measured data correlated better as the fit-up stresses became less significant. It was concluded that the stresses were below yield throughout construction and that once composite action was achieved then significant correlation was possible (Galambos et al. 2000).

The computer program used by Galambos et al. was called the University of Minnesota Steel Curved Girder Bridge System Analysis Program (UM) and detailed by Huang (1996). The program utilized a grillage method that is a stiffness-based finite-element formulation. The elements were 3-dimensional, 2-node curved beam elements on a 2-dimensional planar grid. The beams had 4 degrees of freedom per node including out-of-plane displacement and rotations as well as a warping degree of freedom, but the two translational displacements and the rotation about an axis perpendicular to the plane of the curve were neglected and deemed insignificant. The program modeled cross frames as truss elements and added additional degrees of freedom at the supports to account for the translational displacements of these nodes (Galambos et al. 2000).

A full scale laboratory test was conducted at the FHWA Turner-Fairbanks Structures Laboratory using a 90 ft. simple span bridge with 3-girders and a radius of curvature of 200 ft. A plan view of the test setup is shown in Figure 2.2. To ensure the girders remained elastic throughout the multiple tests the girders were fabricated with AASHTO M270 Grade 70W steel and additional cross frames were placed between girder lines 1 and 2. Resistant gages were used on the cross frames and bracing members, while vibrating wire strain gages were used on the girder. Select locations utilized displacement and rotation transducers to measure displacements. While a total station was used to measure global deformations (Linzell et al. 2004). The b_f/D ratio of the girders ranged from 1/3 for the inside girder to 1/2 for the exterior girder. The dimensions of the girders that were tested are provided in Table 2.1.

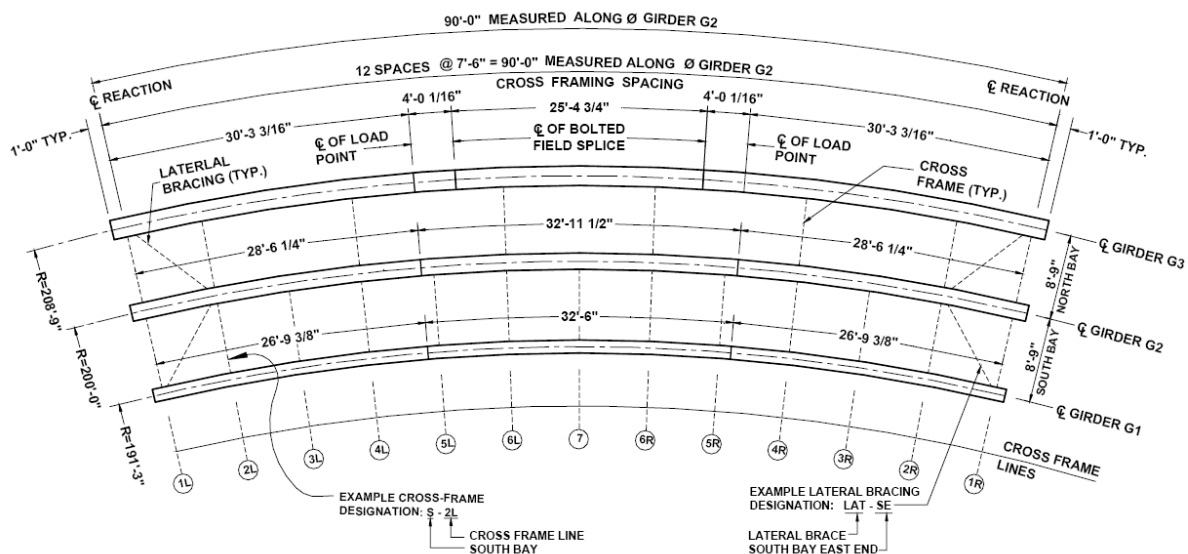


Figure 2-1: Plan View of Test Frame

Figure 2.2: Plan View of Test Frame at FHWA Turner-Fairbanks Structures Laboratory (Hartmann 2005)

Table 2.1: Plate Girder Dimension for Erection Test (Linzell et al. 2004)

| Girder Plate Dimensions | | | | |
|-------------------------|-------------------------------------|---------------------------------|------------------------|----------------|
| Locations | Flanges $b_f \times t_f$ (in) | Web $h_w \times t_w$ (in) | Radius of Curvature | Span Length |
| G1 | 16 x 1-1/16 | 48 x 7/16 | 86'-1" | 191'-3" |
| G2 | 20 x 1-3/16 | 48 x 1/2 | 90'-0" | 200'-0" |
| G3 | 24 x 2-1/4 | 48 x 1/2 | 93'-11" | 208'-0" |

Six single girder erection tests were conducted to examine the response of a single girder to a variety of lateral support conditions. Two twin-girder erection tests were conducted and one three-girder erection test was conducted. Each test consisted of shoring the girder to the shop specified camber, designated the “no-load” situation, and then the shoring was removed until the system fully deflected under the self weight. The shoring was then reinstalled to bring the specimen back to the “no-load” condition. The tests were not intended to reproduce actual construction conditions, but rather to gain data for cases in which falsework are used to stabilize curved girders during construction. The conclusion from the erection test showed that the V-Load method gives conservative predictions for the exterior girder and unconservative predictions for the interior girder (Linzell et al. 2004).

The bridge was modeled using ABAQUS finite element software. The interior two girders had 5 plate elements through the depth of the web and beam elements to represent the flanges. The cross frames and bottom braces were modeled with truss elements. The exterior most girder utilized plate elements for the web and the flange with a denser mesh closer to the center of the girder. The test indicated that it is beneficial to minimize the radial restraint when constructing curved I-girders. It also showed that a detailed shell element based finite element analysis model could provide an acceptable level of predictability of erection behavior. Additionally, simplifying analytical representations of the cross frame connection detail may lead to discrepancies between the predicted and measured behavior, specifically in the radial load distributions as the model was not as stiff in this aspect as measured and the exclusion of the gusset plates (Linzell 1999). Figure 2.3 shows the test frame at the FHWA Turner-Fairbanks Structures Laboratory.



Figure 2.3: Test Frame at FHWA Turner-Fairbanks Structures Laboratory (Hartmann 2005)

Beyond the initial testing phase at the FHWA Turner-Fairbanks Laboratory, several additional component tests were conducted to determine the effect on the vertical bending capacity of web slenderness, flange slenderness, and stiffener spacing. The results showed that the web slenderness and stiffener spacing had a negligible effect on the vertical bending capacity (Hartmann, 2005). Increases in the compression flange slenderness tended to decrease the bending capacity of the girder system.

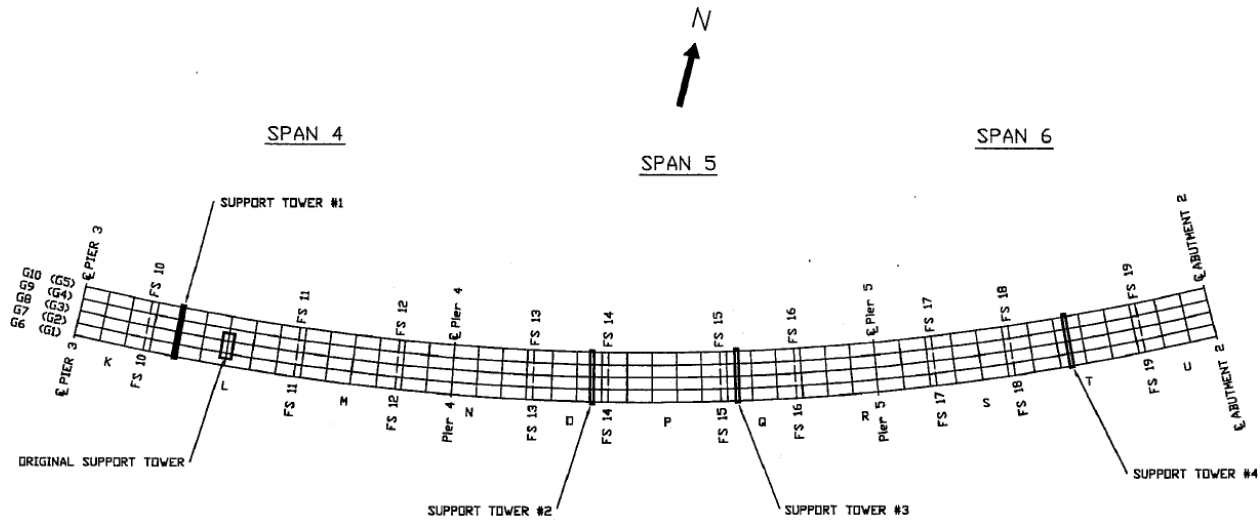
One of the most recent tests on a full scale bridge that experienced unexpected deflections and rotation during the girder erection process was documented by Bell (2004). The bridge was one of two side-by-side horizontally curved steel I-girder bridges built for an I-99 Interchange in State College, Pennsylvania. The bridge consists of five 10.5 ft. deep singly symmetric steel plate girders spaced at 9.75 ft. with radii of curvature varying from 1920 ft. to 1959 ft. The structure is a 6-span bridge with two 3-span continuous units. The focus of the research was on the second unit, which is referred to as spans 4, 5, and 6. Sixteen removable strain transducers and twelve vibrating wire strain gages were used to monitor the strain at different locations including the girder flange tips and cross frame members. Additionally, surveying data from a third party was collected and utilized to calibrate a 3-D finite element model developed in SAP2000. With the calibrated model Bell was able to conclude that for erection procedures involving lifting single girder lines, it is best to begin with the outer girder (largest radius) and construct the bridge toward the inside of the curve. However, for bridges erected with pairs of girders the erection sequence should be reversed and the inner girders should be lifted first. The use of top lateral bracing stiffens the girders and reduces the deflections. Temporary supports can reduce the deflections when compared to erection sequences that do not use temporary supports. Table 2.2 and Table 2.3 provide a summary of the girder dimensions and geometry. Figure 2.4 is a plan view of the bridge with the girder line, field splice, and support tower locations.

Table 2.2: Girder Plate Dimension Range (Bell, 2004)

| Girder | Top Flange Plate | | Web Plate | | Bottom Flange Plate | |
|--------|------------------|-----------|-----------|-----------|---------------------|-----------|
| | Width | Thickness | Depth | Thickness | Width | Thickness |
| | (in) | (in) | (in) | (in) | (in) | (in) |
| G1 | 20 – 35 | 1.5 – 4 | 126 | 0.8125 | 26 – 43 | 1.75 – 3 |
| G2 | 17 – 34 | 1 – 3 | 126 | 0.8125 | 18 – 40 | 1.5 – 3 |
| G3 | 16 – 28 | 1 – 3 | 126 | 0.8125 | 18 – 34 | 1.25 – 3 |
| G4 | 16 – 28 | 1 – 3 | 126 | 0.8125 | 18 – 34 | 1.25 – 3 |
| G5 | 17 – 34 | 1 – 3 | 126 | 0.8125 | 22 – 40 | 1.25 – 3 |

Table 2.3: Geometric Summary (Bell, 2004)

| Girder | Radius | Span 4 | Span 5 | Span 6 |
|--------|---------|--------|--------|--------|
| | (ft) | (ft) | (ft) | (ft) |
| G1 | 1959.36 | 298.84 | 336.5 | 268.79 |
| G2 | 1949.61 | 297.35 | 334.83 | 267.45 |
| G3 | 1939.86 | 295.85 | 333.16 | 266.11 |
| G4 | 1930.11 | 294.36 | 331.48 | 264.78 |
| G5 | 1920.36 | 292.86 | 329.80 | 263.44 |

*Figure 2.4: Plan View of Bridge Studied by Bell (2004)*

2.5 Computational Efforts

Currently there are several commercially available software programs capable of analyzing horizontally curved I-girder bridges. Many of the programs consist of 2-D grillage models that are useful for design calculations of various load cases of the completed structure and include. Two of the most widely used grillage programs consist of MDX and DESCUS. These design software packages are intended to ease the book keeping involved in the various load cases, force envelopes, and code checks. However, the 2-D models are not capable of analyzing the girders during construction and can miss critical information that can only be obtained from a full 3-D analysis. Alternatively, there are several general 3-D finite element

programs available including ANSYS, ABAQUS, LUSAS, ADINA, and BSDI. These programs can model most any structural problem, but lack the user-friendly interface necessary for widespread use in the design community. These 3D packages also do not include pre-defined load cases or AASHTO checks.

One of the first analytical methods used to design curved girders was introduced by U.S. Steel in 1963 (Richardson). This method, known as the V-load method, was investigated by Fiechtl et al. (1987) and they presented a report on the development and evaluation of the method. The V-load method accounts for the girder curvature by applying self-equilibrating vertical loads on the girder. Fiechtl's report compares these results with refined finite element analysis for a variety of bridge configurations. The following steps are presented to summarize the V-load method used widely as a preliminary analysis technique.

1. Apply the loads of the curved girder to an approximated straight girder with a length equal to the arc length of the curved girder (known as P-Loads).
2. Determine the moments and shears along the girder length from this analysis.
3. Determine the moments at each diaphragm line.
4. Use (2.3) or (2.4) to find the V-Loads at each diaphragm location.
5. Apply the V-Loads at the diaphragms.
6. The V-Loads are applied as point loads at the diaphragm location.
7. For a 2-girder system the V-Load is downward for the outer girder and upward for the inner girder.
8. For multiple girders the V-Load is assumed to be linearly distributed between the outer and inner girders.
9. Therefore the V-Load is proportional to the distance from the centerline of the bridge.
10. Determine the moments and shears for this analysis.
11. Sum the moments and shears from steps 2 and 5 to determine the final moments and shears for the girder.

For Two Girders:

$$V = \frac{M_{p1} + M_{p2}}{RD/d} \quad (2.3)$$

For Multiple Girders

$$V = \frac{\sum_{i=1}^{N_g} M_{pi}}{C(RD/d)} \quad (2.4)$$

Where:

M_p = The moment for each diaphragm line due to the
P – Load of the i^{th} girder
R = Radius of the girder
D = Spacing between girder
d = Arc length between diaphragms

$C = A$ constant distribution factor for multi – girder bridges

$$C = \frac{1}{6} \frac{N_g(N_g + 1)}{(N_g - 1)} \quad (2.5)$$

$N_g =$ Number of girders

Note: d should be measured along the radius line of R . The internal angle is the important aspect $\phi = d/R$. Therefore any girder R will work if the d is measured along that girder.

The conclusion from the study showed that the V-load method is accurate for non-composite sections, but did not perform well for composite action due to the shear transfer by the deck. For two-girder systems the analysis is slightly conservative for the outer girder while the solution is slightly unconservative for the inner girder when compared to the finite element models. The V-load method has greater error for bridges with skewed supports.

The difficult structural analysis problems present in the design of highway bridges have utilized many techniques over the years. Zureick and Naquib (1999) synthesized the available analysis methods and evaluated the strengths and limitations of each technique. The authors divided the methods into approximate methods and refined methods. Approximate methods include the plane-grid method which models the bridge as an assemblage of two-dimensional (2D) grid members with one translational and two rotational degrees of freedom. The space-frame method models the bridge as idealized three-dimensional (3D) straight members, with the effect of warping not usually included. The V-load method models the bridge using equivalent straight girders with span length equal to the arc length and adds self-equilibrating vertical shear forces at the diaphragm locations to take the curvature into account.

Zureick and Naquib (1999) also discussed the refined methods which include the finite element method that models the bridge by discretizing the structure into small divisions defined by specifically numbered nodes. The behavior of the elements and the entire structure are a function of the nodal quantities which serve as the primary unknown. The authors recognize that the finite element method is one of the most general and accurate methods, but requires significant amount of time to implement. The finite-strip method divides the bridge into narrow strips with radial supports and provides some simplicity over the finite element method, but does not offer the flexibility. The finite-difference method superimposes a grid on the structure and the governing differential equations are replaced by algebraic difference equations and solved at the grid points. The slope deflection method establishes partial differential equations in terms of the slope-deflection equations and solved assuming a Fourier series. In conclusion, the approximate methods are suitable for preliminary design and while the finite element method is the most involved it's also the most flexible with respect to configurations and boundary conditions. It was noted that the development of commercial finite element codes with incorporated graphical interfaces would expedite the modeling and allow the user to view results.

Chavel and Earls (2006 a) analyzed the Ford City Veterans Bridge PA State Route 128 over the Allegheny River. The bridge consisted of a three-span system with curved end span. The end spans are 322 feet and the center span is 417 feet. The bridge consists of four 14 feet deep girders spaced at 13.5 ft. There was very little bridge erection data. To validate the geometric nonlinear finite element analysis using ABAQUS the data from Linzell's test (1999) was used. The authors were unable to predict several alignment problems experienced during construction with the results from the model. This was attributed to inconsistent detailing of the girder, which was discussed more fully in a subsequent article by Chavel and Earls (2006 b). This second article highlights the problems experienced with the erection of the Ford City

Veterans Bridge. The erection problems were attributed to detailing inconsistencies. The girders are normally detailed to be plumb in the no-load condition or in computational models before the girders experience the deflections and rotations associated with self weight. The issue of inconsistent detailing becomes more important as for larger, stiffer, girders or smaller radii girders.

Nevling et al (2006) utilized the results from a field study on a three span curved bridge with five girders to compare different analysis programs. The goal of the project was to assess the accuracy of different analysis levels. The authors established three levels of analysis to compare to the field data: manual, 2D grillage, and 3D finite element method (FEM). For the manual analysis a line girder method of analysis from the AASHTO (1993) *Guide Specification for Horizontally Curved Highway Bridges* and the V-load method were used. Three commercially available 2D grillage software programs were compared including SAP2000, MDX, and DESCUS. The 3D FEM models were created in SAP2000 and independently by Bridge Software Development International (BSDI). The authors reported that the 3D mesh used was coarse due to BSDI requirements. The result of the work concluded that both the 2D and 3D models produced girder vertical bending moment distributions that generally correlated well with the field test distributions and provided improved accuracy over the manual methods. Thus it was recommended that 2D analysis provides a reasonable approach when compared to a coarse 3D mesh.

Coletti and Yadlosky (2008) authored a paper discussing challenges and proper usage of computer models for steel bridges. They specifically addressed the importance of properly understanding the fundamental assumptions and analytical implication of boundary conditions for different levels of analysis, the effect of representing a complex structure in a simple model, and the influence of span length, curvature, and skew on the construction tolerances and fit-up. Several examples are presented to highlight the importance of each issue.

As part of his dissertation Chavel (2008) utilized ABAQUS 6.3 to model a curved skewed bridge in King of Prussia, Pennsylvania and perform a series of parametric geometrically nonlinear analysis. The single span bridge had a radial abutment and a second abutment at a 38.8 degree skew. The model utilized four-node shell elements with a maximum aspect ratio of 2:1 to model the girders and the cross frames were modeled with 3-D beam elements. The research focused on two aspects of the construction: the erection sequence and the cross frame detailing. With respect to the previous, Chavel recommended that bridge engineers investigate each stage of steel erection for horizontally curved steel I-girder bridges in order to limit the problems that may develop in the field during construction and to highlight more difficult portions of the procedure for the erection. Figure 2.5 is a plan and isometric view of the bridge modeled by Chavel in ABAQUS.

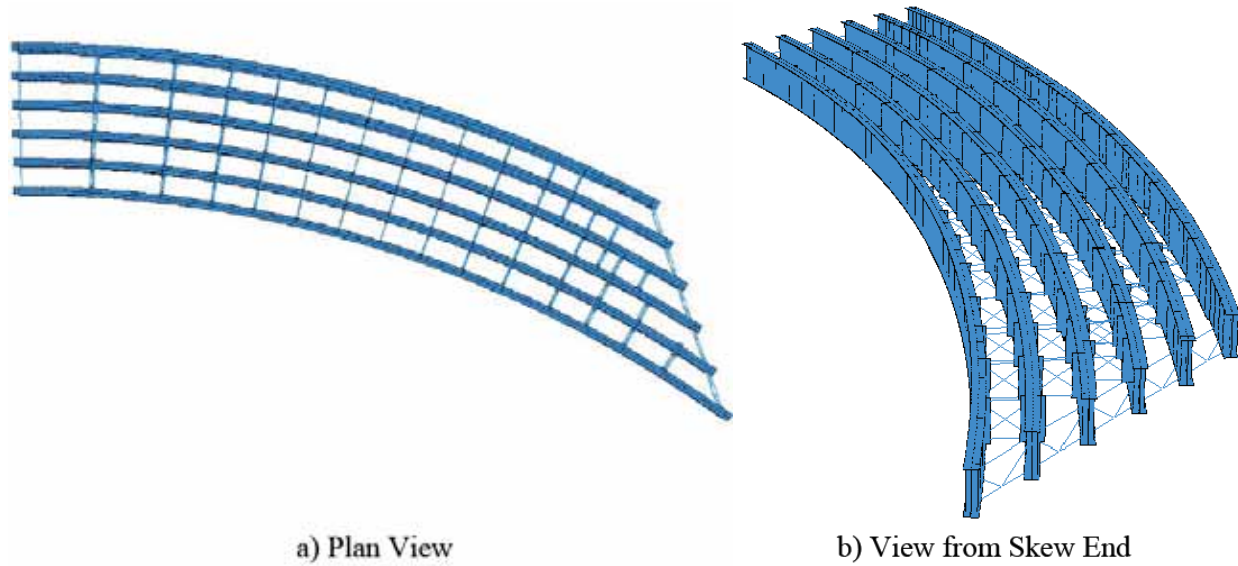


Figure 2.5: Plan and Isometric Bridge Modeled by Chavel (2008)

Another recent publication discussing the modeling issues associated with steel bridges during construction was published by Ozgur et al. (2009). In the paper the authors use much of the material featured in Chavel (2008) including the King of Prussia, PA bridge. Additionally, the author describes an approximate method to determine uplift of the bearings during constructions by utilizing (2.6).

$$\xi = \frac{s_c}{w \cos(L_{as}/2R)} \quad (2.6)$$

Where:

w = The width of the bridge

L_{as} = Arc Length of the bridge

R = Radius of curvature

s_c = Distance from the centroid of the bridge to a chord line through the inner most bearings of the bridge

The author recommends a limit of 0.8 for ξ which works for simple span singularly curved bridges.

A final note on the analysis of curved girders should include the work of Tung and Fountain (1970) on the approximation of torsion by the M/R-Method which is a historically sited computation method often used in the preliminary design of curved steel bridges. Tung and Fountain's idea is to approximate the torsional component of a curved bridge by dividing the moments by the radius of curvature. This is a good approximation used during preliminary designs of box girders, but the method does not work for I-girders, because two of the assumptions stated by the authors include no cross sectional distortion and negligible warping torsion. While these assumptions are applicable for box girders and other closed or semi-closed box girders with adequate bracing, I-girders have a significant amount of torsional stiffness from warping torsion rendering this method erroneous for I-girder applications.

2.6 State of Practice (Code Requirements)

There are several bridge design codes that specify requirements for curved I-girders during construction. Some of these specifications provide specific recommendations while others only provide general guidance. The following paragraphs discuss the stated requirements of several codes and include the preferred practices for the state of Texas. These are given to provide an understanding of the codified state of practice for bridges during construction.

The AASHTO LRFD Bridge Design Specification (2007) is published by the American Association of State Highway and Transportation Officials (AASHTO) providing a Load Resistance Factor Design (LRFD) guideline for bridge engineers to use in the design of all types of bridges. There is some discussion of erection in the specifications including Section 2.5.3 which discusses the design objectives during construction. This section states, “Constructibility issues should include, but not be limited to, consideration of deflection, strength of steel and concrete, and stability during critical stages of construction.” Chapter 4 is dedicated to the structural analysis of bridges and in Section C4.6.1.2.1 states,

“Since equilibrium of horizontally curved I-girders is developed by the transfer of load between the girders, the analysis must recognize the integrated behavior of all structural components. Bracing members are considered primary members in curved bridges since they transmit forces necessary to provide equilibrium.”

This requirement suggests a certain level of analysis is required for curved bridges above that of a similarly complex straight bridge. The commentary continues by stating,

“Small-deflection theory is adequate for the analysis of most curved-girder bridges. However, curved I-girders are prone to deflect laterally when the girders are insufficiently braced during erection. This behavior may not be well recognized by small-deflection theory. Classical methods of analysis usually are based on strength of materials assumptions that do not recognize cross-section deformation. Finite element analyses that model the actual cross-section shape of the I-girders can recognize cross-section distortion and its effect on structural behavior.”

This brings up two important ideas discussed in this report: the need for 3D finite element analysis and the idea of small-deflection theory. Recommendations are given for when each are necessary. The recommendation of using finite element analysis to model the bridge cross-section and bracing members is accomplished by the UT Bridge program developed as part of this research and discussed later in the report.

Chapter 6 of AASHTO LRFD Bridge Design Specification discusses the design of steel bridges. Section 6.5.1 states that the limit states should be investigated “for each stage that may be critical during construction, handling, transportation, and erection.” Section 6.7.4.2 discusses specific limitations on the unbraced length of curved I-girder bridges by mandating that all intermediate cross frame or diaphragm spacing (L_b) shall not exceed:

$$L_b \leq L_r \leq \frac{R}{10} \leq 30' \quad (2.7)$$

Where:

L_r = Limiting unbraced length
 R = Radius of curvature

$$L_r = \pi r_t \sqrt{\frac{E}{F_{yr}}} \quad (2.8)$$

Where:

r_t = Effective radius of gyration for lateral torsional buckling
 F_{yr} = Compression – flange stress at the onset of nominal yielding within the cross section

F_{yr} includes residual stress effects, but does not include compression-flange lateral bending, taken as the smaller of $0.7F_{yc}$, and F_{yw} , but not less than $0.5F_{yc}$. F_{yc} and F_{yw} are the yield stress of the compression flange and the web, respectively.

$$r_t = \frac{b_{fc}}{\sqrt{12 \left(1 + \frac{1}{3} \frac{D_c t_w}{b_{fc} t_{fc}} \right)}} \quad (2.9)$$

Where:

b_{fc} = Width of the compression flange
 t_{fc} = Thickness of the compression flange
 t_w = Thickness of the web
 D_c = Depth of the web in compression in elastic range

This gives very specific cross frame spacing depending on the cross sectional properties used by the designer. Section 6.10.2.2 provides other guides for the cross sectional proportioning including an equation setting the limit of the flange width to a sixth of the depth of the web. This would allow a twelve foot deep beam to have a two foot flange width. While this may be sufficient for straight girders, the complication of torsional forces in a curved girder can lead to a problematic and even dangerous structural element with such a slender flange designed near this limit.

The AASHTO LRFD Bridge Construction Specifications (2004) provide the required construction practices as stated by AASHTO. Section 11.6 discusses the erection of steel structures and states in Section 11.6.4.3 that “Cross frames and diagonal bracing shall be installed to provide stability and ensure correct geometry. Temporary bracing, if necessary at any stage of erection, shall be provided by the Contractor.” This section provides suggestions, but does not give guidance as to how to determine “if necessary.” There is no standard on the level of analysis or factor of safety to provide to determine the need for temporary supports.

The AASHTO/NSBA Steel Bridge Erection Guide Specification (2007) is published jointly by AASHTO and the National Steel Bridge Alliance (NSBA) with the intent to standardize and facilitate construction of steel bridges in the United States. Chapter 2 of this document specifically discusses the erection procedure and requires that a contractor provide a detailed erection procedure to the owner prior to the start of construction. Section 2.3 b) states the submitted procedures should contain, “calculations to substantiate structural adequacy and stability of girders for each step of bridge assembly.” There is no mention of the type of procedure or the level of analysis required. Instead, the Specification stipulates that these calculations be completed as part of the erection plan. Chapter 6 of this document specifically discusses the lifting procedure and states that “crane and materials must be located such that the

lift is safe and within the crane manufacture's capacity." Section 6.3 states that "Girders shall be stabilized with falsework, temporary bracing, and/or holding cranes until a sufficient number of adjacent girders are erected with diaphragms and/or cross frames connected to provide the necessary lateral stability and to make the structure self-supporting." Again this requirement is given without guidance for accomplishing the task. The details for the level of analysis or factor of safety to employ are not discussed. The commentary associated with Section 6.3 states that "Removal of falsework, temporary bracing, and holding cranes shall be in accordance with stability provided in the erection procedure."

Engineers not satisfied with the previously mentioned codes can research sources of recommendations including the TxDOT Preferred Practices for Steel Bridge Design, Fabrication, and Erection. This document is published by the Texas Department of Transportation (TxDOT) to provide optimal quality and value in steel bridge design within Texas. In Section 2.2.1 it states that "for curved girders, flange width should be approximately one-third the web depth and no less than 30 percent of the web depth. The extra width for curved girders enhances handling stability and helps keep lateral bending stresses within reason." This limit of one-third the web depth is twice as wide as the one-sixth limit specified by AASHTO. This disparity was one of the reasons for the funding of the current project. The Preferred Practices also state, "flange width affects girder stability during handling, erection, and deck placement. Keep the girder length (field section length) to flange width ratio below 85." This last recommendation gives guidance on the length of field sections and provides for a conservative limit to ensure transportation and erection safety. Section 2.2.4 provides additional cross-sectional proportioning recommendations and states that the recommended depth given in AASHTO 2.5.2.6.3 should be increased by 10% to 20% for curved girders. The total superstructure depth to span length ratio should be 1: 0.033 – 1: 0.04 according to the TxDOT Preferred Practices. Section 2.6 states that for curved girders, TxDOT prefers that diaphragms or cross frames be placed at 15 to 20 ft maximum to help limit flange bending stresses and cross frame/diaphragm member forces.

Another source of information about the current state of practice in construction and erection of curved I-girder is the recent NCHRP Synthesis 345 report (2005). This report titled *Steel Bridge Erection Practices, a Synthesis of Highway Practices* documents a survey sent to state departments of transportation, contractors, and fabricators. Chapter 4 summarizes the erection issues and solutions encountered by the survey participants. With respect to the lifting of curved girders, it was noted that picking at two points usually eliminates any later stability problems, as long as the line between the pick points runs through the center of gravity of the girder. The erectors also gave rules of thumb for cross-sectional proportioning stating that unbraced length to compression flange width (L/b) of 60 or less provides stability during transportation and erection, but also stating that it could be increase to as much as 80 with further stress calculations to verify the safety. Any L/b value greater than 80 would require a temporary support (falsework or holding crane) to provide stability according to the erectors. These rules of thumb are value tools for the engineer to take from the experience of the erectors, but they do not provide the analysis process to accomplish "further stress calculations." Chapter 5 reports the problems experienced by the survey participants and include five states reporting stability problems with girders in various stages of construction before the final condition. Instabilities were reported for girders without adequate cross frame bracing attached, cantilevered girders over the pier to a field splice, and also due to wind loadings during construction. Another problem reported by eight states was unanticipated lateral or rotational deformations of the

girders during the deck placement. These concerns highlight the need for robust computational tools to assist engineers in predicting the behavior of these bridges at a vulnerable state.

Chapter 3. Field Tests

3.1 Introduction

This chapter provides a summary of the field tests conducted as part of the research project. The material that is presented includes the geometry and layout used to monitor the behavior of a steel girder unit during the erection and concrete deck placement. As discussed in the review of past research conducted on curved I-girders presented in Chapter 2, there is a significant void in the availability of field studies on curved I-girders during early stages of construction. This chapter describes the steps taken to correct this deficiency and includes the first test on curved steel I-girders during lifting of which the authors are aware.

A brief discussion about the data acquisition system used to measure the behavior is also provided. The system was first used to monitor two steel girders and two cross frames from a curved bridge on the direct connector from SH 130 to US 71 in Austin, Texas. Strain changes were monitored during the lifting, erection, and concrete deck placement of the girders and cross frames. In addition, measurements were also made of the deflections and rotations that occurred during the concrete deck placement. The second instrumentation was of two girders at the Hirschfeld Steel Company in San Angelo, TX. Girder stresses and twists were measured during lifting from well established support conditions. The instrumentation that was used is discussed in the following sections. The information from the field tests was gathered to provide data for verification of the finite element models and provide guidance on issues that bridge engineers face when designing curved steel plate I-girders. While a summary of the results are given within this chapter a comprehensive presentation of the information can be found in Schuh (2008) and Farris (2008).

3.2 Data Acquisition system

Before describing the field specimens and instrumentation processes, a brief description of the data acquisition systems is warranted. The field work utilized several different sensors including strain gages, rotational gages, and a laser distance meter. Foil strain gages measure the strain change in the girder by utilizing the electrical resistance change in the gage amplified by a Wheatstone bridge to detect a microstrain. The rotational gages utilized accelerometers to determine the rotational change of the girder in the field. The laser distance meter sends a laser to the target object and records the time it takes for the beam to return providing an accurate distance measure to the 1/16 of an inch. The data was collected and stored using CR5000 Campbell Scientific dataloggers. To increase the number of sensors that could be monitored for a given data logger, multiplexers were utilized. Up to 16 strain gages (16 differential channels) can be connected to each of the AM416 Multiplexer and up to 7 multiplexers can be connected to the datalogger. A full description of all the data acquisition systems is given by Schuh (2008) and Farris (2008).

3.3 SH 130/US 71 Bridge Instrumentation

The first field investigation was conducted on a bridge located east of the Austin Bergstrom Airport on SH 130 as indicated in Figure 3.1. Bridge 88 is a direct connector between east-bound US 71 to north-bound SH 130 and is comprised of four continuous horizontally curved steel girder units and five precast prestressed concrete beam units. The bridges are

numbered along SH 130 from North to South and the instrumented bridge is therefore named Bridge 88 through this naming convention.

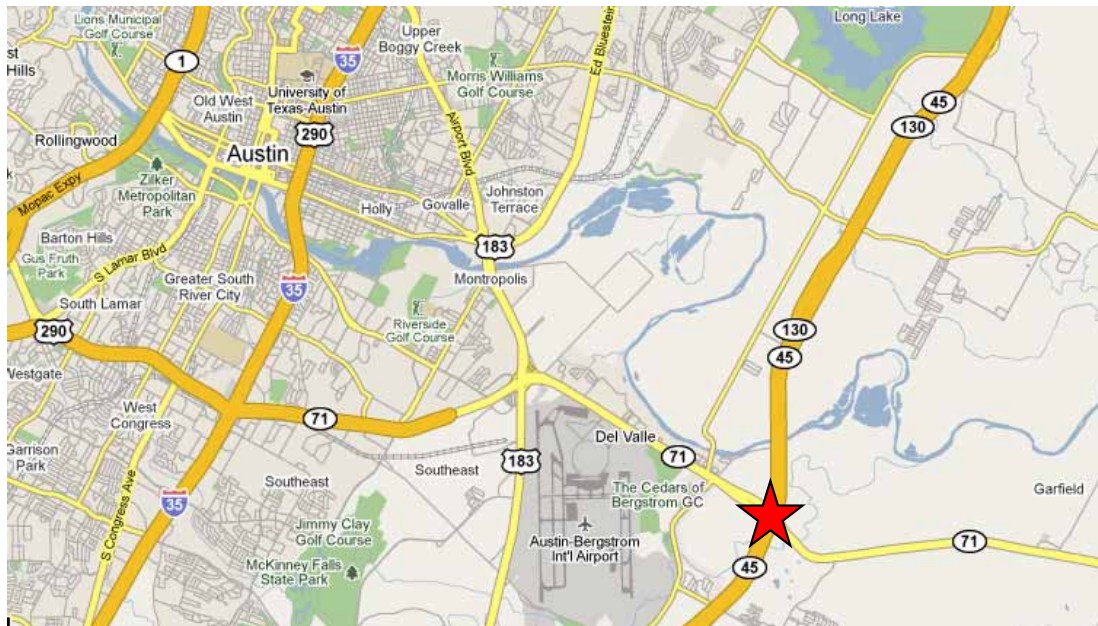


Figure 3.1: Bridge 88 Location (Google Maps 2009)

The third steel unit, which contains Spans 14, 15, and 16, was chosen for instrumentation and field monitoring. The three-span continuous girder system has spans of 185', 205', and 158.5' with a radius of curvature of 1206' at the base line. The basic cross-sectional layout is depicted in Figure 3.2. The center to center spacing between adjacent girders is 10'-4". Strain gages were placed on the girders labeled 3 and 4, which were located on the outside of the curved bridge. Two cross-frames that will be referred to as X1 and X2 were also instrumented. Figure 3.2 shows the plan layout of the bridge, with Span 14 magnified to show the location of the instrumented girders and cross frames. Also pictured is the elevation view of Girders 3 and 4 with the instrumented cross sections detailed. The full description of the bridge geometry and instrumentation setup for Bridge 88 is given by Schuh (2008) and Farris (2008).

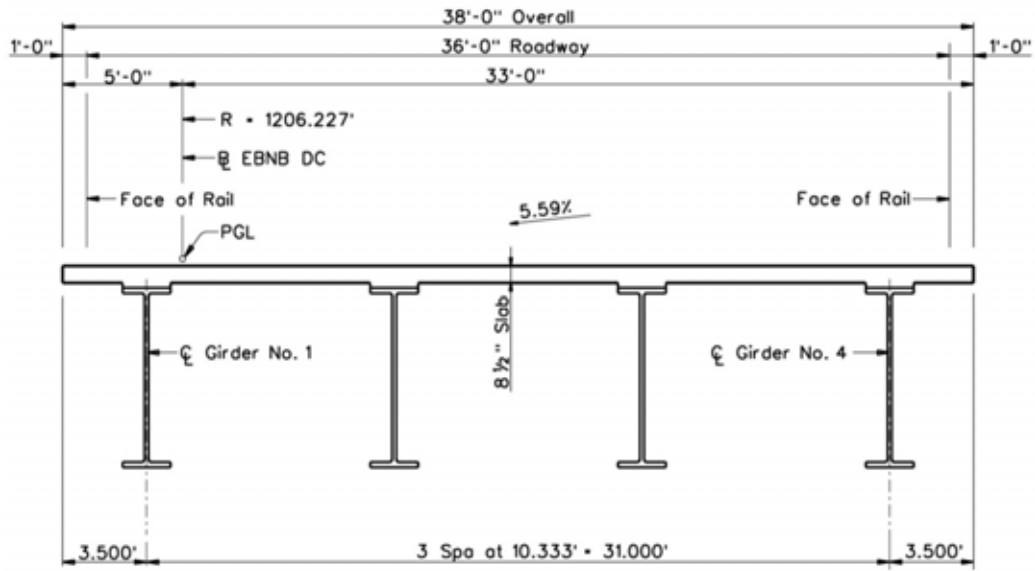


Figure 3.2: Typical Roadway Cross Section

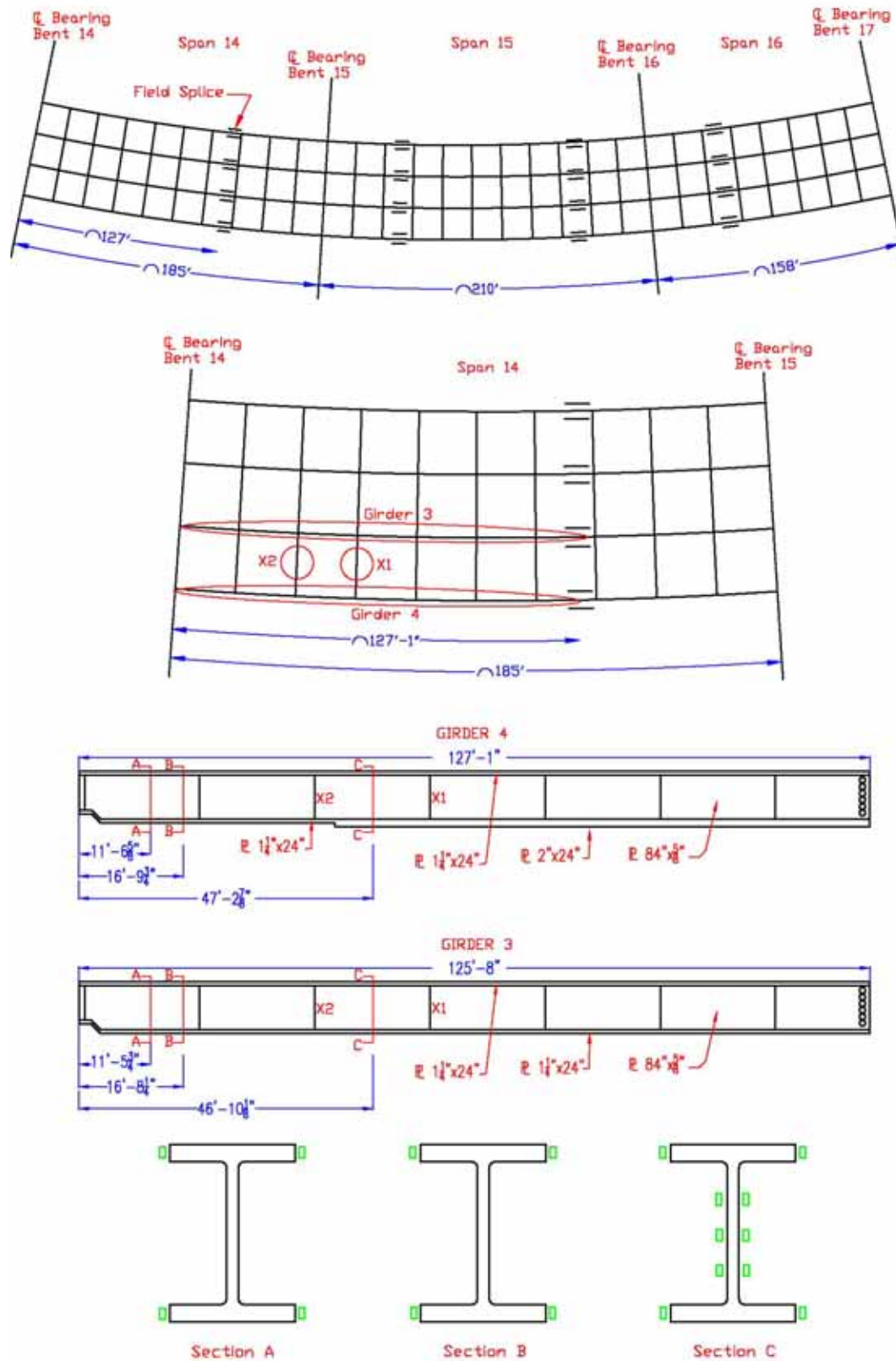


Figure 3.3: Unit 6 Bridge Framing Plan & Girder Elevations w/ Gage Locations

The cross frames were comprised of four L5" x 5" x ½" angle sections which is a standard TxDOT cross frame commonly used in curved I-girder bridges. The two top and bottom horizontal struts have lengths of 8'-7" while the two diagonals are 9'-1" in length. The angles were instrumented with four strain gages that were positioned on both sides of the angle legs at a location 1" from the tip of the angle leg. The goal of the instrumentation was to measure the axial force components in the angle members during the concrete placement. Four strain gages were used for this task so that the effects of bending of the angle could be accounted for. The bending was accounted for using expressions developed by Fan (1999). Figure 3.4 provides a schematic of the cross frames and gage locations on the four members.

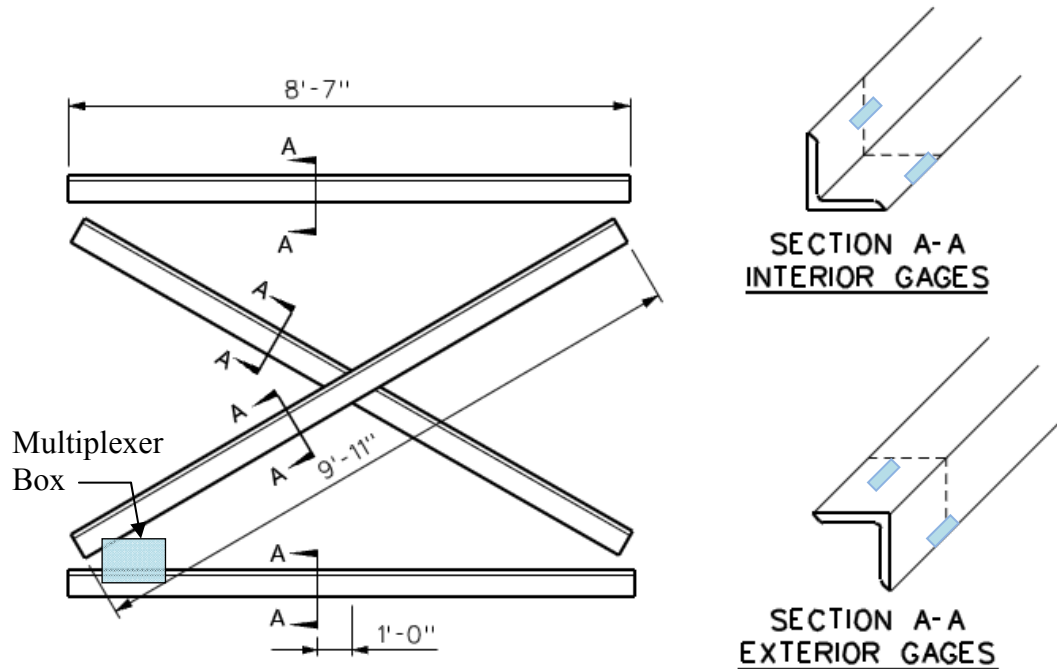


Figure 3.4: X1 and X2 Elevation with Gage Locations

3.4 Hirschfeld Lift Test Instrumentation

In addition to the studies of the bridges during construction, two curved girders were also instrumented at the Hirschfeld Steel Company in San Angelo, TX. The purpose of these tests was to monitor the displacement behavior of the curved girders during lifting with well established support conditions. Although tests were conducted during lifting of the girders at the SH130-US71 outlined in the previous section, the support conditions of the girders during lifting were unclear. The girders at SH130-US71 were supported on wooden timbers and the actual support points were difficult to ascertain. In addition, the points of support in the girders were very close to the lifting points and therefore stress changes during lifting were relatively small. Special support brackets were fabricated for the Hirschfeld lift tests so that the conditions prior to lifting were very clear. In addition, the support points could be easily adjusted to provide larger changes in the support conditions during lifting. The girders were moved into a staging area in the steel yard where they were instrumented with strain gages, tilt sensors, and the data acquisition system. Figure 3.5 shows the elevation view of Girders 16C4 and 14C2 with the instrumented cross section detailed. These girders are part of the same direct connector as Girder

4 and Girder 3 in the SH130-US71 bridge, which lead to the girders bearing similarities with regard to their geometry. A more detailed description of the girders and instrumentation setup are given by Schuh (2008).

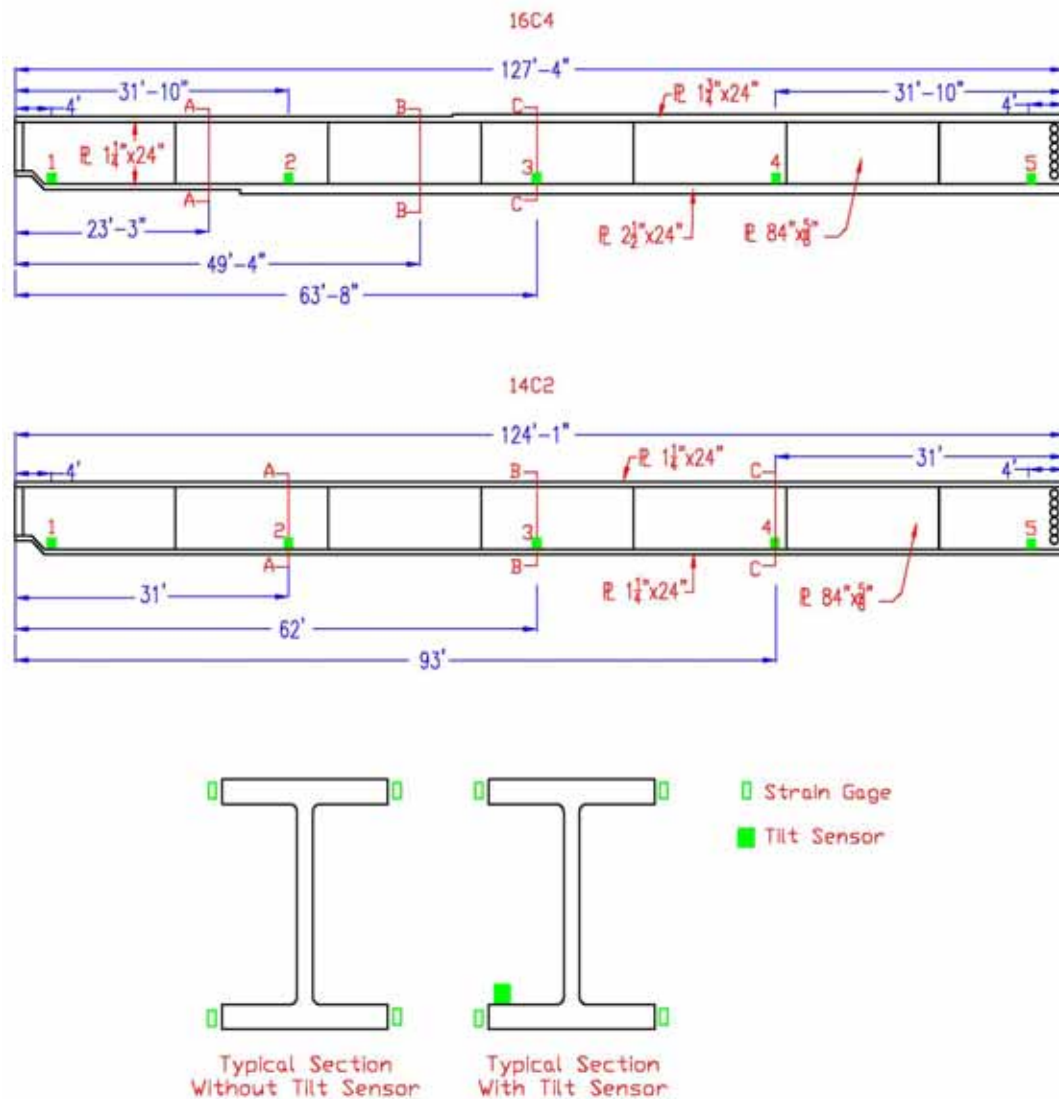


Figure 3.5: Hirschfeld Girder Elevations w/ Gage and Tilt Sensor Locations

3.5 Data Reduction Technique

The purpose of the instrumentation was to measure strains from which bending and warping stresses could be isolated. These stresses provided valuable information for improving the general understanding of girder behavior during the early stages of construction as well as for validating analytical models for studying girder behavior during these critical stages. This section illustrates how the bending and warping stresses presented in the results were calculated from the strains collected from the gages during the lifting process.

3.5.1 Bending and Warping Stress Interaction

An important aspect to interpret the strain measurements from the field studies is having a clear understand of the relationship between the bending and warping stress distributions that are present in the flanges of curved I-girders. Bending stresses from vertical bending vary linearly down the depth of the cross section, with the maximum values occurring at the top and bottom flanges. The bending stress is assumed to be essentially constant through the relatively small thickness of the flanges. Because warping stresses are caused by lateral bending of the flanges, the variation of stresses across the flange width are linear. The individual stress components from bending and warping stresses can be isolated using principles of superposition. Figure 3.6 illustrates the bending and warping stress distributions at the flanges, as well as their interaction.

3.5.2 Bending and Warping Stress Isolation

During the girder lifts, stresses at the flange tips were obtained from the strain gages. These stresses are denoted as σ_L and σ_R , referring to the left flange tip stress and right flange tip stress, respectively. For all girders involved with this study, this convention makes σ_L correlate to the inside with respect to horizontal curvature and σ_R with the outside. The characteristics of the combined stress distribution were used to isolate the bending and warping stress components. This process is presented in Figure 3.7, and in the expressions given in (3.1), and (3.2).

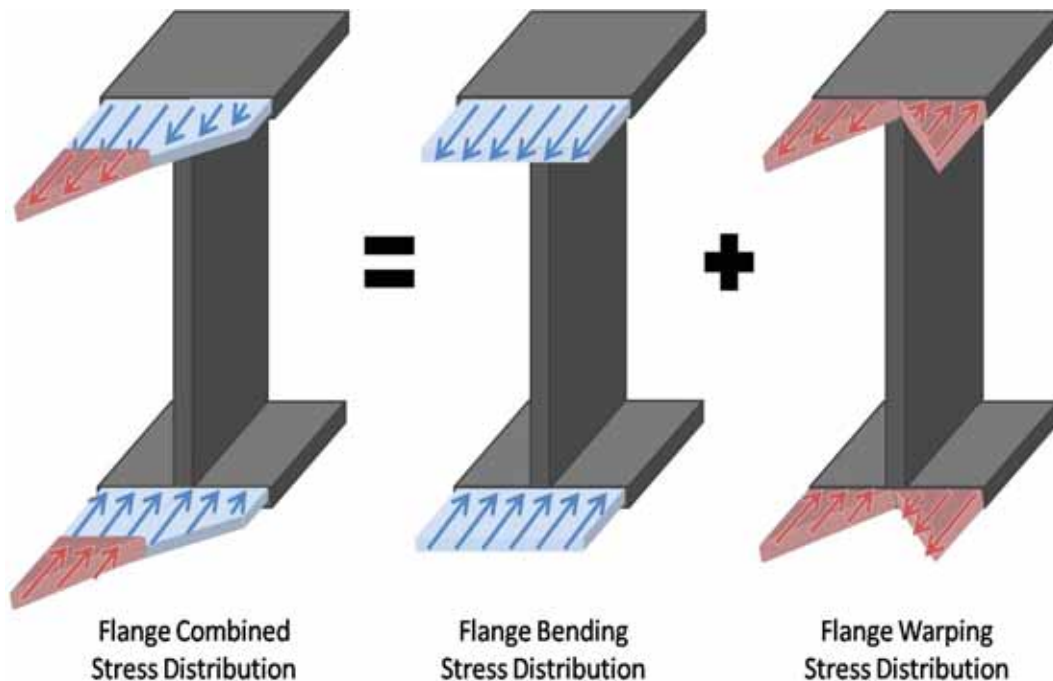


Figure 3.6: Curved I-Girder Flange Stress Distributions

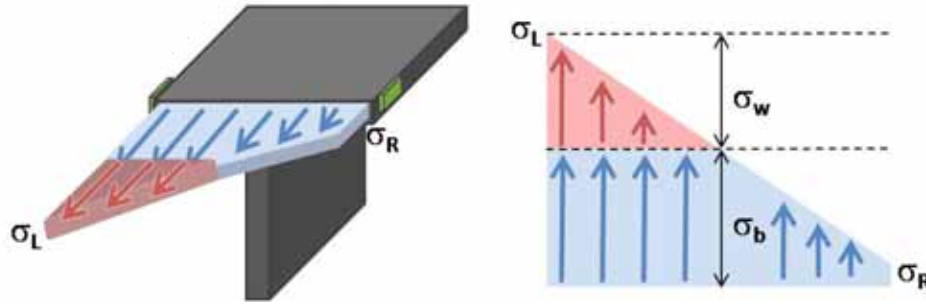


Figure 3.7: Bending and Warping Stress Isolation

$$\sigma_{bending} = \frac{(\sigma_L + \sigma_R)}{2} \quad (3.1)$$

$$\sigma_{warping} = \frac{(\sigma_L - \sigma_R)}{2} \quad (3.2)$$

The data presented in the following sections gives the bending and warping stress calculated using (3.1) and (3.2). Further discussion of bending and warping stress distributions specific to the tests is also presented. Based upon (3.2), positive warping stress changes indicate higher combined stresses being present on the flange tip located on the inside of the horizontal curvature of the girder.

3.6 Description and Results of SH 130/US 71 Bridge Erection

This section explains the time line and process by which the girders and cross frames of Span 14 of the SH 130/US 71 direct connector were lifted and erected into place. Results from the girder lift and erection are presented. The purpose of the tests was to collect data to validate analytical models.

3.6.1 SH 130/US 71 Direct Connector Erection

The girders were initially located in a large staging area and supported on heavy timber dunnage. A 60 foot spreader bar with two lift clamps lifted the girders and supported them during the erection. The spreader bar and lift clamp apparatus are shown in Figure 3.8.



Figure 3.8: Spreader Bar and Lift Clamp Apparatus

Timelines for both the Girder 4 and Girder 3 lifting and erection is shown in Figure 3.9. The timeline begins when the data acquisition system on Girder 4 was activated at 13:45. For both girders, the dataloggers were programmed to record strain data every 2 minutes. Once the girders were lifted into place on the pier, girder splices were made with snug tightened bolts. Following typical erection procedures, approximately half of the bolts were installed into the splices before the girders were released from the crane. At this stage, cross frame to girder connections consisted of a single snug tightened bolt at the top and bottom of the cross frame. Girder 4 was lifted first, followed by Girder 3 with cross frames attached. A temporary holding crane (second crane) was used to support Girder 4 until Girder 3 was erected and the cross frames were installed between the girders. The following subsections detail the respective lift for each girder.

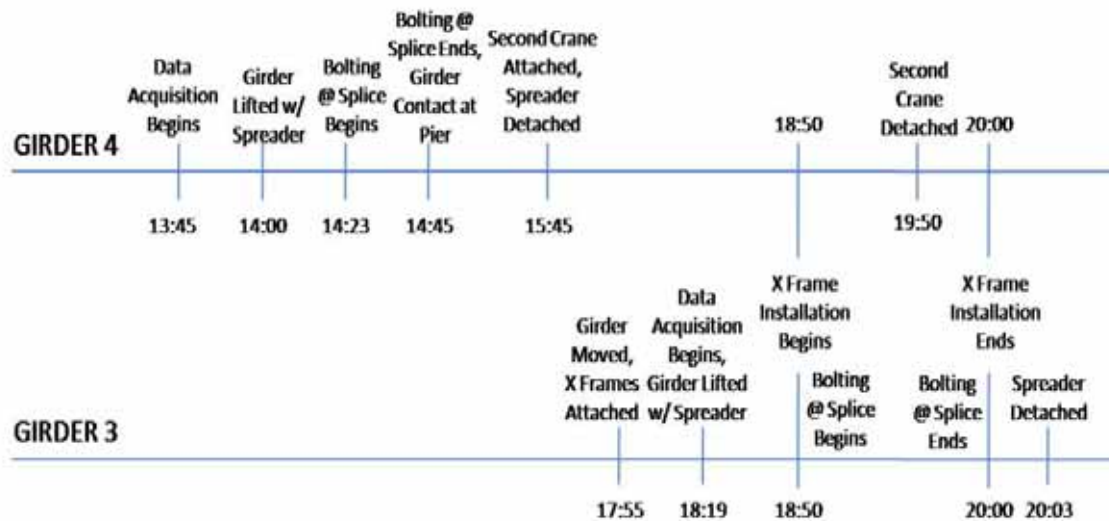


Figure 3.9: Erection Timeline for Girder 4 & 3

3.6.2 SH 130/US 71 Girder Erection Results

The following section presents figures showing a stress time history of Girder 4 and Girder 3 during their lifting and erection. Specific events of the lift are highlighted and can be correlated to the timeline presented in Figure 3.9. From these figures, the different states of stress experienced by the girders and the stress changes associated with different operations can be observed. The full presentation of the data is given by Schuh (2008).

Girder 4 Graphical Results

All stress changes shown for Girder 4 in this section indicate the change relative to the state of stress prior to the lift when the girder was supported by timbers on the ground. Very small changes in stress were recorded at the gage locations during the initial lifting with the spreader bar. The reason for the small changes in stress is that the change in vertical boundary conditions was very small, because the timber support locations were relatively close to the lifting points as shown in Figure 3.10.

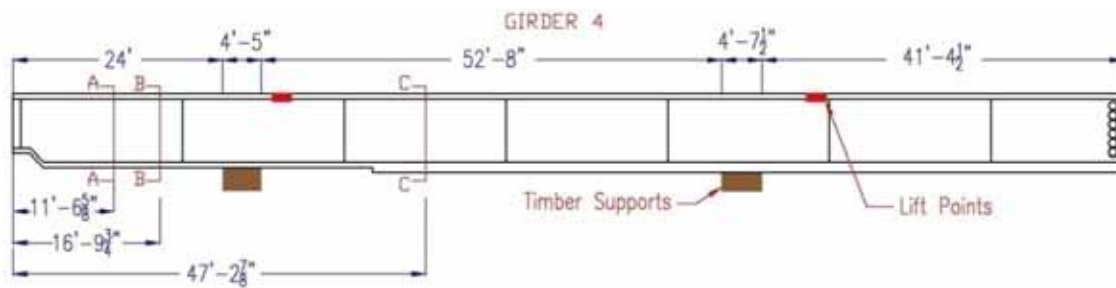


Figure 3.10: Girder 4 Timber Support Locations w/ Gaged Sections

Figure 3.11 shows the graph of Girder 4's bending and warping stress changes at the top flange of Section C during the lifting process. A slight change of less than 1 ksi occurred once the girder was placed on the pier and the splice was completed at 14:45. The first significant stress change occurred when the second crane was attached and the spreader bar was removed from the girder at 15:45. The support conditions changed, causing a significant change in the moment along the girder. Figure 3.11 details the approximate moment expected when the girder was supported by the 60 foot spreader bar during the lift at 14:00 versus the moment once the spreader was detached and the girder was supported at the pier and splice, with a 29 kip stabilizing force provided by the second crane (15:45, see Figure 3.9).

These predicted changes in moment correlate with the observed bending stress changes at the top flange of Section C, shown at the dashed line on the girder detail in Figure 3.11. Once the spreader bar was removed from Girder 4, the bending stress change at this location underwent a brief spike of approximately -2 ksi (negative values denote compressive stress changes), before settling at about -0.75 ksi. The warping stress change at the top flange of Section C showed a similar brief spike (-6.5 ksi) before settling at an approximate compressive stress of 2.5 ksi.

The second significant stress change occurred during the installation of the cross frames between Girders 4 and 3 from 18:50 to 20:00. The data shows that the bending and warping stress changes during fit-up are significant, with bending stress undergoing maximum changes of 2.5 ksi and warping showing max changes of 7 ksi. The removal of the second crane from Girder 4 and the spreader from Girder 3 at 19:50 and 20:03, respectively, led to the girders acting as a continuous bridge with the rest of Unit 6, though the splices and cross frames were connected with only a small number of bolts, tightened snug at this stage. During this time, bending stresses changed -3 ksi and warping changed +4.5 ksi. These changes associated with this final state can be seen in the data presented in Figure 3.11.

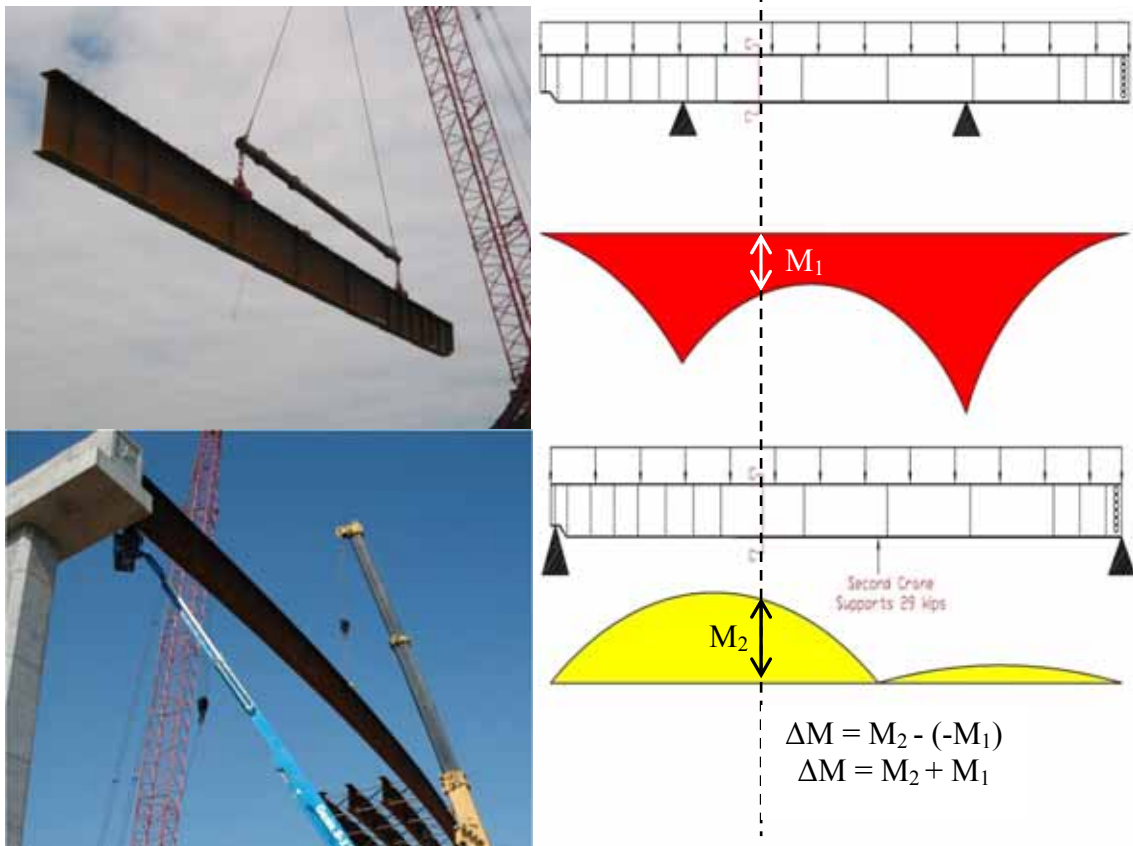
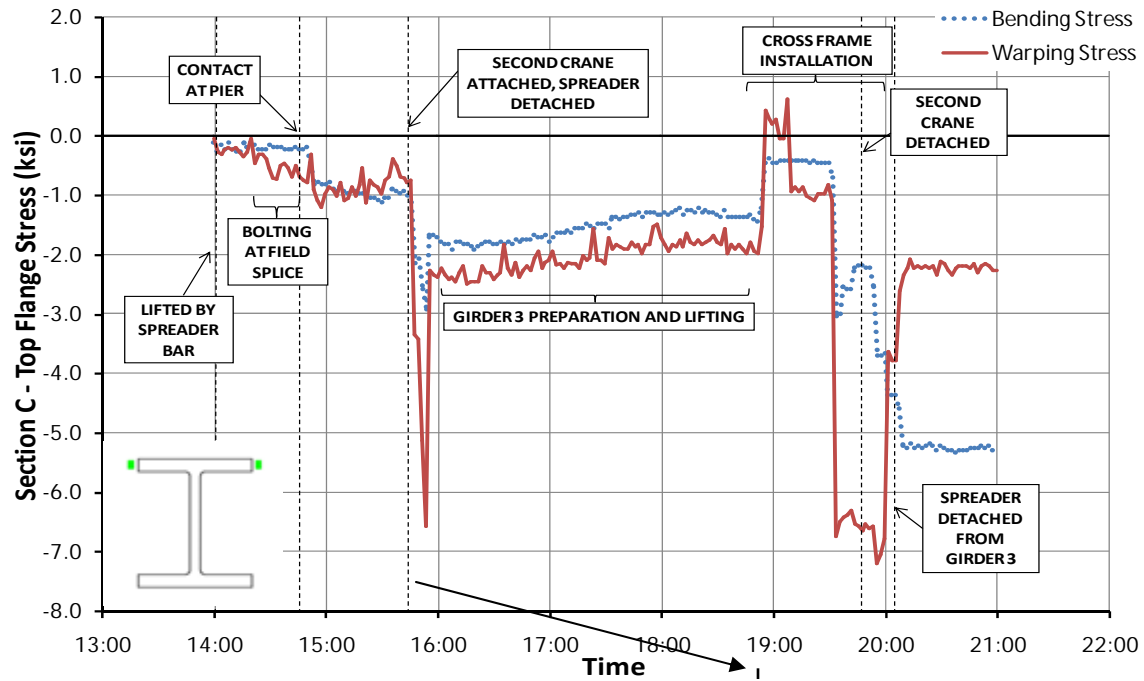


Figure 3.11: Girder 4 Stress Change at Section C Top Flange

Summary of Girder 4 Results

A summary of the stress change values observed from the data during the erection events is provided in Table 3.1. As mentioned earlier, negative bending stress values denote stress changes of a compressive nature while positive values indicate tensile stress changes. For warping stresses, negative values correlate with higher combined stresses being present on the exterior flange tip of the girder.

Table 3.1: Girder 4 Stress Change Summary

| Location | Stress | Flange | Girder 4 Stress Change During Specified Event (ksi) | | | |
|-----------|---------|--------|--|---|-------------------------------------|---|
| | | | Second Crane Attached, Spreader Detached (15:45) | Cross Frame Installation* (18:50-20:00) | Second Crane Detached (19:50) | Spreader Detached From Girder 3 (20:03) |
| Section A | Bending | Top | -0.5 (-0.75) | 0.5 | -0.5 | -0.25 |
| | | Bottom | 0 (+0.5) | 0.5 | +0.5 | +0.25 |
| | Warping | Top | -0.5 (-1.25) | 1.5 | +0.75 | +0.25 |
| | | Bottom | +0.75 (+0.75) | 0.75 | +0.5 | 0.0 |
| Section B | Bending | Top | -0.75 (-1.25) | 1 | -0.75 | -0.5 |
| | | Bottom | +0.5 (+1.0) | 0.75 | +0.75 | +0.5 |
| | Warping | Top | -0.75 (-2.0) | 2.5 | +1.0 | +0.5 |
| | | Bottom | +0.5 (+1.25) | 1.25 | +0.5 | -0.25 |
| Section C | Bending | Top | -0.75 (-2.0) | 2.5 | -2.5 | -0.5 |
| | | Bottom | +0.25 (+1.25) | 2 | +1.5 | +0.5 |
| | Warping | Top | -3.0 (-6.0) | 7 | 0.0 | +4.5 |
| | | Bottom | +0.25 (+1.25) | 2.25 | 0.0 | -0.5 |

*Stress changes during cross frame installation given as max changes independent of sign

() denotes initial stress change before values settle once operation is complete

The general trends in the stress change time histories were the same for each section of Girder 4. Around 15:45 when the second crane was attached and the spreader bar was removed, all flanges exhibited pronounced changes in stress (value in parentheses, see note) before settling to values indicative of a more modest change (indicated by the first value in the table). While the cross frames were being installed between Girder 4 and 3 from 18:50 to 20:00, significant stress changes took place, with warping stress changes being more pronounced at all sections. These values were reported as max changes, because multiple fluctuations occurred, presumably due to ratcheting of the cross frames into place and fit up.

Typically, notable changes in stress occurred near the end of cross frame installation when the second crane was detached at 19:50. Though difficult to fully dissociate from changes associated with cross frame installation and fit up, the removal of the second crane appeared to correlate with a change in bending and warping stresses. Similarly, the detachment of the spreader bar from Girder 3 at 20:03 caused a final change in stress before the stresses stabilized after all operations were complete.

Summary of Girder 3 Results

The bending and warping stress changes for each instrumented section during the two primary events are listed in Table 3.2. The same sign convention used with the Girder 4 erection applies to Girder 3. Like the trends with the Girder 4 erection, the trends observed in the stress change time histories of Girder 3 were the same for each section. However, one gage was lost during the erection. Data was only collected from the strain gage on the right flange tip, making

isolation of bending and warping stresses impossible. However, the stress history of this gage follows the same trends as the other gage sections.

Table 3.2: Girder 3 Stress Change Summary

| Location | Stress | Flange | Girder 3 Stress Change During Specified Event (ksi) | |
|-----------|---------|--------|---|--|
| | | | Cross Frame Installation (18:50-20:00) | Spreader Detached From Girder 3 (20:03) |
| Section A | Bending | Top | NA | NA |
| | | Bottom | +1.0 | +1.0 |
| | Warping | Top | NA | NA |
| | | Bottom | +1.0 | -0.5 |
| Section B | Bending | Top | -1.5 | -1.25 |
| | | Bottom | +1.5 | +1.25 |
| | Warping | Top | -0.5 | +1.5 |
| | | Bottom | +1.25 | -0.75 |
| Section C | Bending | Top | -2.75 | -2.75 |
| | | Bottom | +2.75 | +2.75 |
| | Warping | Top | -2.0 | -1.0 |
| | | Bottom | +2.25 | +1.0 |

A significant change in bending and warping stress was observed during the cross frame installation between 18:50 and 20:00 at each location. The removal of the spreader bar from Girder 3 led to a stress change in Girder 3, as it did for Girder 4.

3.6.3 SH 130/US 71 Girder Erection Conclusions

The results obtained from the lifting and erection of Girder 4 and Girder 3 can be used to make important conclusions about their general behavior. First, bending and warping stress changes during cross frame installation can be significant. Forcing of the girder into place for fit-up purposes or ratcheting of cross frames appears to induce high bending and warping stresses relative to other stages of erection, particularly in the fascia girder, Girder 4. A warping stress change of 7.0 ksi was observed at the top flange of Section C of Girder 4, which was the highest stress change recorded during the study of girder erection.

Second, locations closer to midspan (Section C in this case) appear to be the more critical sections with regard to bending and warping stresses at all stages of erection. All of the maximum stress values observed for both Girder 4 and Girder 3 occurred at Section C, providing evidence to support this conclusion.

Ultimately, though some results showed relatively large stress change values that led to the conclusions above, most of the observed stress changes were under 3 ksi in magnitude. Noting that reported results are changes in stress from a previous stress state, the magnitude of these changes would make it seem that the possibility of an unpredictably large stress state occurring during erection on this particular bridge is small. However, because these results are stress changes from an indeterminate state of stress, it is difficult to determine more precise stress magnitudes from this portion of the study. The researchers had no control over the support conditions of the girders. The dunnage that was used to support the girders consisted of heavy

timbers that were spread over regions of approximately 20' along the girder length in some instances (Figure 3.12). The actual contact points between the bottom flanges and the wood timbers were very difficult to assess.



Figure 3.12: Dunnage Used for Girder Support

For the purposes of obtaining more appropriate data for the validation of the finite element model during lifting stages, additional studies with known support conditions were necessary. The following section details the Hirschfeld lift tests and the results obtained from a more controlled testing environment where the boundary conditions were established.

3.7 Description and Results of the Hirschfeld Lift Tests

This section details the method by which girders 16C4 and 14C2 were tested at the Hirschfeld Steel Company yard. The test setup and procedure are detailed, as well as the results for the two girder tests. The Hirschfeld lift tests were undertaken to capture the stresses and rotations associated with lifting a curved girder segment with a crane. This process was repeated to ensure reliability in the data. Two different girder support locations were tested.

3.7.1 Girder Supports

So as to ensure known support conditions, two identical supports were fabricated. The supports provided a statically determinate structure with well-known support conditions. The supports are shown in Figure 3.13. The supports were fabricated at the Phil M. Ferguson Structural Engineering Laboratory. The base consisted of three 2" x 6" timbers bolted together using ½" diameter bolts spaced evenly along the length. The diagonal struts were composed of 4" x 4" timbers, with a single ¾" diameter bolt connecting them to the base. The single bolt allowed the struts to swivel relative to the base and make girder contact between the top flange and the web. The top ends of the struts were beveled to provide a good contact point with the web. The supports were oriented with the struts located on the side of the girder necessary to stabilize the curved girder from rotating while on the supports.



Figure 3.13: Wood Supports

3.7.2 Girder Lifting

The girders were lifted using a MI-JACK with a lift clamp spacing of approximately 40 feet. Figure 3.14 show the MI-JACK and lift clamp apparatus. The lifting clamps on the MI-JACK were representative of the lifting clamps frequently used on the lifting cranes used in the field.



Figure 3.14: MI-JACK Travelift Provided By Hirschfeld Steel and Lift Clamp Apparatus

3.7.3 Test Procedure

The fabricated wood supports were placed at two support locations, S1 and S2, along each girder. Support location S1 was located near the ends of the girder, while S2 was closer to

the lift points. The S1 support locations were intended to induce a moment distribution that would maximize the change in moment (and thus stress) during girder lifting. This would alleviate the complicating issue that had been present for the SH 130/US 71 girder erection, where the moment distributions had been very similar during the lift and while it was supported on the ground by timbers; a situation which yielded small changes in stress.

A timeline of this testing procedure is shown in Figure 3.15. Each girder's timeline begins when the data acquisition system was activated prior to lifting and ends when the girder was placed on timbers and the lift clamps were removed. For both girders, the dataloggers were programmed to scan every 12 seconds. For each location, the girder was placed on the supports for approximately 1-2 minutes, lifted up for approximately 1-2 minutes, replaced on the supports for 1-2 minutes, and lifted again while the supports were moved to the next location.

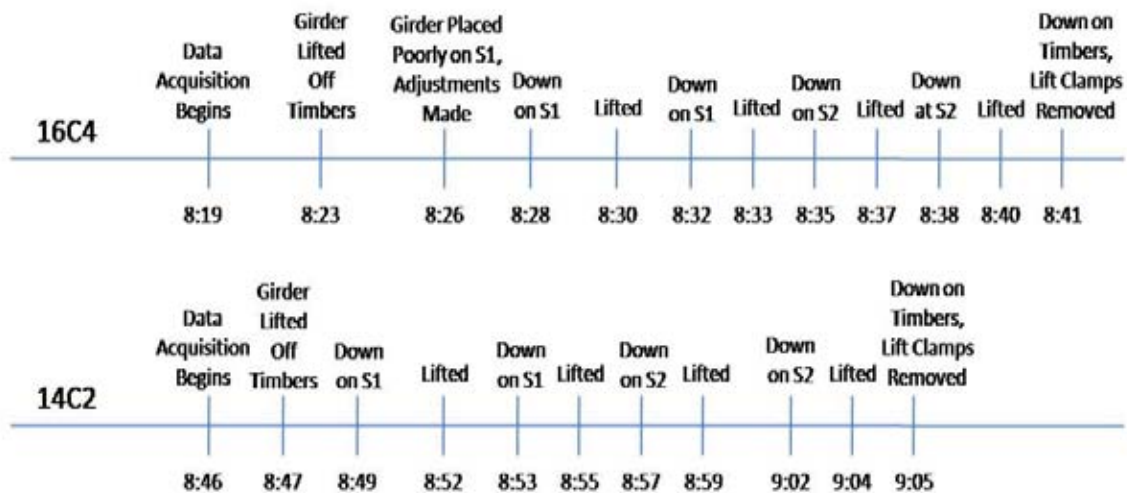


Figure 3.15: Test Timeline for 16C4 & 14C2

3.7.4 Hirschfeld 16C4 Lift Tests Results

The following section presents some of the stress and rotation time histories for 16C4's lift tests. The data is separated into the graphs (Figures 3.16–3.21) associated with the girder supported at S1 and the graphs associated with the girder supported at S2. Bending and warping stresses are shown on separate plots to display the behavior of the instrumented cross section (top and bottom flange). The data was zeroed using the results from the girder while it was supported by the lift clamps in the air. Therefore, the data represents the change in stress or rotation between the ground and the lifted positions. The full presentation of data is provided in Schuh (2008).

It is important to note the erratic nature of the stress and rotation data during the initial attempted placement of the girder at S1 (8:26). This data was neglected due to problems placing the girder on the supports properly. In addition, problems were encountered in placing the girder on timbers after being lifted from S2 at the conclusion of the test (8:40). Adjusting the girder to place it properly prevented the girder's rotations from settling at the typical values exhibited in the air, as shown in Figure 3.17.

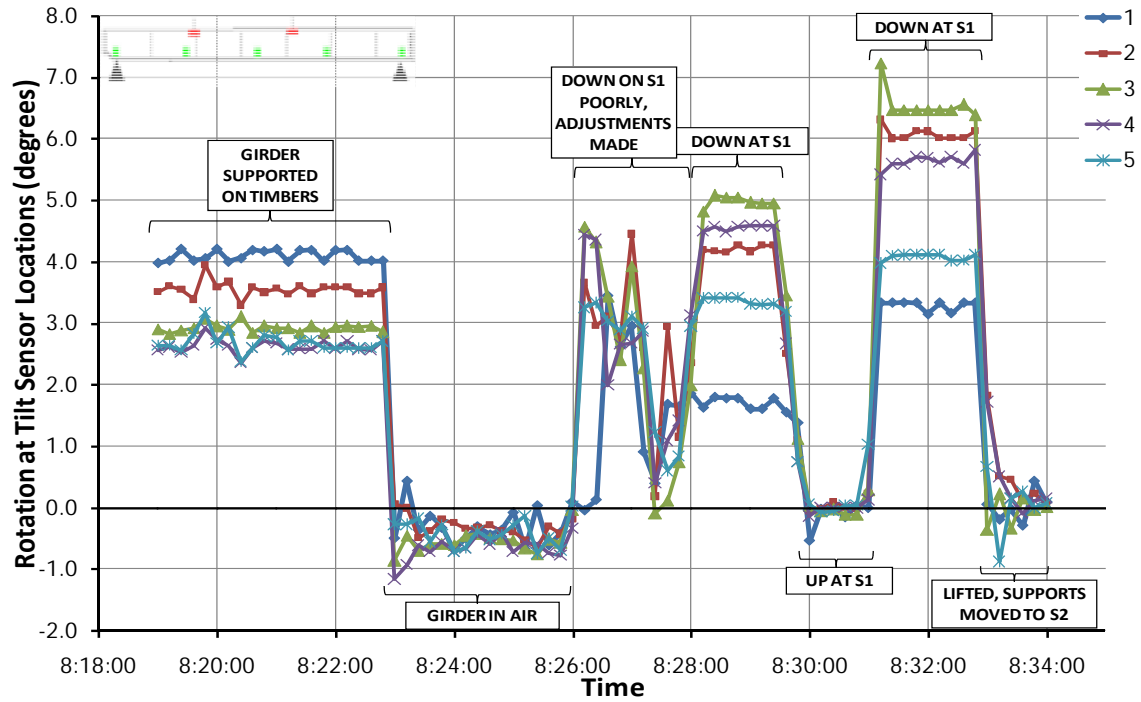


Figure 3.16: 16C4 Rotation Changes for Support Location S1

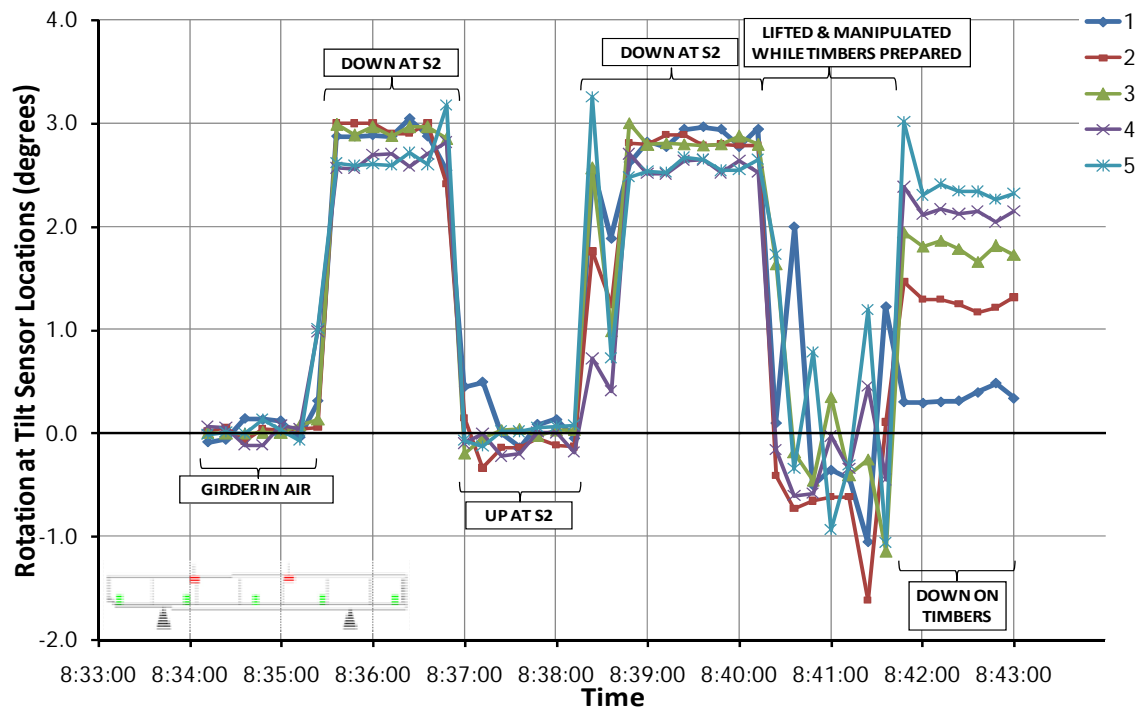


Figure 3.17: 16C4 Rotation Changes for Support Location S2

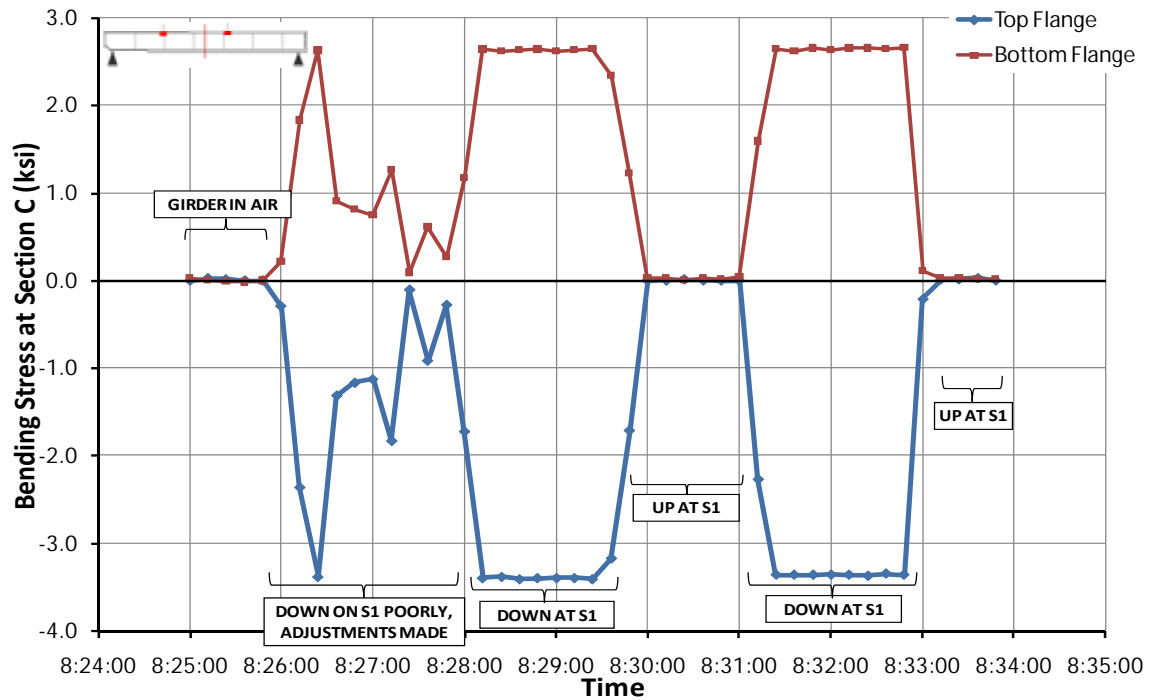


Figure 3.18: 16C4 Bending Stress Change at Section C for Support Location S1

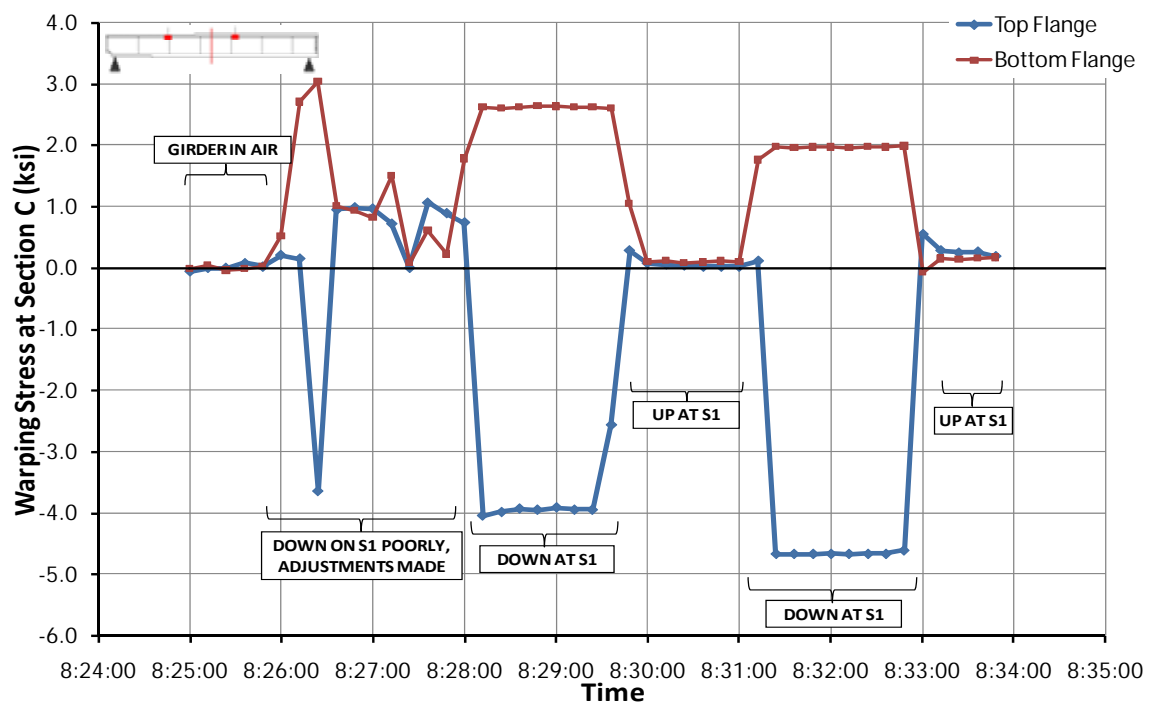


Figure 3.19: 16C4 Warping Stress Change at Section C for Support Location S1

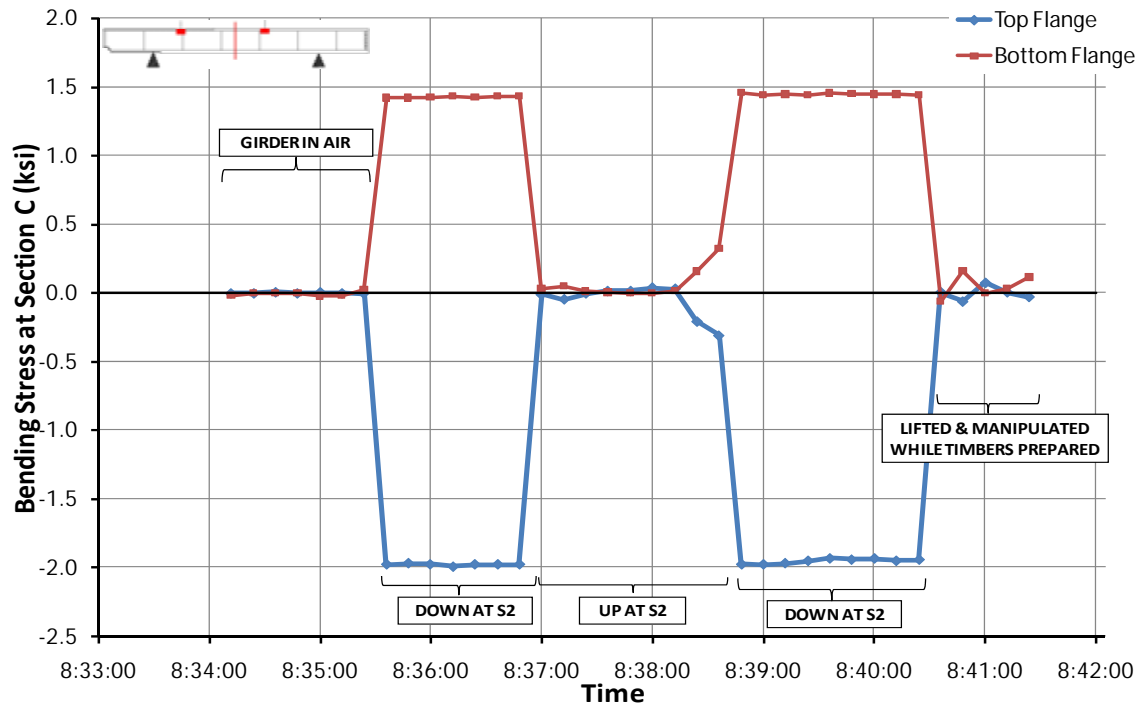


Figure 3.20: 16C4 Bending Stress Change at Section C for Support Location S2

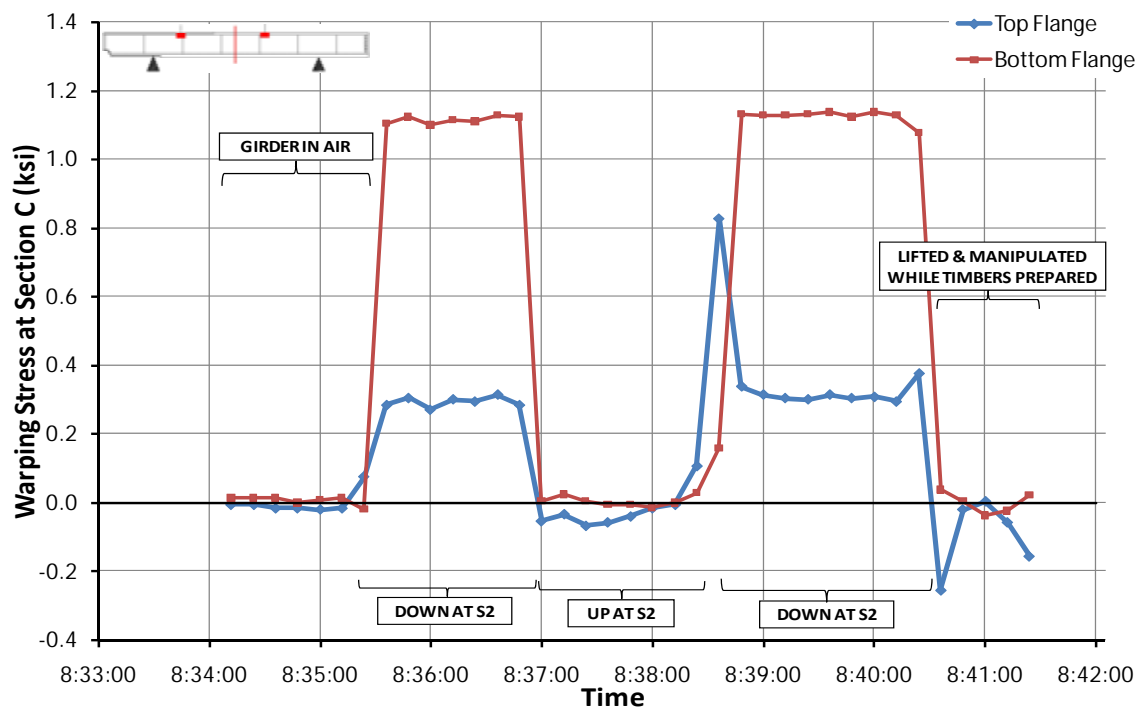


Figure 3.21: 16C4 Warping Stress Change at Section C for Support Location S2

Rotations

A summary of the rotation changes observed at each tilt sensor location when 16C4 was placed on S1 and S2 is provided in Table 3.3. The values are given in degrees and are all of the same sign because the girder exhibited a notable rigid body rotation due to the girder curvature in all cases presented in this study. This aspect of curved I-girder lifting is discussed more thoroughly in Chapter 4.

Table 3.3: 16C4 Rotation Change Summary

| Location | 16C4 Rotation Change During Event (Degrees) | |
|---------------|---|------------|
| | Down on S1 | Down on S2 |
| Tilt Sensor 1 | 3.3 | 2.9 |
| Tilt Sensor 2 | 6.0 | 2.9 |
| Tilt Sensor 3 | 6.5 | 2.9 |
| Tilt Sensor 4 | 5.7 | 2.7 |
| Tilt Sensor 5 | 3.1 | 2.7 |

For the changes in rotation at S1 shown in Figure 3.16, the values were taken as those observed during the second placement of the girder on S1. This was due to the significant differences during the first placement suggesting that even when the girder was repositioned at 8:26, the rotations remained affected. The second placement was therefore was a better representation of the behavior.

When the girder was placed on S2, the rotation changes at all tilt sensors were approximately the same. This indicates that the observed rotations can be attributed entirely to the rigid body rotation of the girder. When the girder was placed down on S1, a maximum rotational change of 6.5 degrees occurred at Tilt Sensor 3, at the midspan of the girder. This indicates that the girder experienced an additional cross sectional twist due to the torsional load applied by its own self weight. The understanding of both rigid body rotation and cross sectional twist is important to understanding the girder behavior and discussed more in Chapter 4.

Stresses

A summary of the stress change values at the instrumented sections of 16C4 when it was placed on S1 and S2 is provided in Table 3.4. The stress changes associated with placement on S1 are larger than those for S2. As mentioned earlier, this is caused by more dramatic differences between the moment diagram of S1 and the moment diagram of the girder while lifted. Conversely, the moment diagram of S2 is relatively similar to the lifted diagram, as evidenced by the lower changes in stress in Table 3.4.

Table 3.4: 16C4 Stress Change Summary

| Location | Stress | Flange | 16C4 Stress Change During Specified Event (ksi) | |
|-----------|---------|--------|---|------------|
| | | | Down on S1 | Down on S2 |
| Section A | Bending | Top | -1.9 | 0.0 |
| | | Bottom | +2.4 | 0.0 |
| | Warping | Top | -3.2 | +0.4 |
| | | Bottom | +4.0 | +0.4 |
| Section B | Bending | Top | -3.7 | -1.9 |
| | | Bottom | +2.3 | +1.2 |
| | Warping | Top | -3.1 | +0.2 |
| | | Bottom | +6.2 | +1.1 |
| Section C | Bending | Top | -3.4 | -2.0 |
| | | Bottom | +2.6 | +1.4 |
| | Warping | Top | -4.7 | +0.3 |
| | | Bottom | +2.6 | +1.1 |

*Table gives larger stress change if repeatability does not exist

Section A is the only cross section of 16C4 that is doubly symmetric; however, the magnitudes of the stress values at the top and bottom flange are slightly different by approximately 0.5 ksi. Section B and C are singly symmetric, with the centroid below midheight because the bottom flange is larger than the top flange. The measured results confirm this, with larger magnitude bending stresses present at the top flange. The largest bending stress change observed was at Section B's top flange when the girder was placed on S1, which induced a change of -3.7 ksi.

The relative sign of the warping stress change was different for S2. Unlike the opposite signs exhibited by the flanges for S1, the top and bottom flange warping stress change had the same sign when the girder was placed on S2. Both classic theory and the results from the SH 130/US 71 erection show that the warping stresses are of opposite direction (sign) in the top and bottom flange of a given cross section. However, a finite element analysis on the girders during lifting also showed this same behavior, attributing the change to weak axis bending. When the girder undergoes the observed rigid body rotation relative to its position on S2, a component of the self weight induces bending about the weak axis. The weak axis bending produces a stress gradient opposite to the warping stresses present in one of the flanges (the top in this case) and with those in the bottom flange. The result is the appearance of warping stresses acting in the same direction in both flanges, although it is actually the result of weak axis bending overshadowing the warping stresses in one flange and yielding a small positive value in the case of 16C4. The maximum warping stress change was +6.2 ksi at the bottom flange of Section B when the girder was placed on S1.

3.7.5 Hirschfeld 14C2 Lift Test Results

Results are presented in this section demonstrating stress and rotation time histories for 14C2's lift tests. The graphical results are similar to 16C4 and are therefore not presented here. A full documentation of the results can be found in Schuh (2008).

Rotations

A summary of the rotation changes observed at each tilt sensor location when 14C2 was placed on S1 and S2 is provided in Table 3.5. The sign convention follows the same convention as was used for 16C4.

Table 3.5: 14C2 Rotation Change Summary

| Location | 14C2 Rotation Change During Event (Degrees) | |
|---------------|---|------------|
| | Down on S1 | Down on S2 |
| Tilt Sensor 1 | 3.1 | 3.7 |
| Tilt Sensor 2 | 4.6 | 2.6 |
| Tilt Sensor 3 | 5.4 | 3.1 |
| Tilt Sensor 4 | 4.0 | 2.5 |
| Tilt Sensor 5 | 2.0 | 2.6 |

For the rotational changes at S2 shown in Schuh (2008), the values were taken as those observed during the first placement of the girder on S2. During the second placement on S2, the girder made slight contact with the ground at the dapped end due to the camber, which may have caused less rotation at Tilt Sensor 1 than would have normally occurred. This contact was not observed in the stress change results and can be considered to have negligible impact on the tests; however, the first placement was tabulated to account for this in the presentation of the rotational results.

The maximum twist that 14C2 underwent when placed on S1 was 5.4 degrees at midspan (Tilt Sensor 3). Similar to the results presented in the other test, the rotational difference for points along 14C2 varied from the ends of the girder where the supports prevented twist to the center of the girder where the maximum cross sectional twist occurs. For S2, the maximum rotation was 3.7 degrees occurring at the dapped end (Tilt Sensor 1).

Stresses

The values of the measured stress changes at the instrumented sections of 14C2 when it was placed on S1 and S2 are provided in Table 3.6. The stress changes associated with placement on S1 are larger than those for S2 for the same reasons as mentioned earlier for 16C4.

All of the cross sections of 14C2 are doubly symmetric. The magnitudes of bending stress changes during placement on both S1 and S2 reflect this, with absolute values being the same at the top and bottom flange for all sections. In addition, Sections A and C were located at the approximate quarter points, which is close to the location of the S2 supports. Because the lift locations were very near the gage and support locations, no bending stress change was observed at Sections A and C. However, small warping stresses were still observed. The maximum bending stress change for 14C2 was recorded at Section B's top and bottom flange when placed on S1, with values of -3.3 ksi and +3.3 ksi, respectively.

Table 3.6: 14C2 Stress Change Summary

| Location | Stress | Flange | 14C2 Stress Change During Specified Event (ksi) | |
|-----------|---------|--------|---|------------|
| | | | Down on S1 | Down on S2 |
| Section A | Bending | Top | -2.5 | 0.0 |
| | | Bottom | +2.5 | 0.0 |
| | Warping | Top | -2.5 | +1.2 |
| | | Bottom | +2.6 | +1.5 |
| Section B | Bending | Top | -3.3 | -1.1 |
| | | Bottom | +3.3 | +1.1 |
| | Warping | Top | -5.1 | +1.1 |
| | | Bottom | +4.7 | +1.3 |
| Section C | Bending | Top | -2.5 | 0.0 |
| | | Bottom | +2.5 | 0.0 |
| | Warping | Top | -2.5 | +0.6 |
| | | Bottom | +3.3 | +0.7 |

*Table gives larger stress change if repeatability does not exist

The same weak axis bending phenomenon occurred for the S2 stress changes in 14C2 as was noted for 16C4. As shown in the table, all warping stresses for S2 are positive, which is attributed to the weak axis bending introduced by the rotating of the girder. The maximum warping stress change was -5.1 ksi at the top flange of Section B when the girder was placed on S1.

3.7.6 Hirschfeld Lift Tests Conclusions

The Hirschfeld lift tests provided rotation and stress data for calibrating the finite element model. By using a simple test setup with two statically determinate supports, the data obtained from the tests can be appropriately compared with analytical models for validation purposes. In addition to the data, conclusions can be taken from the lift tests.

Rigid body rotation is an important issue when lifting curved I-girders. Depending on how the girder is lifted, the rigid body rotations can create significant serviceability problems. In addition, the torsion applied by the self weight produces cross sectional twist that must be accounted for in the deformations of curved girders during lifting. Difficulty in placement and fit up could follow during girder erection if both rigid body rotation and cross sectional twist are not accounted for in the construction analysis. Also, the situation observed with the warping stress changes at S2 (same signs in both flanges) can present itself, which is a difficult stress state to predict for designers and erectors.

As in the earlier study, the measured warping stresses during lifting of the curved I-girders were generally equal if not greater than measured bending stresses. The data from these tests provided valuable information for validating the finite element that was used to perform parametric studies on the stability behavior of curved I-girders during early stages of erection and construction.

3.8 Description and Results from SH 130/US 71 Concrete Placement

3.8.1 Introduction

For many horizontally curved girders, the critical loading stage often occurs during the construction stage, prior to composite action with the concrete deck. The steel section must support the entire construction load during this phase. This section discusses the measurements and timeline during the concrete placement of Bridge 88. Most of the horizontally curved steel girder bridges that are constructed in Texas follow a traditional concrete pouring sequence that involves placing the positive dead load moment regions of the continuous unit first, followed by the negative dead load moment regions (area over the supports). Contrary to this common practice, the instrumented bridge was poured continuously from beginning to end. Concrete placement began at the North end of the bridge on Span 16 and proceeded along the length of the bridge to Spans 15 and 14. Recalling from the description earlier in this chapter, the instrumentation was placed in Span 14 which was the last region of concrete placement. The geometry and gage locations were also discussed previously. Following data collection, the data was reduced and processed. In addition to strain gages, the bridge was instrumented with 16 tilt sensors to measure twist of the girders. Data from the tilt sensors during the concrete placement was reported by Fasl (2008).

3.8.2 SH 130/US 71 Direct Connector Concrete Placement

In addition to being a critical component in the strength of a composite steel girder, the quality of the concrete bridge deck is extremely important for the bridge to meet its functional requirements. The concrete deck plays an important role in the bridge satisfaction of the traveling public as they cross the bridge. Therefore, extra care is taken to ensure that the ride quality is smooth and that the final concrete deck satisfies durability requirements to provide a quality surface with minimal maintenance issues. Because of the high volume of concrete and significant role that the bridge deck plays in the overall structure, the construction of the deck is an “event” that involves meticulous planning, coordination, and testing so that this stage of construction runs efficiently. Just scheduling the numerous concrete trucks to arrive at the site on time takes extreme planning so as to avoid problems in the delivery of hundreds of cubic yards of concrete to the bridge site. There are a number of critical aspects to consider in the planning of the concrete cast to ensure quality control of the finished deck. One key aspect is that the ready mix trucks will not be delayed by traffic or that the temperature during placement is not too high or too low so as to affect the hydration of the cement in the concrete. Because of the effects of traffic and hot weather, many deck casts are done during the nighttime hours when the temperature is cooler and traffic is much more predictable. The casting of the deck on the test bridge began at night and was completed in the morning. Once the concrete truck arrives on site, the concrete is poured into a truck that pumps the concrete up to the bridge deck. Figure 3.22 shows the pump that was used to place the concrete on the instrumented bridge.



Figure 3.22: Bridge 88 Unit 3 Concrete Deck Placement

As the concrete is pumped onto the deck and in between the deck reinforcing, a screed, as shown in Figure 3.23 and Figure 3.24, distributes the concrete transversely on the bridge and also vibrates and levels the freshly poured concrete. The picture in Figure 3.23 was taken at the start of the concrete pour at 1:30am. Transverse screeds are used because they permit the rapid placement of wide decks while reducing the amount of hand finishing. Supporting a rotating drum, auger, and pan drag, transverse screeds have a carriage system that is supported by screed rails on each side of the deck. The screed travels the length of the placement as the drums, augers, and pan drag move back and forth on the carriage. Additional vibrating of the concrete by construction workers, before the screed passes over, is also required. After the deck is finished and textured, a membrane curing compound is typically sprayed on the surface of the deck. The membrane curing compound forms a thin film on the surface of the deck to prevent evaporation of moisture from the surface of the concrete. Preventing evaporation of the moisture from the surface of the concrete is critical to maintaining proper hydration of the cement particles in the concrete, which is the mechanism by which the concrete gains strength.



Figure 3.23: Concrete Deck Placement at beginning of pour



Figure 3.24: Transverse Screed used in deck construction

The third steel unit of this bridge, which contains the instrumented girders and cross frames in Span 14, was scheduled for pouring the concrete deck on April 16, 2008. Deck placement on Unit 3 began at 1:30 a.m. with Span 16 and finished Span 14 at 11:20 a.m. Public safety necessitated intermittent lane closures of the roadways below the bridge as concrete directly above the various lanes was placed. Because the instrumented sections were above the roadway, access to the instrumented sections was limited until the lanes were closed below those sections of the bridge. The timeline in Figure 3.25 gives a history of the deck placement and highlights the important milestones.

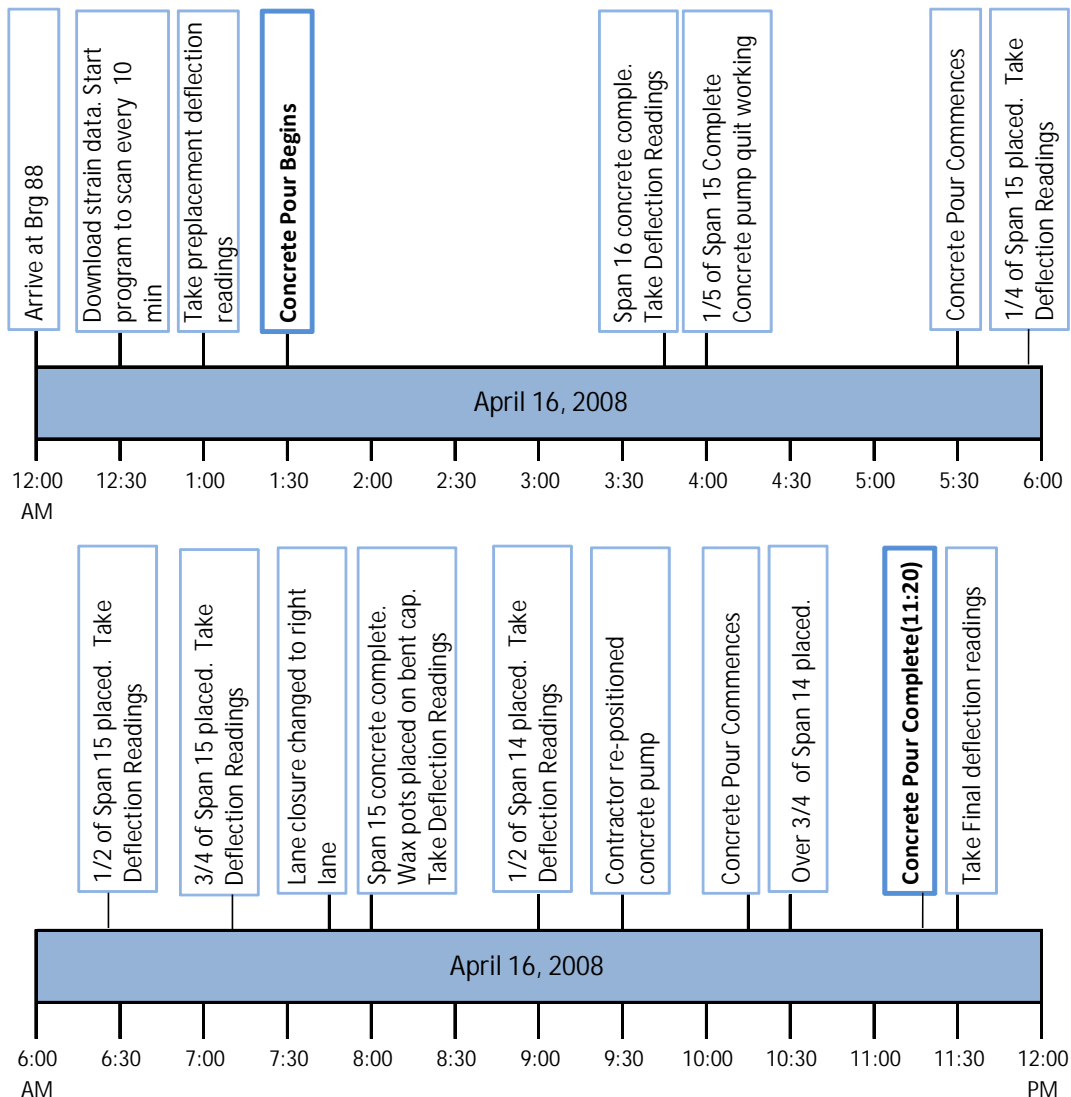


Figure 3.25: Bridge 88 Unit 3 Concrete Deck Placement Timeline

Strain and rotation readings were recorded every 10 minutes during placement of the concrete deck. Two separate data loggers were used on the bridge to record respective data from the strain gages and the tilt sensors. The dataloggers, which were located on the flanges of the girders, were each connected to a booster cable to increase the signal so that strain gage data

could be downloaded through an extended connection cable to the lap top positioned on the top of the bridge. The booster cable also saved time because it decreased the need for using a man-lift for downloading the data. A similar cable was connected to the data logger for the tilt sensors; however, the cable was inadvertently severed by construction activity on the bridge. Therefore only pre-pour and post-pour rotation data was collected. At 1:00 a.m., initial vertical deflection readings were taken to provide baseline readings before the bridge deck was placed. Completion of the concrete placement on the first span (Span 16) occurred at 3:45 a.m. and deflection readings were taken at this time. After 1/5th of the second span (Span 15) was placed, the remote control on the concrete pump arm began to malfunction, leading to a lengthy delay. Work did not recommence until 5:30 a.m. after a second pump truck was setup. During the concrete pour of Span 15, several deflection readings were taken as shown on the timeline in Figure 3.25. Before the third span (Span 14) was poured, the contractor closed the right lane of the underlying roadway, which is a requirement to maintain a safety below the concrete placement. The lane closure was helpful to the research crew because deflection readings could be taken easily and safely.

3.8.3 Summary of Results for Girders 3 and 4

Figures 3.26–3.29 present a representative sample of the strain gage data from the concrete deck placement. Numerical tables for specific placement events are also presented (Tables 3.7–3.10). The graphs presented in this section display the bending stress measured along the depths of girders 3 and 4. The warping stresses along the depth of the girders 3 and 4 are also provided. The complete data set including graphs for all the instrumented locations and a full description of the results is provided by Farris (2008).

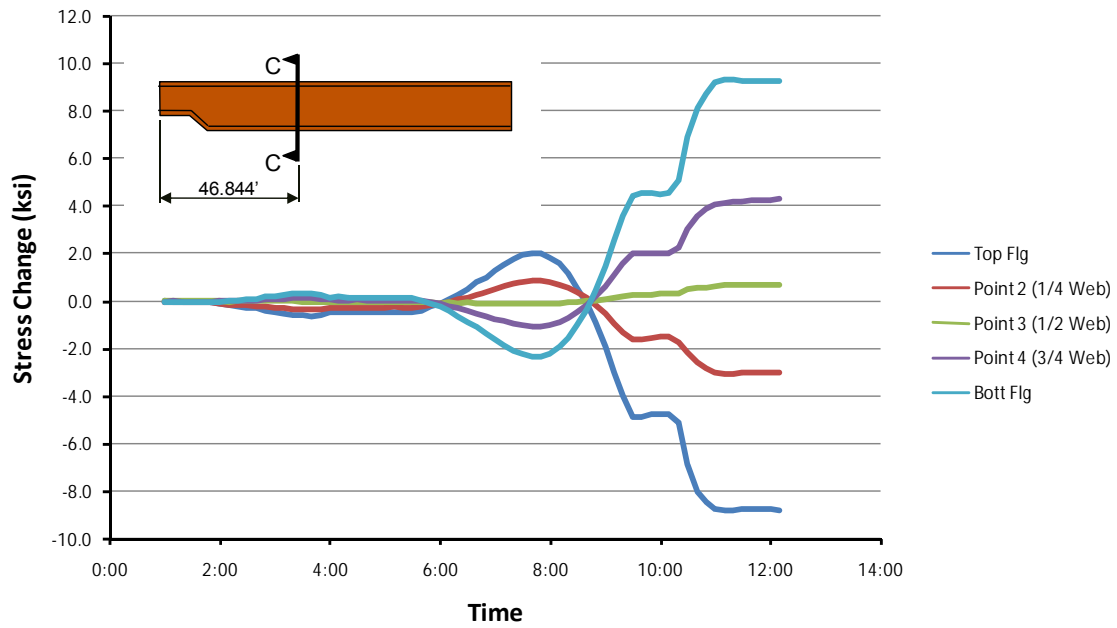


Figure 3.26: Girder 3 Bending Stress Change at Section C

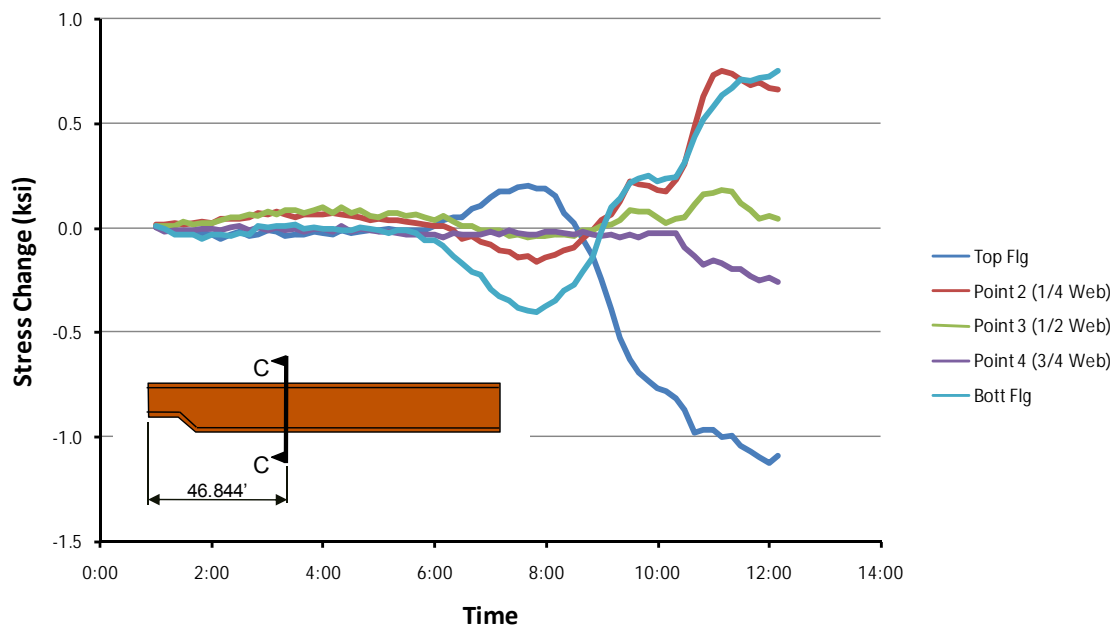


Figure 3.27: Girder 3 Warping Stress Change at Section C

Table 3.7: Girder 3 Flange Stress Change Summary

| | | | Girder 3 Stress Change During Concrete Pour (ksi) | | | |
|-----------|---------|--------|--|---|--------------------------------------|----------------------|
| Location | Stress | Flange | 1/2 Span 15 Poured (6:25 a.m.) | Span 15 Pour Complete (8:00 a.m.) | 1/2 Span 14 Poured (9:00 a.m.) | Span 14 Complete* |
| Section A | Bending | Top | 0.034 | 0.333 | -0.56 | -4.276 |
| | | Bottom | -0.285 | -0.626 | 0.193 | 2.823 |
| | Warping | Top | -0.03 | -0.057 | -0.1666 | -0.549 |
| | | Bottom | -0.023 | -0.047 | -0.024 | -0.038 |
| Section B | Bending | Top | N/A | N/A | N/A | N/A |
| | | Bottom | -0.406 | -0.888 | 0.365 | 3.973 |
| | Warping | Top | N/A | N/A | N/A | N/A |
| | | Bottom | -0.014 | -0.037 | -0.028 | -0.159 |
| Section C | Bending | Top | 0.526 | 1.887 | -1.897 | -9.898 |
| | | Bottom | -0.825 | -2.153 | 1.532 | 9.404 |
| | Warping | Top | 0.049 | 0.186 | -0.242 | -1.154 |
| | | Bottom | -0.171 | -0.377 | -0.020 | 0.934 |

* Represents total change in stress for construction activity.

Table 3.8: Girder 3 Web Stress Change Summary

| | | | Girder 3 Stress Change During Concrete Pour (ksi) | | | |
|-----------|------------|-----------|--|---|--------------------------------------|----------------------|
| Location | Stress | Web | 1/2 Span 15 Poured (6:25 a.m.) | Span 15 Pour Complete (8:00 a.m.) | 1/2 Span 14 Poured (9:00 a.m.) | Span 14 Complete* |
| Section C | Bending | Top 1/4 | 0.155 | 0.799 | -0.531 | -3.138 |
| | PL Bending | Top 1/4 | -0.049 | -0.143 | 0.041 | 0.552 |
| | Bending | Mid | -0.092 | -0.124 | 0.062 | 0.626 |
| | PL Bending | Mid | 0.008 | -0.034 | 0.013 | -0.150 |
| | Bending | 3/4 depth | -0.407 | -1.010 | 0.640 | 4.756 |
| | PL Bending | 3/4 depth | -0.028 | -0.014 | -0.037 | -0.470 |

* Represents total change in stress for construction activity.

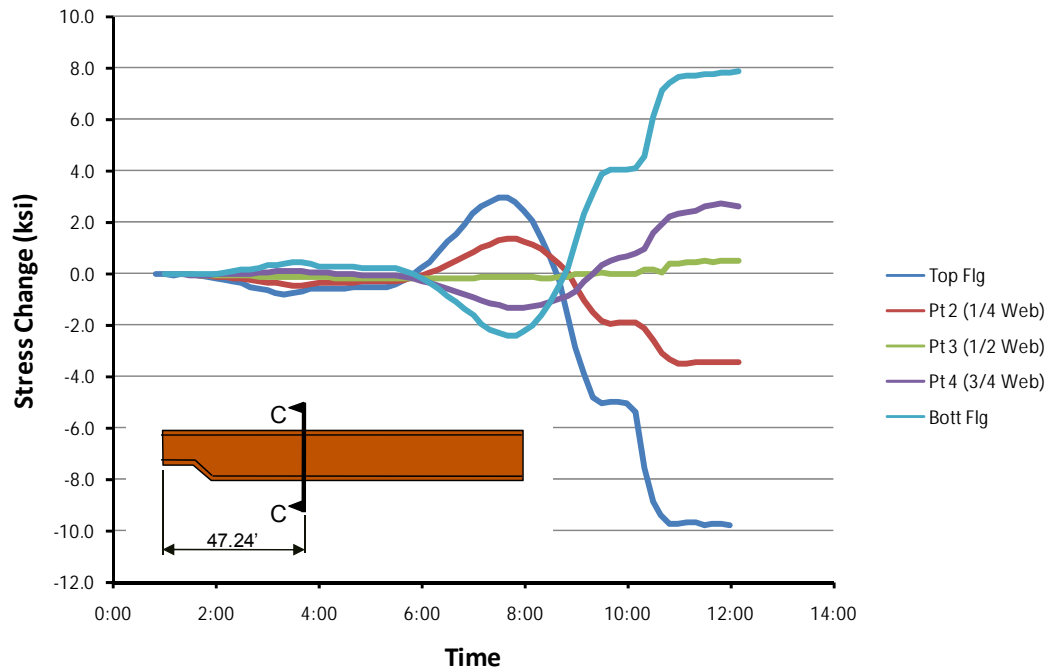


Figure 3.28: Girder 4 Bending Stress Change at Section C

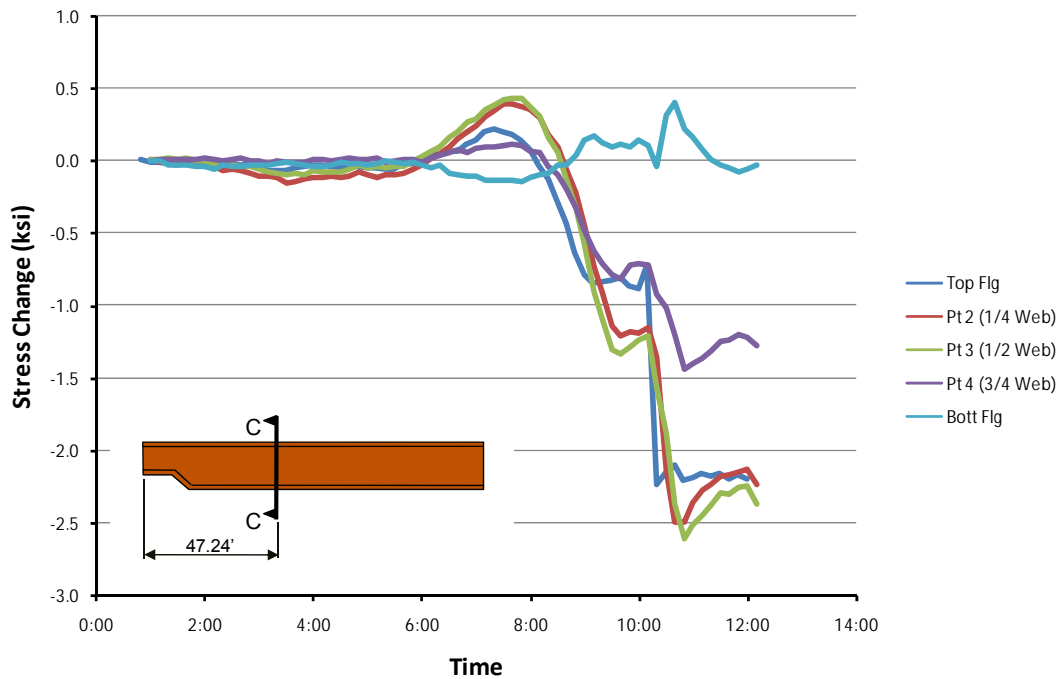


Figure 3.29: Girder 4 Warping Stress Change at Section C

Table 3.9: Girder 4 Flange Stress Change Summary

| | | | Girder 4 Stress Change During Concrete Pour (ksi) | | | |
|-----------|---------|--------|--|---|--------------------------------------|----------------------|
| Location | Stress | Flange | 1/2 Span 15 Poured (6:25 a.m.) | Span 15 Pour Complete (8:00 a.m.) | 1/2 Span 14 Poured (9:00 a.m.) | Span 14 Complete* |
| Section A | Bending | Top | 0.156 | 0.586 | -0.228 | -3.394 |
| | | Bottom | -0.416 | -0.855 | 0.734 | 2.926 |
| | Warping | Top | -0.007 | -0.100 | -0.271 | -0.910 |
| | | Bottom | 0.161 | 0.142 | -0.073 | -0.068 |
| Section B | Bending | Top | 0.289 | 0.9504 | -0.4722 | -4.680 |
| | | Bottom | -0.410 | -1.093 | 0.716 | 4.754 |
| | Warping | Top | 0.049 | -0.018 | -0.208 | 0.036 |
| | | Bottom | 0.056 | 0.075 | 0.275 | -0.398 |
| Section C | Bending | Top | 0.853 | 2.790 | -1.418 | -11.083 |
| | | Bottom | -0.891 | -2.259 | 1.202 | 8.236 |
| | Warping | Top | 0.043 | 0.139 | -0.631 | -2.268 |
| | | Bottom | -0.083 | -0.106 | 0.142 | -0.267 |

* Represents total change in stress for construction activity.

Table 3.10: Girder 4 Web Stress Change Summary

| | | | Girder 3 Stress Change During Concrete Pour (ksi) | | | |
|-----------|------------|-----------|--|---|--------------------------------------|----------------------|
| Location | Stress | Web | 1/2 Span 15 Poured (6:25 a.m.) | Span 15 Pour Complete (8:00 a.m.) | 1/2 Span 14 Poured (9:00 a.m.) | Span 14 Complete* |
| Section C | Bending | Top 1/4 | 0.334 | 1.259 | -0.477 | -3.206 |
| | PL Bending | Top 1/4 | 0.095 | 0.355 | -0.434 | -1.813 |
| | Bending | Mid | -0.147 | -0.091 | -0.003 | 0.585 |
| | PL Bending | Mid | 0.170 | 0.375 | -0.574 | -1.276 |
| | Bending | 3/4 depth | -0.579 | -1.301 | -0.707 | 3.921 |
| | PL Bending | 3/4 depth | 0.067 | 0.074 | -0.473 | -0.313 |

* Represents total change in stress for construction activity.

Tables 3.7 and 3.8 summarize the stress change at certain times during the concrete placement of Unit 3 for Girder 3. Similarly, Tables 3.9 and 3.10 summarize the stress change for Girder 4. Negative bending stress denotes a compressive stress change, while a positive bending stress denotes a tensile stress change. For warping stress, negative values are associated with higher combined stresses being present on the exterior flange tip of the girder.

Overall, the recorded warping stress change during the concrete placement for Girder 3 was low. The maximum value of the total warping stress change occurred at Section C, on the

top flange, with a stress change of -1.2 ksi. The maximum total warping stress change in the web occurred in the top quarter depth of the web, at 0.55 ksi. The maximum total bending stress change in the flange area occurred at Section C in the top flange with a value of -9.9 ksi. Unlike the warping stress change in the web, the maximum bending stress change in the web occurred on the bottom quarter of the web, with a value of 4.8 ksi. As stated previously, the maximum values are given as the total stress change due to the construction activity.

Most of the stress changes for Girder 4 had slightly higher values than Girder 3. The maximum value of warping stress change occurred at Section C, on the top flange, with a magnitude of -2.3 ksi. This is roughly twice the amount of change in maximum warping stress as Girder 3, in the same location. The maximum total change in warping stress in Girder 4, in the web at Section C, was -1.8 ksi at the top quarter depth. The maximum change in total bending stress occurred in the top flange at Section C, with a value of -11.1 ksi. This is the maximum change in bending stress overall. The instrumented web recorded a maximum change in bending stress at the bottom quarter depth of the web (Section C), with a value of 3.9 ksi.

3.8.4 Cross Frames X1 and X2

To increase the torsional stiffness of the bridge and also to brace the girders before the concrete deck cures, cross frames are installed between each adjacent girders. As previously described, the cross frames on the SH 130/US 71 Direct Connector are comprised of four angles; two diagonals and two struts. The angles that make up the cross frames transmit axial forces from the vertical loads on the girders. This section discusses the cross frame results as well as the data reduction technique used to transform the strain data from the gages to axial forces. The axial forces were used to validate finite element models of curved bridge systems. The method used for determining the axial forces in the angles for this specific bridge was summarized previously by others (Fan 2000). The methods and research for determining the axial forces using the regression method can be found in sited reference or given by Farris (2008).

Summary of Cross Frame Results

A summary of the results from the strain gages attached to the instrumented cross frames during the concrete deck placement is provided in the following section. A full presentation of the data and description of the results is given by Farris (2008).

Figure 3.30 provides a graph of the axial force time history for Cross Frame X2 members during the concrete deck placement. Significant events in the concrete deck placement are shown in the graph. A summary of the axial forces in Cross Frame X2 is provided in Table 3.11. The negative values represent compressive axial forces, whereas the positive values represent tensile axial forces. The results show the gradual increase in axial force of the three of the members (X2-1, X2-3, X2-4) up until half of the concrete is poured on Span 14. The time span between the events of half of Span 14 concrete being poured to the end of the concrete pour, the axial forces increase dramatically. This is because after half of Span 14 is poured, the concrete placement approached Cross Frame X2 and was then directly over the position. The results also show that one of the diagonals (X2-3) transmitted close to 6 ½ times the amount of axial force than the other diagonal (X2-2). Another point worth noting, is that members X2-1 and X2-3 are loaded in compression (negative axial forces) before Span 14 was poured, but after Span 14 was poured were in tension. This is true for members X2-2 and X2-4, but in the opposite manner (tensile to compressive). The maximum axial force was in member X2-3, which is a diagonal member, with a magnitude of 13.78 kips.

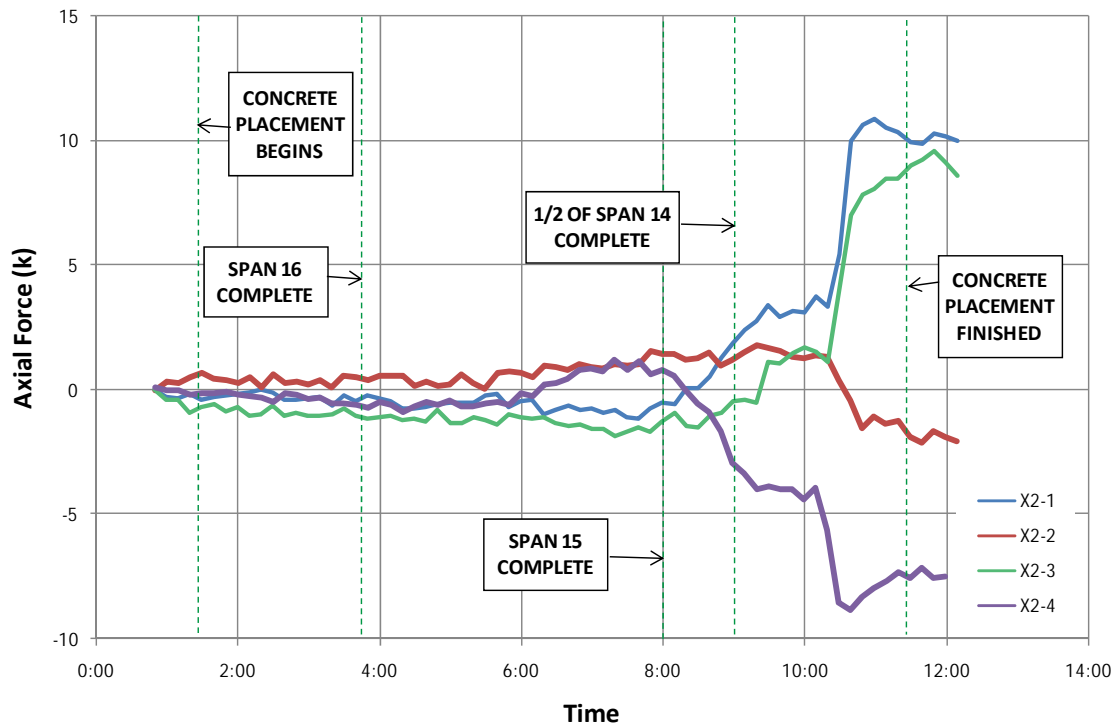


Figure 3.30: Cross Frame X2 Axial Force

Table 3.11: Cross Frame X2 Axial Force Summary

| | | X2 Axial Force During Concrete Pour (kips) | | | |
|--------|----------------------|--|---|------------------------------------|-----------------------|
| Member | Location | ½ Span 15 Poured (6:25 a.m.) | Span 15 Pour Complete (8:00 a.m.) | ½ Span 14 Poured (9:00 a.m.) | Span 14 Complete * |
| X2-1 | Top horizontal | -0.840 | -0.507 | 1.862 | 11.98 |
| X2-2 | Diagonal | 0.954 | 1.463 | 1.211 | -4.10 |
| X2-3 | Diagonal | -1.324 | -1.265 | -0.432 | 13.78 |
| X2-4 | Bottom horizontal | 0.239 | 0.621 | -1.635 | -3.60 |

* Represents total change in axial force for construction activity.

3.8.5 Vertical Deflection Results

Results presented in this section focus on the vertical deflection results from the SH 130/US 71 Direct Connector Unit 3 concrete pour. Deflections were measured using a laser distance meter that had an accuracy of 1/16". More information regarding the laser distance meter and methodology is given by Farris (2008). Baseline readings were taken prior to the

placement of the concrete. At pivotal time periods during the concrete pour, deflection readings were recorded. For repeatability, at each location during each recorded event, three readings were taken, and the final reading reported is the average of the three initial readings. The results from this field experimentation were used in the validation of finite element models of curved girder systems.

Mid Span Deflection Readings

Vertical deflection readings were taken at the mid span of Span 14 on all four girders. The mid span was chosen as an isolated location because relatively large deflection and torsional deformations of the four girder system were expected in this region. Figure 3.31 represents the vertical deflection at the mid span for each girder during the concrete pour of Unit 3. A negative vertical deflection value represents a downward deflection while a positive vertical deflection value represents an upward deflection. Significant events were recorded during the concrete placement to correlate the deflection readings to certain times during the pour. At 3:45 a.m. the concrete for Span 16 was finished and all of mid span readings for the girders resulted in negative deflection readings. At this stage during the concrete pour, Girder 3 deflected the most at -0.50 inches. After a quarter of the second span (Span 15) was placed, a positive deflection of 0.40 inches was measured for Girder 1. According to Figure 3.31, this does not follow the trend of the other three girders. This is also distinctive because Girder 1 is positioned on the inside of the horizontal curve, which means that it would typically deflect the least. Similar to Girder 1, the vertical deflections of Girders 2, 3, and 4 increase in the positive direction, but not by the same magnitude. At the time when half of the second span (Span 15) was poured, the girders seemed to converge to a positive deflection ranging from 0.21 to 0.52 inches. As one could predict, Girder 4 deflected the most at this stage of construction. After three-quarters of Span 15 was placed, the girders began deflecting upward (positive direction), and continued to deflect upward at mid span until the concrete pour on Span 15 was complete.

As concrete was poured on the last span (Span 14), which is the span containing the instrumentation, the vertical deflection readings began to reflect the weight of the wet concrete on the instrumented span and deflected downward. The change from positive to negative vertical deflection from the time between completing Span 15 and pouring half of Span 14, averaged around 2.25" for the four girders. The last readings, which were taken at the end of the concrete pour, indicated that Girder 4 deflected the most (-2.96") and Girder 1 deflected the least (-2.41"). Girders 2 and 3 had similar deflection values of -2.69" and -2.67", respectively. One aspect worth noting about the graph shown in Figure 3.31 is that the girders may not have exactly the same deflection readings at the different stages of the concrete pour, but they all follow a similar trend. This reinforces the idea that the girders deflected simultaneously and acted collectively in torsion as a unit, which was expected because they are connected by cross frames.

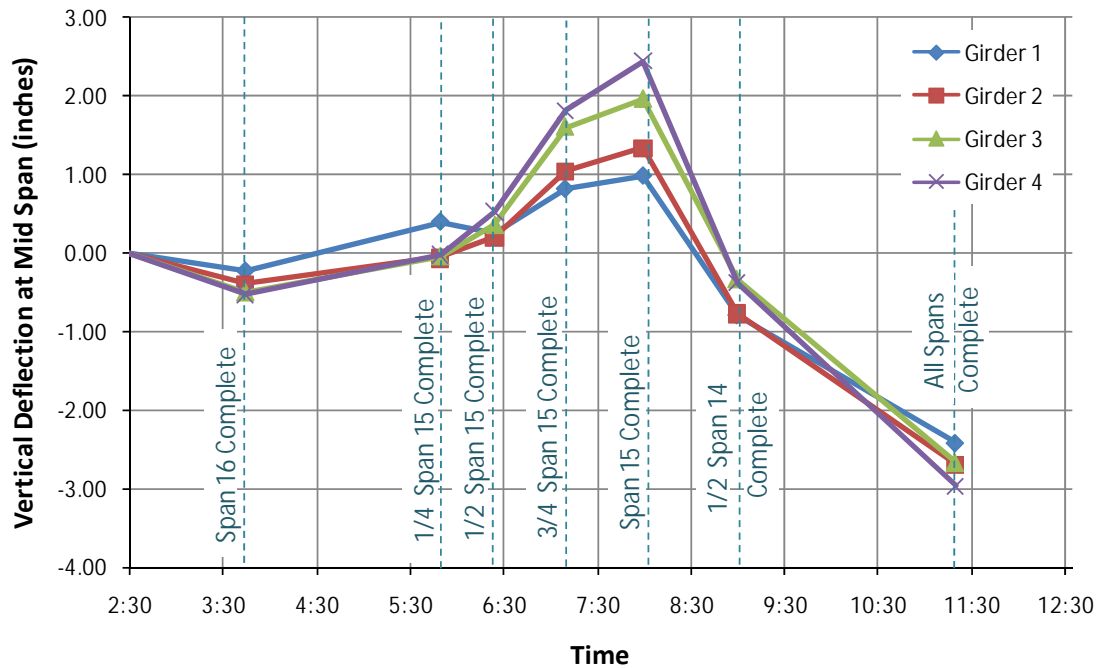


Figure 3.31: Vertical Deflection Readings at Mid Span 14

Girders 3 and 4 Vertical Deflection Results

This section provides a comparison of the vertical deflection results of Girders 3 and 4 of Span 14 of the SH 130/ US 71 Direct Connector. As outlined earlier, deflection readings were taken at five locations: near the pier (Bent 14), at $\frac{1}{8}L$, $\frac{1}{4}L$, $\frac{3}{8}L$, and $\frac{1}{2}L$. Figure 3.32 describes the specific locations along the girders that were monitored. The term, “L,” refers to the total span length of the girder at Span 14. A negative vertical deflection value represents a downward deflection and a positive vertical deflection value represents an upward deflection.

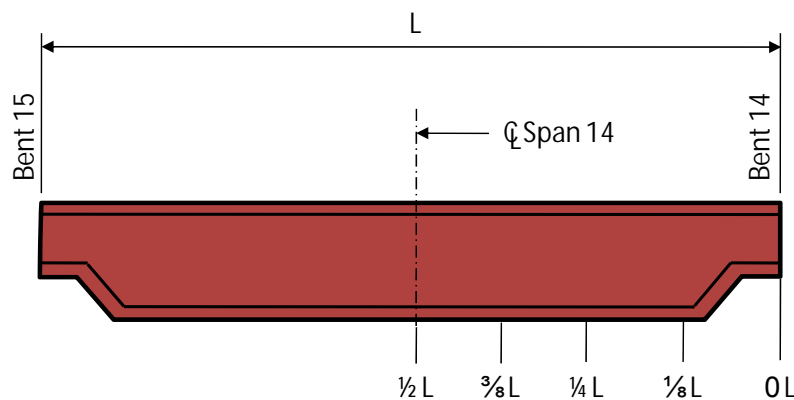


Figure 3.32: Vertical Deflection Reading Locations

After the concrete pour was complete on the first span (Span 16), the data showed negative vertical deflection readings from the mid span of the girders to the pier. The girder deflections then switched to an upward progression in deflection with the next reading after one

quarter of the second span (Span 15) was poured at a time of 5:50am. Girders 3 and 4 deflected upward after half of Span 15 was poured. The next vertical deflection readings were taken after three-quarters of the concrete was poured on Span 15. During the time between half of Span 15 being poured and three-quarters of Span 15 being poured, Girder 4 at $\frac{1}{2}$ L (midspan), deflected upward 1.29". Significant changes in the Girder 3 deflection during this same time period also occurred at the $\frac{1}{2}$ L location, with an upward deflection magnitude of 1.25". There was an upward movement on Girders 3 and 4 at all of the locations measured along the girders at this point in time. Furthermore, after concrete placement on Span 15 was complete, another deflection reading was taken, and it indicated a continued positive upward deflection progression. It was not until 9:00 a.m., when half of the last span (Span 14) was poured, that the girders began to develop a negative vertical deflection magnitude. The change in deflection is noteworthy at this point in time, because the girders began behaving as one would expect for a continuous girder bridge. Tables 3.12 and 3.13 provide a summary of the behavior of the girders relating to vertical deflection during the concrete pour.

Table 3.12: Vertical Deflection Readings Along Girder 3

| | | Vertical Deflection Along Girder 3 (inches) | | | | |
|-------|----------------------|---|--------|--------|--------|--------|
| Time | Event | 0 L | 1/8 L | 1/4 L | 3/8 L | 1/2 L |
| 3:45 | Span 16 Complete | 0 | -0.021 | -0.146 | -0.333 | -0.500 |
| 5:50 | 1/4 Span 15 Complete | 0 | 0.167 | 0.083 | -0.104 | -0.042 |
| 6:25 | 1/2 Span 15 Complete | 0 | 0.417 | 0.521 | 0.521 | 0.354 |
| 7:10 | 3/4 Span 15 Complete | 0 | 0.708 | 1.167 | 1.437 | 1.604 |
| 8:00 | Span 15 Complete | 0 | 0.792 | 1.354 | 1.667 | 1.958 |
| 9:00 | 1/2 Span 14 Complete | 0 | -0.229 | -0.458 | -0.625 | -0.333 |
| 11:20 | All Spans Complete | 0 | -1.125 | -2.229 | -2.771 | -2.667 |

Table 3.13: Vertical Deflection Readings Along Girder 4

| | | Vertical Deflection Along Girder 4 (inches) | | | | |
|-------|----------------------|---|--------|--------|--------|--------|
| Time | Event | 0 L | 1/8 L | 1/4 L | 3/8 L | 1/2 L |
| 3:45 | Span 16 Complete | 0 | -0.312 | -0.396 | -0.333 | -0.521 |
| 5:50 | 1/4 Span 15 Complete | 0 | -0.125 | -0.125 | -0.021 | -0.021 |
| 6:25 | 1/2 Span 15 Complete | 0 | 0.167 | 0.458 | 0.729 | 0.521 |
| 7:10 | 3/4 Span 15 Complete | 0 | 0.563 | 1.354 | 1.938 | 1.812 |
| 8:00 | Span 15 Complete | 0 | 0.729 | 1.583 | 2.313 | 2.438 |
| 9:00 | 1/2 Span 14 Complete | 0 | -0.396 | -0.500 | -0.312 | -0.375 |
| 11:20 | All Spans Complete | 0 | -1.646 | -2.479 | -2.750 | -2.958 |

Girders 3 and 4 Vertical Deflection Summary

The vertical deflection results for Span 14 are typical of a continuous girder bridge. When the preceding spans were poured, the girders in the last span could be characterized with some uplift, but as the concrete pour progressed onto the last span, the girders started to change from an upward deflection to a downward deflection. The maximum deflection recorded on Girder 4 occurred at $\frac{1}{2} L$, after all spans were complete, with a magnitude of -2.96." Subsequently, the maximum recorded deflection for Girder 3 occurred at $\frac{3}{8} L$, after Unit 3 was completely finished, with a magnitude of -2.77."

3.8.6 Horizontal Thermal Expansion Results

This section focuses on the results of thermal effects on Span 14 of the SH 130/US 71 Direct Connector (Bridge 88). During daily thermal cycles on most materials, the material expands and contracts as it heats up and cools down, respectively. Continuous steel girder bridges, with their long spans, can experience large thermal movements as the temperature changes. Although most steel bridges undergo non-uniform temperature gradients in the vertical, transverse, and longitudinal direction, this project only focuses on thermal expansion results in the longitudinal direction. The thermal expansion was measured using a wax horizontal displacement device shown in Figure 3.33. The wax trace boxes were developed for research on the thermal expansion of steel bridges and have been previously discussed in Grisham (2005) and Chen (2008). As the bridge expands, the stylus, which is attached to the bearing plates of Girders 1 and 4, records the maximum longitudinal movement.



Figure 3.33: Wax Trace Box for Measuring Bearing Movements

The wax trace boxes for measuring thermal bridge movements were placed on Bent 14 of Bridge 88 on April 16, 2008 at 8:15 a.m. and removed on May 8, 2008 at 7:00 p.m. The devices

recorded the maximum thermal movement that Unit 3 experienced during this time frame. The temperature at the time of placement was 55°F. After Span 14 was poured (11:20 a.m.), which completed the concrete placement for Unit 3, the measured thermal movement for Girder 1 was 0" and for Girder 4, 0.15." The recorded temperature at this time was 70°F.

On May 8, 2008, when the wax device was removed from Bent 14, the measured longitudinal movement was 0.615" as shown in Figure 3.34. The temperature at this time was 86 °F. The maximum temperature that Bridge 88 experienced during the time period of April 16th through May 8th was 90 °F and the minimum temperature was 42 °F (www.weatherbug.com).

The actual measured thermal movements can be compared with theoretical thermal expansion values that can be calculated according to the AASHTO LRFD Design Bridge Specifications (2007). Theoretical thermal movement is referred to in AASHTO as design thermal movement for uniform temperature change. The following equation, which uses the extreme bridge design temperatures, is used to calculate the design thermal movement range, Δ_T , which is outlined in Section 3.12.3 of AASHTO (2007).

$$\Delta_T = \alpha L(T_{Max} - T_{Min}) \quad (3.3)$$

Where:

α = Coefficient of Thermal Expansion (in/in/F)

L = Expansion Length (in)

T_{Max} = Maximum Design Temperature

T_{Min} = Minimum Design Temperature

To evaluate the maximum and minimum design temperature, AASHTO refers to two figures that are a schematic of temperature contours drawn on a picture of the United States. The design engineer is instructed to use one figure to determine the maximum design temperature and another to determine the minimum design temperature, by locating the bridge site on the map and interpolating between the temperature contours. Because Austin, Texas weather data was available, the AASHTO contour maps were not used to calculate the temperature range for the theoretical thermal expansion; therefore the actual temperatures during the field test were used. Because the temperature at the installation of the wax devices (8:15 a.m.) was 55°F and the temperature increased to 70°F at 11:20 a.m., the change in temperature used in the first theoretical thermal movement calculation was 15°F. The change in temperature used in the second set of calculations was 48°F, which is equal to the maximum temperature that occurred from April 16 to May 8 (90°F) subtracted by the minimum temperature occurrence (42°F) during the same time period. The design thermal coefficient for steel was taken as 6.5×10^{-6} in/in/°F. The expansion length was determined by assuming that the thermal neutral point occurs at the mid span of Span 15. This assumption is consistent with the findings of Chen (2008) who found that pier flexure often occurs in bridges even with "fixed" bearings so that the true thermal fixed point is often close to the center of mass of the bridge. Therefore, the total expansion length used to calculate the theoretical thermal movement for Girder 1 was 282.89 ft and 290.28 ft for Girder 4. By adding the length of Span 14 to half of the length of Span 15 for each girder, the total expansion length can be resolved. Table 3.14 references the span lengths for Unit 3 of Bridge 88.

Table 3.14: Bridge 88, Unit 3 Girders 1 and 4 Lengths

| | Plan Sheet Girder Lengths (ft) | | | L* (ft) |
|----------|--------------------------------|---------|---------|---------|
| | Span 14 | Span 15 | Span 16 | |
| Girder 1 | 180.52 | 204.74 | 154.05 | 282.89 |
| Girder 4 | 185.27 | 210.01 | 158.13 | 290.28 |

*Expansion Length

Table 3.15 compares the calculated theoretical thermal expansion values with the field measured values. The theoretical expansion values are significantly higher than the field measured values. This is an indication that the theoretical expansion calculation is conservative in evaluating this behavior. It is also worth noting that in just the small amount of time between when the wax trace boxes were installed (8:15 a.m.) to when the concrete deck was complete (11:20 a.m.), there was thermal movement, although minor, within the steel unit. Figure 3.34 and Figure 3.35 show the wax thermal expansion device in the field and the method for determining the total thermal bridge movement.

Table 3.15: Summary of Thermal Movement on Unit 3

| Summary of Thermal Movement | | |
|-----------------------------|--|----------------------------|
| | After Span 14 Poured (4/16/08 - 11:20 a.m.) | |
| | Field Measured (in) | Theoretical Expansion (in) |
| Girder 1 | 0 | 0.33 |
| Girder 4 | 0.15 | 0.34 |
| | After Thermal Effects (05/08/08 – 7:00 p.m.) | |
| | Field Measured (in) | Theoretical Expansion (in) |
| Girder 1 | 0.60 | 1.06 |
| Girder 4 | 0.615 | 1.09 |

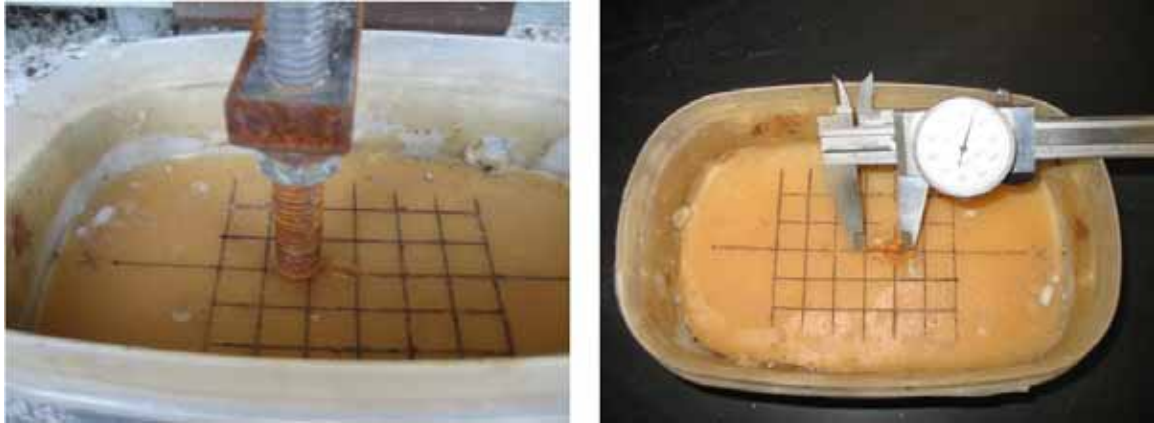


Figure 3.34: Wax Thermal Expansion Device Measurement



Figure 3.35: Wax Device attached to Bent 14

3.8.7 SH 130/US 71 Concrete Placement Summary

The data showed that significant change in bending stress occurred when concrete placement was completed on the last span (Span 14) on all of the girder sections monitored. There was minimal amount of change in warping stress in the bottom flange region, and less than 1 ksi of change in warping stress in the top flange region on all sections monitored. The web region of Girder 4 produced higher bending and plate bending stresses than Girder 3. The bottom quarter point of the web region in Girders 3 resulted in higher stresses than the web midpoint and bottom quarter points that were instrumented, whereas the top quarter point of the web had higher stresses in Girder 4.

The vertical deflection results were typical of a continuous girder bridge. When the preceding span were poured, the girders in the last span could be characterized with some uplift, but as the concrete pour progressed onto the last span, the girders changed from an upward deflection to a downward deflection.

The actual horizontal displacement results relating to the thermal expansion behavior of Unit 3 were much less to the calculated theoretical values. This is an indication that the theoretical expansion calculation is conservative in evaluating this behavior.

3.9 Field Test Conclusions

This chapter provided a summary of the field tests conducted as part of the research project. Descriptions and results from both the test on direct connector SH 130/US 71 and the Hirschfeld lift test are presented. The information collected during this study was used in the verification of the finite element models developed for the parametric studies as well as the finite element design tools discussed later in this report. The data collected here also provides others in the structural engineering community a resource for comparisons with finite element models and analytical solutions to ensure the latest predictions of the behavior of horizontally curved steel I-girder bridges have a sound experimental basis.

Chapter 4. Lifting of Curved I-Girders

4.1 Introduction

The lifting of curved girders is an important step in the erection process. During the course of this research project significant strides were made towards understanding the behavior of curved I-girders during lifting. The work documented in this chapter describes the state of practice as obtained from a survey of industry experts. In addition, three of the critical issues that need to be addressed by the engineer when considering the lifting of girders are also addressed: buckling, deformations, and stresses. Although local buckling of plate elements needs to be considered during construction, most I-girders with practical proportions are usually controlled by lateral-torsional buckling. A linear buckling analysis can be used to determine the critical buckling load, but the analysis is applicable for problems with small pre-buckling deformations. This will often not be the case for curved girders as deformation came became significant from the torque applied by self-weight. This chapter provides a description of a methodology to predict the deformations of curved I-girders during lifting. Additionally, the stresses need to be checked to ensure the girder does not yield during the construction process. Except for extremely slender girders, yielding is not usually a problem unless the girders experience excessive deformations. However, the stress calculations should include both strong and weak axis bending as well as warping normal stresses from the torque applied. The combination of these three critical issues was incorporated into an Excel spreadsheet program named UT Lift that was developed and verified as part of the project. Descriptions of the spreadsheet as well as the assumptions made during its development are provided in the chapter.

4.2 Erection Practices for Lifting of Horizontally Curved I-Girders

4.2.1 Introduction

This section provides a summary of the results of a questionnaire created to survey various steel curved I-girder erection contractors, inspectors, and engineers. The questionnaire focuses on the common practice for lifting curved I-girders, including spreader beam length, number of cranes, lift points, shore towers, and length of girder segments lifted. The purpose of developing the survey was to verify that the research project solutions incorporate the typical range of parameters that occur in actual practice. A total of 12 people were surveyed with this Questionnaire, representing contractors, construction engineers, inspectors, from 12 companies located in the United States. The responses from the survey are numbered from 1 through 12, representing each person participating in the study. A copy of the Questionnaire can be found in Appendix A.

4.2.2 Question 1: Typical Lifting Scenario

The objective of Question 1 of the Questionnaire was to determine the typical lifting scenarios that are employed by various contractors. The first part of this question asked what the range of girder segment lengths are, when one girder segment is lifted and then spliced in the air. This situation involves lifting a single girder and placing it on the bent cap at one end and temporarily supporting the girder with a crane or shore tower. This is repeated until a complete span of girder segments is lifted and the cross frames are connected. Then the shored span of girders is spliced in the air, between piers, to the next segment of girders at the field splice

location. Figure 4.1 shows the air splice stage of construction for the first connecting girder segment for the instrumented bridge near the Austin airport. Figures 4.2 and 4.3 give an example of the typical temporary shoring used to provide falsework for curved I-girders during construction.



Figure 4.1: Air Splice



Figure 4.2: Shore Tower Supporting Curved Girders



Figure 4.3: Shore Tower Beam Supporting I-Girders

The length of a girder segment is most often controlled by the transportation hauling length. The maximum single girder segment lifted that the surveyed participants reported was 150' and the minimum was 20'. Table 4.1 organizes the minimum and maximum lengths that were reported. Participants 4, 5, and 6 did not give a minimum and maximum length, but gave an explanation of single segment erection and air splicing. The response from Participant 4 stated that the size of the pieces lifted depends on the lengths that can be transported to the site, the size of the crane available and the bending stresses that can be tolerated without buckling. He also said that their company cannot erect girders one at a time in the beginning because the first girder usually has an unbraced length in excess of what is acceptable. They try to erect I-girders with a single crane when possible and avoid using shoring towers. Participant 5 indicated that the segment length depends on the stability of the girder and the capacity of the crane. He also reported that length is not a problem if the girder remains stable for picking and placing. The sixth participant commented on the topic of air splicing. In response to Question 1, they stated that splicing in the air can be difficult if the girder webs are not on the same grade or exactly plumb. They went on to say that for continuous units, falsework must be used to support one girder as the other is lifted for splicing. This method will work well if girders are either too long or too heavy to be pre-spliced on the ground, or available cranes are too small to lift heavier loads. Another noteworthy comment from Participant 6 is that falsework must be adequately protected if it is adjacent to a travel way, which means that this method is oftentimes more costly and time consuming especially on multi-level interchanges where the upper levels are high above the ground. Participant 10 responded to this question by first stating that the first lift should always be a pair of girders. He stated that single or double crane lifts requiring cranes over 250 ton cranes increase the cost of the erection.

Table 4.1: Single Girder Segment Reported Lengths

| Participant | Profession | Min. Length | Max. Length |
|--------------------|-----------------------|--------------------|--------------------|
| 1 | Engineer/Contractor | 60' | 120' |
| 2 | Engineer/Contractor | 80' | 100' |
| 3 | Contractor | -- | 120' |
| 4 | Engineer/Contractor | -- | -- |
| 5 | Construction Engineer | -- | -- |
| 6 | Engineer/Contractor | -- | -- |
| 7 | Inspector | 20' | 120' |
| 8 | Inspector | -- | 150' |
| 9 | Contractor | 100' | 140' |
| 10 | Engineer/Contractor | -- | -- |
| 11 | Construction Engineer | 64' | 154' |
| 12 | Fabricator/Contractor | 50' | 150' |

The profession of each Participant is also given in the table above. The participants that are labeled “Construction Engineer” work for an engineering firm that is specifically hired by erection contractors to engineer curved I-girder erections. Participants that are labeled “Engineer/Contractor,” are erection engineers that work for construction companies that erect curved I-girders. If a participant’s profession is labeled “Contractor” in Table 4.1, then that person is a superstructure manager or superintendent at an erection construction company.

The second part of Question 1 targeted the range of girder lengths lifted when segments are spliced on the ground and lifted into place. This type of splice is referred to as a ground splice and allows longer girder lengths to be lifted (Figure 4.4). The maximum length reported for a curved girder that was ground spliced and lifted was 300'. The ranges of spliced girder lengths are organized in Table 4.2. Participant 5 commented that if the spliced girder is stable and the crane can pick it, then “you can go to a length that determines the weight and stability.” In reference to Participant 6’s maximum length response of “no limit,” he states that if girders are spliced and paired, the only limitation is the multi-crane setup locations, total lift capacity, and reach.



Figure 4.4: Ground Spliced Curved I-Girders

Table 4.2: Pre-spliced Girder Segment Reported Lengths

| Participant | Min. Length | Max. Length |
|-------------|-------------|-------------|
| 1 | 60' | 250' |
| 2 | 80' | 150' |
| 3 | -- | < 200' |
| 4 | -- | -- |
| 5 | -- | -- |
| 6 | -- | No Limit |
| 7 | 150' | 290' |
| 8 | -- | 300' |
| 9 | 240' | 280' |
| 10 | --- | 160' |
| 11 | -- | -- |
| 12 | 160' | 286' +/- |

4.2.3 Question 2: Spreader Beams

The second question focused on the use of spreader beams and what the protocol is for curved I-girder erection. Spreader beams, which are connected to the crane with large cables, attach to the girder lifting clamps on the top flange of the girder, as shown in Figure 4.5, and are used to provide multiple lift points and control the inward force that the top flange is subjected to during lifting. Question 2 queries the use of spreader beams and lengths that are typically used. It also asks if the size of the spreader beam is pre-determined before the girder arrives on the construction site or does the contractor have various sizes of beams on hand to choose from. Figure 4.5 shows an example of a type of spreader beam used in curved I-girder construction. In this case, the spreader beam was a pipe section that could be extended or reduced in length by interchanging segments with the intermediate bolted pipe flange connections.



Figure 4.5: Spreader Beam Connected to I-Girder

All of the curved I-girder erection specialists that were surveyed use spreader beams. It is necessary to use spreader beams in order for the beam clamps to hang vertical. The use of other lifting devices such as slings would not allow the beam clamps to hang vertical, which could cause them to slip, the girder could roll, or cause excessive flange deformation when the girder is lifted (Participant 10). Four out of twelve of the participants mentioned the use of adjustable spreader beams. The consensus of the survey indicated that the size of the spreader beam is pre-determined and engineered before the girder arrives on the construction site. This can be expected due to complex stability issues and the delicate nature of curved steel I-girder erection. Because erection plans are required before the girders can be lifted, the size of the spreader beam

is usually included in this set of construction documents. The erection contractor may use the spreader beam that is in their inventory or a new one can be designed. Participant 5 said that the length of the spreader beam is determined by the radius of the curve. He described the importance of the spreader beam intersecting the center of gravity of the curved I-girder. This is referred to the *line of support* and is also described in later in this chapter of this report. The parametric study later in this chapter concluded that approximately half the segment length was the optimal length for a spreader beam (L_{Lift}) used to lift one girder segment to maximize the buckling strength. Participant 6's company tries to use two cranes to handle individual and spliced curved girders. He goes on to say that a lifting beam can also be used in lieu of multiple spreader beams to make solo lifts. Participant 12 determines the length based on the lateral-torsional bending stress limit given by AASHTO. Table 4.3 represents the typical spreader bar lengths that each person surveyed has dealt with during curved I-girder erection. One participant, who is an engineering specialist in this field, said that the erector has multiple spreader beams, including adjustable beams, so there will always be an appropriate size for almost any length of girder.

Table 4.3: Reported Spreader Beam Lengths

| Participant | Reported Lengths |
|-------------|-----------------------|
| 1 | 22', 42', 60', 80' |
| 2 | 25' & 40' |
| 3 | 10' – 100' |
| 4 | 20' – 50' |
| 5 | All Sizes, 60' Common |
| 6 | 5' – 150' |
| 7 | -- |
| 8 | 40' & 80' Typ. |
| 9 | 20' – 70' |
| 10 | -- |
| 11 | All Sizes |
| 12 | 10' – 50' |

4.2.4 Question 3: Cranes

Cranes are the nucleus of the third question of the Questionnaire. The employment of one or two cranes is surveyed in order to understand the typical lifting scenario that the majority of the construction industry utilizes. The Questionnaire also asked the question: If two cranes are used, is it typical to employ spreader beams for each crane? Figure 4.6 depicts a single crane used to lift a curved I-girder into place.



Figure 4.6: Crane Lifting Curved I-Girder

The majority of the people surveyed reported that it is more desirable to use one crane. Therefore, they typically use one crane and a spreader bar for curved I-girder erection. Contractors typically prefer the use of one crane due to the high cost of renting this type of heavy construction equipment. A common response to whether one or two cranes are employed was that it depended on the segment length, which affects the weight of the member. With this in mind, the capacity of the crane becomes an issue as the girder segment gets longer. Stability of the curved I-girder was also mentioned as a determining factor. Available site access and

mobilization of the girder transport truck and crane were also notable answers to this question. Overhead obstructions, such as a power line, that might interfere with a single crane were also given as a reason for using two cranes.

The answers from the second part of Question 3, which asked if spreader beams are used with two cranes, varied, but brought up noteworthy responses. A common thread among many of the responses was that the load magnitude determined the need for spreader beams attached to the two cranes. The effect that the load has on localized top flange bending was also cited as a factor considered on this topic. Participant 4 mentioned that if two cranes are used, it is preferable that they are as nearly identical as possible with respect to boom length and working radius.

4.2.5 Question 4: Girder Tilt

A question relating to girder tilt was incorporated into the Questionnaire to evaluate the importance that various contractors, engineers, and inspectors place on this topic. The geometry of curved girders can cause excessive rotations during construction. This is due to the fact that the center of gravity does not lie on the centerline of the girder and therefore there is an eccentricity between the line of support and the center of gravity. Figure 4.7 illustrates the relationship between girder tilt, line of support, and eccentricity. The last part of Question 4 assesses the typical rotation tolerances that various contractors allow.

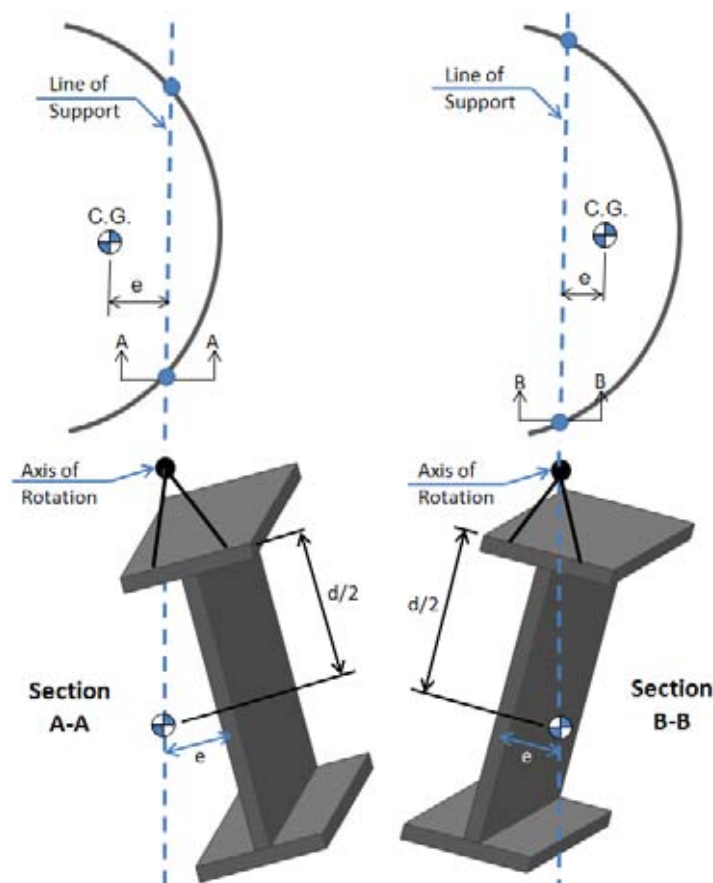


Figure 4.7: Effect of Eccentricity on Curved I-Girder Tilt (Schuh, 2008)

The consensus from the survey participants was that tilting of the girder is a concern when lifting curved I-girders. More than one survey participant indicated that the end rotation of each plate girder at the splice end location is of great concern. This has an impact on how the girder line is connected at the splice location (Figure 4.8). Participant 4 stated that when brought into initial contact, ideally the end rotation of each girder segment should be so that the bottom flanges touch first and the web splice closes as the load is released by the crane. Another typical response from the survey was that if the girder is lifted from the correct location, which is calculated and reported in the erection plans, girder tilt should not be a problem. A common response to the second part of this question, which asks about rotation tolerances, was that the participant did not have a specific tolerance value, but rotation of the girder was definitely a concern and engineered to minimize this effect. Participant 12 stated that a limit of 4 degrees is used especially when using beam clamps to prevent slippage of the clamps. Additionally, this participant stated the few degrees may be acceptable, but it depends on the radius of curvature and the stiffness of the girder. The reported typical rotation tolerance varied among participants, as shown in Table 4.4. One difficulty with three of the responses is that they did not provide a lateral translation limitation based upon the girder depth. Therefore, a 2 inch deformation limit will have a more significant impact on a 60 inch deep girder compared to a 90 inch deep girder. The answer from participant 2 provides a limit that relates to the relative twist of the girder section.



Figure 4.8: Girder Segment Ends Connected at Splice

Table 4.4: Reported Typical Rotation Tolerances

| Participant | Rotation Tolerance |
|-------------|--------------------|
| 2 | 2" per 7' depth |
| 3 | < 2" |
| 6 | 1" |
| 11 | 1" - 2" |
| 12 | 4 degrees |

4.2.6 Question 5: Determining Lifting Points

Question 5 evaluates the common engineering and construction practice for determining the lifting locations along a curved girder. All of the survey participants indicated that the lifting locations are determined through structural analysis. Unbraced flange length, compression flange stresses, and the ability of the top flange to sustain load transfer to the beam clamps were some of the engineered requirements mentioned. More than one participant stated that a two point lift is preferable to eliminate the “roll.” Typical analysis involves evaluating each girder to determine the center of gravity and then completing a stress analysis to establish the appropriate lift points. Figure 4.9 depicts a girder segment being lifted.



Figure 4.9: Lifting Curved I-Girder Segment

4.2.7 Question 6: Problems or Concerns

Finally, the last question surveyed the participants about problems or concerns that they have about lifting horizontally curved I-girder segments and what other aspects of this subject should be considered in this research project or future research projects. This question gives the participants a chance to address their concerns about all aspects of curved I-girder construction and it gives bridge design engineers as well as academia an insight into the real issues that are left unexplored. Table 4.5 organizes the responses for Question 6 into four topics: Shoring, Erection, Tight Radius of Curvature, and Unbraced Length.

Table 4.5: Topics of Question 6 Responses

| Participant | Topic Discussed |
|-------------|---------------------------------|
| 1 | Shoring |
| 2 | Erection |
| 3 | Erection |
| 4 | Unbraced Length (Lifting) |
| 5 | Tight Radius/Erection |
| 6 | Stability |
| 7 | Shoring |
| 8 | Erection/ Shoring/ Tight Radius |
| 9 | Shoring |
| 10 | Tight Radius |
| 11 | Unbraced Length (Lifting) |
| 12 | Erection |

Shoring

The above table demonstrates the variety of responses received concerning Question 6, yet several focus on similar topics. One of the topics referenced the most was shoring, which could be due to the high cost of installing and designing falsework to support curved I-girders during erection. Participant 1 indicated the need for the development of criteria for field engineers to determine when shoring is necessary to maintain a certain elevation of erected girders. He noted that on occasion girders could be safely erected without shoring, but this practice may often result in the girder final elevations falling below the required profile grade.

Participants 7 and 8's concerns lie with the premature removal of temporary shore towers, improperly locating falsework, and non-existent falsework and the effects that this has on the structural system. The ninth participant mentioned that due to site access issues, girders must be shored, despite the unwelcomed expense. His concern involved the phase of construction when I-girder spans are erected over traffic at elevated heights and when the shoring should be disengaged.

Erection

Issues relating to erection were also the subject matter that was referenced often in the responses to Question 6. Participant 2 expressed the need for simple expressions to evaluate the requirements for single point I-girder lifts. A noteworthy response from Participant 3 centered on the effect of splice locations pertaining to girder erection. He stated that many times the first girder that is in a set requires a holding crane or shore tower to temporarily support it until the adjacent girder is erected. When erecting over the top of an existing bridge, it is difficult to support the first girder. His resolution to this scenario is to strategically place the girder splice to ensure that the center of the girder can be supported during these specific situations. Such an idea is ideal for design-build contracts, because the design engineer must know the methods and means that the girders will be erected while designing the superstructure of the bridge. Participant 5 questions the need for erecting curved I-girders in pairs and would like to see this topic examined more closely. Finally, the eighth participant is concerned with the affects that the girder clamp (Figure 4.5), used to lift the girder, has on putting tension on the fillet welds at the top flange to web weld.

Tight Radius of Curvature

The next topic was related to tight radius of curvatures on curved I-girders. Participant 5 speculated on whether the standard calculation methods for stability are affected by extreme curvatures and if they are, what would be the limit of this circumstance. His response also highlighted on the effect that a tight radius has on the erection of a second girder (adjacent girder). Should the girder be blocked at the ends along with installing a central cross-frame before disengaging the lifting crane or should more cross-frames be installed. The eighth participant briefly questioned the length of spreader bar utilized to lift curved I-girders that have tight radius of curvatures. Participant 10 remarked on the problems concerning curved I-girder bridges with tight radius of curvatures and steep cross slopes. In his experience, this scenario sometimes prevents the I-girders in the span or unit from cambering until almost all the dead load of the concrete is placed.

Unbraced Length

As mentioned in Chapter 5, design specifications lack in-depth criteria for horizontally curved I-girder lifting. Therefore, the topic of unbraced length was also given as response for this question by more than one participant. Participant 4 reflected on the equation in the American Association of State Highway and Transportation Officials (AASHTO) *LRFD Bridge Design Specifications* (2007) for allowable bending stress and whether it was applicable for long unbraced lengths (50' to 100'). The subject of unbraced length was also contemplated by Participant 11 who commented that this question was discussed extensively in their office. Their

questions initiated with respect to the top flange of the girder and whether this lifting point constitutes as a brace point against lateral-torsional buckling.

4.3 Buckling of Curved I-Girders during Lifting

4.3.1 Introduction

The buckling of I-girders is a concern especially, when the unbraced length becomes large and the lateral or torsional stiffness becomes small. This is true for any point in the construction process. While the girder is lifted there is no bracing provided and therefore a reasonable check should be made to ensure the safety of girders during the vulnerable state. As stated previously in question 1 of the questionnaire the methods used to lift curved I-girders varies from erector to erector. The most critical scenario from a buckling stand point is a girder lifted with two lift points. This is the minimum number of supports necessary to lift the girder, but maximizes the unbraced length and provides no restraint to rigid body rotation about the axis defined by the lift points. Thus the parametric finite element analysis that was conducted as part of this project focused on this critical lifting approach and conclusions concerning other more stable lifting methods are discussed in the conclusions.

The quickest analytical check of girder stability is a linear eigenvalue buckling analysis. An eigenvalue buckling analysis predicts the buckling shape (eigenvector) and the multiplier (eigenvalue) of the applied load that will cause buckling. Utilizing this approach a better understanding of the behavior is obtained, but the conclusion for curved I-girders is limited by the assumptions inherent in the analysis technique. The linear eigenvalue buckling analysis assumes that the displacement of the system will remain small prior to buckling. This is a reasonable assumption for straight girders, but does not accurately describe the curved girder system. The curvature acts like an initial imperfection resulting displacements which increase as the load is applied leading to second order effects that decrease the buckling capacity of the curved girder system. Thus a full geometric nonlinear analysis that takes the effects of deformations into account was utilized to accurately predict the buckling behavior. Both eigenvalue and geometric nonlinear analysis were performed as part of a parametric study conducted to establish the design guidelines necessary for safe and economic lifting of curved I-girders. A description of the methods used and a summary of the results is provided in the following section.

4.3.2 Parametric Finite Element Model

To understand the behavior of curved girders during lifting it was desirable to perform a series of analyses with a wide range of parameters to improve the understanding of the girders over a range of support and loading conditions. The parametric study was completed using the finite element analysis software, ANSYS, which provides a user defined parametric language. The parametric language allows the user to develop a manageable set of input files that cover a wide range of modeling scenarios. The parametric language provides a method to quickly change specific user defined variables and develop the models necessary to fulfill the parameter matrix. For the problems studied on this research project, the flexible parametric language allowed for variation in the radius of curvature, depth of the girder, length of the girder, plate thicknesses, and lift locations. The variables considered in the parametric study included radius of curvature (R), flange width to depth (b_f/D), length to depth (L/D), and lift point location (a/L) which are

shown with their range in Table 4.6. Figure 4.10 is a schematic of a girder with the parameters defined.

Table 4.6: Eigenvalue Parametric Study Variables

| Variable | Maximum | Minimum |
|-----------------------------------|----------|---------|
| Radius of Curvature (R) | Straight | 250' |
| Flange Width to Depth (b_f/D) | 1/3 | 1/6 |
| Length to Depth (L/D) | 10 | 25 |
| Lift Point Location (a/L) | 0.1 | 0.4 |

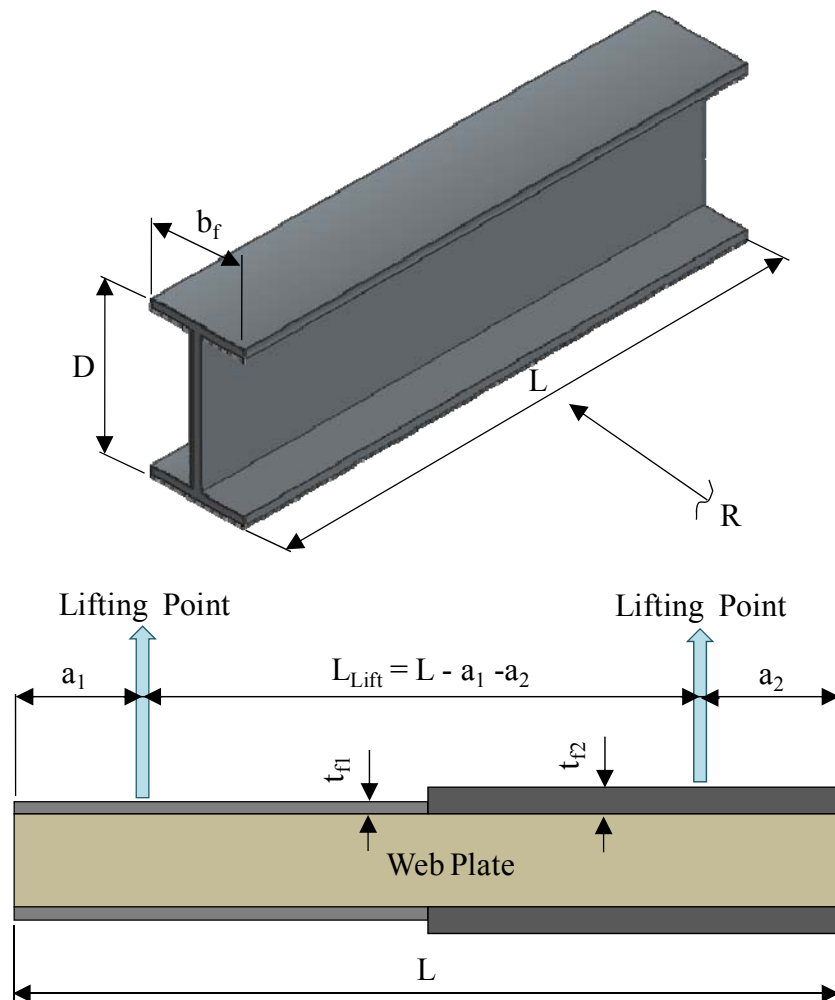


Figure 4.10: Girder Parameter Definitions

The average lifting location is used for a when nonprismatic girders are lifted with $a_1 \neq a_2$. This is shown in (4.1).

$$a = \frac{a_1 + a_2}{2} \quad (4.1)$$

The model consisted of 8-node shell elements (SHELL93) that have six degrees of freedom at each node. The shell elements were used to model the flanges, web, and stiffeners. The boundary conditions that constrain the girder were initially troublesome due to the mathematical singularity in the stiffness matrix. The singularity results from a lack of global degree of freedom constraints, namely the rotation about a line defined by the lifting points. In actuality the girder will rotate such that the center of gravity is at its lowest point rendering the minimum potential energy of the system. To find the solution with the model a weak spring was added to the bottom of the girder transversely at the lifting locations to provide a small amount of restraint to rigid body rotation. Field results from the Hirschfeld lift tests were used to make sure that the stiffness of the lateral springs provided a system similar to that found in practice. The spring acts like friction in the lifting clamp. Figure 4.11 and Figure 4.12 are two screen shots of the ANSYS model used to calculate the buckling capacity of a curved I-girder during lifting. Figure 4.13 is a picture from one of the tests conducted at Hirschfeld Steel Plant.

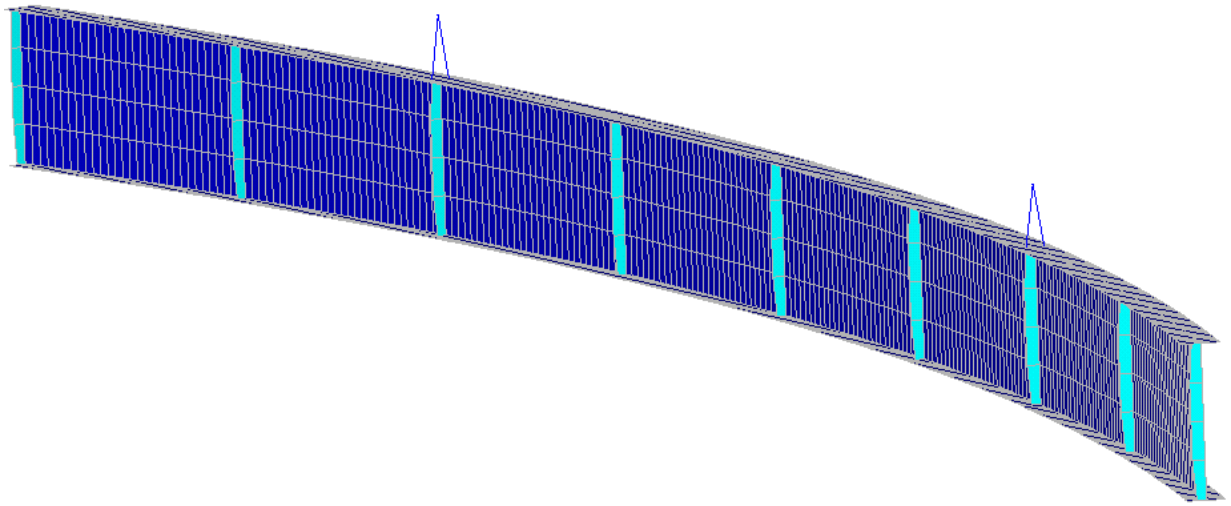


Figure 4.11: ANSYS Model of a Curved I-Girder during lifting

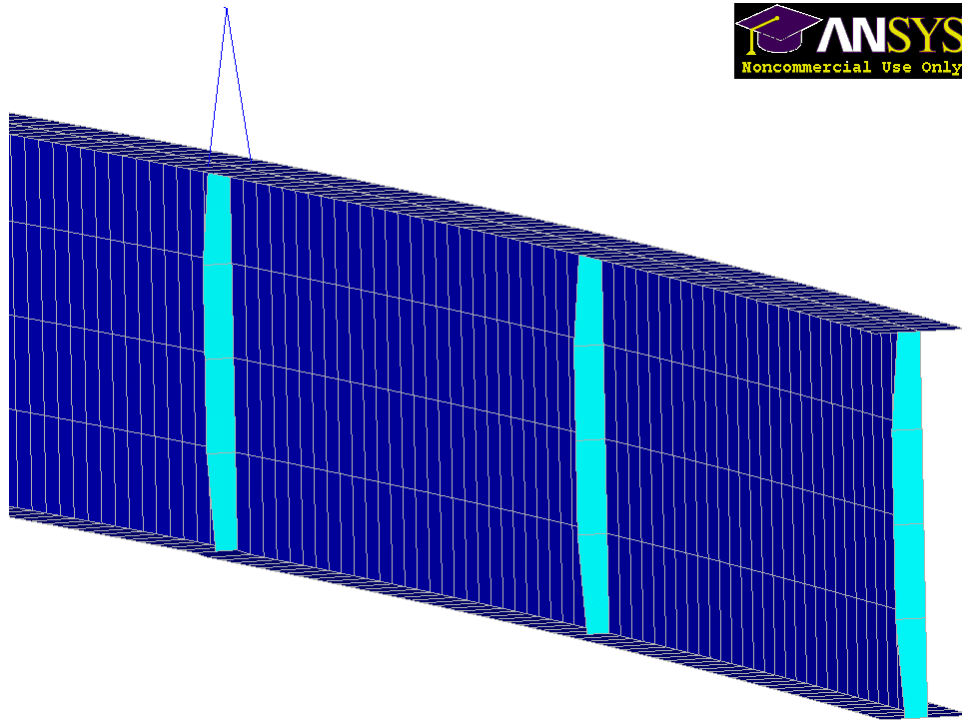


Figure 4.12: Close-up of the ANSYS Model of a Curved I-Girder during lifting



Figure 4.13: Actual I-Girder Lifted during Field Test

4.3.3 Eigenvalue Buckling

As mentioned earlier, the eigenvalue is a multiplier of the applied loads that will cause buckling. For all the cases studied, the only load was the girder self weight and thus an eigenvalue less than 1.0 would indicate that the girder would buckle under its self weight, which is obviously undesirable. However, it is uncommon for engineers to perform a full 3-D eigenvalue analysis of a girder and thus simplified methods have been developed to provide the essential information without the complicated analysis. The simplifying assumption is that lateral-torsional buckling will control the stability behavior of the girder during lifting. This is a reasonable assumption and one that was evident in the buckled shapes produced by the analysis as shown in Figure 4.17.

The solution for lateral-torsional buckling of a beam under uniform moment was provided in Timoshenko and Gere (1961). This equation is given in Chapter 1 of this report. However, this solution can provide very conservative solutions if significant moment gradient exists along the length of the beam. . Thus a moment gradient factor, C_b , is applied to the critical buckling moment to account for the nonuniform moment. This approach has been applied to several structural systems when considering buckling, but had not until now been applied to I-girders during lifting.

Prismatic Girders

The study of prismatic girders during lifting was completed by Schuh (2008) and a full description of the parametric study is given in his thesis. Representative samples of the graphs presented by Schuh are provided in this section (Figures 4.14–4.16) along with the resulting equation derived to account for the moment gradient.

The parameter with the greatest influence on the eigenvalue of the girder during lifting is the lifting location (a/L). The follow graphs present the effect of varying a/L on the eigenvalue for beams with various degrees of horizontal curvature, span-to-depth ratios, and also the flange width to depth ratio (b_f/D).

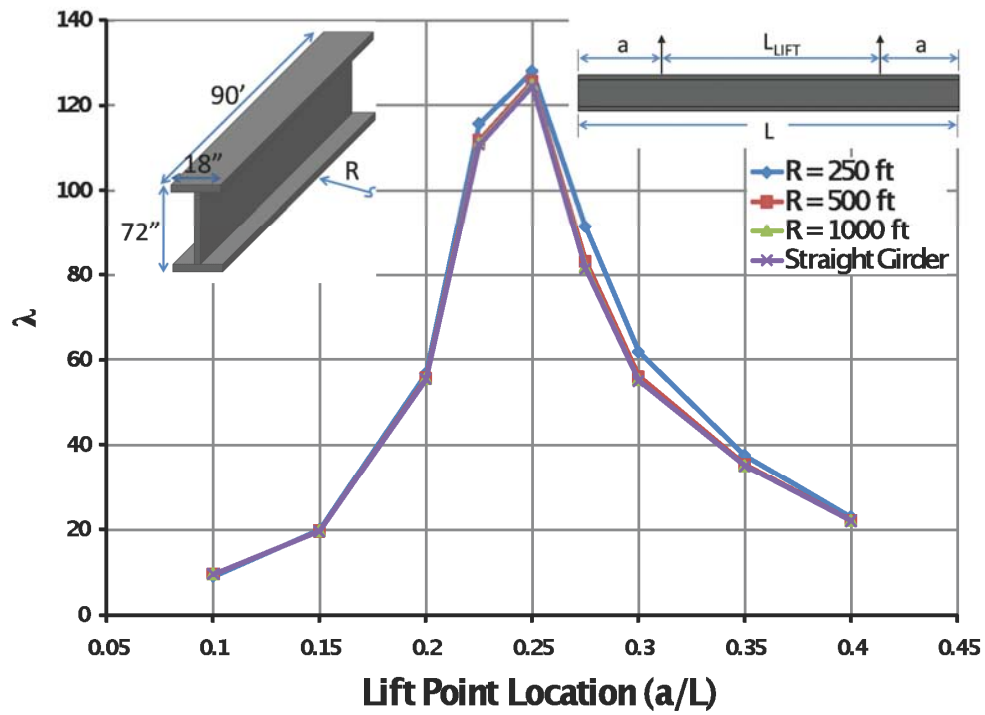


Figure 4.14: Effect of Lift Location and Radius of Curvature on the Eigenvalue

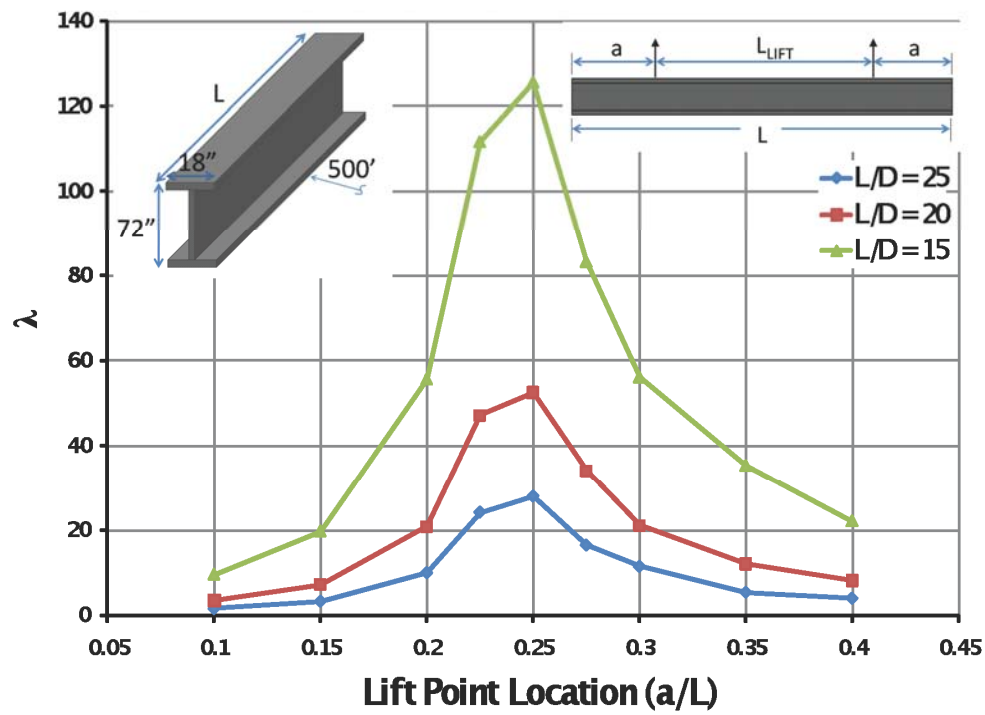


Figure 4.15: Effect of Lift Location and L/D on the Eigenvalue

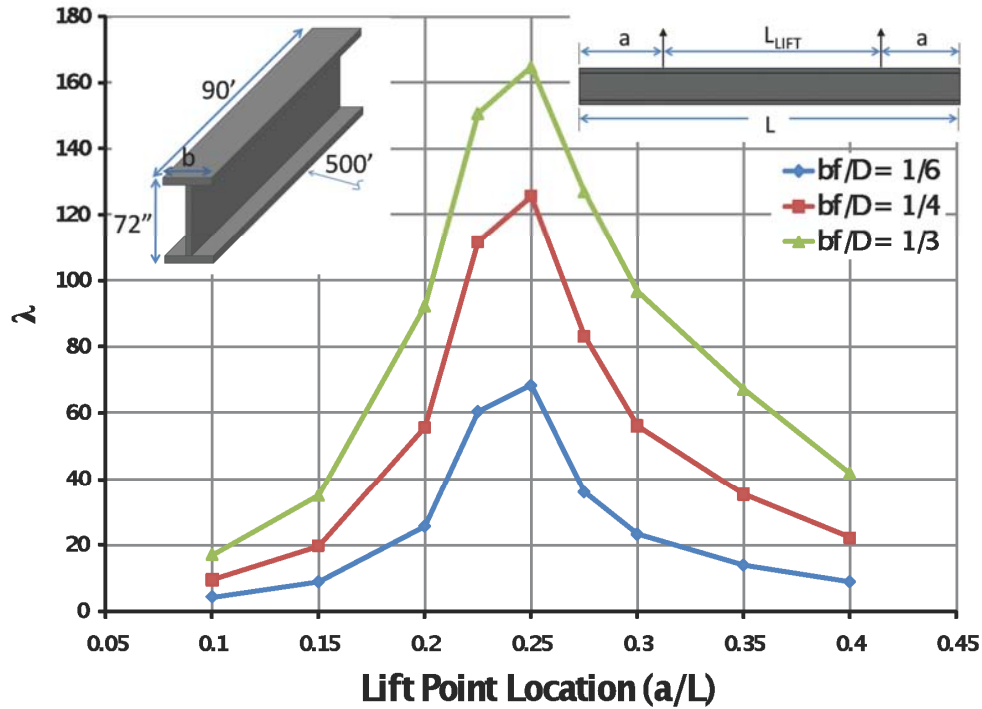


Figure 4.16: Effect of Lift Location and b_f/D on the Eigenvalue

As shown in Figure 4.14–4.16, the maximum eigenvalues are achieved at an a/L of 0.25. The eigenvalue decreases quickly when the lift location deviates from this configuration. The smallest eigenvalues occurred at the extremes of the lifting points that were considered, at values of a/L of .1 and .4. The effect of changing a/L is similar in all of the plots. Additionally, the radius of curvature had a negligible effect on the eigenvalue while the b_f/D and L/D had some effect, but less than the lifting location (a/L).

The buckled shapes are shown for a/L values of 0.1 through .4 in Figure 4.17. The locations of the lifting attachments are identified in the figure. For an a/L of 0.1, the girder buckles with the top flange in single curvature. This is due to the top flange being primarily in compression along most of the segment length when the lift locations are near the ends. As a/L increases, the torsional displacements become more prominent. When the eigenvalue reaches the maximum value at an a/L of 0.25, there is very little twist at the lift points; however, the predominant deformation along the rest of the girder length is a pure twist. When the lift point locations are greater than a/L of 0.35, the buckling deformation is dominated by the overhang section with the largest lateral deformations on the bottom flange due to the compression from the cantilever-like support conditions.

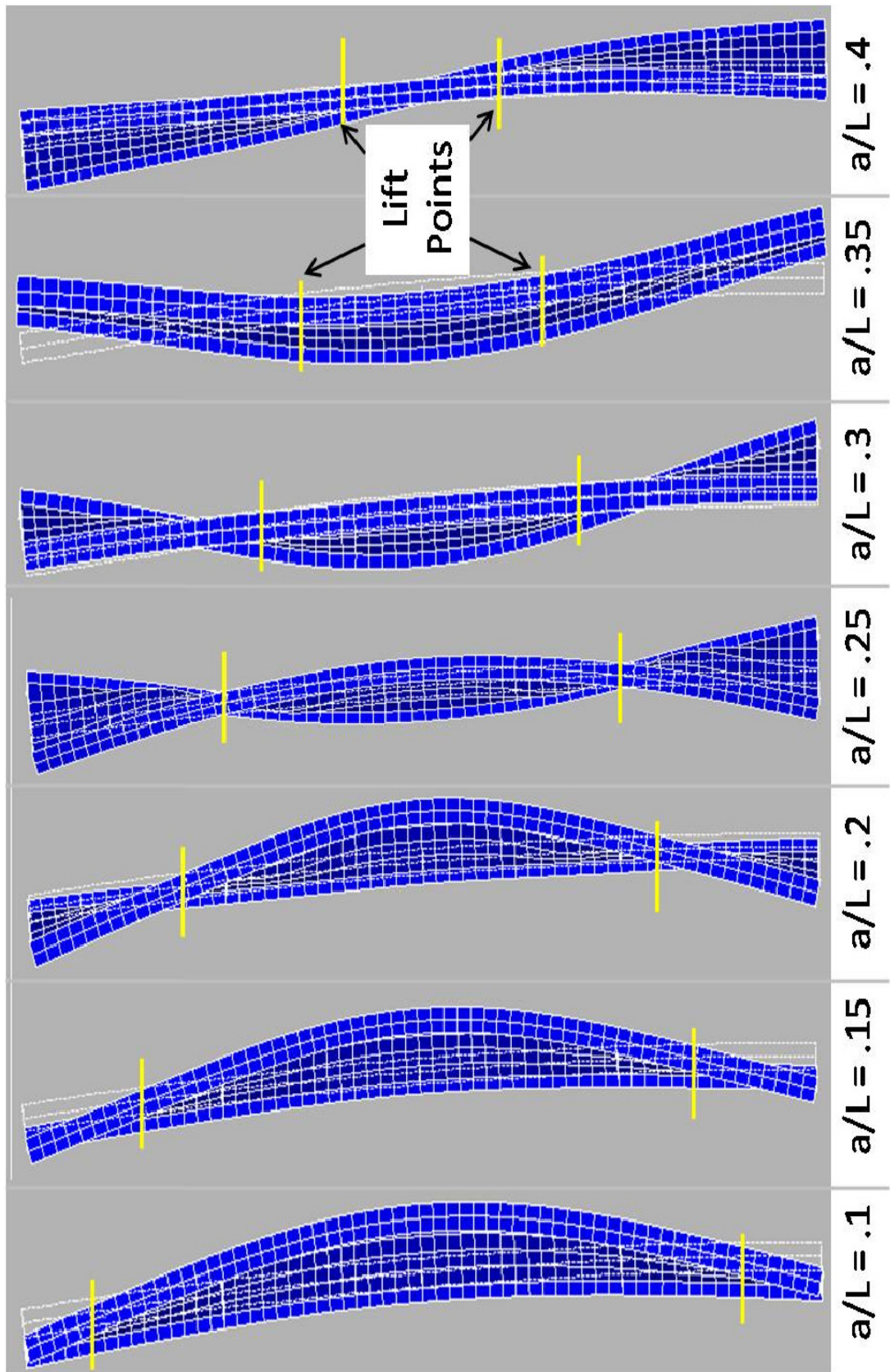


Figure 4.17: Curved Girder Buckled Shapes for $L/d = 10$, $b/d = .25$, $R = 500$ ft

As stated in Chapter 1, once the eigenvalue is obtained from the results presented in this section, (1.3) can be used to observe trends in C_b , the proposed adjustment factor to account for the effects of lifting on curved I-girders. The C_b value from the FEA studies was found for a given lifting geometry by comparing the eigenvalue buckling capacity for the lifting geometry with the equation for uniform moment loading given by (1.1). The C_b factor is the ratio of the maximum moment along the girder length with the buckling capacity for uniform moment given by (1.1). The expressions used to evaluate C_b are given in the following equations and Figures 4.18 and 4.19.

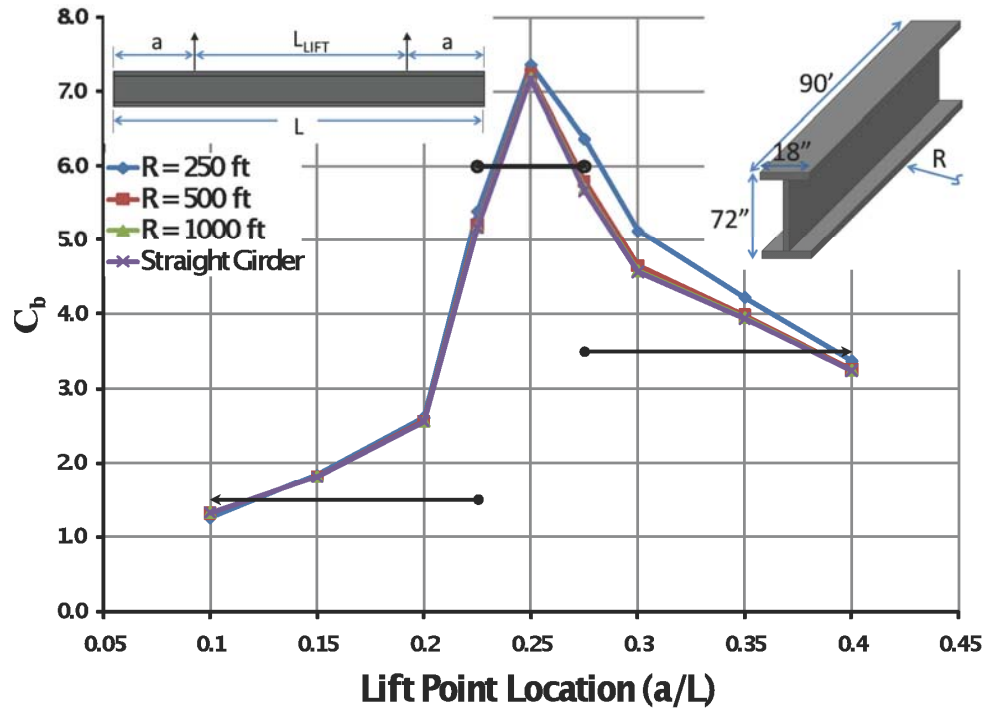


Figure 4.18: C_b vs. a/L for Given Radius of Curvatures

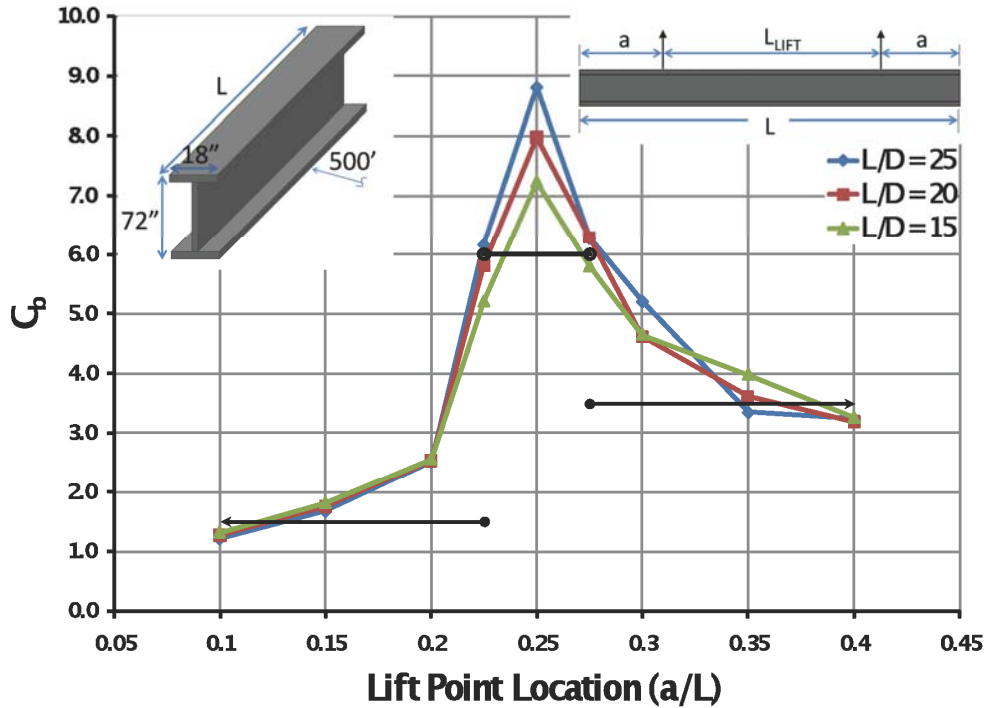


Figure 4.19: C_b vs. a/L for Given Span to Depth Ratio

From the trends presented in the figures, the expression for C_b was formulated and given in (4.2). This expression is shown in Figure 4.18 and Figure 4.19 as a black trend line.

$$C_b = 1.5 \text{ for } \frac{a}{L} \leq 0.225$$

$$C_b = 6.0 \text{ for } 0.225 < \frac{a}{L} < 0.275 \quad (4.2)$$

$$C_b = 3.5 \text{ for } \frac{a}{L} \geq 0.275$$

Nonprismatic Girders

The study of nonprismatic girders during lifting was completed by Farris (2008) and a full description of the parametric study is given in her thesis. The follow is a representative sample of the graphs presented by Farris with the resulting equation derived to account for the moment gradient. The parametric study began with a non-prismatic girder with two flange plate transitions. The flange sizes were varied by changing the thickness of the flange. The first and third cross sections of the girder had top and bottom flange thicknesses of 1.25 in. The second (middle) cross section has a top and bottom flange thickness of 2.00 in. The comparison studies within this section were all analyzed with symmetric lifting points.

Figures 4.20–4.23 present the effect of varying a/L on the eigenvalue and also show this effect for another parameter as well.

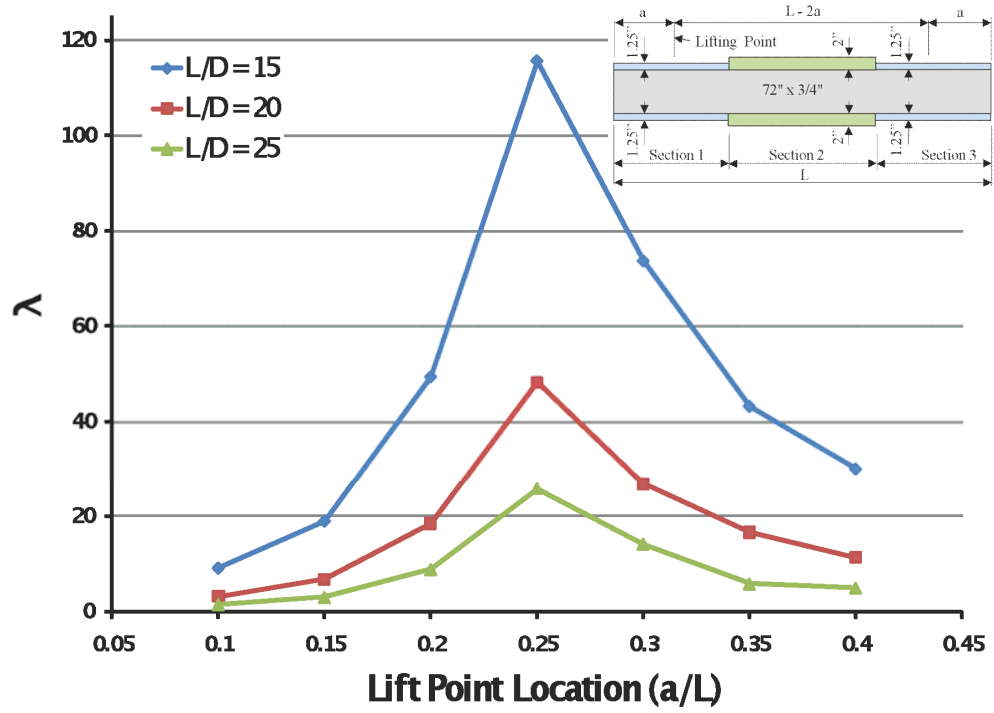


Figure 4.20: Effect of Lift Location and L/D on the Eigenvalue

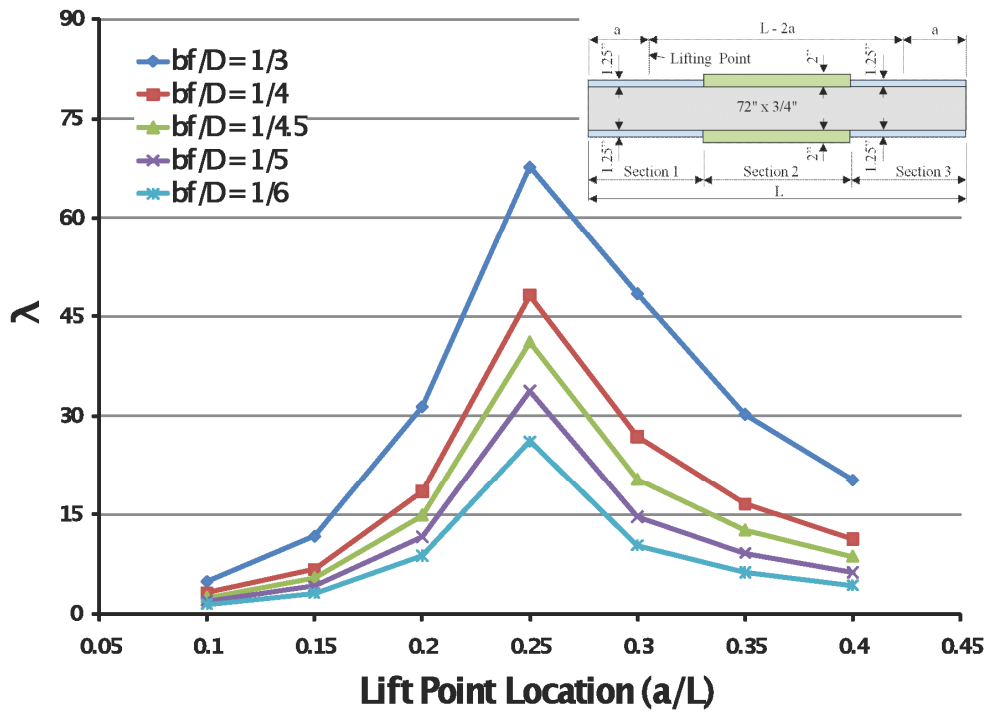


Figure 4.21: Effect of Lift Location and b_f/D on the Eigenvalue

The purpose of presenting the L/D and b_f/D study is to illustrate the behavior of the eigenvalue as a function of girder lifting point. In general, the girder is less stable when the lifting points are very close to the ends of the girder ($a/L = 0.10$) compared to lifting points that are moved closer towards the mid section of the girder ($a/L = 0.4$). The highest buckling capacity was observed at an a/L value of 0.25.

To investigate the effects that the length of the spreader beam (L_{Lift}) has on the eigenvalue buckling analysis, various lengths were chosen ranging from 20' to 85'. As L_{Lift} decreases, the length of the cantilever increases (a_1 or a_2). The length of the girder for this study was fixed at 120'. The web plate was 72" x $\frac{3}{4}$ " which produces a girder with an L/d ratio close to 20. The location of the top and bottom flange plate transition was varied to investigate the behavior of the I-girder as the sections were modified. Depending on the lifting geometry, different regions of the girders controlled the buckling mode.

The optimal spreader beam length (L_{Lift}) was calculated with the spreadsheet mentioned earlier and discussed in detail later in the chapter. The optimal length is presented as the length of the spreader bar to lift the curved I-girder to produce zero rigid body rotation or tilt.

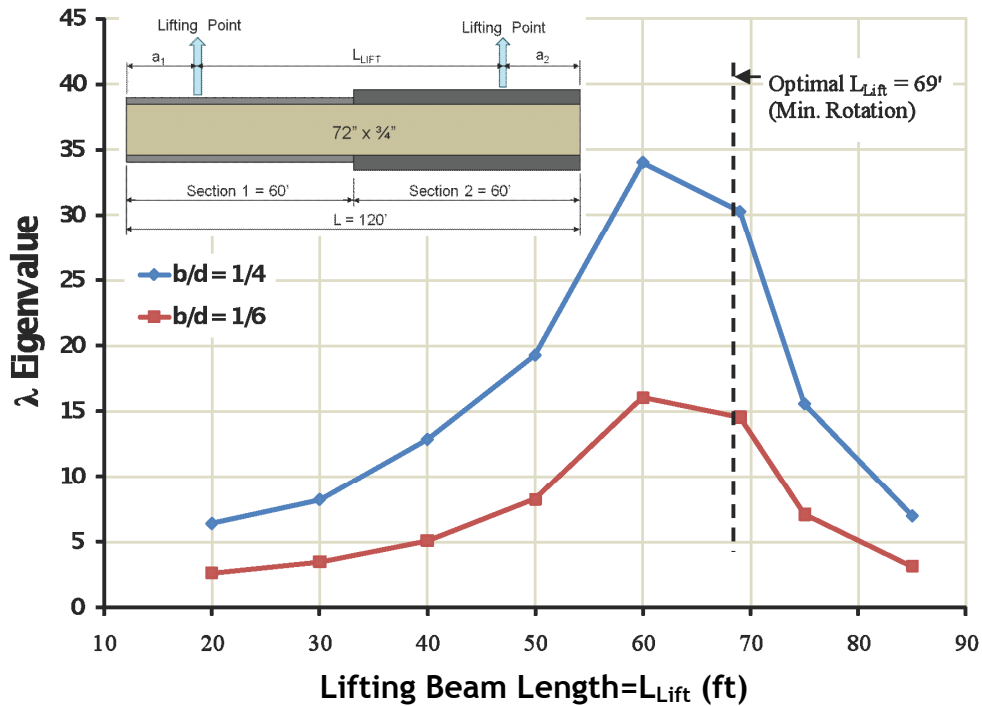


Figure 4.22: λ vs. L_{Lift} (Section 1=Section 2 = 60')

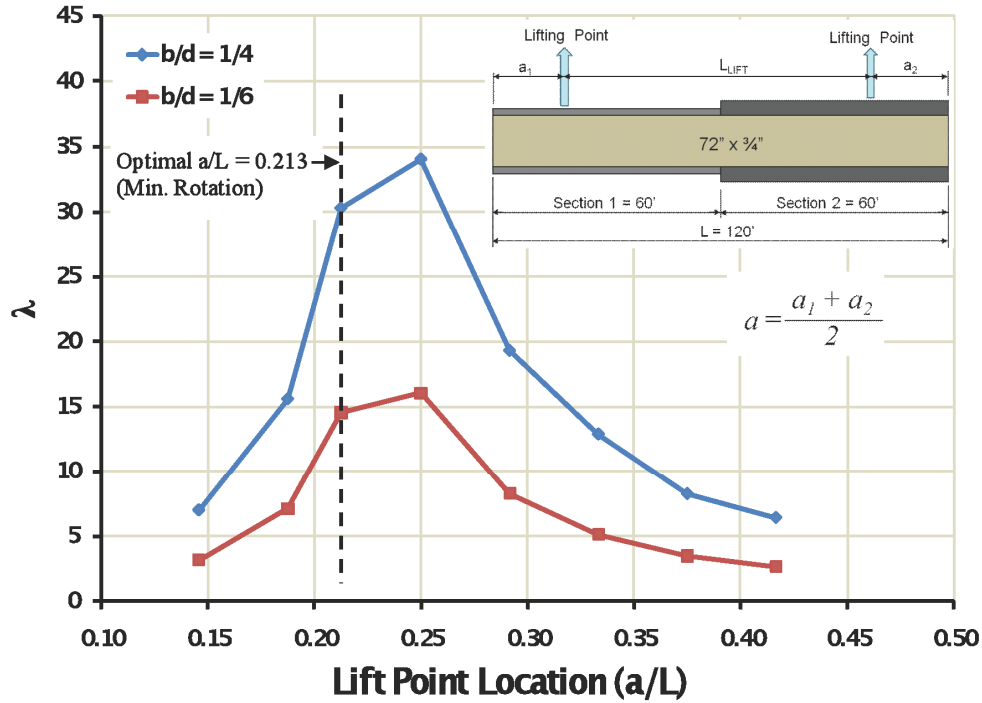


Figure 4.23: λ vs. Average a/L (Section 1=Section 2 = 60')

For the case shown, the eigenvalue is greater for a b_f/D ratio of 1/4, which can be expected because the longer flanges add stability during lifting. The optimal spreader beam is close to 70' for zero rotation during lifting, but this location is not the optimum location for maximum stability. While the location that produces zero rigid body rotation is near the maximum stability location it remains a reasonable location to lift curved girders. The effect of the radius of curvature and the L/D ratio was also investigated for each of the cases (flange plate transitions) presented in this section, but the results from these studies were similar to previous results already outlined.

Finally, the simplification discuss previously for prismatic girders, namely that lateral-torsional buckling is the assumed critical mode, was applied to nonprismatic girders and a moment gradient factor, C_b , was derived. A complexity with non-prismatic girders is the question of what section properties (J , I_y , C_w) to use in the buckling equation. Additionally, the defined unbraced length (L_b) was studied to determine the effect on the moment gradient factor. After studying the effects of the different parameters on the buckling capacity, it was concluded that a conservative approach should be taken. Thus it is recommended that to calculate the lateral-torsional buckling capacity (M_o) the entire length of the lifted section should be used for the unbraced length and the cross section with the smallest geometric properties should be used. The maximum moment occurs at either the lift locations or in the region between the lift locations. Depending on the location of the lift points, the girder will buckle in one of the two locations; the cantilever or the mid region. The controlling maximum moment will be taken as the absolute maximum moment wherever it may occur. The expressions used to evaluate C_b are given in the following equations and Figures 4.24 and 4.25.

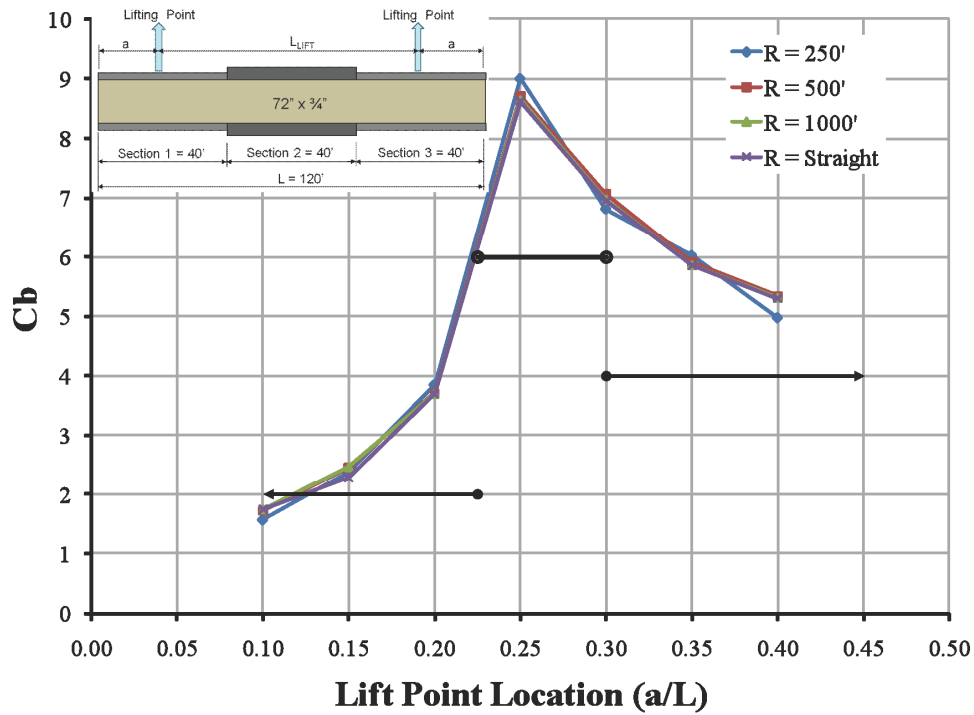


Figure 4.24: C_b vs. a/L for Given Radius of Curvatures (Symmetric Lift)

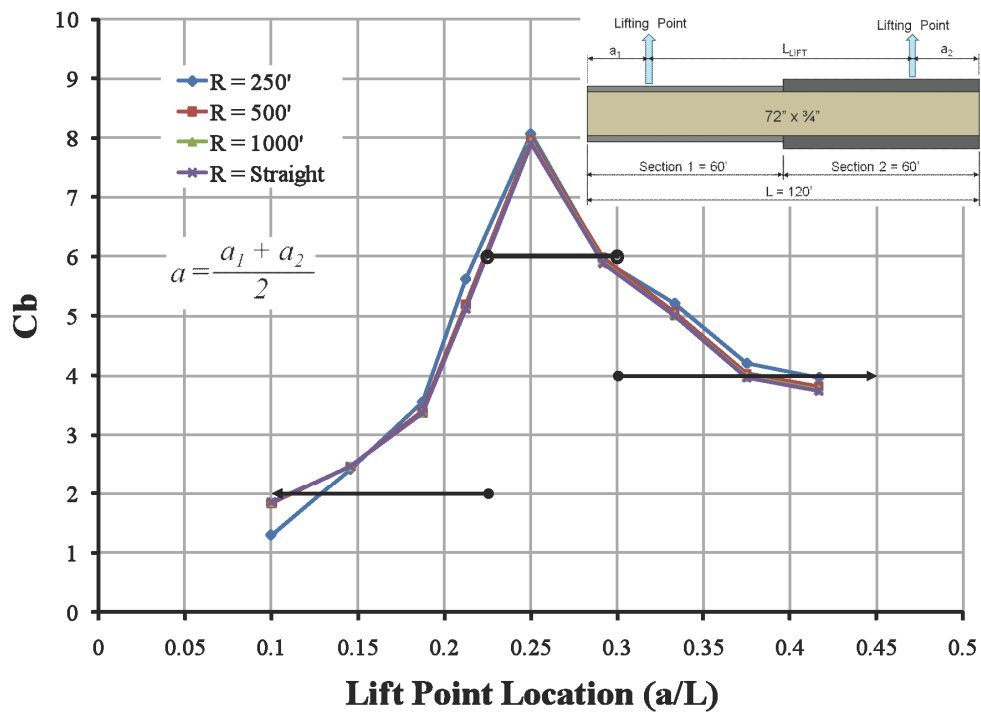


Figure 4.25: C_b vs. a/L for Given Radius of Curvatures (Unsymmetric Lift)

The expression in (4.3) was formulated for the moment gradient factor, C_b , using the trends presented in the previous figures. This expression is represented as the black trend line in the previous figures.

$$\begin{aligned} C_b &= 2.0 \text{ for } \frac{a}{L} \leq 0.225 \\ C_b &= 6.0 \text{ for } 0.225 < \frac{a}{L} < 0.3 \\ C_b &= 4.0 \text{ for } \frac{a}{L} \geq 0.3 \end{aligned} \tag{4.3}$$

The results from the eigenvalue buckling analysis in this section showed that the radius of curvature had very little effect on the critical buckling load. In addition, the magnitudes of the eigenvalues showed that the critical load was often significantly higher than the girder self-weight. While the effect of girder curvature does not significantly impact the eigenvalue solution, girder curvature does have an impact on the actual girder displacements. The next section describes the nonlinear behavior of the girders as a function of girder curvature and lifting geometry. The eigenvalue solutions presented in this chapter serve as an important limit to the girder behavior.

4.3.4 Eigenvalue Buckling Analysis Conclusions

The basic assumptions that were made in the eigenvalue analyses is that the girders experienced small displacements prior to buckling, had a linear stiffness, and also that lateral-torsional buckling was the dominate failure mode instead of a local instability.

The eigenvalue buckling analysis is a quick and accurate assessment of straight I-girders and provides an indication of stability of curved girders. It should be noted that the graphs and equations given for prismatic girders are different from those given in Schuh's thesis due to a change in the assumed unbraced length (L_b). To ensure consistency the unbraced length was altered to match the work of Farris which assumes the entire girder length as the unbraced length rather than using the longer of the cantilever overhang or the distance between the lift points as applied by Schuh. When these corrections were made it became clear that the recommended expressions given in (4.2) and (4.3) were different and that the equations used by Farris were slightly unconservative. The reason for this discrepancy is that Farris assumes the smallest cross sectional properties for the entire length which the eigenvalue buckling analysis accounted for the "stiffer" portion of the nonprismatic beam. The result was a higher moment gradient factor (C_b). Thus the following assumptions were included in the development of the moment gradient factor:

- 1) Lateral-torsional buckling is the dominant buckling mode.
- 2) The girder will experience small displacements prior to buckling.
- 3) The unbraced length used to calculate the moment capacity is the entire length of the girder.
- 4) The smallest geometric properties are used to calculate the moment capacity for nonprismatic girders.

The following recommendations are given for the lifting of I-girders:

- 1) The C_b factors derived for prismatic girders also should be used for non-prismatic girders.
- 2) The predicted buckling capacity provides accurate solutions for straight girders.
- 3) The predicted buckling capacity provides an indication of the stability for curved girders.
- 4) The lifting location is the greatest factor in determining the girder stability and is maximized at approximately $a/L = 0.25$, but for prismatic girders exactly at $a/L = 0.238$.

4.3.5 Geometric Nonlinear Buckling

The result of the eigenvalue parametric studies showed that girders lifted near there quarter points provide the greatest stability to the system. However, as many of the previous figures showed the radius of curved did not significantly affect the eigenvalue buckling capacity. A more refined analysis was performed and the graphically presentation is shown in Figure 4.26.

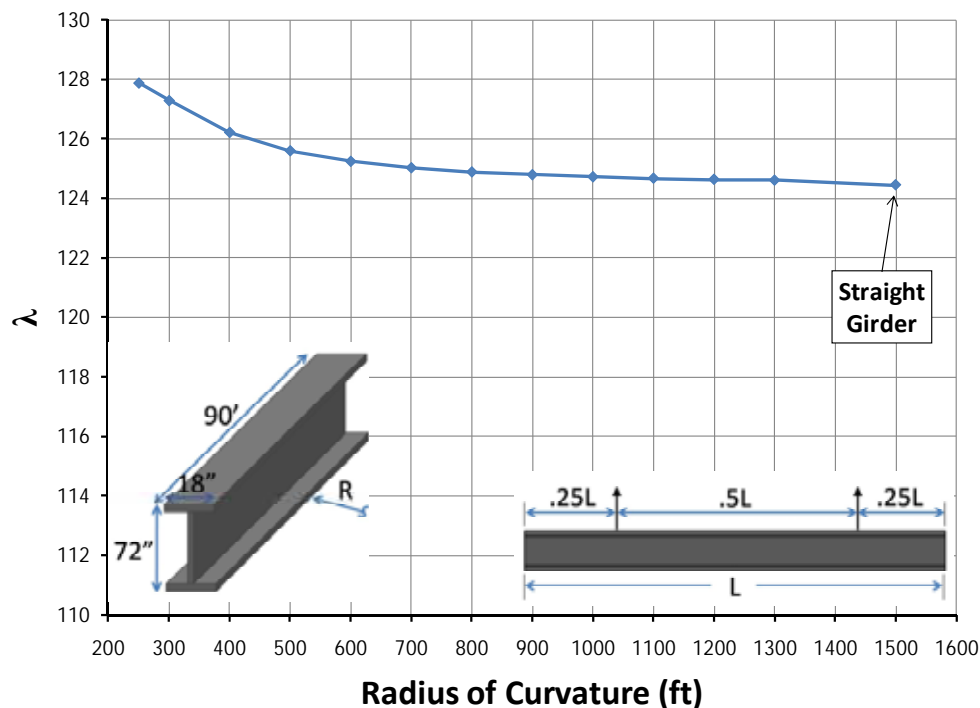


Figure 4.26: Effect of Radius of Curvature on the Eigenvalue

The analysis would indicate a slight increase in stability with a decrease in the radius of curvature. This has been attributed to two primary factors: 1) small displacement assumption of eigenvalue analysis and 2) arching effect in resisting the buckling mode. The first factor is extremely important to the conclusions drawn from the research. The eigenvalue buckling analysis assumes small displacements of the system prior to buckling, which is generally true for straight girders as the load does not induce out-of-plane displacement before buckling occurs. However, this is not the case for curved girders which can have both torsional and weak axis

bending forces applied resulting in out-of-plane displacements that do not fit the eigenvalue buckling assumption. These displacements would seem to reduce the eigenvalue, but it is also notable that the buckled shape given by the eigenmode does not have a magnitude associated with it. Thus for a given displaced shape both positive and negative mode shapes are possible and for highly curved girders the eigenmode must bend the girder against the curvature providing the system a kind of arching restraint. These two features limit the applicability of eigenvalue buckling solutions for highly curved girders.

Thus a 3-D geometric nonlinear analysis was performed to accurately capture the behavior of the curved I-girders during lifting. Due to the linear elastic material properties utilized in the models, two criteria were identified to limit the applicability of the solutions to fit practical conditions. Based upon the information gained from the survey of erectors, contractors and engineers a serviceability limit state of 1.5 degrees of girder rotation was used to ensure proper girder fit-up for aerial splices. In addition, a strength limit state of half of the yield stress ($F_y/2$) was also applied to prevent inelasticity from the combination of stresses during lifting and residual stresses. For all the nonlinear analyses the only loads applied to the girder was the self weight. Although other loads such as wind are possible, erectors typically have stringent limits on wind speed that would preclude girder lifting in windy conditions. As discussed previously, the eigenvalue represents the multiple of the applied load in the analysis that will cause buckling. Because the applied loading consisted of girder self-weight, in the following figures the abscissa is a multiple of the self weight with the ordinate representing the out-of-plane displacement of the top and bottom of the girders. Deformations are shown for both the end and middle of the girder. All cases presented in this section have a flange to depth ratio of $1/4$. Figures 4.27 and 4.28 represent “straight” girders with an $L/500$ imperfection which is a typical manufactures tolerance for I-girders. Figures 4.29 and 4.30 are curved girders with a radius of curvature of 500'. Two lift locations are used in these examples $a/L = 0.2$ and $a/L = 0.25$. Three vertical lines showing the load limits corresponding to the rotation limit of 1.5 degrees, half the yield limit, and the eigenvalue are labeled on the graphs.

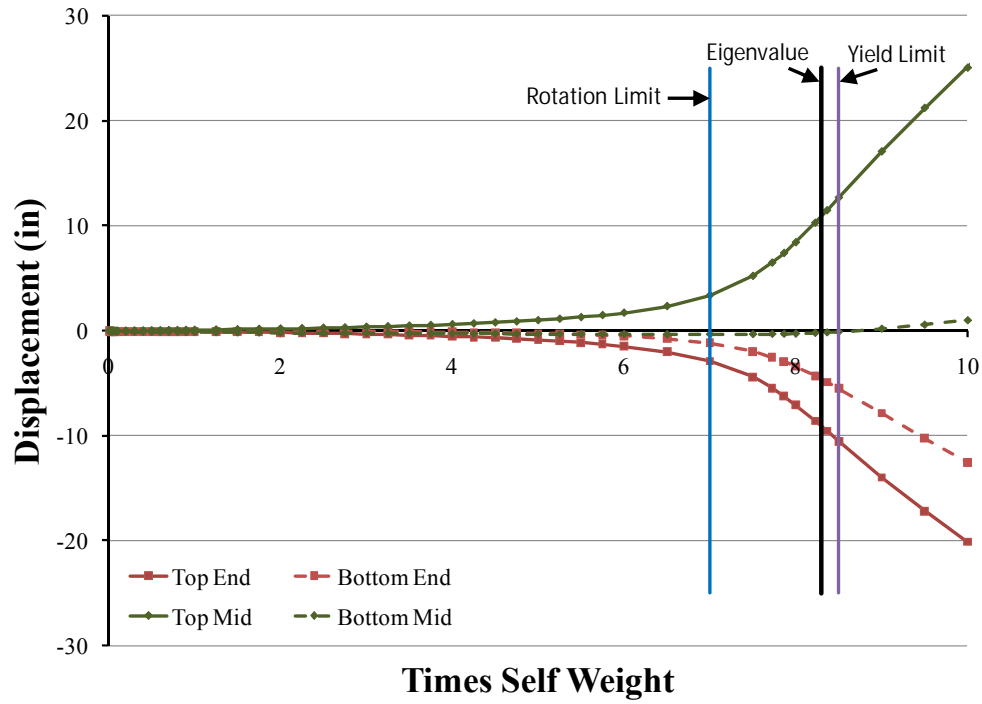


Figure 4.27: Flange Lateral Displacement for Girder with $a/L = 0.2$ $b_f/D = 0.25$ $R = Str.$

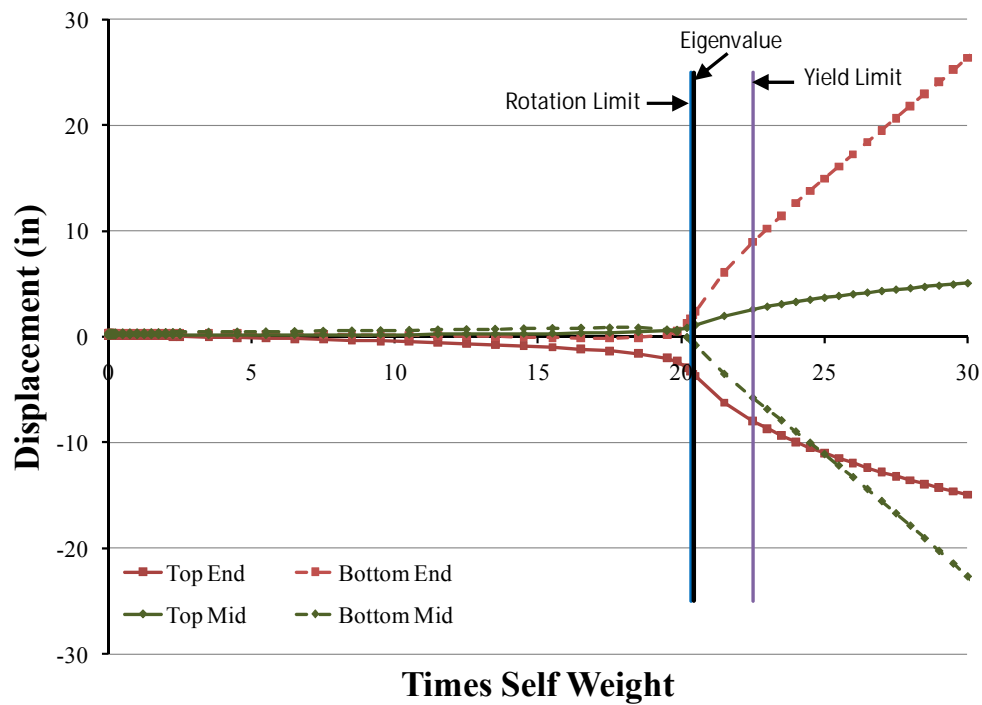


Figure 4.28: Flange Lateral Displacement for Girder with $a/L = 0.25$ $b_f/D = 0.25$ $R = Str.$

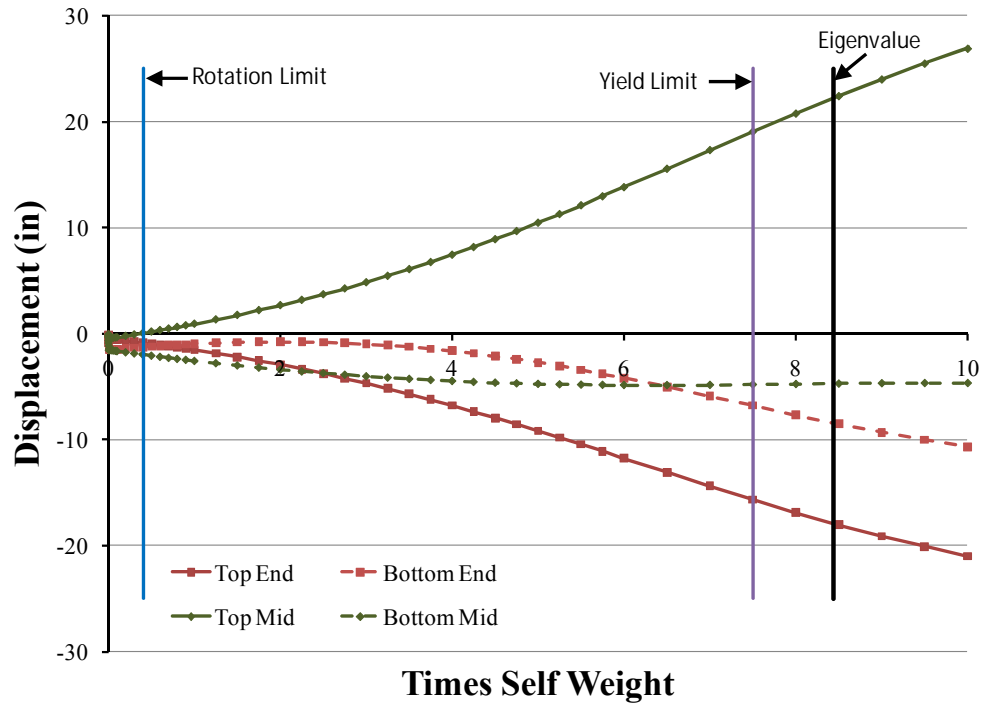


Figure 4.29: Flange Lateral Displacement for Girder with $a/L = 0.2$ $b_f/D = 0.25$ $R = 500'$

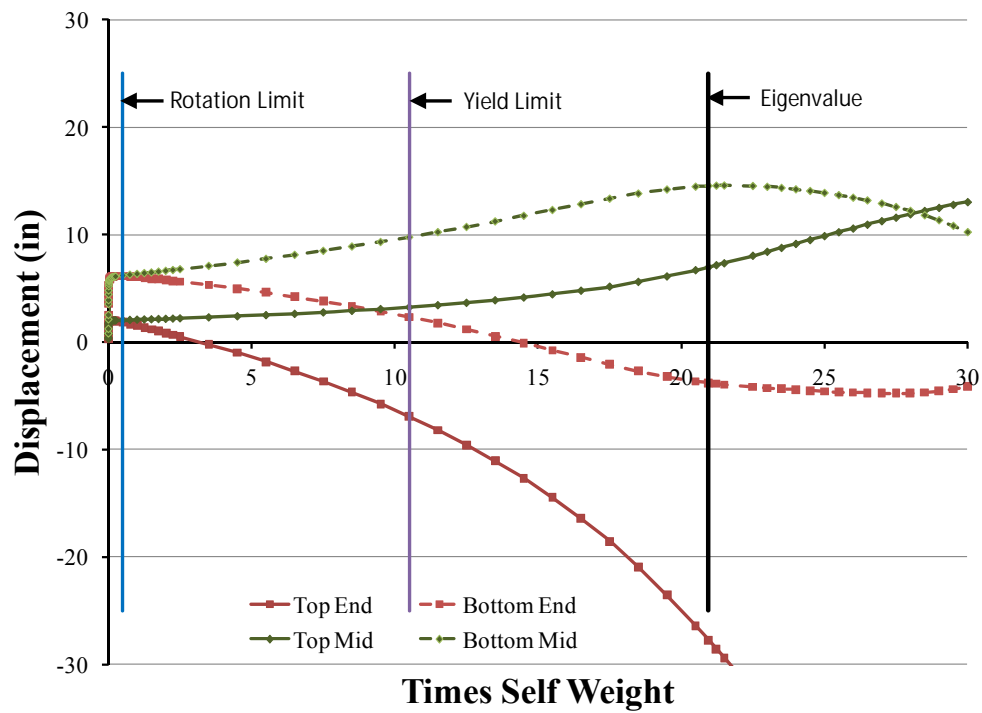


Figure 4.30: Flange Lateral Displacement for Girder with $a/L = 0.25$ $b_f/D = 0.25$ $R = 500'$

The straight girder systems shown in Figures 4.27 and 4.28 generally behave as expected from an eigenvalue analysis. The girders deflect very little until they approach the eigenvalue buckling load and then diverge quickly afterwards. This indicates that the eigenvalue provides a good estimate of the buckling capacity of straight girders. On the contrary, results for the girders with significant curvature shown in Figures 4.29 and 4.30 experience substantial deformations immediately with the rotation limit quickly reached. In both of the later cases the rotation limit is reached then the yield limit and finally the eigenvalue. This would indicate that the eigenvalue is an unconservative estimate for the limiting capacity of highly curved girders. It should be noted that for Figure 4.30 the girder is lifted such that an initial rigid body rotation occurs and thus the additional rotation necessary to reach a limit is relatively small.

The most important finding from all of the analytical cases is that the rotation limit controlled for most curved I-girders. The results from these studies indicate the importance of controlling girder rotation during lifting. The following section provides an overview of analytical expressions that were developed as part of this study for predicting the rigid body rotation for curved girders with various lifting locations.

4.4 Curved I-Girder Deformation Behavior during Lifting

4.4.1 Introduction

Feedback from experts in erection practices, field test results, as well as solutions from analytical models discussed earlier in this chapter demonstrated the importance of girder rotations during lifting of curved girders. Girder rotations can be divided into the rigid body rotation and the cross sectional twist. For straight girders and mildly curved girders, the rotational behavior is of significantly less of a concern and the results of a linear eigenvalue buckling analysis will sufficiently predict the lifting behavior. The buckling of a non-prismatic straight girder can be approximated by applying Timoshenko's lateral torsional buckling equation and modifying it with an appropriate C_b factor given by Farris (2008). Nevertheless, engineers should consider all possible limit states when evaluating a girder during lifting. Possible limit states include both strength and serviceability limit states. The recommended strength limit state from this study is half the steel yield strength ($F_y/2$). This would prevent yielding during the construction by the combination of lifting stresses and residual stresses. The serviceability limit is less definitive with the controlling factor being ease of construction. To quantify this rotational limit a nationwide survey was conducted of contractors, inspectors, and engineers regarding typical practices in the industry. This was described earlier in this chapter and a conclusion that an end rotation of 1.5 degrees was an acceptable limit. For curved girder the serviceability limit state controls the behavior for most cases and thus it was imperative to derive an analytical approach to predict the behavior of curved I-girders during lifting.

The rotational behavior of curved girders during lifting has two components; the rigid body rotation (θ_{rigid}) and the cross sectional twist (θ_{twist}). The rigid body rotation is a function of the girder geometry and the lifting locations and is independent of the girder stiffness. The cross sectional twist must reflect both the St. Venant and Warping torsional stiffness components. While there are exact solutions to the torsion of open sections that reflect specific boundary conditions and applied loading, there is not a general solution available due to the high variability. It was therefore necessary to find an approximate solution to the twist of an open section subjected to nonuniform torque. Based upon a search of the literature a 1-D two node, 2 degree of freedom per node C^1 continuous finite element formulation was found for open

sections subjected to nonuniform torsion (Mohareb and Nowzartash, 2003). A C^1 continuous finite element is a measure of the parametric continuity of the element shape functions at the element boundary. Practically speaking, C^1 continuity indicates that the primary variable and the derivative of the primary variable are continuous at the boundary between two elements. For this particular element the cross sectional angle of twist (ϕ) and the change in the cross sectional angle of twist (ϕ') are continuous at the element boundary. An accurate prediction of the girder behavior can be determined by combining both parts of the girder rotation.

4.4.2 Rigid Body Rotation

For a straight girder, the center of gravity (C.G.) of the segment is located along the girder's center line. For any lifting configuration of the girder there is no eccentricity between the line of support created by the lift points and the center of gravity. Therefore, no rigid body rotation will occur about the longitudinal axis of the girder when it is lifting in the air. Curved girders complicate this situation as the C.G. is shifted from the girder center line which usually has the properties of a circular arc for bridge structures to match the highway geometry. In roadway design it is typical convention to use circular geometry for the horizontal alignment and parabolic geometry for the vertical alignment. Figure 4.31 is a plan view schematic drawing that shows the C.G. location of both a straight and curved girder.

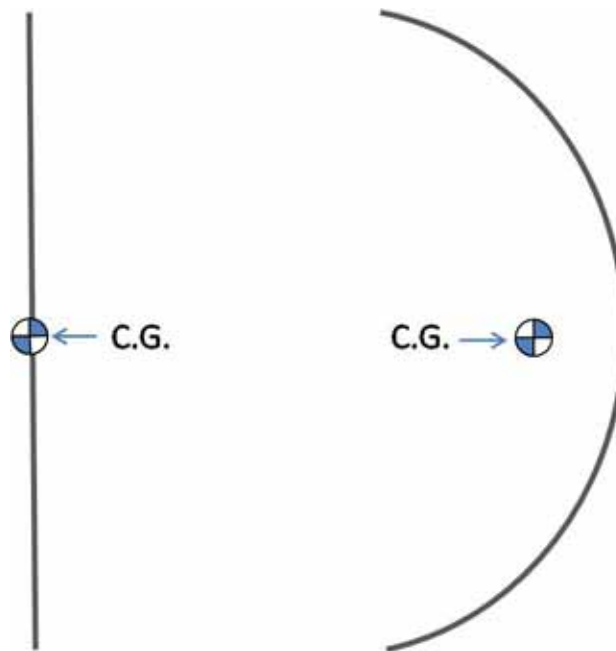


Figure 4.31: Plan View Schematic of Curved and Straight Girder Center of Gravity (Schuh 2008)

The line of support for lifting is defined by a line that passes through the lifting apparatus. Many girders are lifted with a single crane and spreader beam resulting in two lift clamps that define the line of support. Figure 4.32 is a picture of a girder being lifted in this manner.



Figure 4.32: Lifting of a Horizontally Curved Steel I-Girder with 1 Crane & 2 Lift Clamps

For a system in which the center of gravity does not align with the line of support the girder, a rigid body rotation about the line of support will occur until the center of gravity is collinear with the lift clamps. The rotation stabilizes the system by minimizing the total potential energy. Two factors contribute to the rigid body rotation, the center of gravity location (a function of the girder geometry) and the lift locations. The rigid body rotation is not affected by the girder stiffness. To determine the center of gravity, a series of equations were derived for nonprismatic girders with any configuration of cross frames attached to the girder. The cross frame locations and orientation are important because the weights of the braces can lead to significant torsion to the girder segment. Polar coordinates were used in the development with the origin at the center of radius of the girder. Figure 4.33 is a schematic of a curved girder with many of the variables defined for the derivation.

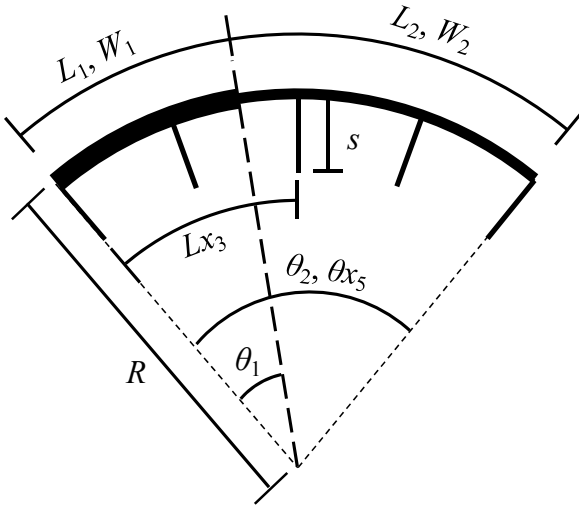


Figure 4.33: Variable Definition for C.G.

L_1 : Length of Section 1
 L_2 : Length of Section 2
 W_1 : Weight per Unit Length of Section 1
 W_2 : Weight per Unit Length of Section 2
 $\theta_0 = 0$
 θ_1 : Internal Angle from the Beginning of the Girder to the End of Section 1
 θ_2 : Internal Angle from the Beginning of the Girder to the End of Section 2
 s : Cross Frame Width
 Lx_3 : Length along the Girder to X-Frame 3
 θ_{x_3} : Internal Angle from the Beginning of the Girder to X-Frame 3
 R : Radius of Curvature of the Girder

Thus it can be shown that the total weight of the girder system can be defined by (4.4) for the general case:

$$Total\ Weight = R \sum_i^n W_i (\theta_i - \theta_{i-1}) + \sum_j^m Wx_j \quad (4.4)$$

Where: n = number of different girder cross sections
 m = number of cross frames
 Wx_j = is the weight of a cross frame

The next step in determining the center of gravity is to calculate the angular distance to the center of gravity (Figure 4.34).

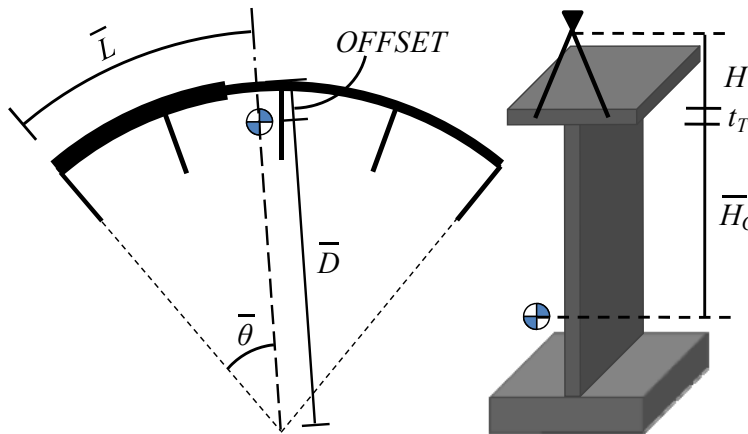


Figure 4.34: C.G. Location

Center of Gravity
 $\bar{\theta}$: Angular Distance to C.G.
 \bar{L} : Length along Girder to C.G.
 \bar{D} : Radial Distance to C.G.
 H : Height of Axis of Rotation above the Top of Girder
 t_T : Top Flange Thickness
 $H_{C.G.}$: Depth to C.G.
 $OFFSET$: Radial Distance of C.G. from the Girder Centerline

The angular distance from the beginning of the girder to the center of gravity is determined by taking a weighted average of the segment's centroids located at the angular center of each cross section. The generalized form of the equation for determining the angular distance to the center of gravity is determined by the following equation:

$$\bar{\theta} = \frac{\frac{R \sum_i^n W_i (\theta_i^2 - \theta_{i-1}^2)}{2} + \sum_j^m W x_j \theta x_j}{R \sum_i^n W_i (\theta_i - \theta_{i-1}) + \sum_j^m W x_j} \quad (4.5)$$

The following equation determines the location along the length of the girders to center of gravity:

$$\bar{L} = \bar{\theta} R \quad (4.6)$$

The radial distance to the center of gravity is determined by taking the weighted average of the girder projected onto the $\bar{\theta}$ radial line. This is shown schematically in Figure 4.35 for the girder in Figure 4.34.

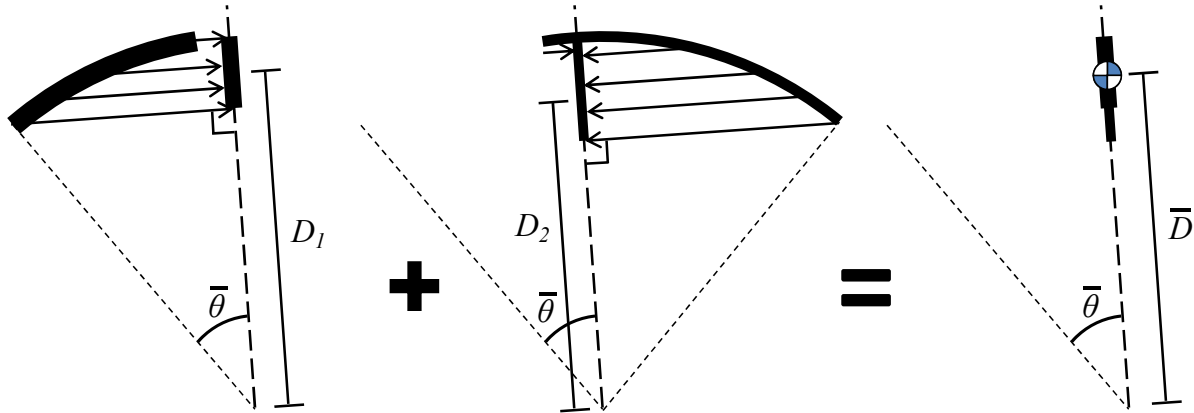


Figure 4.35: Schematic of Method used to Obtain Radial Distance to C.G.

The radial distance can be determined by the generalized form given in (4.7):

$$\bar{D} = \frac{R^2 \sum_i^n W_i [\sin(\theta_i - \bar{\theta}) - \sin(\theta_{i-1} - \bar{\theta})] + (R + \alpha \frac{S}{2}) \sum_j^m W x_j \cos(\theta x_j - \bar{\theta})}{R \sum_i^n W_i (\theta_i - \theta_{i-1}) + \sum_j^m W x_j} \quad (4.7)$$

Where:

$$\alpha = \begin{cases} -1 & \text{if cross frames are only on the inside of the curve} \\ 0 & \text{if cross frames are only on both sides of the girder} \\ 1 & \text{if cross frames are only on the outside of the curved} \end{cases}$$

The offset of the center of gravity from the girder centerline is given by (4.8):

$$OFFSET = R - \bar{D} \quad (4.8)$$

The depth of the center of gravity is determined by taking a weight average of each cross section's C.G. measured from the bottom of the top flange. The generalized form of the equation is given as follows:

$$\bar{H}_{C.G.} = \frac{R \sum_i^n W_i H_{C.G.i} (\theta_i - \theta_{i-1}) + \sum_j^m W x_j \theta x_j}{R \sum_i^n W_i (\theta_i - \theta_{i-1}) + \sum_j^m W x_j} \quad (4.9)$$

To prevent rigid body rotation the line of support must intersect the center of gravity defined by the previous expressions. There are an infinite number of lines that would intersect the C.G. as shown in Figure 4.36. However, assuming a single crane is used to lift the segment, rotational stability of the spreader bar necessitates equal vertical forces at the two lift points (Figure 4.37). This last requirement therefore leads to a unique solution to the problem. This would be the optimum solution with respect to the rigid body rotation.

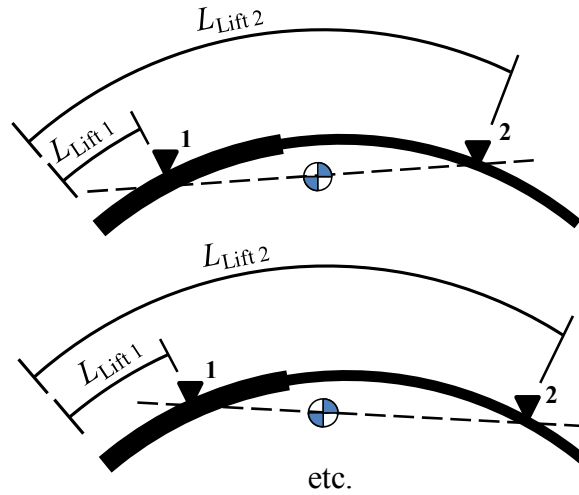
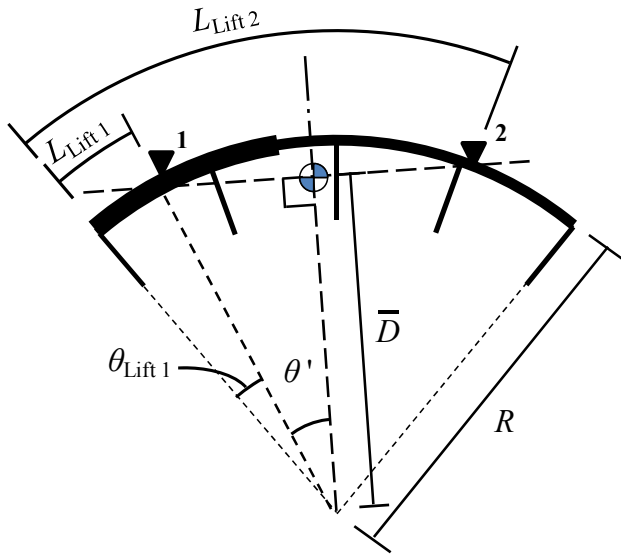


Figure 4.36: Possible Lines of Support that Intersect the C.G.




$L_{Lift\ 1}$: Length along Girder to Lift Pt. 1
 $L_{Lift\ 2}$: Length along Girder to Lift Pt. 2
 $\theta_{Lift\ 1}$: Angular Distance to Lift Pt. 1
 $\theta_{Lift\ 2}$: Angular Distance to Lift Pt. 2
 Center of Gravity
 θ' : Angular Distance from Lift Pts. to Center of Gravity
 \bar{D} : Radial Distance to C.G.
 R : Radius of Curvature of the Girder

Figure 4.37: Zero Rotation/Equal Force Lift Location

The lift points have equal forces if they are an equal distance from the center of gravity. These lift point locations are determined by the following equation and given by (4.13) and (4.14):

$$\cos(\theta') = \frac{\bar{D}}{R} \quad (4.10)$$

$$\theta' = \cos^{-1}\left(\frac{\bar{D}}{R}\right) \quad (4.11)$$

$$\theta_{Lift\ 1} = \bar{\theta} - \theta' \quad (4.12)$$

$$L_{Lift\ 1} = R\theta_{Lift\ 1} \quad (4.13)$$

$$L_{Lift\ 2} = R(\theta_{Lift\ 1} + 2 * \theta') \quad (4.14)$$

The spreader bar is commonly used by a single crane in lifting a girder and can be represented as a chord between the lift points. Figure 4.38 is a picture of a crane using a spreader bar to lift a girder. The practical application of the equations developed in this section allows for the design of the spreader bar length. The expression given in (4.15) gives the length of the spreader bar needed to prevent rotation and minimize the lift clamp capacity requirements.



Figure 4.38: Spreader Bar used by a Single Crane Lifting a Girder

$$\Delta L = 2R \sin(\theta') \quad (4.15)$$

The lift clamp capacity requirements are given by the expression:

$$\text{Lift Load} = \frac{\text{Total Girder Weight}}{2} \quad (4.16)$$

In general, the optimum spreader bar length is not available to the contractor. It is therefore important to calculate the rigid body rotation for a given girder and spreader bar length.

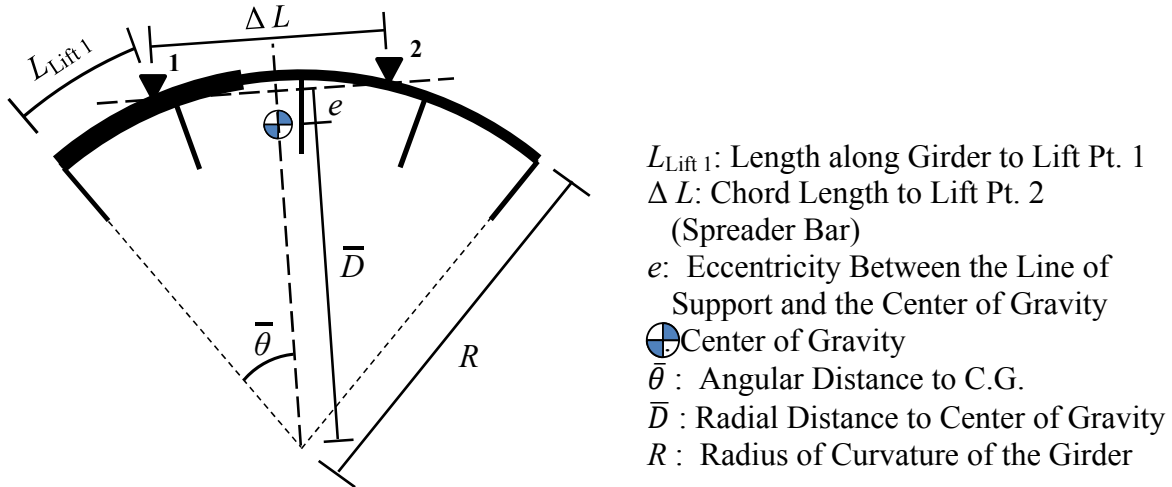


Figure 4.39: Predicted Rotation and Lift Reactions

The eccentricity of the line of support and the center of gravity must be determined. This is accomplished by giving coordinate locations for the three critical points: lift clamp 1, lift

clamp 2, and the center of gravity. Then a formula located in many text as well as the website mathworld.wolfram.com is utilized to determine the minimum distance of the center of gravity from the line of support (eccentricity). Equations (4.17) - (4.20) define the coordinates and (4.21) calculates the eccentricity:

$$L_{Lift\ 1}: (x_1, y_1) = \left(R \sin\left(\frac{L_{Lift\ 1}}{R}\right), R \cos\left(\frac{L_{Lift\ 1}}{R}\right) \right) \quad (4.17)$$

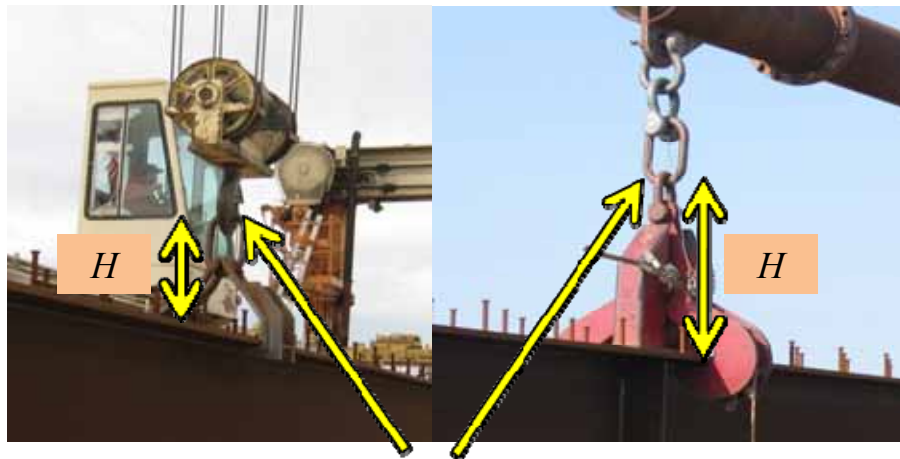
$$\Delta L_{Arc\ Length} = 2R \sin^{-1}\left(\frac{\Delta L}{2R}\right) \quad (4.18)$$

$$L_{Lift\ 2}: (x_2, y_2) = \left(R \sin\left(\frac{L_{Lift\ 1} + \Delta L_{Arc\ Length}}{R}\right), R \cos\left(\frac{L_{Lift\ 1} + \Delta L_{Arc\ Length}}{R}\right) \right) \quad (4.19)$$

$$C. G.: (x_0, y_0) = (R \sin(\bar{\theta}), R \cos(\bar{\theta})) \quad (4.20)$$

$$e = \frac{|(x_2 - x_1)(y_1 - y_0) - (x_1 - x_0)(y_2 - y_1)|}{\sqrt{(x_2 - x_1)^2 + (y_2 - y_1)^2}} \quad (4.21) \quad (\text{mathworld.wolfram.com})$$

The girder lift tests that were performed at Hirshfeld, provided valuable information about the rigid body rotational behavior of the girders. A curved girder segment will generally rotate about the top of the lifting clamps as depicted in Figure 4.40. The axis of rotation's distance of above the top of the girder is denoted by (H) A full definition and complete parametric study of the effect of H on the rotation and stability of curved girders is given in Schuh (2008). This parameter can be defined by the location of the lifting apparatus that is free to rotate as shown, but from calculation purposes the smaller the assumed H the more conservative. Two feet or 24 inches is a practical yet conservative estimate for the height of the axis of rotation for situations where the engineer has no information regarding the lifting apparatus. Figure 4.41 provides a schematic of the rigid body rotation.



Assumed Axis of Rotation

Figure 4.40: Approximating the Height of the Axis of Rotation (Schuh 2008)

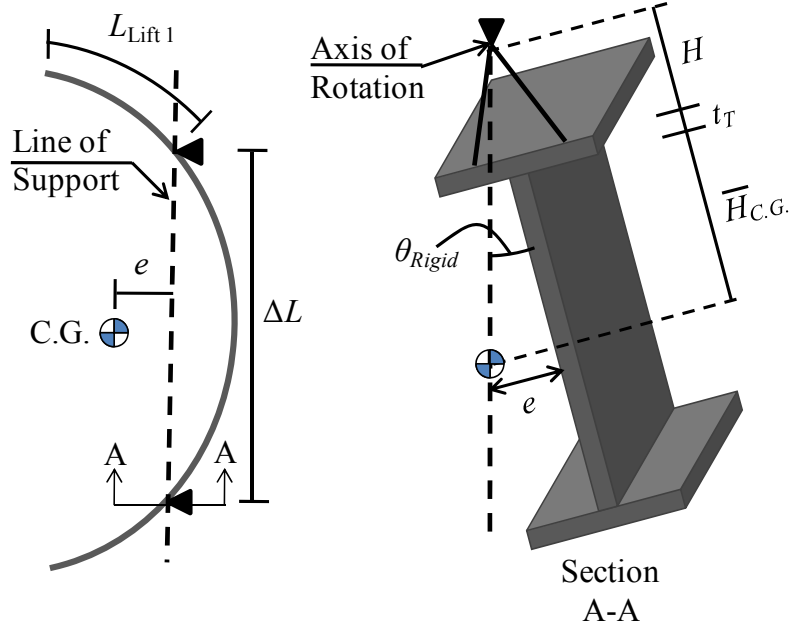


Figure 4.41: Schematic of the Rigid Body Rotation

For a given height of the access of axis of rotation and CG location, the rigid body rotation of the girder is given by the following expression:

$$\theta_{Rigid} = \tan^{-1} \left(\frac{e}{H + t_T + \bar{H}_{C.G.}} \right) \quad (4.22)$$

The lift clamp reactions are calculated by their relative distance from the girder's center of gravity. The equation that calculated these reactions are given by (4.23)–(4.24). These equations assume that the lifting apparatus acts independently as would be the case for two cranes lifting a girder, but for a single girder with a spreader bar the lift clamp reactions must be equal or the girder will rotate along the length. Thus for a single crane the location of the lifting points must be determined using a trial and error procedure.

$$R_{Lift 1} = Total Weight * \frac{(L_{Lift 2} - \bar{L})}{(\Delta L_{Arc Length})} \quad (4.23)$$

$$R_{Lift 1} = \left[R \sum_i^n W_i (\theta_i - \theta_{i-1}) + \sum_j^m W x_j \right] \frac{(L_{Lift 2} - \bar{L})}{(\Delta L_{Arc Length})} \quad (4.24)$$

$$R_{Lift 2} = Total Weight * \frac{(\bar{L} - L_{Lift 1})}{(\Delta L_{Arc Length})} \quad (4.25)$$

$$R_{Lift 2} = \left[R \sum_i^n W_i (\theta_i - \theta_{i-1}) + \sum_j^m W x_j \right] \frac{(\bar{L} - L_{Lift 1})}{(\Delta L_{Arc Length})} \quad (4.26)$$

4.4.3 Cross Sectional Twist

The second part of the rotational behavior of curved girders is the cross sectional twist due to the applied torsion induced by the girders own self weight. The I-girder is an open section that often has a relatively low St. Venant torsional stiffness. The warping stiffness is sensitive to both the support conditions as well as the length of the segment. A schematic of the induced stresses resulting from a torsional load on an I-girder is provided in Figure 4.42.

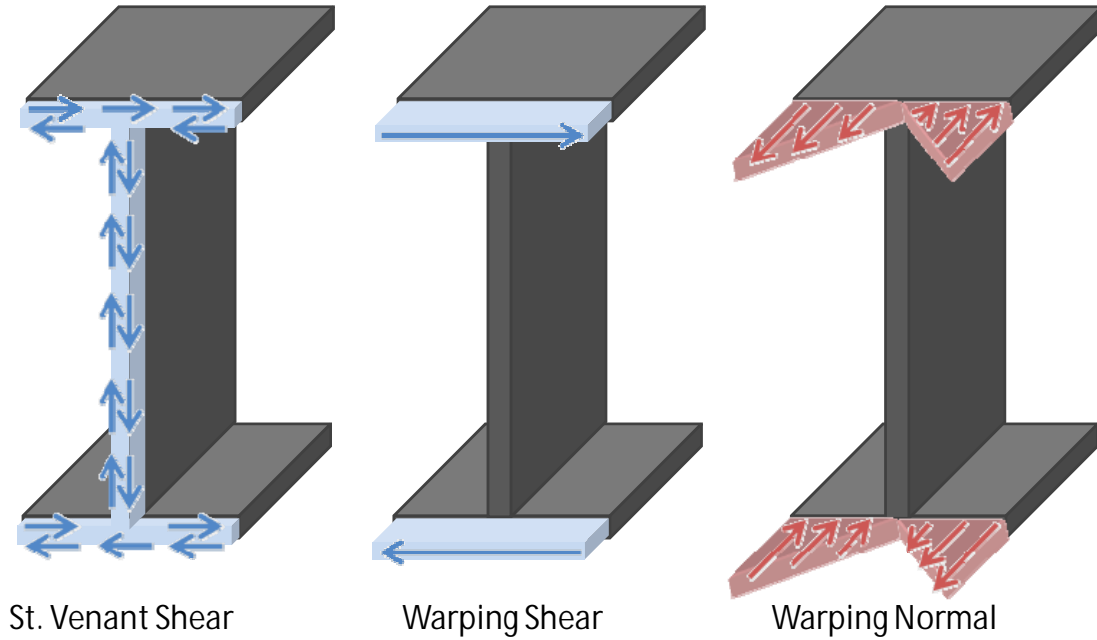


Figure 4.42: Torsion Induced Stress

For any section, the torsion is resisted by St. Venant shear stresses (T_{SV}) and warping restraint (T_W) and therefore the sum of the two must be equal to the total torsion applied to the cross section as shown in (4.27).

$$T(z) = T_{SV}(z) + T_W(z) \quad (4.27)$$

Where:

$$T_{SV}(z) = GJ\varphi'(z) \quad (4.28)$$

$$T_W(z) = EC_W\varphi'''(z) \quad (4.29)$$

Thus the basic differential equation for torsion is given by (4.30):

$$\frac{T(z)}{EC_W} = \frac{1}{k^2} \varphi' + \varphi''' \quad (4.30)$$

Where:

$$k = \sqrt{\frac{EC_w}{GJ}} \quad (4.31)$$

The general solution to the differential equation for torsion is given by (4.32):

$$\varphi(z) = A + B \cosh\left(\frac{z}{k}\right) + C \sinh\left(\frac{z}{k}\right) + \varphi_p(z) \quad (4.32)$$

$\varphi(z)$ is the general solution to the nonhomogenous differential equation for torsion. The constants A, B, and C are determined by the boundary condition of the problem (Engelhardt 2008). The $\varphi_p(z)$ term is the particular solution of the differential equation and depends on the applied distributed twisting moments, $t(z)$, applied to the beam and is given as (Mohareb and Nowzartash 2003):

$$t(z) = EC_w \varphi_p^{iv} - GJ \varphi_p'' \quad (4.33)$$

For specific boundary conditions and loading cases AISC has summarized the solution of the differential equation and given guides for design (AISC 2003). However, for the general case there is no exact solution and thus an approximate solution provides an alternative. A search of the literature revealed a one dimensional, two node, 2 degree of freedom per node C^1 continuous finite element formulation (Mohareb and Nowzartash, 2003). The expression is applicable for open sections subjected to nonuniform torsion such as the case with an I-section girder segment during lifting. By utilizing this formulation a reasonable approximation of the cross sectional twist of a curved I-girder during lifting could be achieved.

The formulation utilizes the following standard finite element equation:

$$[K_e]\{\varphi\} = \{G_{eFE}\} + \{G\} \quad (4.34)$$

Where $[K_e]$: Exact stiffness matrix

$\{\varphi\}$: Nodal displacements (i.e., nodal rotation and change of rotation)

$\{G_{eFE}\}$: Exact nodal fix end forces

$\{G\}$: External nodal forces (applied torques)

The stiffness matrix $[K_e]$ is derived from the solution given by Mohareb and Nowzartash (2003). The nodal fix end forces, $\{G_{eFE}\}$ are calculated by integrating the product of the shape functions $\{N_i(z)\}$ and the applied distributed twisting moment $t(z)$ as shown in (4.35).

$$\{G_{eFE}\} = \int_{z=0}^{z=l} \{N_i(z)\} t(z) dz \quad (4.35)$$

Where the element shape functions ($N_i(z)$) are given by Mohareb and Nowzartash (2003). The applied distributed twisting moment ($t(z)$) is the distribution of forces on the girder that cause the nonuniform torque. Physically it is similar to a shearing force that causes a change in the bending moment of a beam and thus it can similarly be calculated by taking the derivative of the moment diagram. For this particular case the distributed twisting moment is calculated by taking the derivative the torsional moment diagram.

Calculating the Torsional Moment Diagram

The torsional moment diagram is similar to a bending moment diagram, but it is a function of the torque applied to the cross section as a function of the length. To obtain the diagram the girder is “cut” and equilibrium is found between the applied loads and the internal forces. The torsion applied to the cross section is equal to the product of the applied loads and the eccentricity of the load and the cross sectional shear center. However, unlike straight girders these girders are curved in the 2-D plan view space. To calculate the eccentricity of the applied load from the cross sectional shear center at the “cut” X, a line tangent to the girder’s curve at the “cut” is drawn. The eccentricity is the perpendicular distance of the applied load from the tangent line. Figure 4.43 is a schematic of this basic concept which utilizes similar triangles to evaluate the eccentricity.

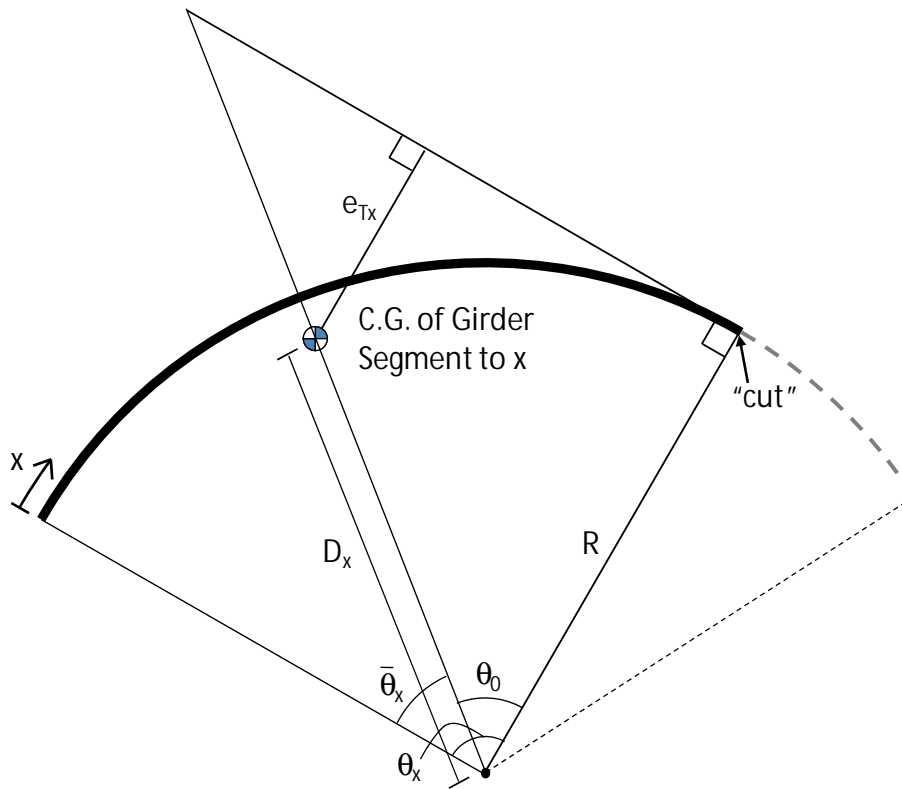


Figure 4.43: Basic Idea for Calculating Torsion Diagram

Where:

x : Length along Girder

D_x : Radial Distance to C.G. of Segment X

R : Radius of Curvature

θ_x : Angular Distance from the Beginning of the Girder to the “cut”

$\bar{\theta}_x$: Angular Distance from the Beginning of the Girder to the C.G. of the Segment X

e_{Tx} : Eccentricity between C.G. and Tangent Line at the “cut”

The eccentricity is calculated by the following expression:

$$\theta_x = \frac{x}{R} \quad (4.36)$$

$$\theta_o = \theta_x - \bar{\theta}_x \quad (4.37)$$

$$e_{Tx} = \left(\frac{R}{\cos \theta_o} - D_x \right) \cos \theta_o \quad (4.38)$$

The concept can be expanded to consider the general case. In general, the girder experiences a rigid body rotation calculated by (4.22). In a plan view as the girder rotates the lift reactions will not be on the same plan view arc of the girder as the shear center. The shear center is a geometric property of the cross section and is shown schematically in Figure 4.44.

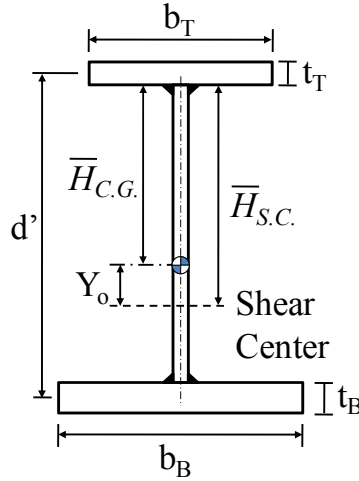


Figure 4.44: Shear Center of a Plate Girder

The equation to calculate the shear center can be found in a variety of sources including (CISC 2002) and shown in (4.39)–(4.41).

$$\alpha = \frac{1}{\left(1 + \left(\frac{b_T}{b_B} \right)^3 \left(\frac{t_T}{t_B} \right) \right)} \quad (4.39)$$

$$\bar{H}_{S.C.} = \alpha d' - \frac{t_T}{2} \quad (4.40)$$

$$Y_o = \bar{H}_{C.G.} - \bar{H}_{S.C.} \quad (4.41)$$

In addition to the eccentricity of the girder's center of gravity from the line of support, it is also necessary to evaluate the rigid body rotation. The rigid body rotation produces an eccentricity of the cross sectional center of gravity and cross sectional shear center from the line of support. The eccentricities of both the center of gravity and shear center are not constant for singly-symmetric girders. Figure 4.45 is a schematic of this concept. Equations (4.42)–(4.44) are

equations that provide these eccentricities with respect to the originally calculated eccentricity (e) calculated by (4.21).

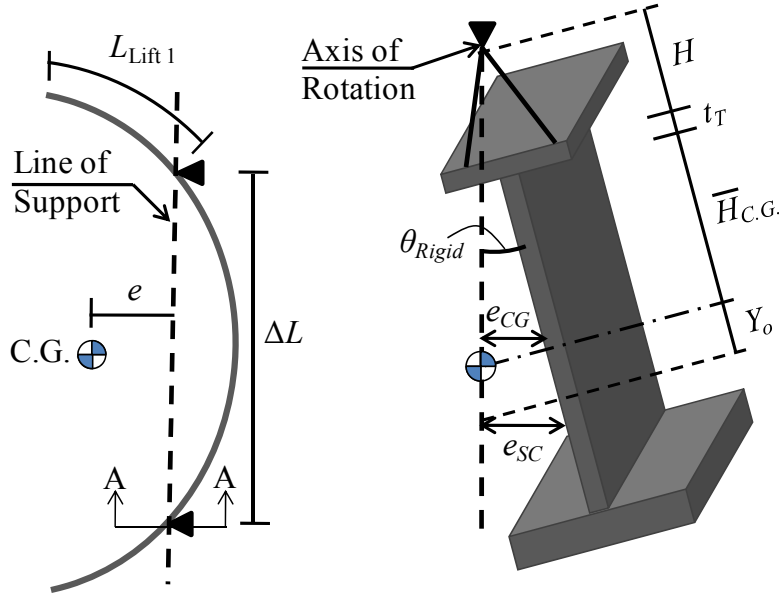


Figure 4.45: Center of Gravity Eccentricity and Shear Center Eccentricity

$$e_{CGi} = e \frac{(H + t_T + H_{CGi})}{(H + t_T + \bar{H}_{CG})} \quad (4.42)$$

$$e_{SCj} = e \frac{(H + t_T + H_{SCj})}{(H + t_T + \bar{H}_{CG})} \quad (4.43)$$

$$e_{Yoj-i} = e_{SCj} - e_{CGi} \quad (4.44)$$

The remaining derivation can be found in the dissertation by Stith (2010). The torque applied to the girder along its length is the sum of the torque applied by the lift clamps and the self weight is and is given by the following expression:

$$T(x) = \sum_i^n (T_{xi}) - T_{Lift1} - T_{Lift2} \quad (4.45)$$

Where:

T_{xi} : Torque applied by the girder self weight from cross section i to the “cut” at X

T_{Lift1} : Torque applied by lift clamp 1 to the “cut” at X

T_{Lift2} : Torque applied by lift clamp 2 to the “cut” at X

n : The number of cross section to the “cut” at X

The typical torsional diagrams for a 125-foot-long prismatic girder lifted at two points are given in the graphs shown in Figure 4.46–4.49. The diagrams are shown with different lift point locations.

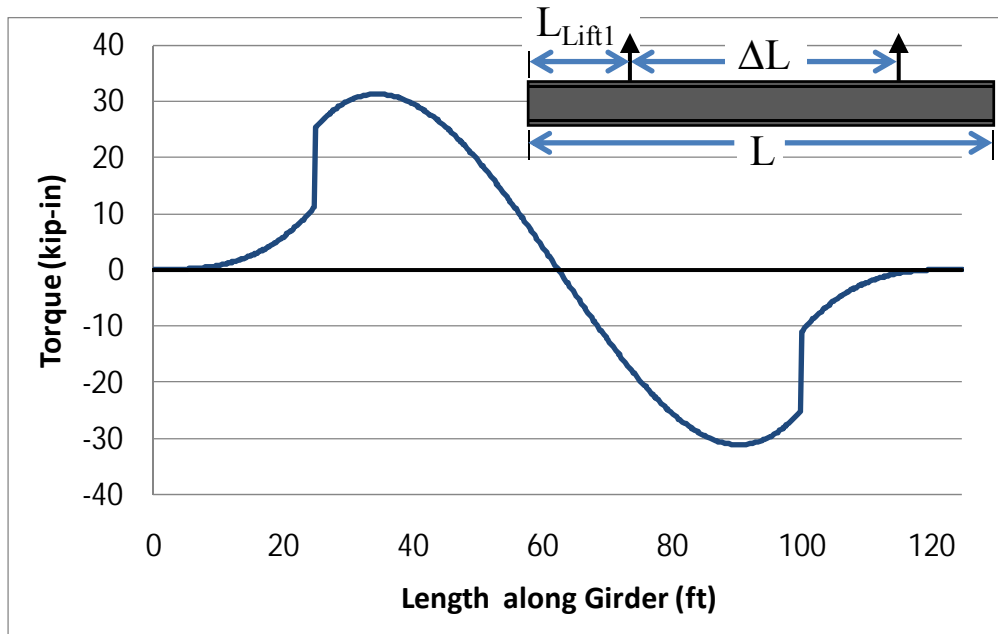


Figure 4.46: Torsion Diagram for $L_{Lift1}/L = 0.2$

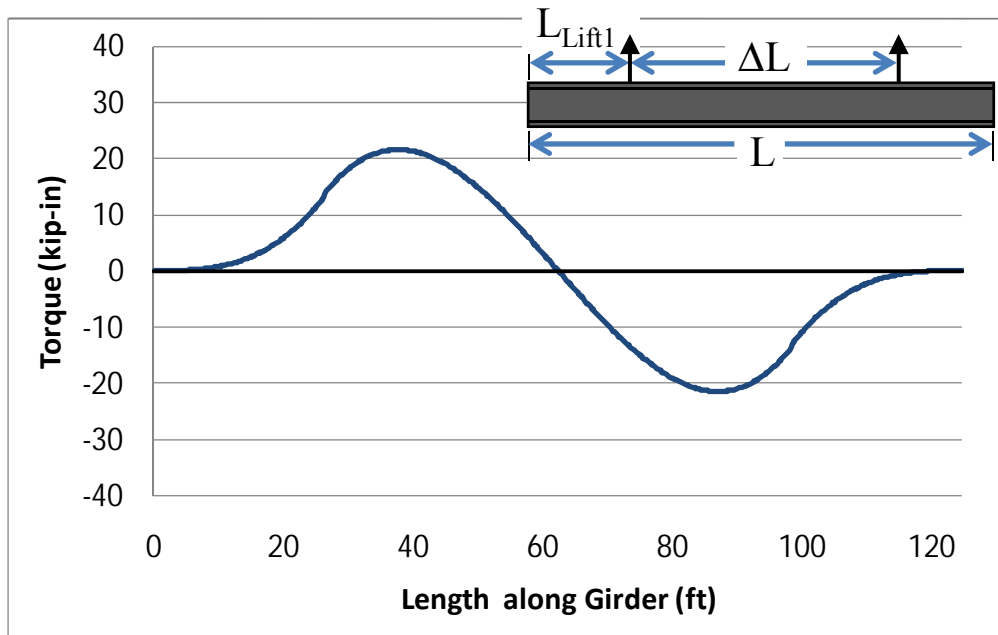


Figure 4.47: Torsion Diagram for $L_{Lift1}/L = 0.211$

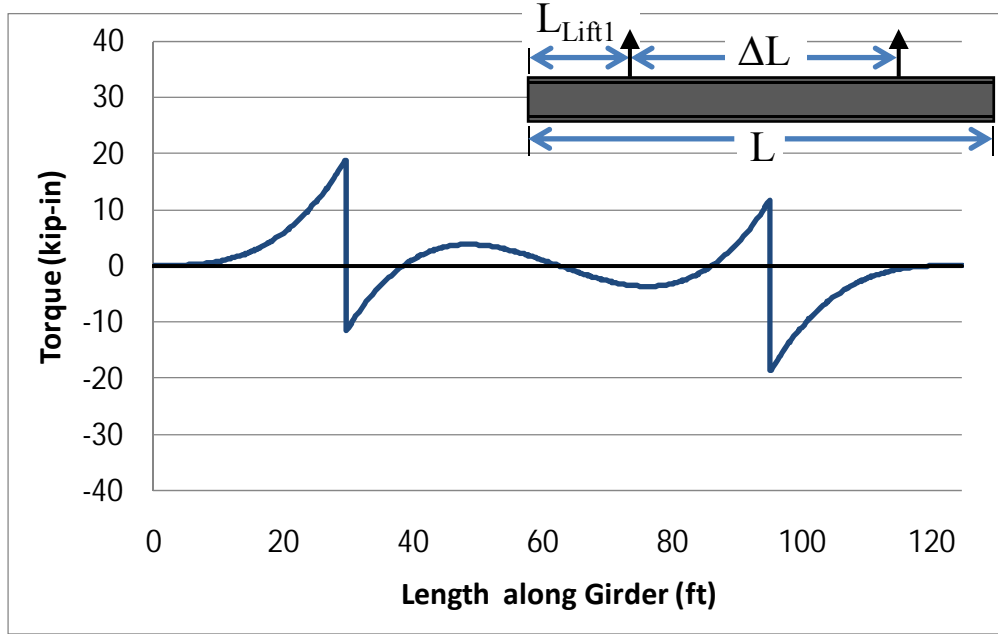


Figure 4.48: Torsion Diagram for $L_{Lift1}/L = 0.238$

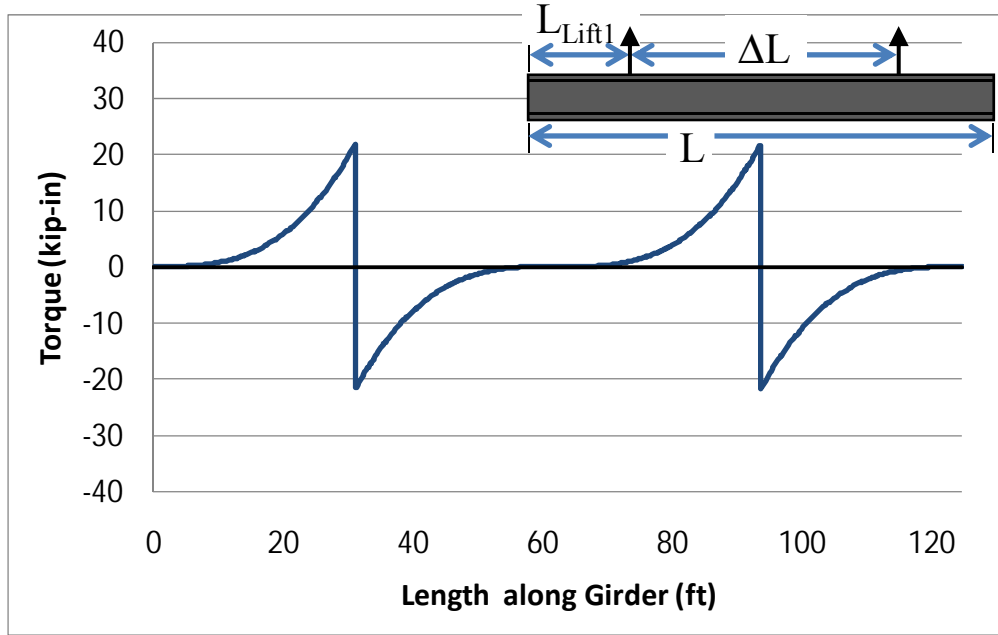


Figure 4.49: Torsion Diagram for $L_{Lift1}/L = 0.25$

Once the distribution of torsion is determined, the derivative of the function can be calculated to obtain the distributed torsion moment. This can be done numerically with many schemes such as central differences, forward difference, or backwards difference. However, to increase the accuracy with a minimal number of elements a higher order approximation of the derivative was chosen called a five-point one dimensional stencil (Numerical Differentiation

www.Wikipedia.org). This numeric differentiation scheme utilizes a quadratic approximation of the derivative. An arbitrarily small h is chosen and the function is given as follows:

$$t(x) = \frac{dT}{dx} = \frac{T(x - 2h) - 8 * T(x - h) + 8 * T(x + h) - T(x + 2h)}{12h} \quad (4.46)$$

With the distributed torsion moment (4.35) can be calculated by means of a numeric integration. The most common numeric integration technique utilizes gaussian quadratures to approximate the integration of a function. The interval of the integration must be transformed from $[a,b]$ to $[-1,1]$ which is accomplished by using (4.47). By evaluating $f(x)$ at the gauss points and multiplying by the appropriate weighting function (4.48) is obtained.

$$\int_a^b f(x)dx = \frac{(b-a)}{2} \int_{-1}^1 f\left(\frac{b-a}{2}x + \frac{a+b}{2}\right) dx \quad (4.47)$$

$$\frac{b-a}{2} \sum_{i=1}^n w_i f\left(\frac{b-a}{2}x_i + \frac{a+b}{2}\right) \quad (4.48)$$

To increase the accuracy of the integration with a minimum of elements five point integration was performed with the following integration points and weighting functions.

| <u>Integration Points</u> | <u>Weighting Function</u> |
|--|--|
| $x_1 = -\frac{\sqrt{245 + 14\sqrt{70}}}{21}$ | $\omega_1 = \frac{322 - 13\sqrt{70}}{900}$ |
| $x_2 = -\frac{\sqrt{245 - 14\sqrt{70}}}{21}$ | $\omega_2 = \frac{322 + 13\sqrt{70}}{900}$ |
| $x_3 = 0$ | $\omega_3 = \frac{128}{225}$ |
| $x_4 = \frac{\sqrt{245 - 14\sqrt{70}}}{21}$ | $\omega_4 = \frac{18 + 13\sqrt{30}}{36}$ |
| $x_5 = \frac{\sqrt{245 + 14\sqrt{70}}}{21}$ | $\omega_5 = \frac{322 - 13\sqrt{70}}{900}$ |

The self weight of the girder was decomposed into components as a result of the rigid body motion and the vertical and out-of-plane displacements were solved simultaneously when solving the cross sectional twist approximation. The out-of-plane displacement alters the location of the center of gravity slightly and thus the rigid body rotation can be recalculated providing additional accuracy of the behavior.

4.4.4 Using L/b_f Ratios

Designers use a series of established guidelines based on experience to ensure stability while handling curved steel I-girders during construction. One of the most well known rules of thumb is to limit the girder length to flange width (L/b_f) ratio to less than 85. The L/b_f limit of 85 was first used by US Steel and is used as a rule of thumb for the stability of straight girders. However, it has been shown in this research project that for curved girders the serviceability deformations are often the critical limit state. The problem with a rule of thumb is that the accuracy will often vary as a function of the geometry or loading condition. As a result, geometric nonlinear FEA studies were conducted to establish the validity of the L/b_f limit of 85 for curved girders with various radii of curvature.

In Figure 4.50, a series of slender girders ($b_f/D = 1/6$) with varying lengths and a constant radius of curvature equal to 1,800 ft are lifted at four different locations ($a/L = 0.20, 0.21, 0.23, 0.25$). The rotations are monitored as the loading on the lifted girder is increased in multiples of the girder self weight and the load at which the girder reaches an end rotation of 1.5 degrees is recorded. The results are then displayed in terms of L/b_f ratio vs. the load that caused an end rotation equal to 1.5 degrees.

A similar methodology is used to obtain the results in Figure 4.51 for a less slender section ($b_f/D = 1/4$) that has a smaller radius of curvature equal to 500 ft.

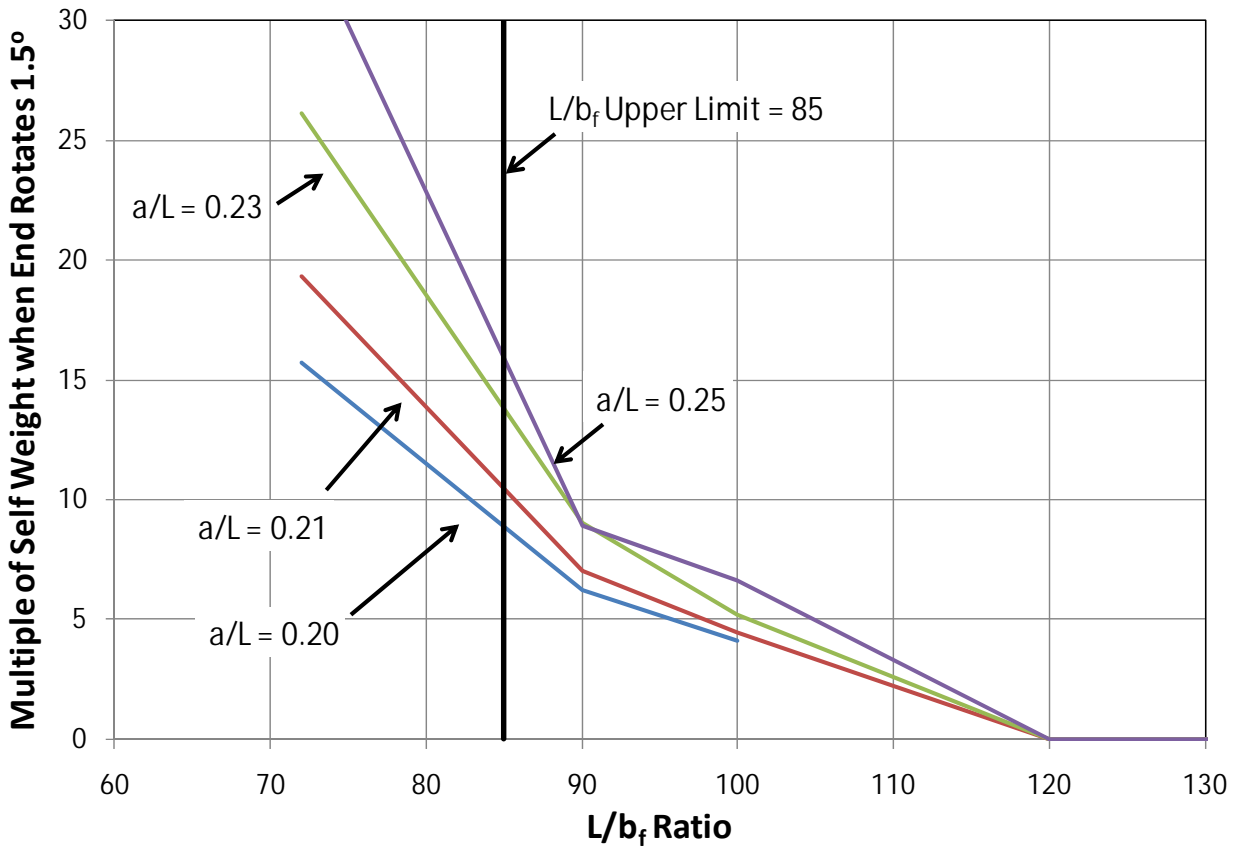


Figure 4.50: Serviceability Limit State [$b_f/D = 1/6$; $R = 1,800$ ft]

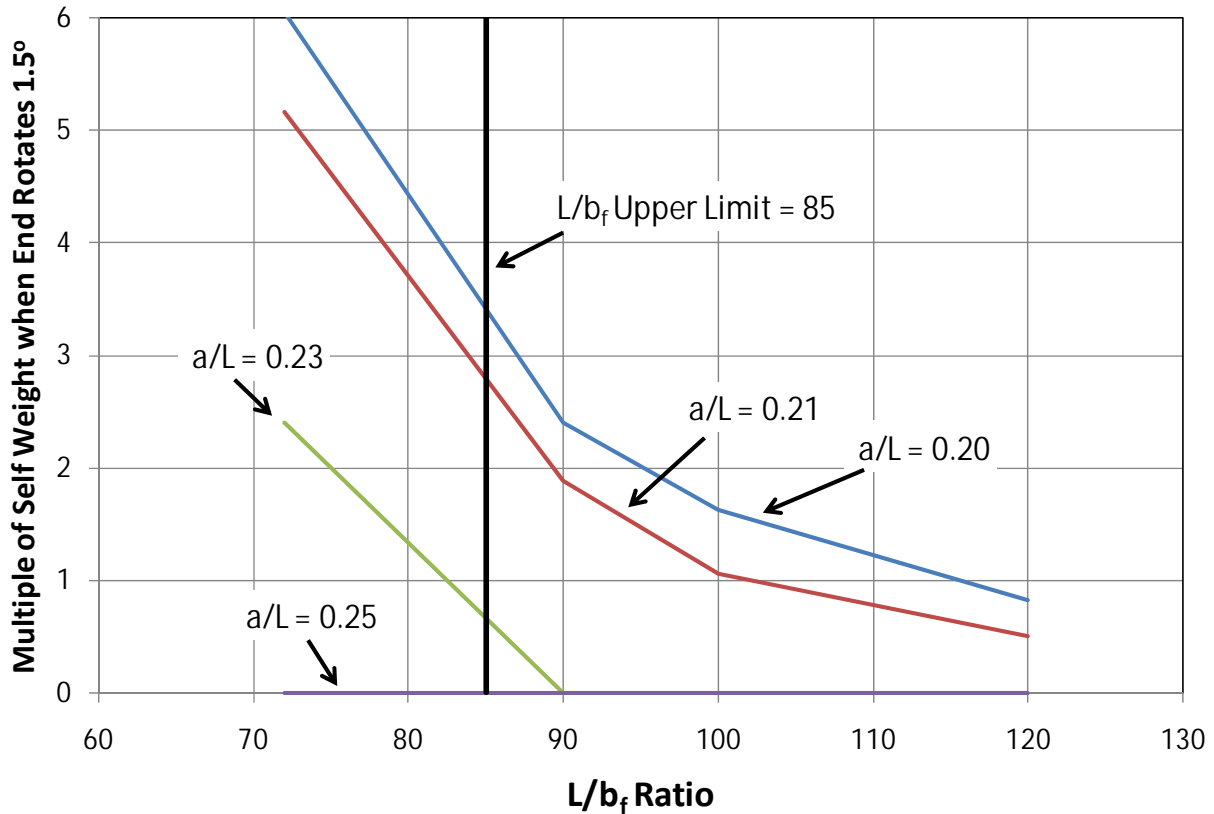


Figure 4.51: Serviceability Limit State [$b_f/D = 1/4$; $R = 500$ ft]

It can be seen in Figures 4.50 and 4.51 that the stability of the system seems to increase by reducing the L/b_f ratio. Yet, the L/b_f ratio is not the only factor that has a significant effect on the stability of the system. As discussed above, the geometry and lifting conditions play a major role in the behavior of curved steel I-girders during lifting. Therefore, even though the girder lifted in Figure 4.50 is more slender ($b_f/D = 1/6$) than the girder lifted in Figure 4.51 ($b_f/D = 1/4$), it takes more load to rotate the end of the girder in Figure 4.50 1.5 degrees because the girder is straighter than the one lifted in Figure 4.51. In addition, it can be seen in Figure 4.51 that when lifting the girder at a location of $a/L = 0.25$, that for all L/b_f ratios the girder reaches the 1.5 degree rotational limit with seemingly no load on it. This is because by lifting this girder at $a/L = 0.25$, the rigid body rotations will always be greater than 1.5 degrees.

The L/b_f ratio provides reasonable control over the behavior in straight girders; however the accuracy for curved girder is dependent on the degree of curvature and the lifting location. Instead of endorsing this rule of thumb for particular situations, design tools are provided that can be used to estimate the behavior during lifting and throughout construction.

4.5 UT Lift Spreadsheet

4.5.1 Introduction and Purpose

To facilitate the use of the expressions that were developed in the last section, an Excel spreadsheet program was developed named UT Lift. The analytical tool is capable of predicting

the behavior of curved I-girders during lifting. The program allows the user to input information about the girder and then the spreadsheet utilizes the previously mentioned equations and techniques to provide a linear approximation of the girder's deformational behavior during lifting.

The spreadsheet provides a tool that will primarily be used by erectors or erection engineers. The program can be used to determine the ideal location for girder lifting as well as the girder deformations for locations different than the ideal location. The program also provides an indication of the safety of a girder during lifting. The program was developed assuming the girder segment is lifted with one crane and two lift clamps. This is a common lifting technique used in the construction of curved I-girder bridges as shown in Figure 4.52. This lifting scenario is one of the most economical due to the use of a single crane and thus one of the most common scenarios. The program will be conservative if a lifting scenario with more than 2 lifting points is used.



Figure 4.52: Lifting of a Horizontally Curved Steel I-Girder with 1 Crane & 2 Lift Clamps

The spreadsheet has been developed with clearly indicated input cells for information on the lifting geometry and highlighting the calculated results. Green colored cells are designated for input to be given and the blue colored cells highlight the notable calculated results. The current spread sheet allows for the analysis of a girder segment with up to 8 different cross sections and 18 cross frames attached.

4.5.2 Girder Input Sheet

The spread sheet is divided into four separate tabs. The first tab (**Girder Input**) contains two pages which are dedicated to the required geometric properties of the girder and the cross frame information including:

- 1) the number of different cross sections along the girder,
- 2) the radius of curvature of the girder segment,
- 3) the plate dimensions for each cross section,
- 4) the arc length measured along the girder's centerline of each cross section,
- 5) the number of cross frames attached to the girder segment during lifting,
- 6) the cross frame width,
- 7) the weight of each cross frame,
- 8) the location of the cross frames, and
- 9) whether the cross frame is on the inside of the curve, the outside of the curve, or on both sides of the girder.

Screen shots of these pages are shown in Figures 4.53 and 4.54.

| | A | B | C | D | E | F | G | H | I | J | K | |
|----|---|-----------|-----------|---|---|---|---|-----------------------------|---|---|---|--|
| 1 | Behavior of Curved Girder During Lifting | | | | | | | | | | | |
| 2 | | | | | L_1 : Length of Section 1 L_2 : Length of Section 2 W_1 : Weight per Unit Length of Section 1 W_2 : Weight per Unit Length of Section 2 $\theta_0 = 0$ θ_1 : Internal Angle from the Beginning of the Girder to the End of Section 1 θ_2 : Internal Angle from the Beginning of the Girder to the End of Section 2 s : Cross Frame Width L_{x3} : Length along the Girder to X-Frame 3 θ_{x3} : Internal Angle from the Beginning of the Girder to X-Frame 3 R : Radius of Curvature of the Girder | | | | | | | |
| 3 | | | | | | | | | | | | |
| 4 | | | | | | | | | | | | |
| 5 | | | | | | | | | | | | |
| 6 | | | | | | | | | | | | |
| 7 | | | | | | | | | | | | |
| 8 | | | | | | | | | | | | |
| 9 | | | | | | | | | | | | |
| 10 | | | | | | | | | | | | |
| 11 | | | | | | | | | | | | |
| 12 | | | | | | | | | | | | |
| 13 | | | | | | | | | | | | |
| 14 | | | | | | | | | | | | |
| 15 | | | | | | | | | | | | |
| 16 | Girder Input: | | | | | | | | | | | |
| 17 | Project : Example Problems | | | | Clear Input | | | User Input | | | | |
| 18 | Girder # : Example Girder 1 | | | | | | | Notable Results | | | | |
| 19 | | | | | | | | | | | | |
| 20 | Number of Cross Sections: | | | | | | | Material Constants: | | | | |
| 21 | NUMSECTIONS = 2 | | | | Girder Scale Factor: | | | E = 29000 ksi | | | | |
| 22 | Radius of Curvature (ft): R | | | | S.F. _{girder} = 1.10 | | | G = 11154 ksi | | | | |
| 23 | R = 1000 ft | | | | | | | p = 490 lbs/ft ³ | | | | |
| 24 | | | | | | | | | | | | |
| 25 | Section 1 | | Section 2 | | | | | | | | | |
| 26 | TFLW | 15 | 15 | | | | | | | | | |
| 27 | TFLT | 1.5 | 2.25 | | | | | | | | | |
| 28 | | | | | | | | | | | | |
| 29 | DEPTH | 72 | 72 | | | | | | | | | |
| 30 | WEBT | 0.625 | 0.625 | | | | | | | | | |
| 31 | | | | | | | | | | | | |
| 32 | BFLT | 1.5 | 2.25 | | | | | | | | | |
| 33 | BFLW | 15 | 15 | | | | | | | | | |
| 34 | | | | | | | | | | | | |
| 35 | | Section 1 | Section 2 | | | | | | | | | |
| 36 | L_i = | 70 | 60 | | | | | | | | | |
| 37 | W_i = | 336.9 | 421.1 | | | | | | | | | |
| 38 | θ_i = | 4.01 | 7.45 | | | | | | | | | |
| 39 | J_i = | 39.61 | 119.77 | | | | | | | | | |
| 40 | C_{wi} = | 1139537 | 1744367 | | | | | | | | | |

Figure 4.53: Screen Shot of UT Lift Girder Geometric Input

| | A | B | C | D | E | F | G | H | I | J | K |
|----|---|-----------|-----------|-----------|-----------|---|-----------|-------|---|---|---|
| 50 | Cross Frame Input: | | | | | | | | | | |
| 51 | Number of Cross Frame Locations: | | | | | Uniform Cross Frame Weights: Constant X-Frame Weight | | | | | |
| 52 | NUMXFRAMES = 7 | | | | | Weight = 250 lbs | | | | | |
| 53 | Cross Frame Width: s | | | | | | | | | | |
| 54 | s = 6.50 ft | | | | | | | | | | |
| 55 | | | | | | | | | | | |
| 56 | Uniformly Spaced Cross Frames: | | | | | All Cross Frames on Inside of Curve, Outside of Curve, or Both | | | | | |
| 57 | Spacing = 20 ft | | | | | Constant X-Frame Spacing | | | | | |
| 58 | Location of the 1 st Cross Frame: | | | | | All I All O All I/O | | | | | |
| 59 | 1st X-Frame Loc. = 0 ft | | | | | | | | | | |
| 60 | | | | | | | | | | | |
| 61 | X-Frame 1 | X-Frame 2 | X-Frame 3 | X-Frame 4 | X-Frame 5 | X-Frame 6 | X-Frame 7 | | | | |
| 62 | $Lx_j =$ | 0 | 20 | 40 | 60 | 80 | 100 | 120 | | | |
| 63 | $Wx_j =$ | 250 | 250 | 250 | 250 | 250 | 250 | 250 | | | |
| 64 | I/O | I/O | I/O | I/O | I/O | I/O | I/O | I/O | | | |
| 65 | $\theta x_j =$ | 0.000 | 1.146 | 2.292 | 3.438 | 4.584 | 5.730 | 6.875 | | | |
| 66 | | | | | | | | | | | |
| 67 | | | | | | | | | | | |
| 68 | | | | | | | | | | | |
| 69 | $Lx_j =$ | | | | | | | | | | |
| 70 | $Wx_j =$ | | | | | | | | | | |
| 71 | I/O | | | | | | | | | | |
| 72 | $\theta x_j =$ | | | | | | | | | | |
| 73 | | | | | | | | | | | |
| 74 | Cross Frame Location along centerline (CL) of the Girder (ft): Lx_j | | | | | | | | | | |
| 75 | Weight of One Cross Frame (lbs): Wx_j | | | | | | | | | | |
| 76 | Inside of Curve, Outside of Curve or Both (I, O, or I/O): I/O | | | | | | | | | | |
| 77 | Internal Angle from Beginning (deg.): θx_j | | | | | | | | | | |
| 78 | | | | | | | | | | | |
| 79 | <div style="display: flex; justify-content: space-around;"> <div> <p>Cross Frames on the Inside: I</p> </div> <div> <p>Cross Frames on the Outside: O</p> </div> </div> | | | | | | | | | | |
| 80 | | | | | | | | | | | |
| 81 | | | | | | | | | | | |
| 82 | | | | | | | | | | | |
| 83 | | | | | | | | | | | |
| 84 | | | | | | | | | | | |
| 85 | | | | | | | | | | | |
| 86 | <div style="display: flex; justify-content: center;"> <p>Cross Frames on Both Sides: I/O</p> </div> | | | | | | | | | | |
| 87 | | | | | | | | | | | |

◀ ▶ 🔍
About Girder Input C.G. & Ideal Lift Calculated Behavior Graphs

Figure 4.54: Screen Shot of UT Lift Girder Cross Frame Input

The project name and the name of the specific girder analyzed can be specified for record keeping purposes. The girder scale factor is multiplied by the girder self weight. This scale factor allows the engineer to match shipping weight if available or accounts for other auxiliary elements (shear studs, stiffeners etc.). The sign convention for the radius of curvature is positive for a right curve looking ahead station from the girders beginning. A “Clear Input” button is

available. Once pressed it will prompt the user to confirm that they want all the input cells to be deleted and it will clear all user input cells. Figure 4.55 is a schematic of a girder cross section with the necessary plate dimensions that include:

- 1) top flange width (TFLW),
- 2) top flange thickness (TFLT),
- 3) web depth (DEPTH),
- 4) web thickness (WEBT),
- 5) bottom flange thickness (BFLT), and
- 6) bottom flange width (BFLW).

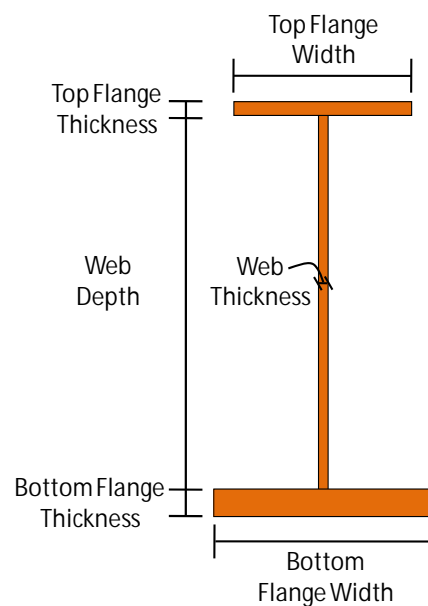


Figure 4.55: Plate Dimensions

The cross frame width is needed to determine the center of gravity of an individual cross frame. The cross frame center of gravity is assumed to be located midway between adjacent girders (girder spacing divide by 2). Therefore, the girder spacing should be specified as the cross frame width. The weight of a cross frame should only include the weight of a single cross frame even if they are located on both sides of the girder for a given location. The cross frames need to be specified as either located on the inside of the curve, on the outside of the curve, or on both sides of the curve for a given cross frame location as shown in Figure 4.56. By selecting “I/O,” the weight will be multiplied by 2 for locations where cross frames are present on both sides of the girder. This is specified for each cross frame location and does not necessarily have to be consistent down the length of the girder. The cross frames locations must be specified in ascending order down the length of the girder. The flexibility of specifying cross frame locations as inside the curve, outside the curve, or both for each individual cross frame would allow an erector to adjust the cross frames that they send up with a segment to help adjust the rigid body rotation if desired.

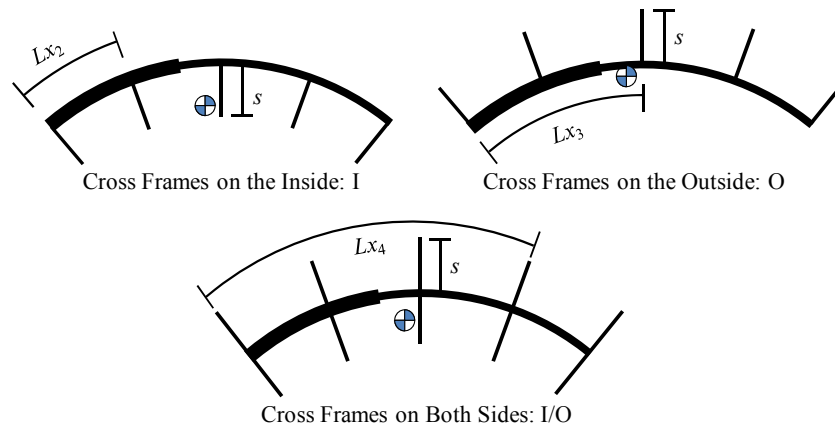


Figure 4.56: Options of Cross Frame Location

For girders with a constant cross frame spacing the “Uniformly Spaced Cross Frame:” section allows the user to specify the cross frame spacing and the first cross frame location. Then the correct input will appear in the cells once the “Constant X-Frame Spacing” button is pressed. There are three buttons: “All I,” “All O,” and “All I/O.” By pressing a button all the cross frames location cells will be propagated with the appropriate value. The program does not require uniform cross frame locations, but these buttons assist users with girders that have constant locations. Once the number of cross sections and the number of cross frames are specified any input located in columns associated with cross sections or cross frames beyond this specified number will be ignored and can be deleted without affecting the analysis.

4.5.3 C.G. & Ideal Lift Sheet

The spreadsheet calculates several useful pieces of information for future calculations and reference as well as comparisons to know information for checking including:

- 1) the total girder length,
- 2) the total girder weight,
- 3) location of the girder segment’s center of gravity,
- 4) the lift clamps location that results in zero rigid body rotation and equal lift clamp forces, and
- 5) the reactions of the lift clamps for the zero rigid body rotation location.

The location of the girder segment’s center of gravity is given as the length along the girder and an offset from the girder centerline. The center of gravity offset is assumed to be on the inside of the curve and thus this direction is considered a positive offset. There are an infinite number of lines that intersect the curve at two points and pass through the center of gravity. However, there exists a lift clamp location that defines a line that results in equal minimized forces and the line passes through the center of gravity. This is optimum with regard to the girder’s rigid body rotation. The reaction for these lift clamps is equal to the total girder weight divided by two. A screen shot of this page is shown in Figure 4.57.

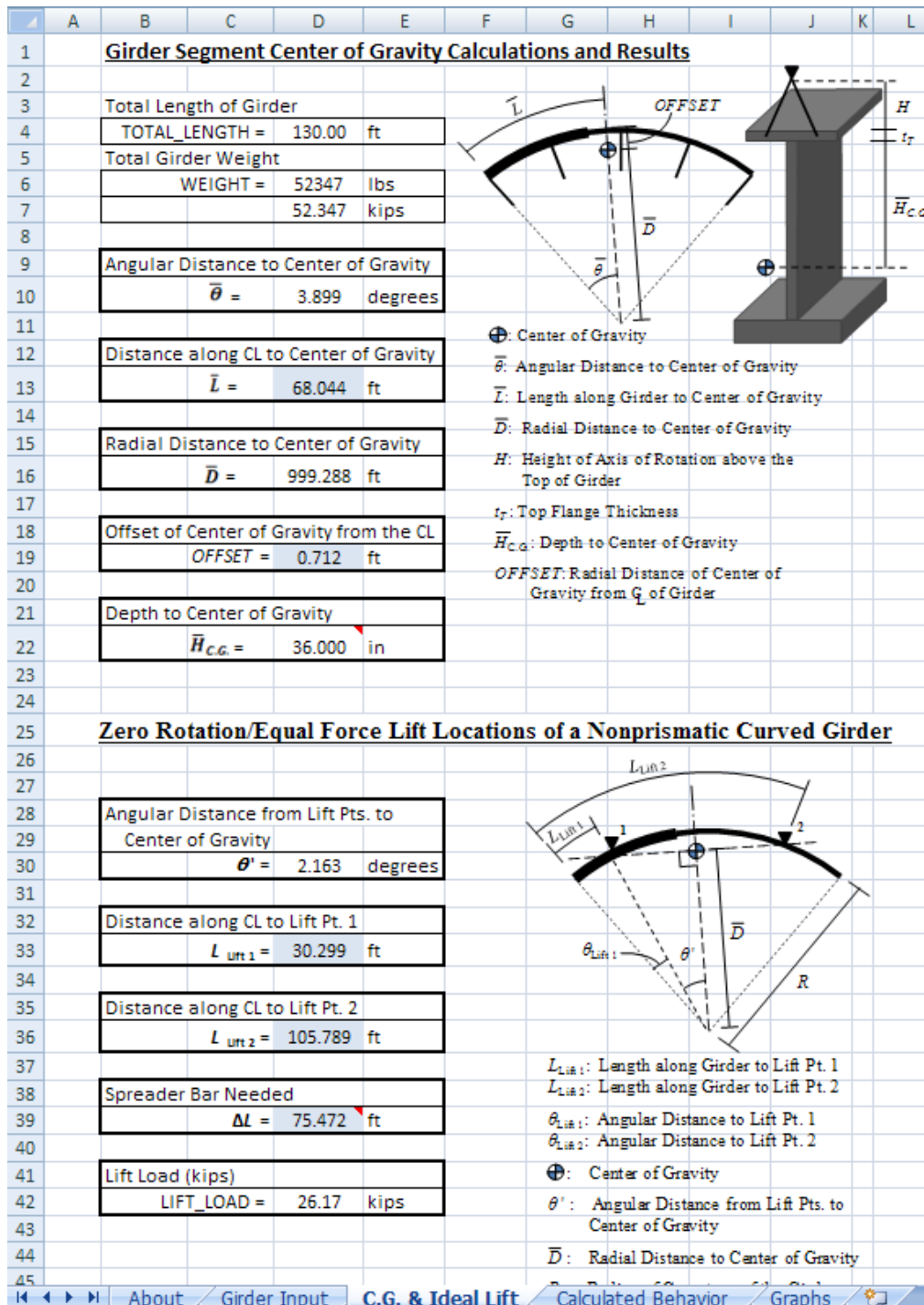


Figure 4.57: Screen Shot of UT Lift C.G. & Ideal Lift Output

4.5.4 Calculated Behavior Sheet

This sheet allows for the behavior of the girder segment lifted at specified locations to be analyzed. This requires the lift clamp locations and the location of the axis of rotation above the top of the girder to be specified by the user. The axis of rotation is the location within the lifting apparatus where rotation is free to occur. For the case of a single crane with two lift clamps

separated by a spreader bar this is the location on the lift clamp that will allow for rotation. Figure 4.58 demonstrates the assumed axis of rotation for two different lift clamps. This height was approximately 30” and has been deemed a reasonable estimate. However, it should be noted that a smaller value will result in larger calculated rigid body rotations or a more conservative estimate.

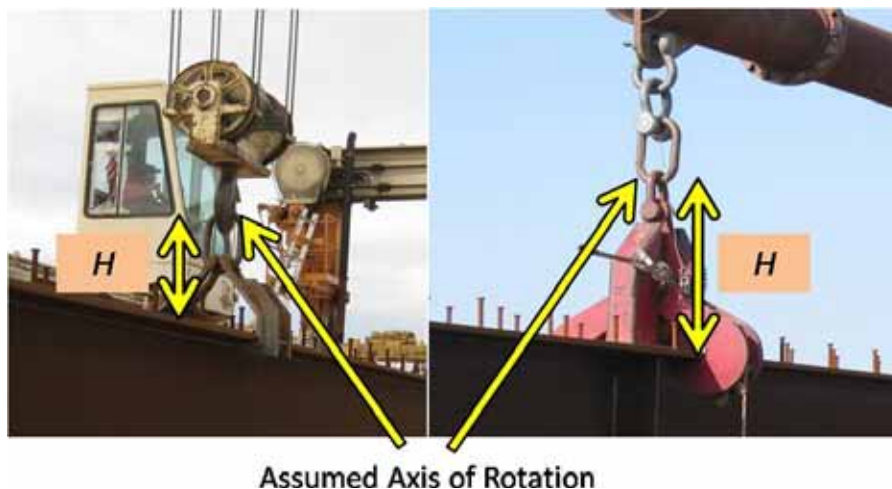


Figure 4.58: Definition of the Height to Axis of Rotation

From the given lift locations the eccentricity of the center of gravity from the line of support is calculated and the subsequent rigid body rotation is given. The reactions of the lift clamps are given and may not be equal as the analysis treats them as independent lift points. For girders lifted with a single crane and a spreader bar, the lift clamp forces must be equal for static equilibrium. A warning is issued for unequal lift forces, but the program will compute an answer even if the forces are not the same. This may be the case for a girder lifted with two cranes. When the “**Calculate Rotation & Stress**” button is pressed, a macro will run that performs the linear finite element analysis discussed previously to approximate the girder’s cross sectional twist.

The results of the analysis are provided on this sheet and include the predicted total rotations and stresses for the lifted girder. The rotations include both the rigid body rotation and an approximation of the cross sectional twist. The given stresses include strong axis bending stresses, weak axis bending stresses, and the warping normal stresses. The maximum stresses are reported at both the lift locations and the midpoint between lift clamps of the girder. The maximum rotations are reported at both the girder ends and the midpoint between lift clamps. The spreadsheet also provides an estimate of the critical buckling load as determined from modified Timoshenko’s lateral torsional buckling equation. The modification and full background of the parameters can be found in Schuh (2008) and Farris (2008). The summary of this work was provided previously in this chapter. The critical buckling load rarely controls the design for lifting of curved girders, but is a reasonable estimate for the lifting of straight girders. Screen shots of these pages are shown in Figures 4.59 and 4.60.

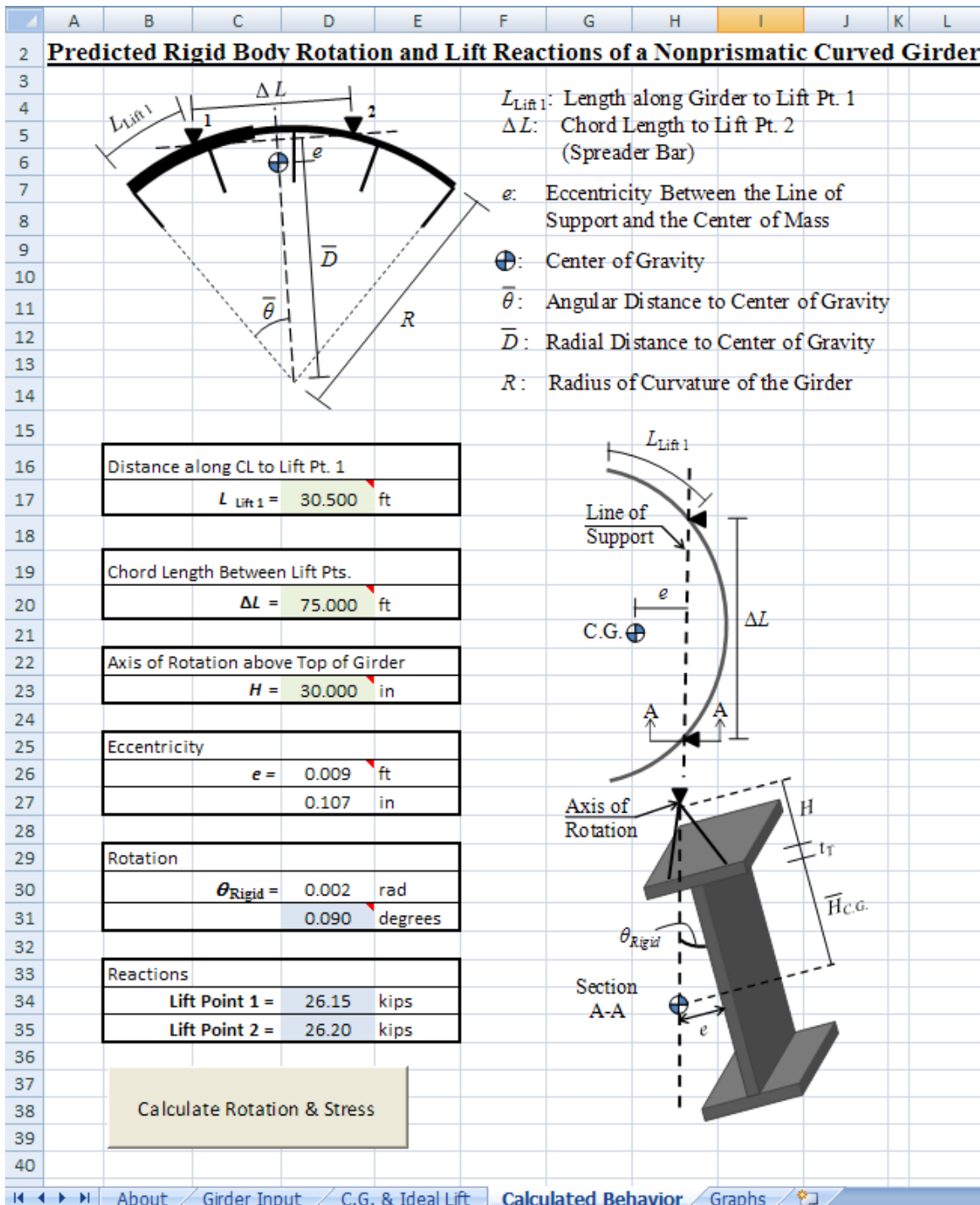


Figure 4.59: Screen Shot of UT Lift Calculated Behavior Input

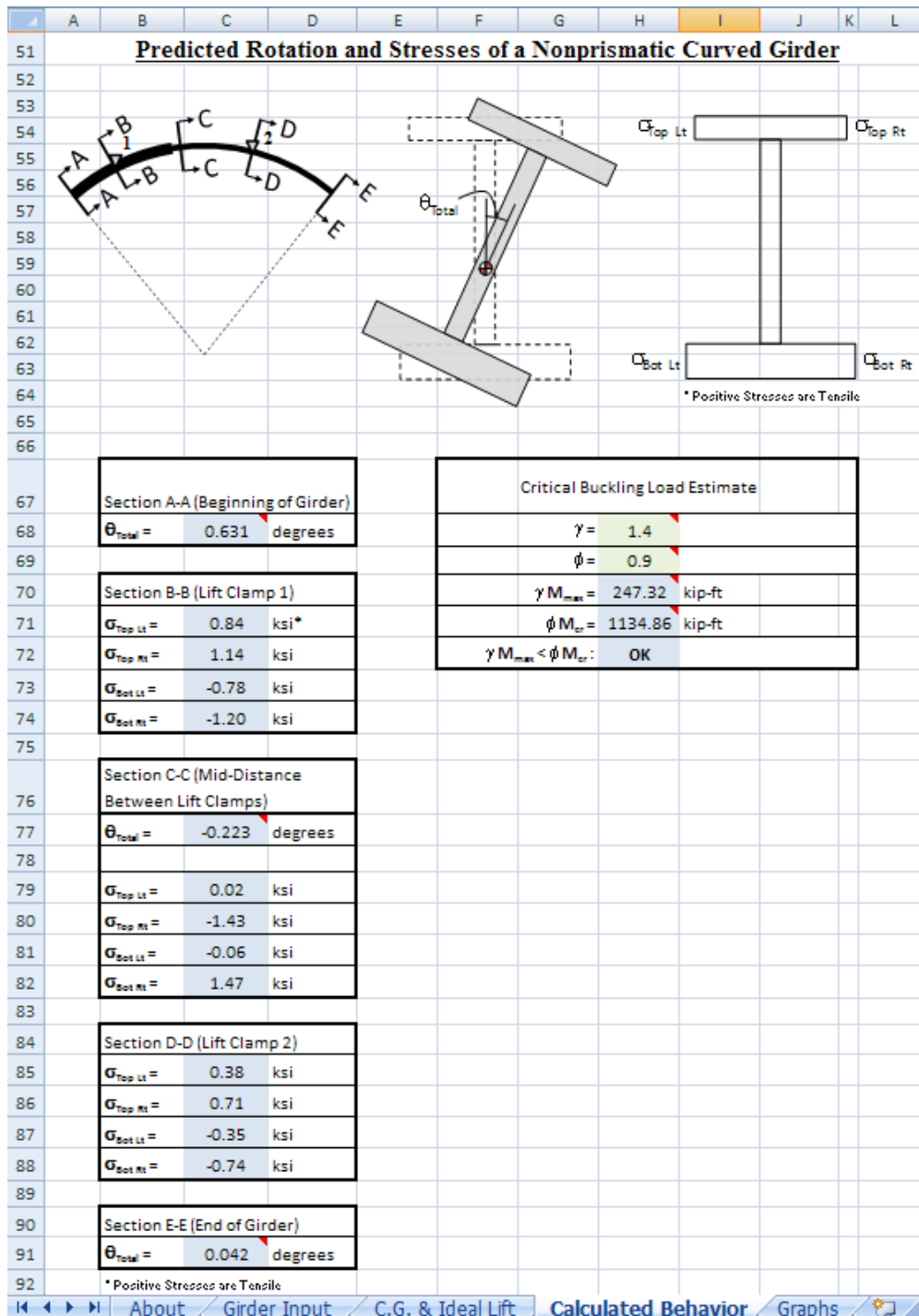


Figure 4.60: Screen Shot of UT Lift Calculated Behavior Output

4.5.5 Girder Deformations and Torsional Diagrams

The analysis tool also provides three useful graphs to assist the engineer in evaluating behavior of the girder during lifting. The first is an out-of-plane displacement graph that gives the displacement of the top and bottom of the girder along its length. The second graph and possibly the most important provides the total rotation of the girder along the length. For

infinitely stiff girders with rigid body rotation the graph would be a horizontal line. As the girder becomes more torsionally flexible the graph will have greater variation in the rotation along the length. Finally the torsion diagram is provided to give the engineer an idea of the torsional force applied to the girder during lifting. A screen shot of this page is shown in Figure 4.61.

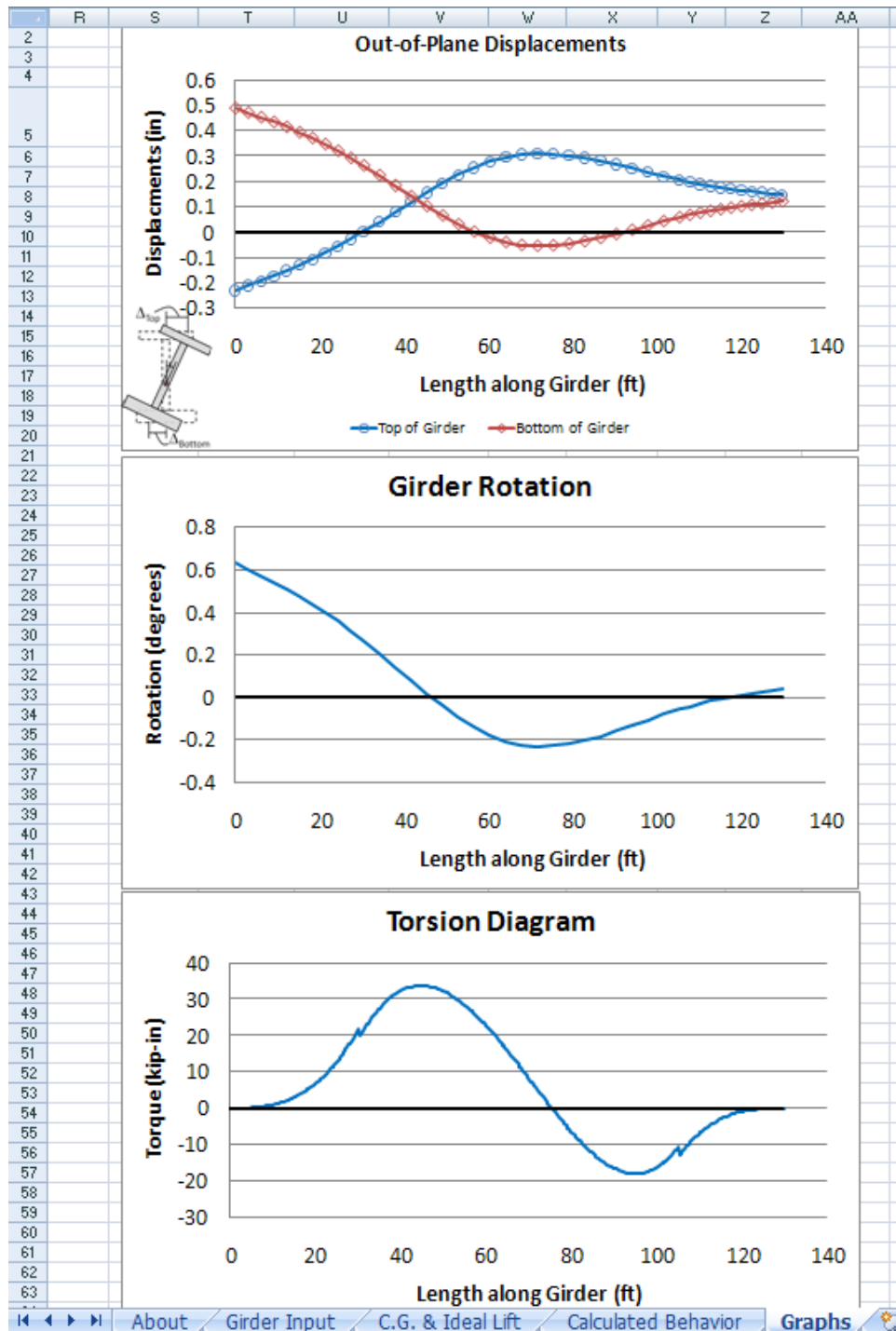


Figure 4.61: Screen Shot of UT Lift Graphical Output

The user should be aware of the program limitation so as to understand the applicability of the results to the problem at hand. There is a limit on geometric inputs as mentioned previously. The cross sectional twist is calculated using a linear finite element analysis and does not iterate to account for nonlinear effects. The research on this project to date has found that 2nd order effects are generally minimal if the analysis is limited to small total rotations ($< \sim 1.5$ degrees). The specific allowable rotation limit should be controlled by the erectors preference.

4.5.6 Verification of UT Lift

Verification of the UT Lift analysis tool was conducted with the 3-D nonlinear finite element model developed in ANSYS and utilized in the parametric study discussed previously. The cross section twist and the rigid body rotation are calculated within UT Lift and the total rotation was compared to a full nonlinear analysis in ANSYS. The following graphs are a set of comparisons between the rotational behavior predicted by UT Lift and the calculated rotation of the mid-height of the girder from the 3-D analysis in ANSYS. Figures 4.62–4.65 provide samples of the verification comparisons.

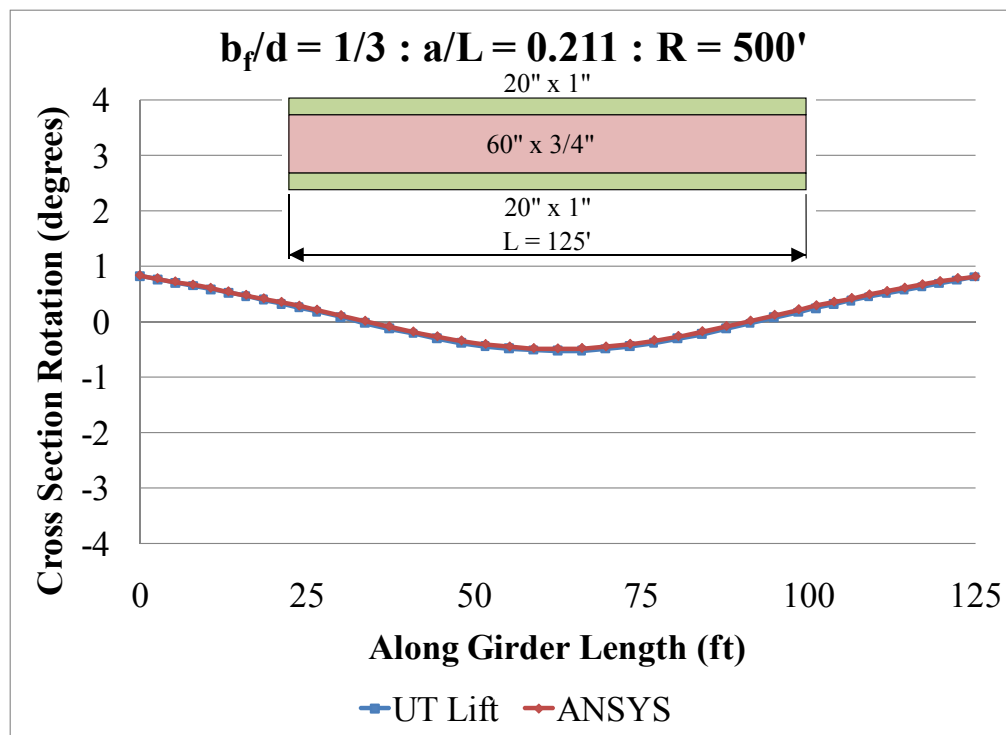


Figure 4.62: UT Lift Validation Graph 1

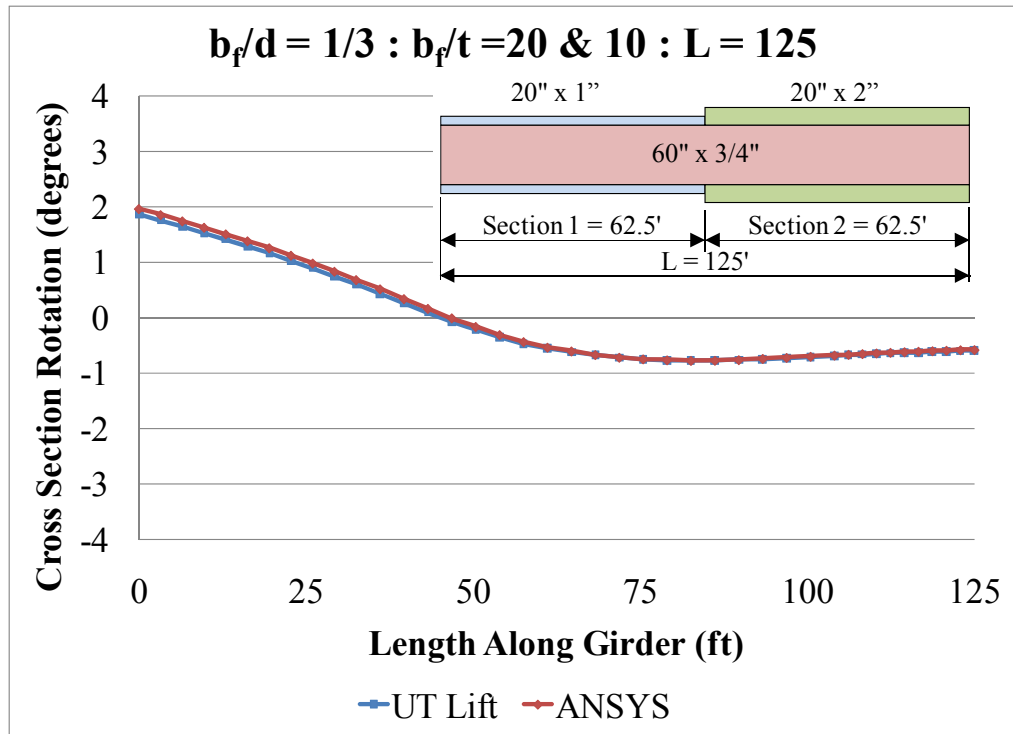


Figure 4.63: UT Lift Validation Graph 2

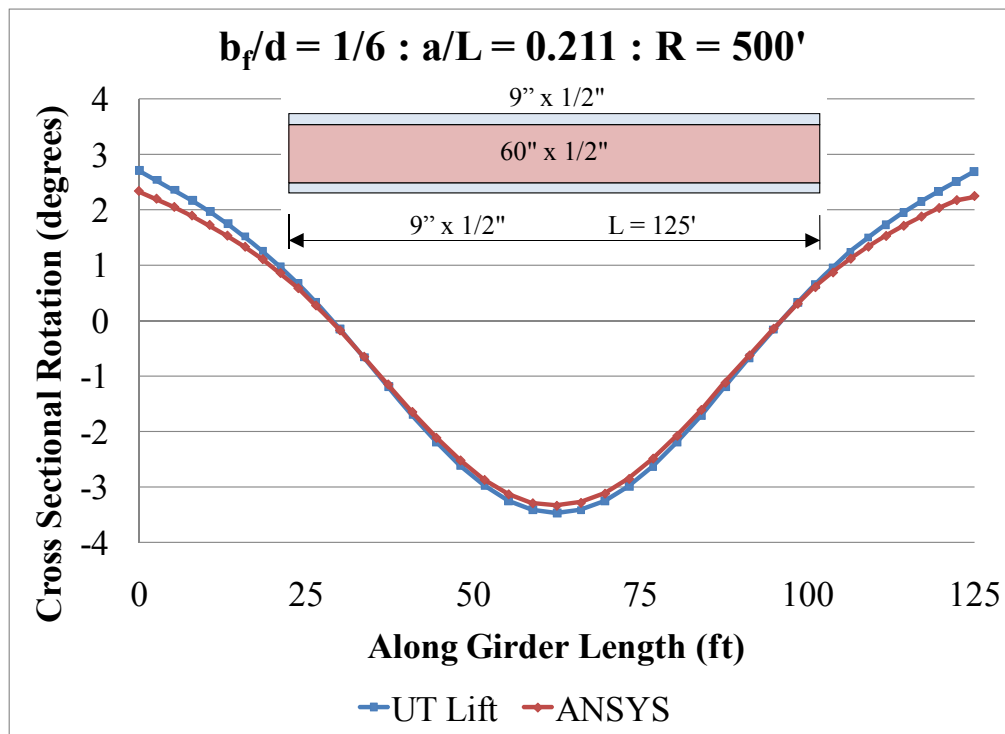


Figure 4.64: UT Lift Validation Graph 3

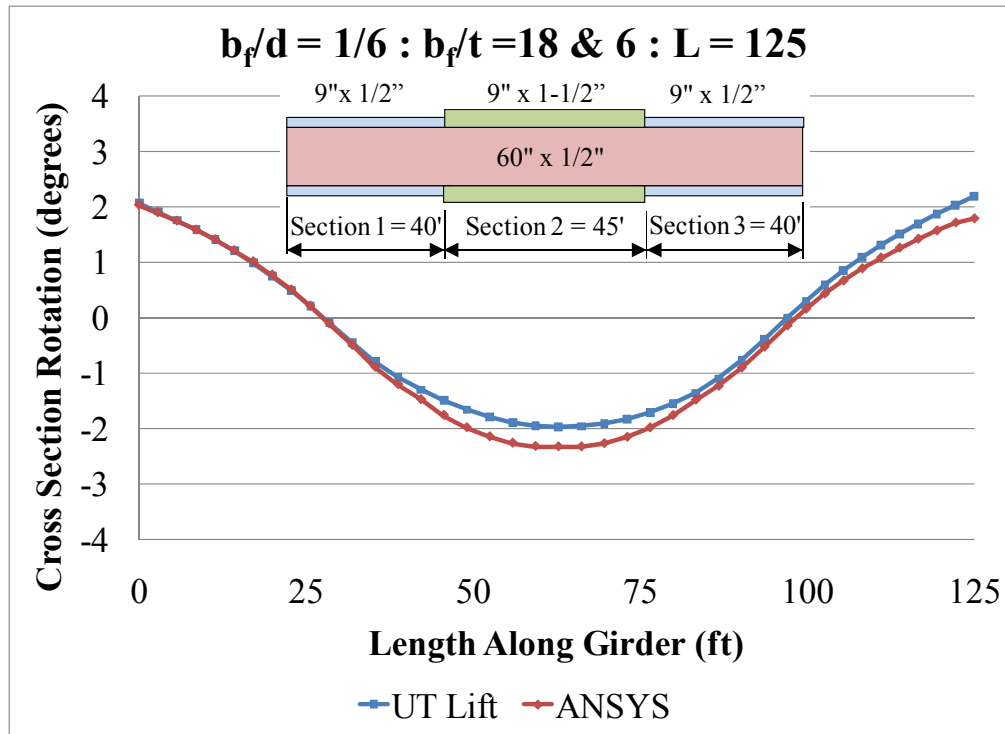


Figure 4.65: UT Lift Validation Graph 4

It should be noted that for the comparisons that were shown the rigid body rotations were relatively small and resulted in very good approximations of the total rotation. For cases with larger rigid body rotations the nonlinear effects especially of the slender girders ($b_f/D \leq 1/6$) the linear approximation of the cross sectional twist deviated more from the nonlinear analysis. Nevertheless, UT Lift provides a quick, accurate, user-friendly analysis tool for engineers and erectors.

This section has provided significant information and analytical solutions for a girder lifted at two points. Another common method for lifting curved girders utilizes two or more cranes for the lifting of long heavy segments with 4 or more lift points. Several parametric analyses were completed to study this behavior and it was found that the use of more than two lift points greatly increases the moment gradient of the girder along its length. This has a significant stabilizing effect on the girder, but does not entirely prevent buckling. It is advantageous for an erector to space the pick points along the length to maximize the moment gradient. Additionally, the height of the axis of rotation from the center of gravity is generally increased for two cranes with separate spreader bars; the axis of rotation is the top of the lifting harness close to the top of the cranes. This increase in the height of the axis of rotation reduces the rigid body rotation experienced by the girder, thus reducing weak axis bending effects. In general, the addition of lifting points is beneficial, but for analysis a conservative approach would be for an engineer to utilize the previous equations and assume the girder is lifted at the center of the two spreader bars for a two crane lift.

4.6 Conclusion

Significant work was completed with regard to the lifting of curved I-girders. A nationwide survey of the state-of-practice was conducted to determine the most common methods used to lift curved girders and establish the greatest challenges facing engineers. Parametric work utilizing eigenvalue buckling analyses and geometric nonlinear analyses were conducted to develop the necessary understanding of curved girder behavior. Equations were developed to calculate the center of gravity of nonprismatic girders with cross frames attached. This allows for a prediction of the rigid body rotation that will occur for girders during lifting. A linear finite element for approximating the rotation of open sections was found, but required the torsion diagram to be developed. This was completed and the entire process was implemented into an Excel based spreadsheet called UT Lift. UT Lift requires input readily available to an engineer and provides a prediction of the behavior of curved I-girders during lifting. Other conclusions from this section include:

- 1) Maximize the moment gradient of the girder by lifting the girder near the quarter points of the girder segment.
- 2) Minimize the rigid body rotation by lifting the girder such that the line of support passes through the center of gravity.
- 3) Minimized weak axis bending by reducing the rigid body rotation.
- 4) Widening the top flange to increase the warping stiffness is the most economical way to increase the torsional stiffness of the open section I-girder and reduce the cross sectional twist.
- 5) Check the girder segment for the strength limit state of $F_y/2$. This stress check should include strong axis bending stresses, weak axis bending stresses, and warping normal stresses.
- 6) Check the girder segment for the serviceability limit state of 1.5 degrees. This rotational check should include both the rigid body rotation and the cross sectional twist.
- 7) Utilize UT Lift for a quick accurate check of the lifting behavior of curved I-girders.

Chapter 5. Partially Constructed Bridges

5.1 Introduction

There are many issues and challenges to deal with when designing a curved I-girder bridge. These challenges primarily deal with the many performance stages that curved I-girder bridges have such as the erection, construction, and in-service stages. When bridge engineers assess the stability of a bridge system, they typically evaluate the system in its final configuration with all cross frames attached and the hardened concrete deck placed. Yet, evaluation of the early stages such as the erection and construction stages can be very difficult because of the limited presence of bracing in the system. In many partially constructed bridges, the system may not be fully braced due to cross frames not being attached. Because of the limited bracing, the bridge system has significantly less torsional stiffness and will rotate more. The larger unbraced length also makes the bridge more susceptible to lateral-torsional buckling. Highly curved bridges may experience relatively large warping stresses as a result of the large torsional moment. In many cases, these warping stresses can be similar or even larger in magnitude to the bending stresses on the cross section. For example, Figure 5.1 and Figure 5.2 show cases where the warping stresses for the given girder are greater than the bending stresses. A holding crane was positioned at approximately 40% of the span length.

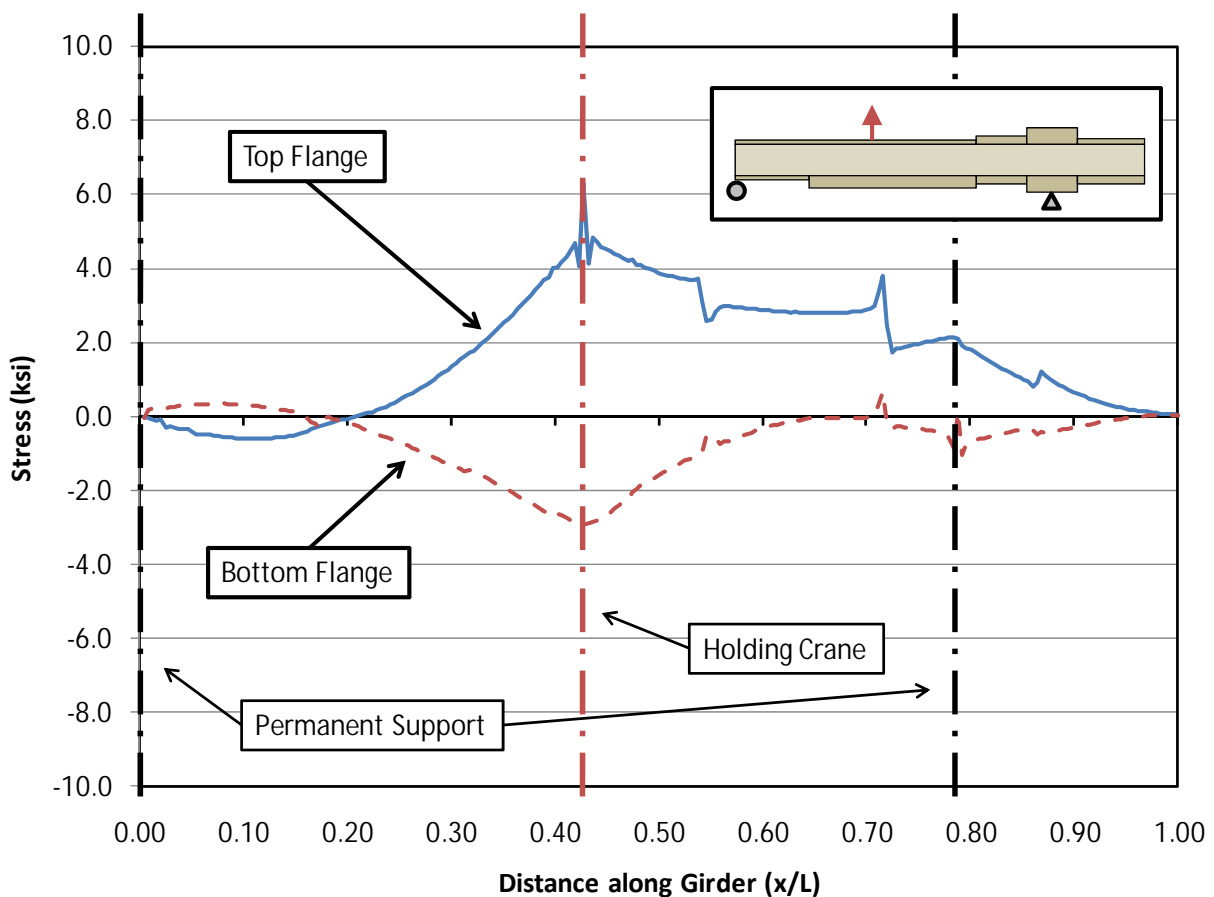


Figure 5.1: Bending Stresses for a Girder being held by a Holding Crane

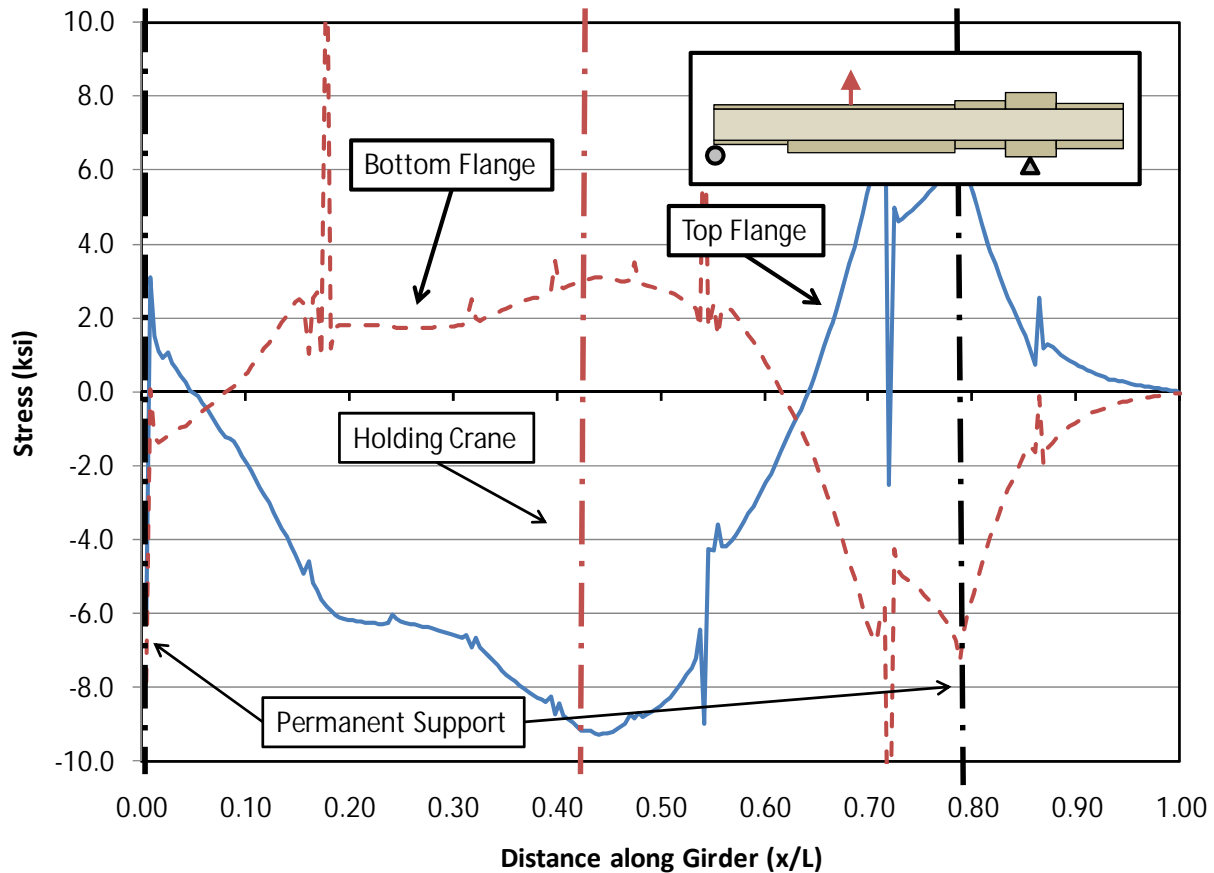


Figure 5.2: Warping Stresses for a Girder being held by a Holding Crane

Traditionally, design engineers and contractors work independently in the design and construction of most bridges. Design engineers are generally responsible for making sure the bridge is able to withstand all strength and service limit states in the end configuration while contractors are generally responsible for the stability of the bridge during erection and construction and to make sure the bridge is constructed as specified by the designer. Unfortunately, these roles may be defined with little communication between the individual parties. Due to a lack of readily available analytical tools, many contractors do not have detailed analytical evaluations of the bridge behavior during early stages of the construction when stability is often critical. Analysis tools such as ANSYS or ABAQUS are not typically found in traditional contracting companies, nor are these packages practical for such use. Sophisticated three-dimensional finite element models are not generally practical for bridge analysis due to the labor intensive efforts that must be put forth in order to produce an accurate model. Instead, many contractors use rules of thumb and experience to ensure stability during erection. Rules of thumb differ from one contractor to another and consistent erection methods are a rarity. Although some rules of thumb may be quite conservative, others may be much less so. Therefore, coming up with design guidelines based on parametric studies rather than rules of thumb are desirable to help allow the contractor and the designer to work together to prevent issues that may occur due to the lack of communication between the two professions.

Lastly, many challenges arise due to the complex geometry of curved I-girders. The center of gravity of a curved I-girder is eccentric to the centerline of the girder. Therefore, the

girder will tend to rotate to maintain static equilibrium. To prevent excessive rotation, three points of vertical support are often provided. Two of these points usually consist of permanent supports in the form of bridge piers or abutments. The third point of support usually consist a temporary support in the form of a shore tower or holding crane. Temporary supports are very expensive because they can require significant efforts to construct and often occupy valuable space that may interfere with traffic flow around the construction site. Cases where a holding crane may be satisfactory over a shore tower are also not well understood.

To improve the understanding the temporary support requirements, parametric studies were conducted using the finite element program ANSYS. As outlined earlier, the three-dimensional FEA models were validated using stress and rotation data gathered from field tests during the Bridge 88 erection and the Hirschfeld Lift Test (see Chapter 3 for more information on the conducted field tests). Using the validated FEA model, both linear and geometric non-linear analyses were completed to determine critical factors in curved I-girder bridges during construction. All analyses conducted made use of linear-elastic materials.

It was important to validate both the linear and geometric non-linear FEA model to be able to determine when second order, non-linear effects become noticeably different from a first order analysis. A geometrically linear analysis assumes displacements are small and that boundary conditions remain the same. A linear analysis assumes a linear function between the applied load vector and the displacements of the system. This relationship can be seen in (5.1) where K_e is the elastic stiffness matrix, Δ is the displacement vector, and P is the load vector.

$$[K_e]\{\Delta\} = \{P\} \quad (5.1)$$

The geometric non-linear analysis that was conducted still assumed that the material stayed in its elastic range, but did not assume that the system displaced small amounts. Instead, the analysis considered displacements when constructing the equilibrium equations. Because the system's geometry is constantly changing for each time step, the loads applied to the system will also change for each time step. Therefore, solving the equilibrium equations becomes an iterative process. Axial forces and membrane forces were also considered in the geometric non-linear analysis. This phenomenon, along with the large displacements, is accounting for in the geometric stiffness matrix term, K_g , in (5.2). Compressive axial/membrane forces use a negative sign convention which decreases the total stiffness of the system (subtracting K_g from K_e) while tensile axial/membrane forces have a positive sign convention increasing the total stiffness of the system (adding K_g to K_e). Typically as a system reaches its buckling capacity, the system starts to displace large amounts and second order, non-linear effects begin to dominate the system. Therefore, it is important to consider the impact of the deformations in the analysis.

$$[K_e + K_g]\{\Delta\} = \{P\} \quad (5.2)$$

5.2 Common Practices

5.2.1 Shore Towers and Holding Cranes

To provide the third point of vertical support for the girders, a shore tower or holding crane is temporarily used until sufficient cross frames can be attached to adequately brace the system. The primary function of a shore tower or holding crane is to reduce deflections and

stresses as well as provide stability to the girder prior to full assembly. A shore tower is a structure that is placed at a specific location along the girder to provide a reaction on the bottom flange. A shore tower can provide restraint to the system in all of the translational directions. A picture of a shore tower is shown in Figure 5.3.



Figure 5.3: Picture showing a shore tower under a partially constructed bridge [Right: KWH Constructors – William Bennett Bridge]

In addition to providing bracing in all the translational directions, a shore tower can also provide rotational restraint of the girder. To prevent the girder from rotating, a common practice is to brace the girder's top flange to the shore tower as seen in Figure 5.4. In the picture on the left, an iron worker is positioning the wood brace to restrain the girder from rotating. In the picture on the right, both the wood compressive brace and the steel-tie tensile brace are in place to prevent the girder from rotating in either direction.



Figure 5.4: Picture showing a shore tower with common rotational restraint on top flange

Although shore towers can be useful to help restrain a girder from moving, there are a few major disadvantages that may make them an undesirable alternative. Shore towers can become cumbersome because they require their own engineering design to make sure they are constructed in such a way that they can withstand the applied load from the girders. Because shore towers are engineered structures that are specific to the bridges location, they require their own construction. This construction process can prove to be lengthy and expensive. Lastly, in order for a shore tower to be constructed, there must be adequate land for the shore tower to stand for the extended period of time that they are required. Therefore, they might not be logistical options for bridge spans that cross existing road ways or other obstacles. Holding cranes can be used to provide a vertical reaction that is typically located on the top flange. A picture of a holding crane clamping onto the top flange can be seen in Figure 5.5. In the picture on the left, the crane with the spreader bar was used to lift the girder into place. The holding crane uses a single lifting clamp to apply a specified upward force to support the girder so that the lifting crane can be released to pick up the adjacent girder. On the right, a close up showing the holding crane attached to the top flange can be seen.



Figure 5.5: Pictures showing a holding crane and its attachment to the top flange of the girder

Unlike shore towers, holding cranes do not typically require large space around the bridge for extended periods of time. Therefore, they can be useful in situations where girders cross existing road ways, bodies of water, or other obstacles. Holding cranes also require less preparation before use and can be used for shorter periods of time. In addition, because of the mobility, the placement can be adjusted to meet last minute changes at the jobsite. The tradeoff for the convenience of a holding crane is that cranes are typically rented on an hourly basis. The price of a holding crane can escalate quickly if adversities arise and the holding crane is required for longer than initially estimated. Holding cranes also do not prevent the girder from translating in both directions orthogonal to the reaction. Therefore, structural analysis should be performed to make sure that the girder does not translate a significant amount when the lifting crane is released.

5.3 Parametric Approach

5.3.1 Parameters Considered

The geometric parameters selected for the parametric work dealing with shore towers and holding cranes were the flange width to girder depth ratio (b_f/D), the girder span length to girder depth ratio (L/D), radius of curvature of the girder (R), and the location of the shore tower/holding crane down the length of the girder. Boundary conditions were also varied when considering the use of a shore tower. Both a small and large stiffness of the bracing connecting the top flange of the girder to the shore tower was considered. Lastly, the load parameters considered when using a holding crane included varying the upward load applied by the holding crane. Figure 5.6 shows the cross sectional variables used for the study on temporary supports.

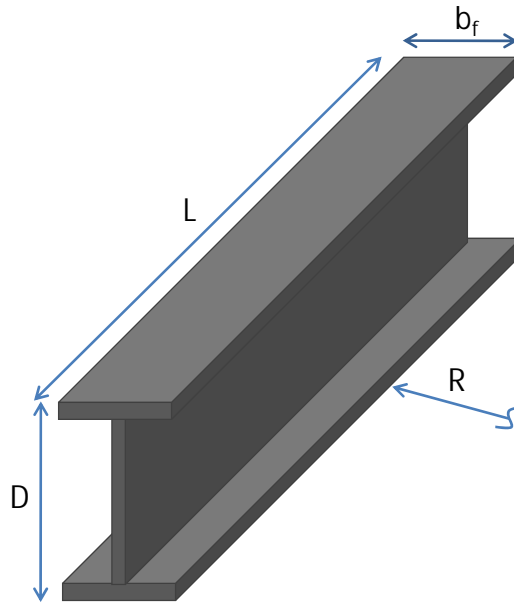


Figure 5.6: Shore Tower Geometric Parametric Definitions

5.3.2 Parameter Definitions

The flange width to depth ratio that the Texas Department of Transportation (TxDOT) recommends in their TxDOT Preferred Practices for Steel Bridge Design, Fabrication, and Erection is $D/3$ (TxDOT 2007). AASHTO on the other hand allows a bridge design engineer to use a flange width to depth ratio as little as $D/6$ as seen in Equation 6.10.2.2-2 of the AASHTO LRFD Bridge Specification (AASHTO 2008). In this study, the range of b_f/D ratios that were used was $1/3$ to $1/6$ to determine the behavior of the girders at the two recommended limits. For all parametric studies completed, the top and bottom flange were kept similar to keep symmetry about both the strong and weak axis of the girder cross section.

The girder span to depth ratio was changed throughout the study to see if it had an effect on the optimal location to place a shore tower. Additionally it was changed to determine if there was a significant effect on the stresses on the cross section for either the geometric linear or non-linear analysis. In trying to model realistic dimensions that might occur in the field, the span to depth ratios that were considered are 26 and 37 and were taken from existing bridge plans.

For any given girder, the radius of curvature is the distance from the centerline of the girder cross section to the middle of the circular segment. For most bridges, arc lengths and tangent lines are used to describe the horizontal profile. The radius of curvatures that were considered in this study ranged from 500 feet to straight (10,000 feet). Most bridges constructed in Texas have a radius of curvatures greater than 800 feet.

To help determine the optimal location to place a temporary support (i.e., shore tower/holding crane), the temporary support position along the length of the girder was varied. The temporary supports location typically varied as a ratio x/L where x is the distance from the start of the girder to the shore tower location and L is the length of the span where the shore tower is located. Figure 5.7 shows the parameter definitions for the location of the temporary supports.

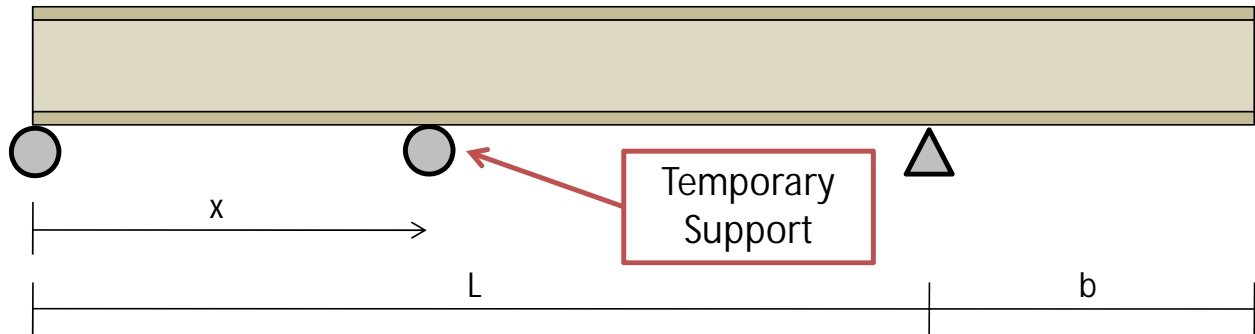


Figure 5.7: Temporary Support Location Parameter Definitions

The stiffness of the brace that connects the top flange of the girder to the shore tower was varied. At first, a very stiff spring equivalent to a 0.5 in² steel rod 10 inches long was used to brace the top flange. It was observed that the top flange of the girder at the location of the shore tower experienced a considerable movement and also experienced large warping stresses. As a comparison, a rigid lateral support was placed in the model. As the stiffness of the rotational support increased, the displacements of the top flange decreased along with the warping stresses on the cross section and the second order effects. Adequate bracing is imperative as the stiffness of the brace on the top flange greatly affects the performance of the temporary support. Figure 5.8 depicts the two different lateral supports used in the ANSYS model.

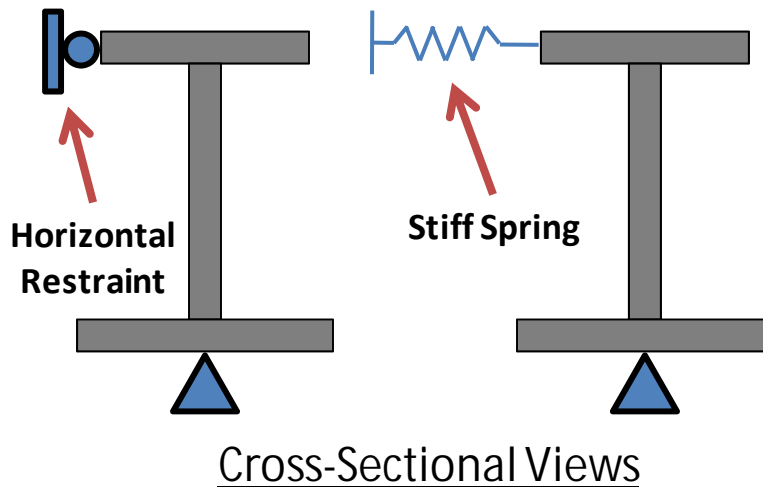


Figure 5.8: Top Flange Lateral Support Options Considered

The vertical load of the holding crane was varied substantially depending on the girder being held in the parametric study. A vertical load of 20 kips to 50 kips at 5 kip intervals was typical for most early parametric work. For later studies, the holding crane load was varied depending on the load that would be equivalent to the vertical reaction of a rigid support placed at the holding crane location. From this starting point, the holding crane load was then varied +/- 5%, +/- 10%, and +/- 20% of the rigid support reaction.

5.4 Parametric Results

5.4.1 Shore Tower Location Results

An important aspect when using a shore tower is determining the location. The shore tower position can dramatically change the system behavior along with the vertical and horizontal reaction that will be induced to maintain the proper orientation of the girder web. Many factors determine where the shore tower should be placed including many non-structural factors. Restricted site access, construction methodology and the stiffness of the girder are some of these factors. The life of a shore tower from erection to removal can be quite lengthy. Therefore, the site where the shore tower is to be constructed needs to be available for the entire duration of service. If there is a road passing underneath that needs to maintain traffic flow, placing a shore tower along the width of the road way may not be acceptable. Additionally, the use of a shore tower may necessitate extra web stiffeners in the girder. The large concentrated load produced by the shore tower will dramatically increase the shear at the location where the shore tower is placed. The increased shear forces may induce web buckling and therefore it is recommended to place the shore tower at a location on the girder where a stiffener is located. Regardless if a shore tower is placed at a stiffener location or not, it is still strongly recommended to do an analysis of the system to make sure that no local yielding occurs and that the stability of the girder web is sufficient at the location of the shore tower.

It is recommended that the shore tower is placed close to the location of maximum positive moment for any given span between two permanent supports. This location will roughly minimize the total deflections that are observed for a given span and will be close to the location that requires the shore tower to hold the minimum amount of load. It is typical to see a contractor lift a section of girder that creates a simply supported beam that cantilevers off on one of the sides as seen in Figure 5.9. For this case, the location of the maximum positive moment can be obtained by (5.3) where L is the length of the simple span, b is the length of the cantilever, and $X_{M,Max}$ is the distance from the beginning of the simple span to the location of maximum positive moment. It should be noted that this equation is only valid for uniform loading situations.

$$X_{M_{Max}} = \frac{L}{2} \left(1 - \frac{b^2}{L^2} \right) \quad (5.3)$$

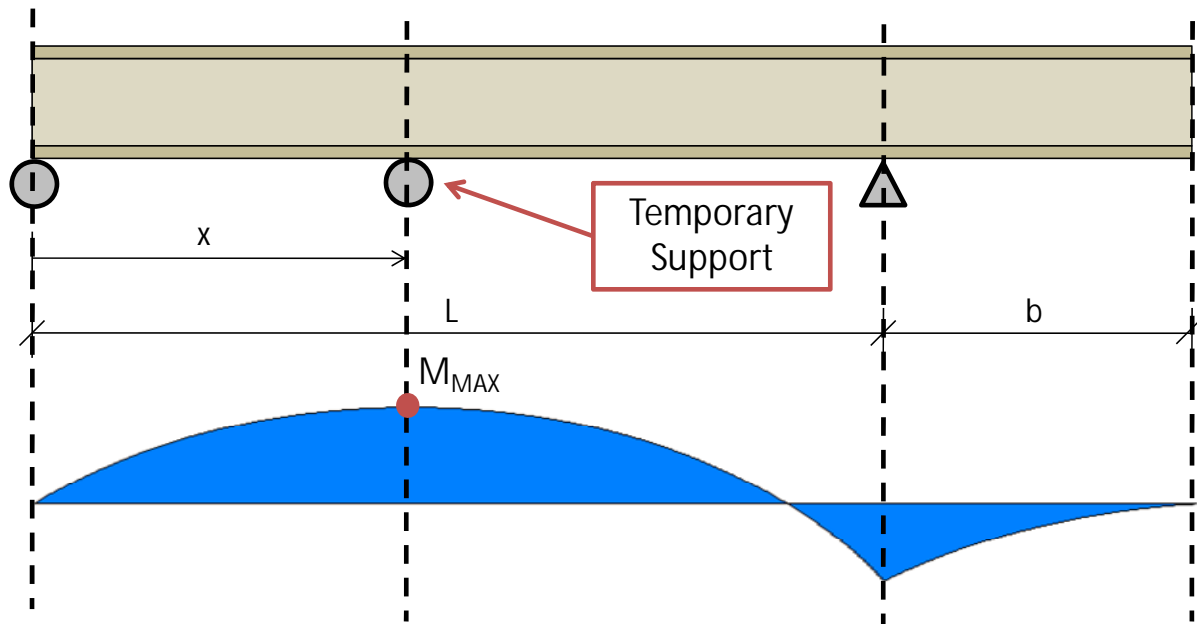


Figure 5.9: Location of Maximum Positive Moment; Simple Span with Cantilever on One Side

In Figure 5.10, a sample girder is shown with a center span of 185 ft. and a cantilever on one side of 51 ft. The temporary support was varied ± 10 ft. and ± 20 ft. on either side of the maximum positive moment. The table shows the required vertical reaction for the shore tower in order to keep the web of the girder vertical. The figure shows a graph of the reaction versus the location (x/L). It can be seen that for this case, the lowest required vertical reaction for the shore tower coincides with the location of the maximum positive moment. Additionally, it can be seen that the shore tower reaction gradually increases as the shore tower position varies from this maximum positive moment.

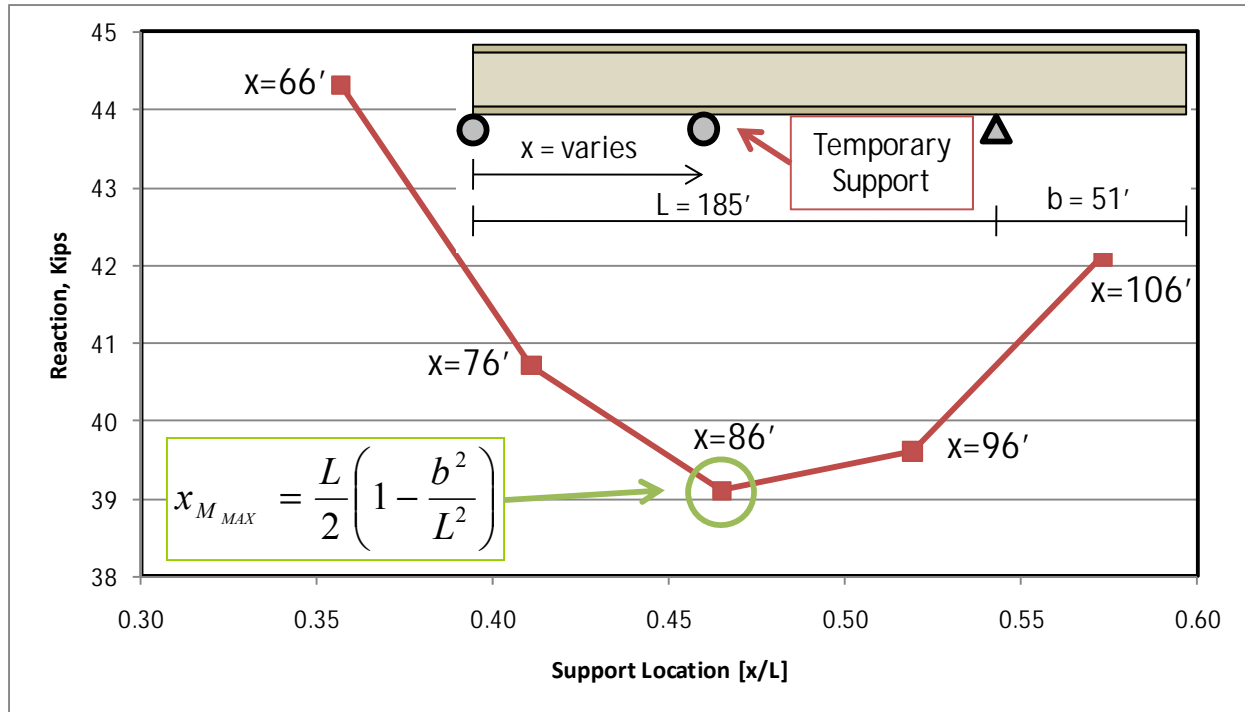


Figure 5.10: Vertical Reactions for Various Locations along a Girder

In Figure 5.12, the vertical displacements down the length of the sample girder shown in Figure 5.10 are graphed for different shore tower positions. Although placing the shore tower at the maximum positive moment location in the simple span portion of the girder (86 ft.) will minimize the girders vertical displacements and reaction, it may not always be the optimal position. Placing the shore tower at the maximum positive moment in the simple span is a good starting point, but further analysis can determine whether or not there is a better place to put the shore tower depending on the individual girder stiffness and geometric properties (Figure 5.11). By placing the shore tower at 76 feet in the sample girder, the displacements along the simple span are actually lower than placing the shore tower at 86 feet. Yet, the displacements at the end of the girder are greater for the 76 foot location. As a general rule, keeping the shore tower location within +/- 5% of the maximum positive moment location in the simple span will result in low displacements, vertical reactions, and reduce the second order effects.

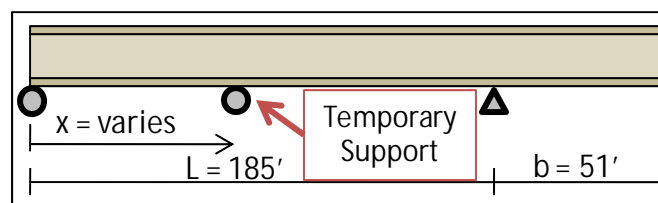


Figure 5.11: Geometry used in Figure 5.12

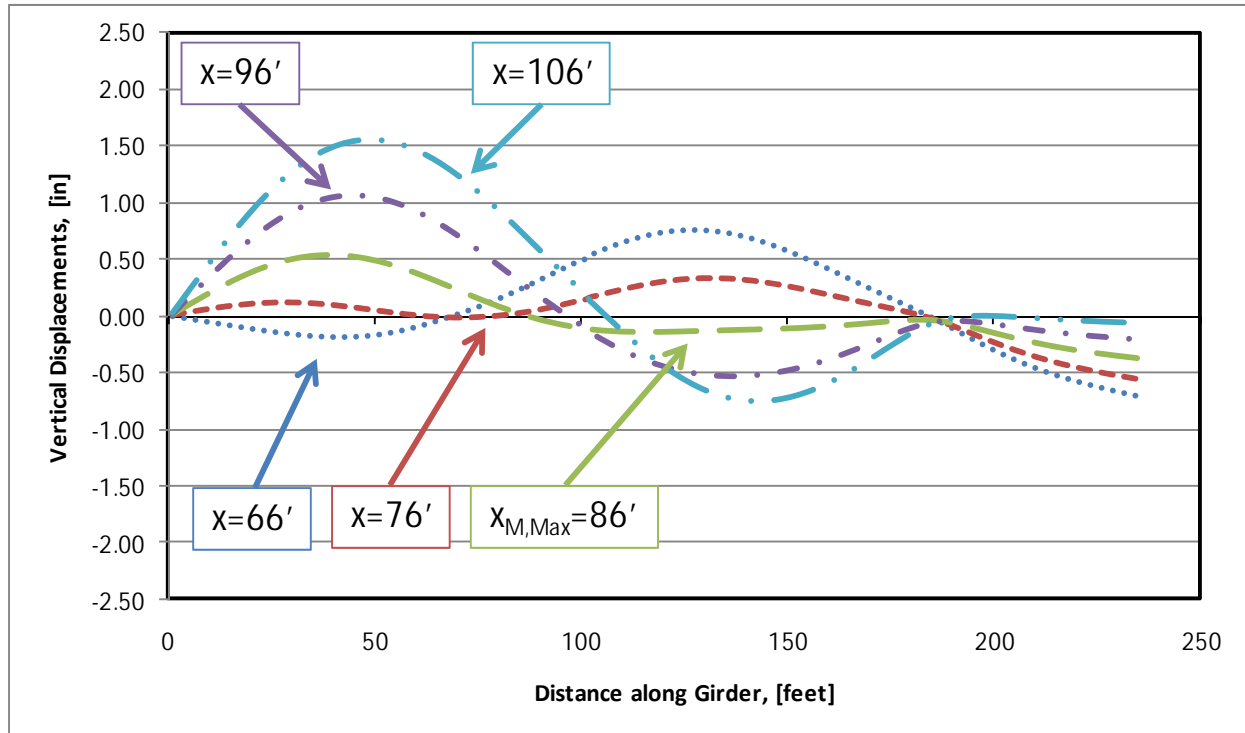


Figure 5.12: Top Flange Vertical Displacements for Various Shore Tower Positions [Linear Geometry]

5.4.2 Holding Crane Location Results

The location of the holding crane affects the required upward force and ultimately hinders the holding cranes ability to control deformations and stresses (Figure 5.13). Like shore towers, many non-structural criteria such as site access, construction methodology, and girder stiffness can affect the erectors ability to be able to place a shore tower in the optimal location. Yet, just like a shore tower, it is desirable to place a holding crane at the point of maximum positive moment between the two permanent supports. This location will give roughly the smallest value for the required crane load to hold and will minimize both displacements and stresses on the girder cross section. In Figure 5.14 the same girder was lifted as in Figure 5.12 except a holding crane was placed at different locations instead of a shore tower. The holding cranes held a force equal to the vertical reactions obtained from the shore tower analysis. It can be seen that by placing a holding crane at the maximum positive moment (86 ft.) the vertical displacements are minimized along the length of the girder. Unlike shore towers, placing a holding crane at the location of maximum postive moment tends to give the lowest displacements and warping stresses of any location along the girder. Therefore, it is reccomended that holding cranes be placed at this location.

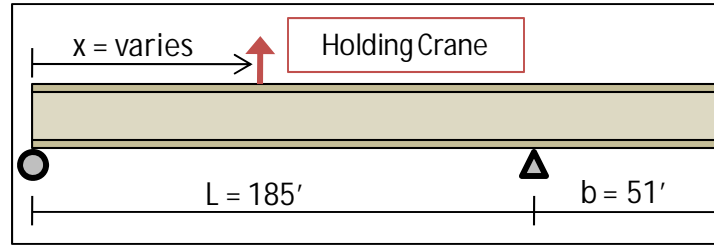


Figure 5.13: Geometry used for Figure 5.14

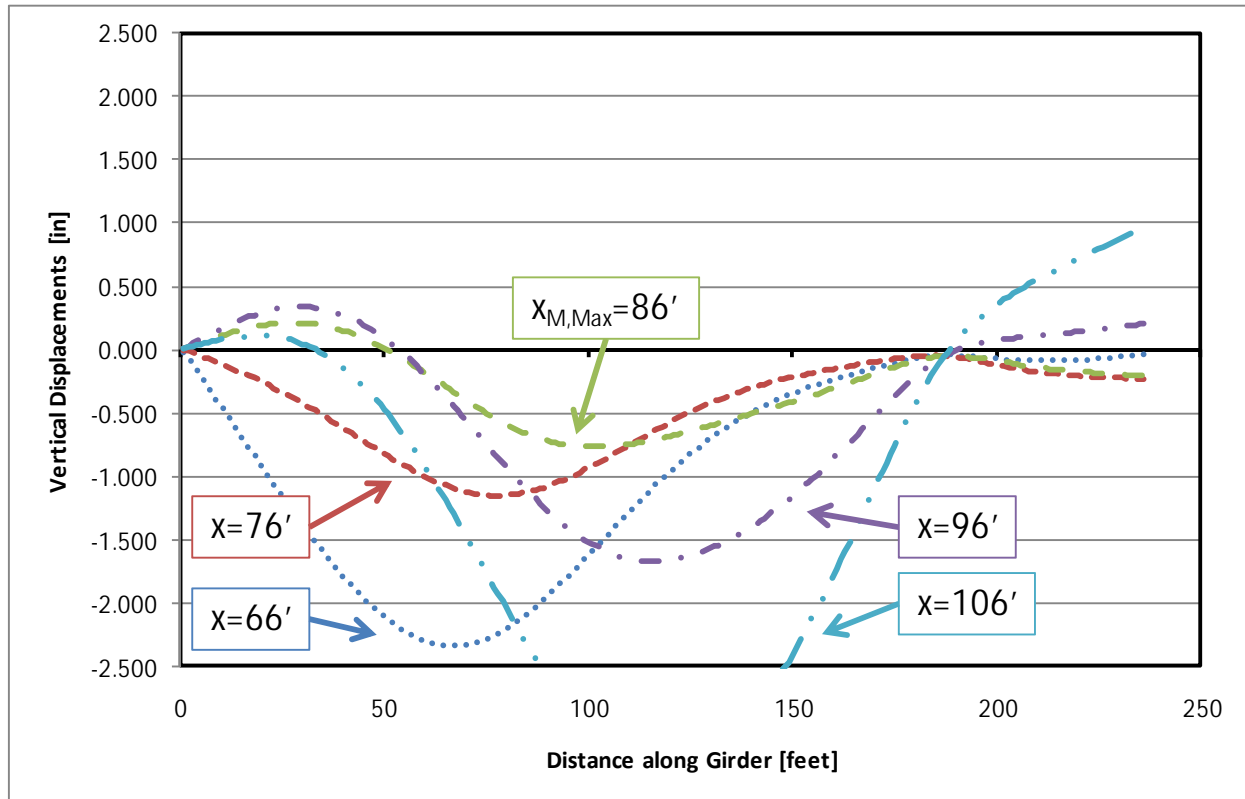


Figure 5.14: Top Flange Vertical Displacements for Various Holding Crane Locations [Linear Geometry]

It should be noted that deviations in holding crane location on the order of $\pm 10\%$ are okay assuming the holding crane is lifting with the optimal load. This concept will be discussed more in the following section.

5.4.3 Holding Crane Lifting Load Results

The load that the holding crane applies significantly affects the behavior of the girder being supported. It is recommended that the holding crane lift with a load that would be equivalent to that of a rigid support placed at the same location. This load allows the web of the girder to remain vertical and minimize deformations helping with fit-up issues. Using a load in the holding crane that differs from this *optimal load* will not keep the girder's web vertical.

A geometrically linear analysis can be used to determine the reaction that would occur at a rigid support for a given location along the length of the girder (Figure 5.15). The difference in reactions for a first order analysis and second order analysis is small assuming the top flange of the girder is properly braced preventing excessive rotations. It is important to model the curvature of the bridge when determining the reaction. Studies were conducted where the reaction at a given support was up to 10% higher if the curvature of the bridge was considered when compared to that of a straight bridge with the same properties. Getting the appropriate reaction for a rigid support is crucial because small deviations from the optimal lifting load can result in dramatic differences in vertical deflections. Figure 5.16 shows three vertical displacement plots of the same girder with different holding crane forces and a b_f/D ratio of about 1/3.5. By changing the holding crane force by only $\pm 5\%$, the maximum vertical displacements can increase by over an inch. For this particular case, the optimal load is 47.8 kips.

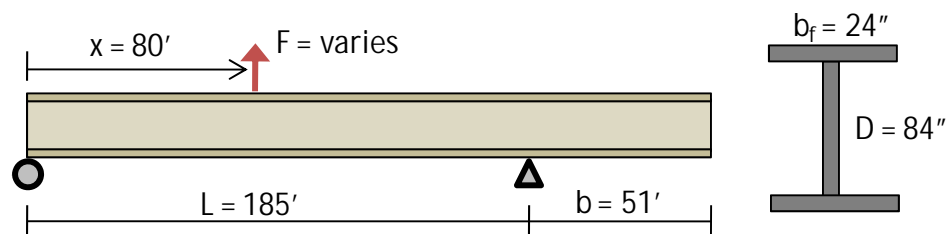


Figure 5.15: Geometry used for Figure 5.16

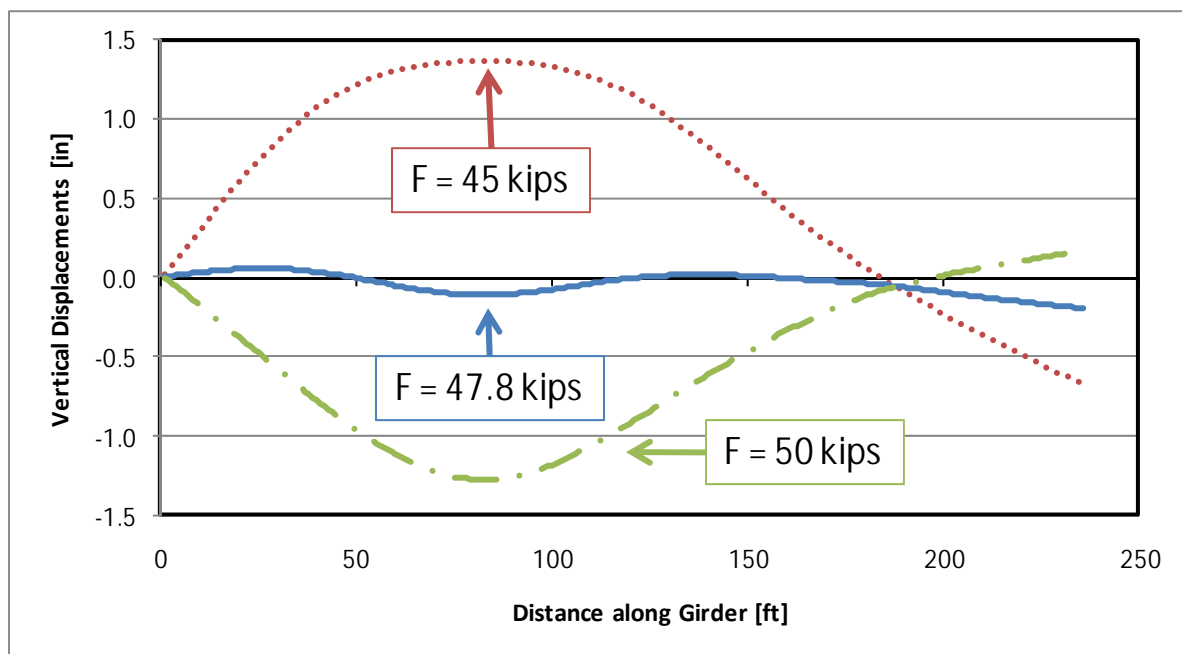


Figure 5.16: Vertical Deflections for Varying Crane Loads

As long as the optimal load is determined correctly and is used as the holding crane, force, then the location of the holding crane becomes less important (although it is still desirable to place the holding crane close to the location of maximum positive moment). For the girder

shown in Figure 5.17, the optimal place to put a holding crane is at 86 feet. As stated above, it is desirable to place the holding crane close to this location. If the holding crane were placed at 80 feet, the optimal lifting load would be 36.5 kips. The b_f/D ratio for the girder in Figure 5.17 is $1/6$. This ratio was used to test the girder slenderness at the AASHTO limit. Figure 5.18 shows the lateral displacements for the girder if it were held at 80 feet which is very close to the optimal holding crane location and with a force of 36.5 kips which is exactly what the optimal holding crane load is for the 80 foot location. This is the ideal case and shows the minimal girder deflections when using a holding crane for this specific case. Figure 5.19 shows the out of plane displacements down the length of the girder when close to the optimal lifting location but not using the optimal lifting load for the 80 foot location. It can be seen that even though the holding crane is close to the optimal lifting location, with a lifting load just 3.5 kips higher than the desired load, the displacements are much larger then in Figure 5.18. Figure 5.20 shows the displacements down the girder when using the optimal lifting load but for a lifting location of 100 feet which is relatively far away from the optimal lifting location. Even though the lifting location is relatively far away from the optimal lifting location, the displacements down the length of the girder are not as severe as seen in Figure 5.19. Therefore, it can be concluded that the holding crane location is less severe than the holding crane load as long as the correct lifting load is used for the selected holding crane location.

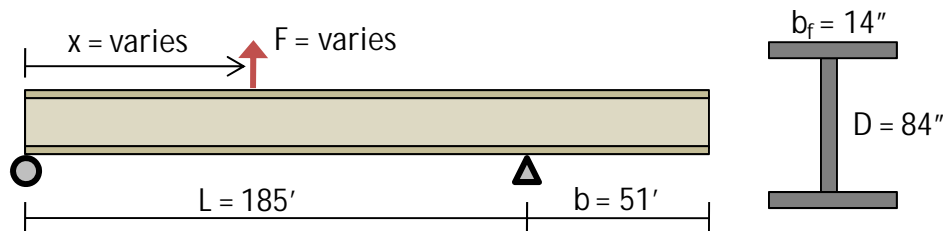


Figure 5.17: Geometry Used for Figure 5.18, 5.19, and 5.20

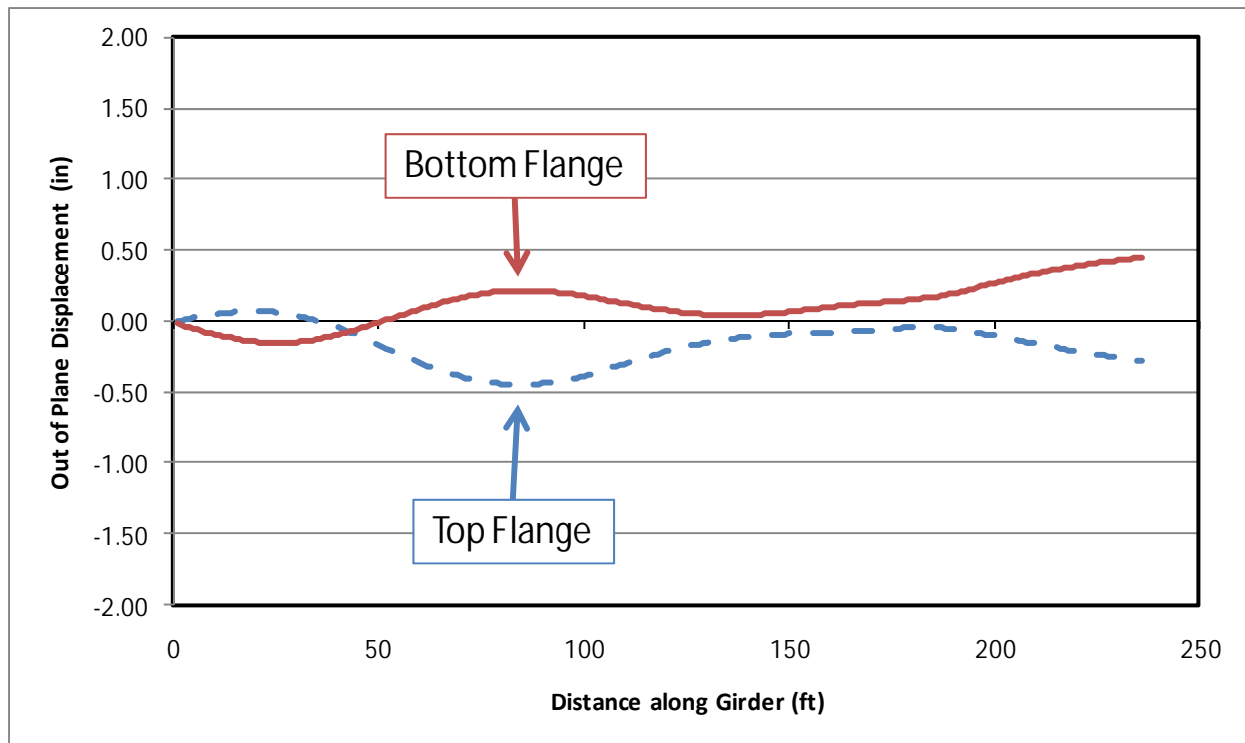


Figure 5.18: Optimal load (36.5 kips) and close to optimal location (80 feet)

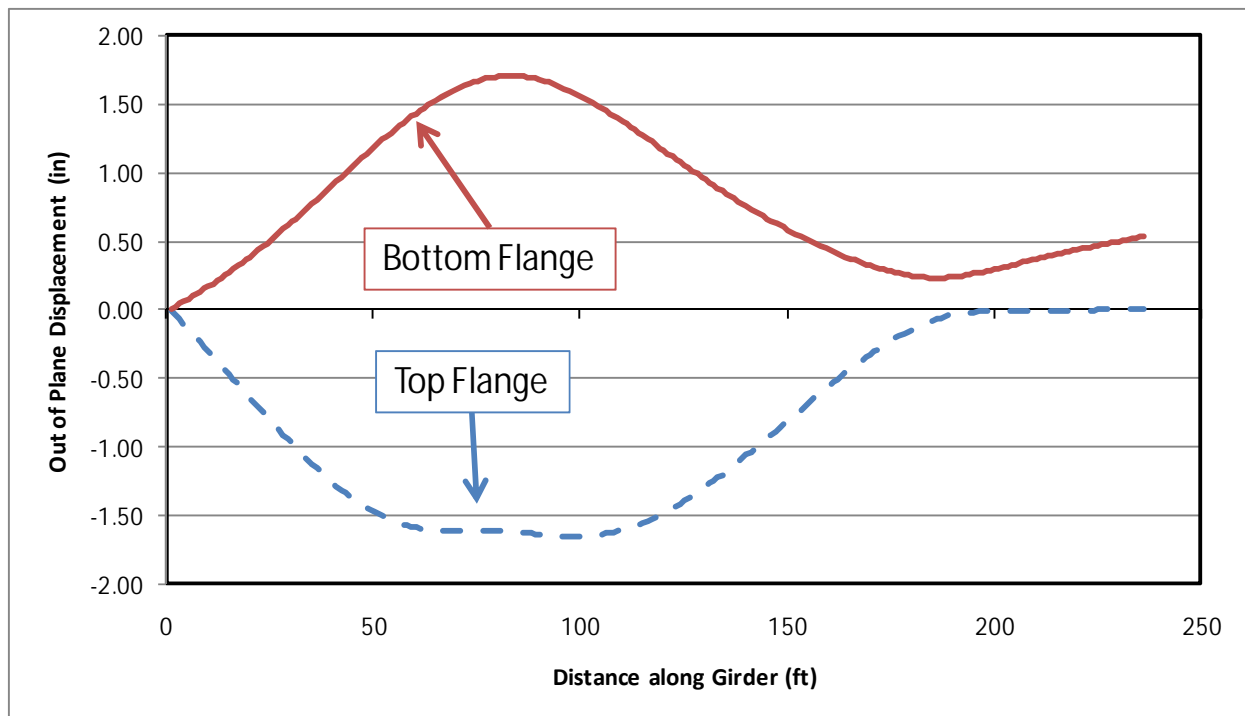


Figure 5.19: Not optimal load (40 kips) and close to optimal location (80 feet)

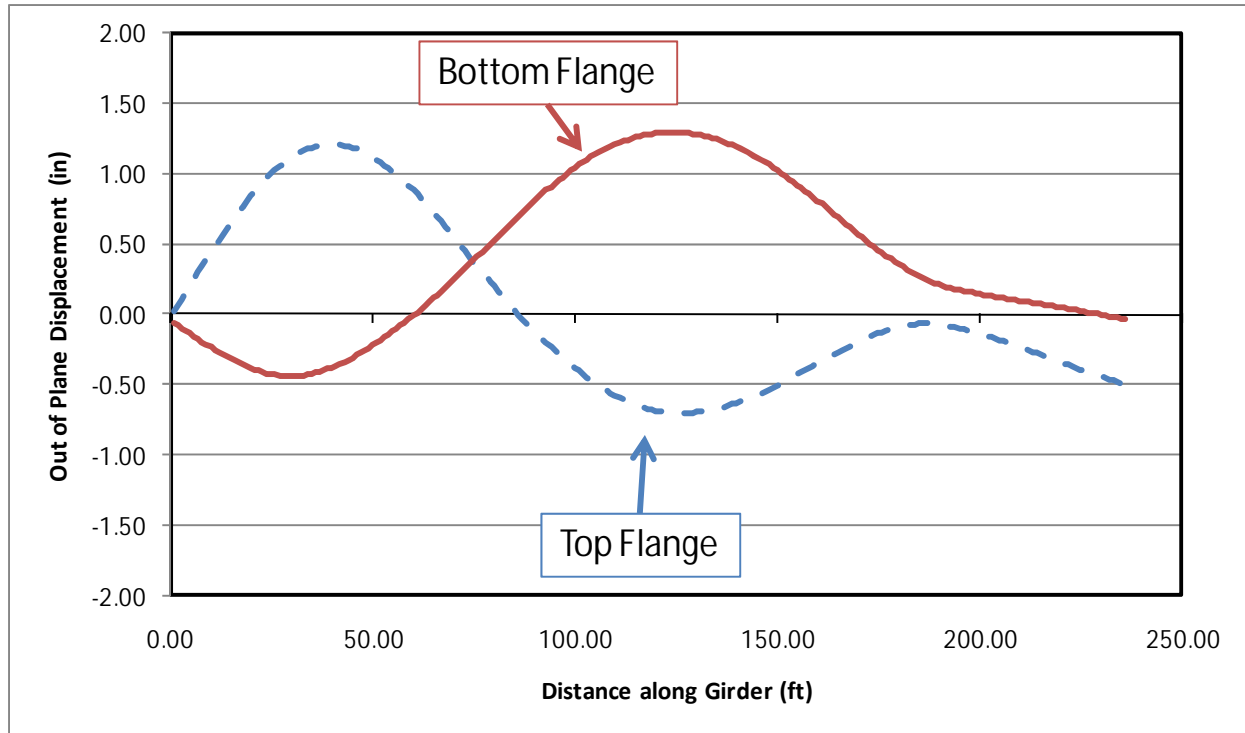


Figure 5.20: Optimal load (37.6 kips) and not optimal location (100 feet)

5.5 Load Height Effects

5.5.1 Shore Towers

Shore towers support a girder on the bottom flange. This is below the girders center of gravity. Therefore, if the girder is not properly braced, then it will begin to rotate at the shore tower location due to its own self-weight. As the girder begins to rotate, the reaction of shore tower will create a component that is orthogonal to the direction of the girders web and create a destabilizing torque about the girders center of gravity. This moment will cause a disturbing force that will continue to tip the girder over increasing the deflections. Figure 5.21 shows the moment that is created by the disturbing force when the girder's top flange is not properly braced.

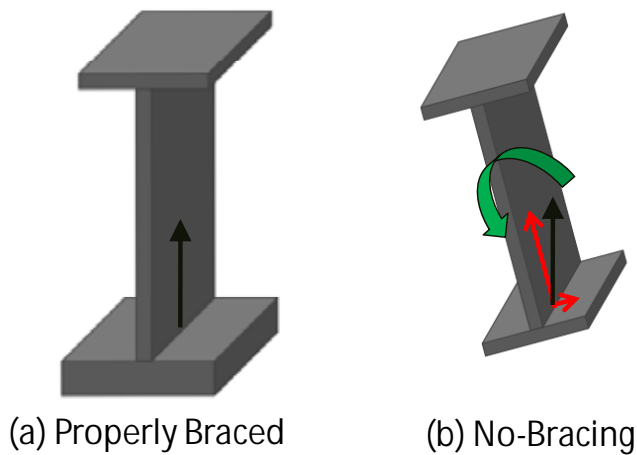


Figure 5.21: Disturbing Force Caused by a Lack of Bracing on the Top Flange

Because the disturbing force is only present after the girder has rotated due to its own self weight, it can only be detected by a second order analysis that includes geometric, non-linear effects (Figure 5.22). When comparing the stresses of a first-order analysis to those of a second-order analysis with a disturbing force present, the bending stresses will be close to the same while the warping stresses and out of plane displacements will be noticeably different. This effect can be seen in Figure 5.23 where the lateral displacements are graphed down the length of the girder for both the first-order and second-order analyses.

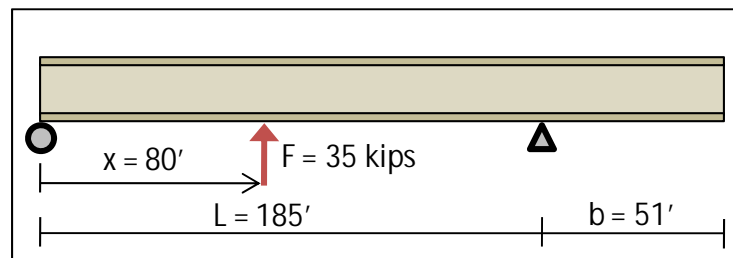


Figure 5.22: Geometry for Figure 5.23

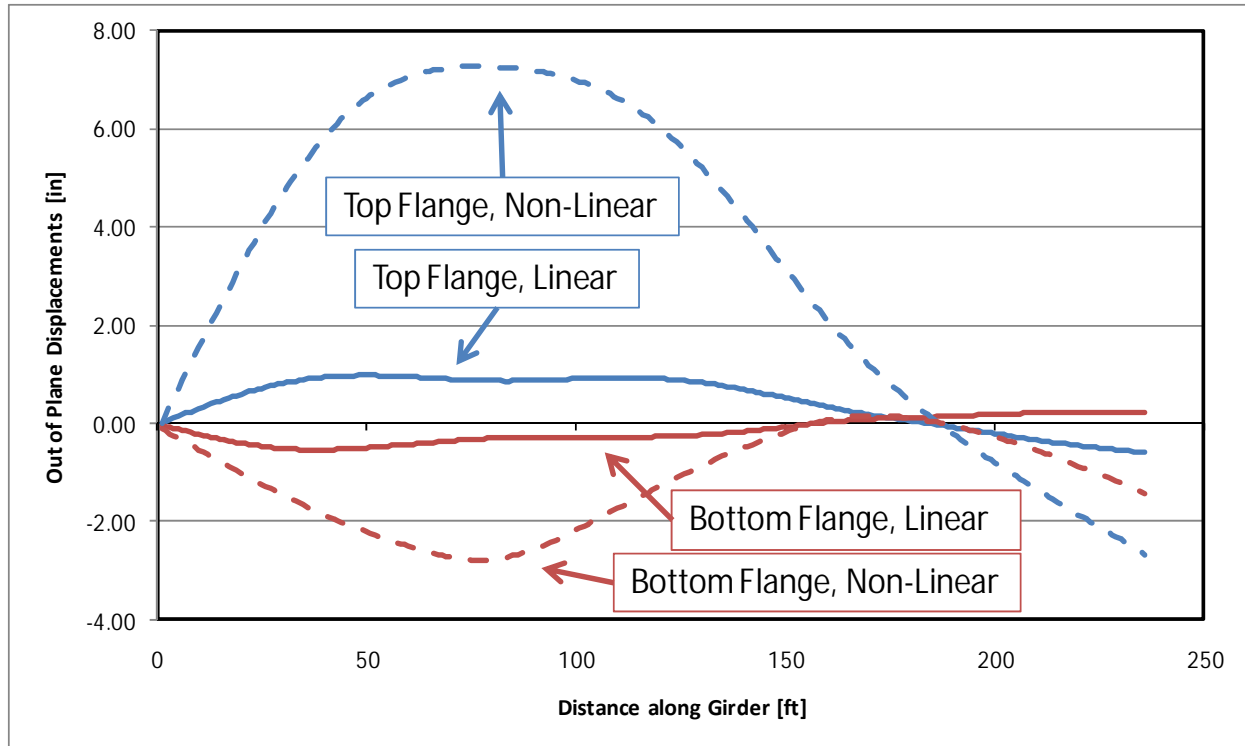
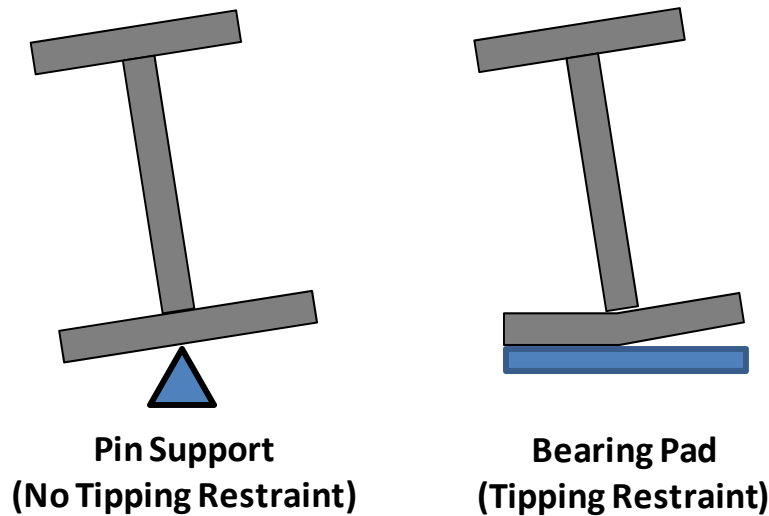


Figure 5.23: Linear and Non-Linear Displacements Along a Girder for a Girder with a Disturbing Force

This phenomenon and lack of conservatism should be well understood by designers. Designers should also be aware that the results shown in Figure 5.18 neglect tipping restraint which is often present in actual bridges. Tipping restraint will provide added stability to the girder by creating a contact surface between the girder and the reaction point. Figure 5.24 contains two girder cross sections: one modeled with tipping restraint and another without tipping restraint.



Cross-Sectional Views

Figure 5.24: Tipping Restraint Schematics

In the ANSYS model, it is assumed that the connection between the girder and the reaction is similar to a knife-edge and provides no tipping restraint. The tipping restraint will reduce the amount that the girder will rotate and therefore reduces the component of the reaction that is orthogonal to the girder's web ultimately lowering the disturbing force.

If the girder is properly braced, many of the load height effects can be avoided. If the girder is not allowed to rotate, then the top flange will not displace causing an additional moment due to the girder self weight about the center of gravity of the girder cross section. As a result, the warping stresses will noticeably decrease and the second order effects are minimal. The vertical bending stresses will stay roughly the same. With proper bracing, the results of the first-order and second-order analyses will be similar and the need to complete a second order analysis becomes less critical.

5.5.2 Holding Cranes

Holding cranes generally support a girder on the top flange. This is above the girder's center of gravity. Unlike shore towers, holding cranes do not have the ability to brace the system in the translational directions orthogonal to the lifting load or in any of the rotational directions. As the girder begins to rotate, the holding crane force that stays vertical will consist of two components relative the girder: a component parallel to the girders web (running through the cross section's center of gravity) and a component perpendicular to the girders web (creating a moment about the center of gravity). This moment causes a restoring force that acts in a direction opposite to that of the rotation and therefore decreases the displacements (Figure 5.25).

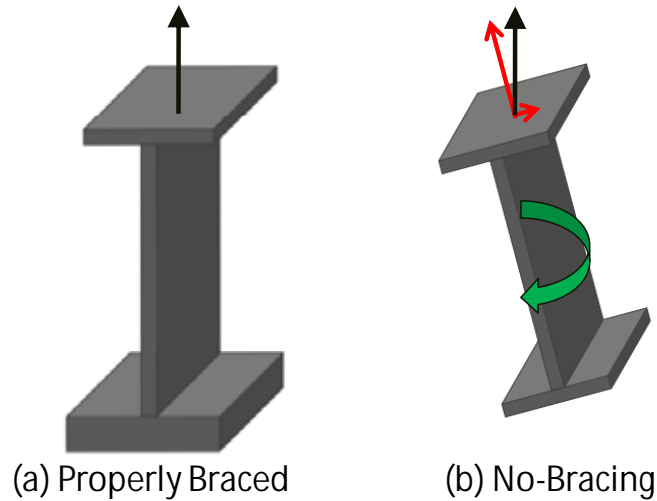


Figure 5.25: Restoring Force Caused by lack of Bracing in Top Flange

Because the restoring force is only present after the girder has rotated due to its own self weight, it can only be detected by a second order analysis that includes geometric, non-linear effects (Figure 5.26). When comparing the stresses of a geometric linear analysis to those of a geometric, non-linear analysis if a restoring force is present, the bending stresses will be close to the same while the warping stresses and out of plane displacements will be noticeably different. This effect is demonstrated in Figure 5.27 where the out of plane displacements are graphed down the length of a girder for both a linear, and non-linear analysis.

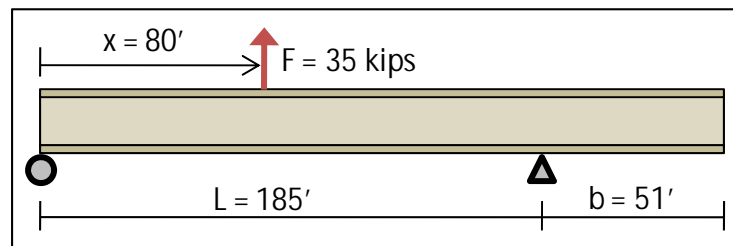


Figure 5.26: Geometry for Figure 5.27

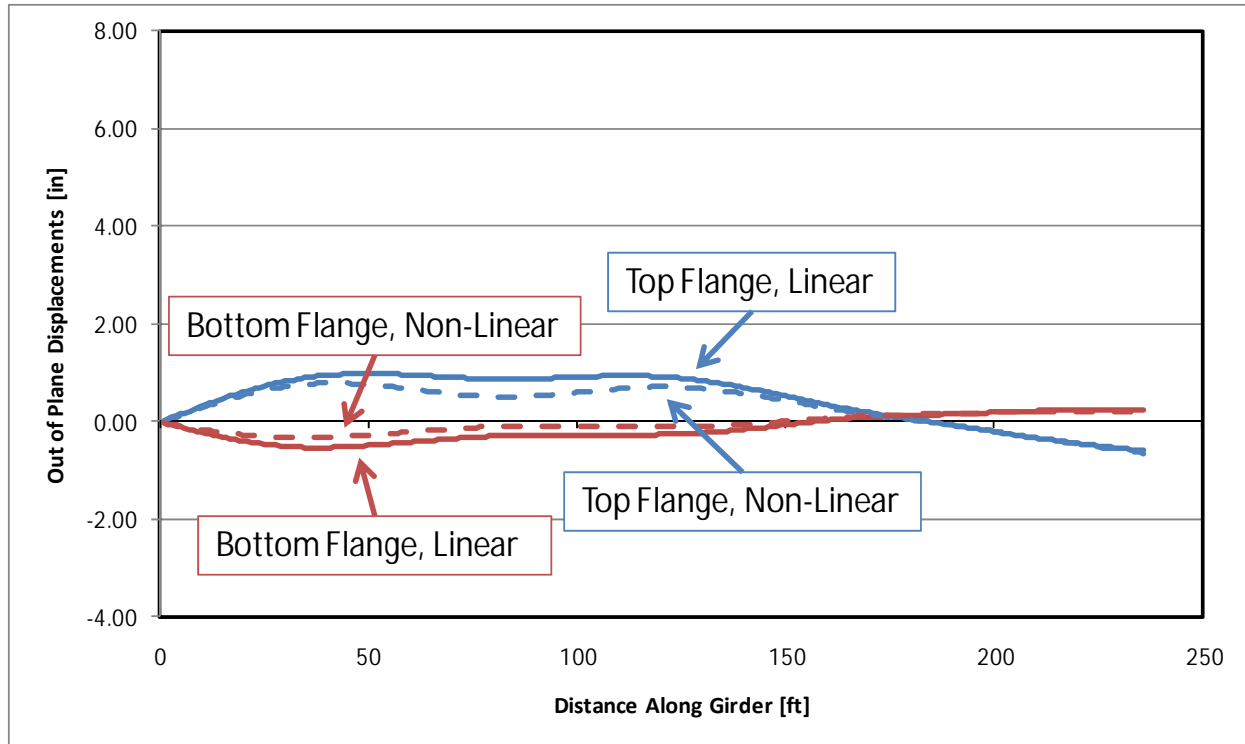


Figure 5.27: Linear and Non-Linear Displacements Along a Girder for a Girder with a Restoring Force

5.5.3 Linear-Elastic Comparison

As stated above, the restoring and disturbing effects can only be calculated using a second order, geometric non-linear analysis that considers geometric deformations. Therefore the linear analysis done on both the top flange and bottom flange loadings should be the same because both were loaded with a 35 kip load. In Figure 5.28 and Figure 5.29, the out of plane displacement results shown above are magnified so the geometrically linear results are more apparent. When the graphs are amplified, it is easy to see that the out of plane displacements down the length of the girder are exactly the same for both the top flange loading and the bottom flange loading as would be expected.

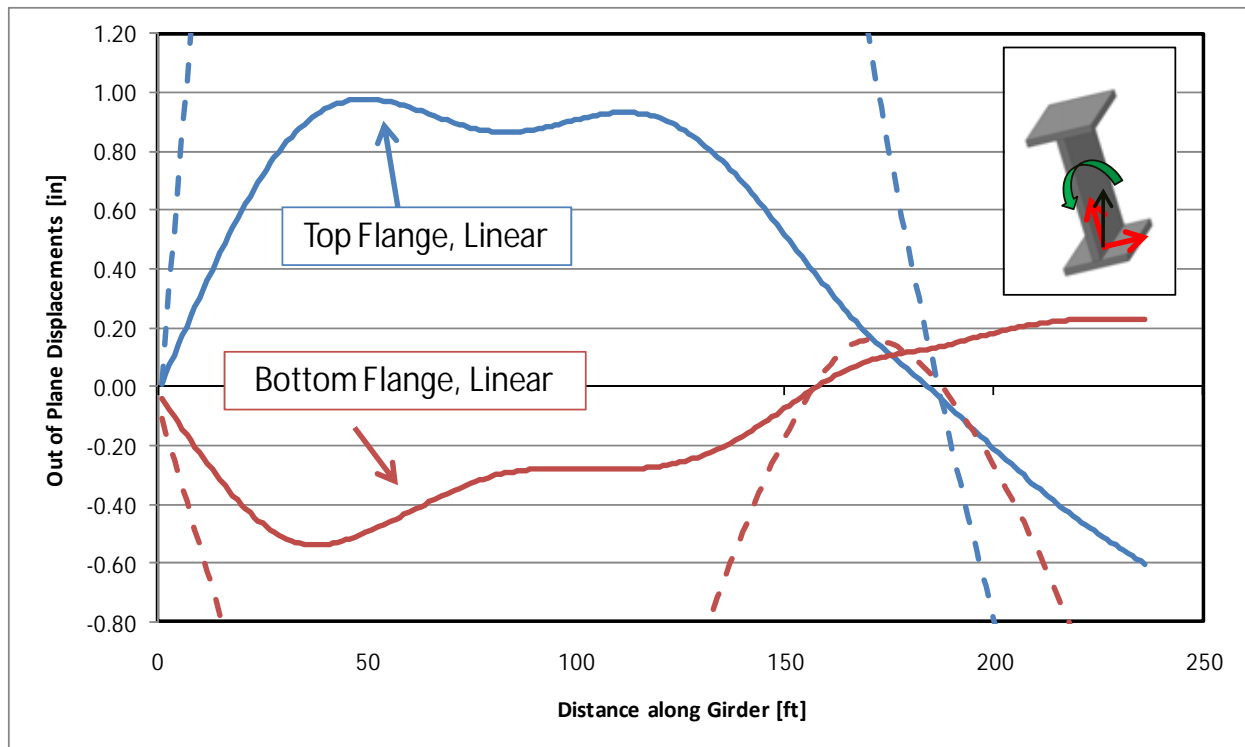


Figure 5.28: Linear Elastic Comparison – Bottom Flange Loading, Disturbing Force

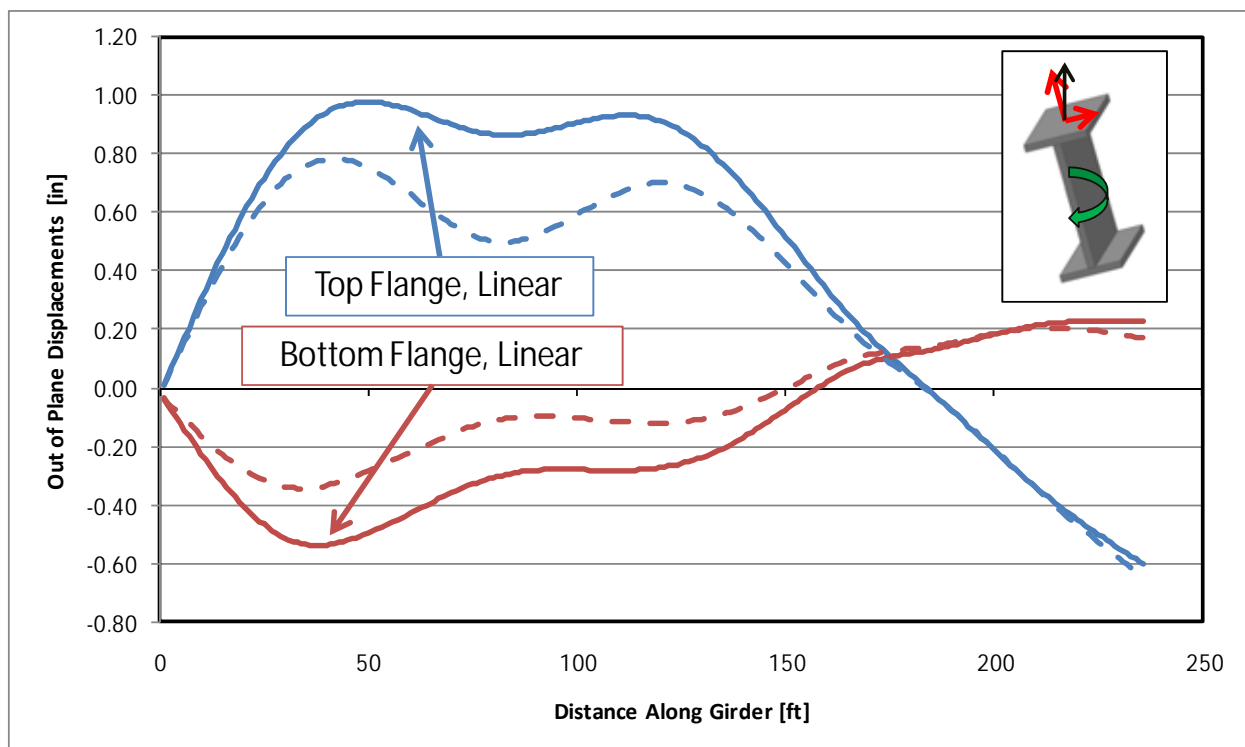


Figure 5.29: Linear Elastic Comparison – Top Flange Loading, Restoring Force

5.6 Critical Stages during Construction

From a stability perspective, the most critical stage in a bridge's life is typically during erection and construction of the concrete bridge deck. As stated before, it is during this time that the bridge is only partially braced. Therefore, shore towers and holding cranes are commonly required to safely erect the bridge. All erection stages should be analyzed without temporary supports to determine if excessive deformations or stresses occur and a temporary support is required.

One of the more critical stages during construction is when a single girder segment has been lifted for a particular cross section along the length of the bridge as seen in Figure 5.30.



Figure 5.30: Single Girder Segment Lifted for a Particular Cross Section

Because there are no other girder segments lifted, there is no bracing along the length of the single segment. As a result, the unbraced length of the single girder segment is significantly longer than the rest of the bridge which is usually the critical stage for girder stability. Once the second girder is erected and some of the cross frames are connected, the two girder system is much more stable compared to the single girder system. Even with the added stability, each erection stage should be checked to confirm whether or not the system alone is stable. Figure 5.31 shows a bridge system with a temporary support located at 80 feet down the girder. Deflections are graphed for the one, two, three, and four girder systems. It can be seen that after the second girder is erected, the bridge's maximum deflection does not decrease much by adding the third and fourth girders. Therefore, this shows the flexibility of a single girder system and the importance of checking the single girder system for stability. It should also be noted that the stability of the system without a temporary support should be analyzed before assuming the girder system is stable after the second girder is erected.

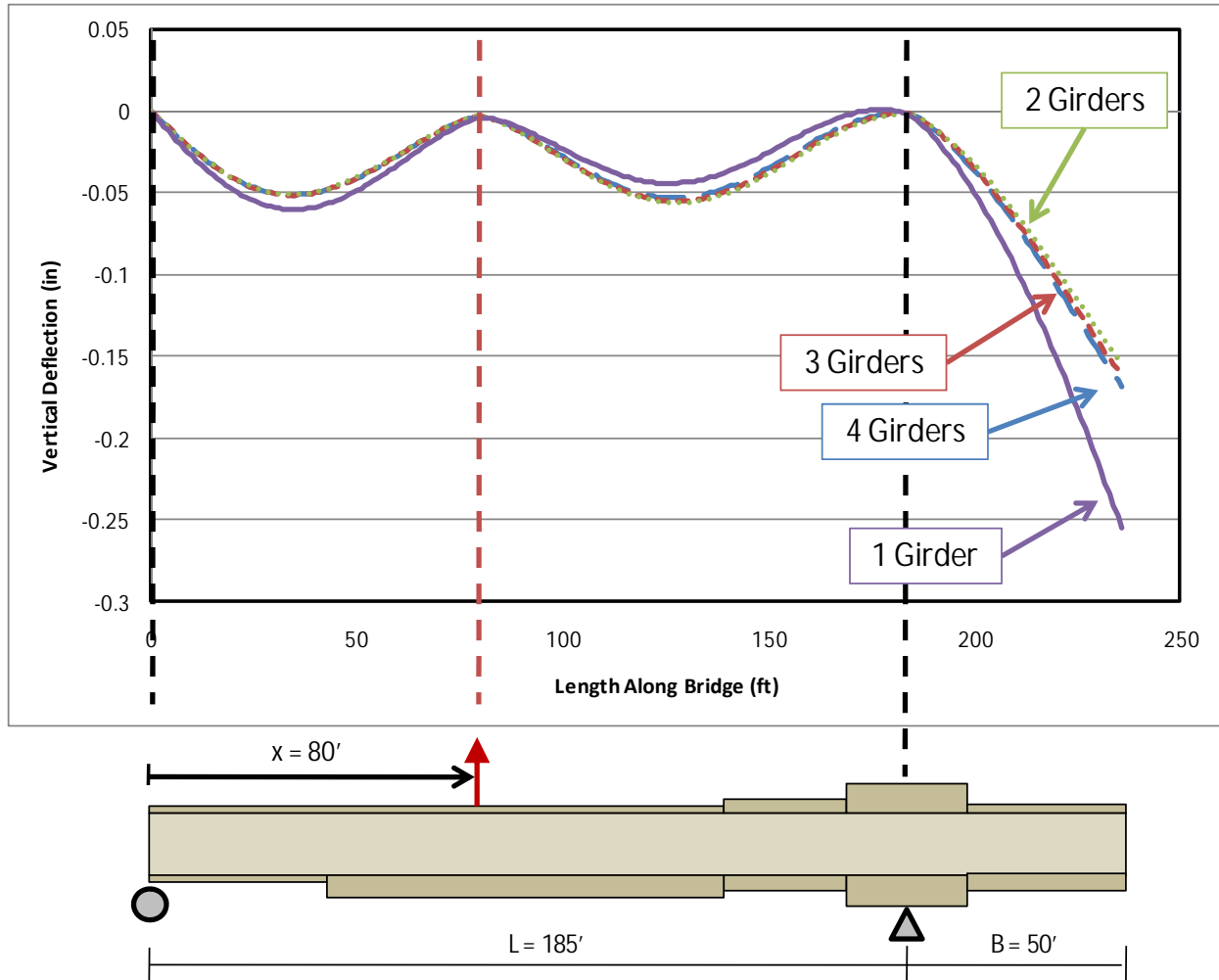


Figure 5.31: One, Two, Three, and Four Girder Erected Systems—Temporary Support at 80'

Another critical stage during construction occurs during the first concrete placement stage on a span. When the concrete is initially poured on a span, the concrete is essentially a fluid that acts as a large dead load on the system and provides no restraint.

5.7 Conclusion

There are many complicated issues when dealing with curved I-girder bridges. The stability of partially erected bridges are perhaps the most complicated to evaluate because of the limited presence of bracing and uncertainty in support conditions. Because of the lack of efficient analytical tools, erection engineers are left with very little guidance on evaluating the erection sequence. Many erectors are forced to rely on rules-of-thumb based upon past experience. Therefore, it is important to come up with guidelines based on research to help both contractors and design engineers better understand the behavior of curved I-girder bridges in the partially constructed state.

Common practices that are used for additional bracing during the partially constructed state include temporary shore towers and holding cranes. Although shore towers are desirable because they prevent translation of the girder in two directions, it is important to make sure that

the top flange of the girder is properly braced to prevent undesirable twist of the cross sections. Additionally, shore towers can be difficult to use because they require their own engineering to ensure that they can withstand the load of the bridge and require adequate land below the bridge to be placed on. Therefore, holding cranes can sometimes be more desirable due to their ability to be used only when needed and minimize time to be placed over obstacles such as busy roads or water.

Many geometric parameters were varied as well as the stiffness of the top flange bracing used for the shore towers and the load parameters used for the holding cranes. For both the shore towers and the holding cranes, it is suggested that they are placed close to the position of maximum moment. When using a 3-D finite element analysis software package, this position can often occur at the location of the highest stresses. Placing a shore tower at the position of highest moment allows the shore tower to be designed for close to the minimum amount of load and will minimize the bending/warping stresses as well as the displacements. When using a holding crane, it is recommended to lift with a value equal to the reaction of a rigid vertical support at the same position. This will keep the web of the cross section vertical and will minimize the second order effects that occur due to twisting of the cross section. It is important to keep the load in a holding crane very close to the reaction of a rigid support placed at the same position because a small deviation from this load can dramatically increase both the warping/bending stresses as well as increase the deflections down the length of the girder. As long as the proper load is lifted with for a given location of a holding crane, the location of the holding crane can vary from the location of maximum moment without causing dramatic changes in the bending/warping stresses and the displacements.

Due to load height effects associated with shore towers and holding cranes, it is important to consider second order effects when conducting an analysis. Because shore towers are supported on the bottom flange, as the girder cross section rotates, a small component of the reaction will help continue to rotate the cross section creating a disturbing force. This can be prevented if the top flange of the girder is properly braced against rotation at the location of the shore tower. Holding cranes, on the contrary, typically support the girder at the top flange. As a result, as the cross section rotates a small component of the holding crane force will be applied in the direction opposite to the rotation of the girder. This creates a restoring force and will help the behavior of the girder. Without using a second order analysis that accounts for geometric deformations, the behavior of a girder will be similar regardless of where on the cross section it is loaded.

Some of the most critical stages of construction occur when a single girder section is lifted or during the first concrete placement on a given span. Both of these stages are critical due to the lack of bracing. Therefore, it is typically desirable to use a shore tower or holding crane to temporarily brace the system until additional bracing can be provided to the system. In general though, it is good practice to check stability of a system anytime support conditions or bracing is changed or large additional loads are applied to the system.

Chapter 6. UT Bridge Program

6.1 General Information

UT Bridge is a three-dimensional finite element program that was developed as part of this research project for the analysis of curved steel I-girders during construction. The program is capable of performing a linear elastic analysis and an eigenvalue buckling analysis during girder erection and also placement of the concrete bridge deck. The program allows for material self-weight, wind loading, point loading, and temporary supports. The program is comprised of three parts: a pre-processor, processor, and post-processor.

6.1.1 Pre-Processor

The pre-processor appears when UT Bridge is opened. This part of the program requires the user to enter the information readily available from bridge plans directly into forms. UT Bridge helps the user easily enter the information by systematically prompting the user for information on a series of fourteen input forms. The first nine forms define the bridge properties, the next three forms define the construction analysis cases, and the last two forms allow the user to define the kinds of analysis to perform. A flow chart showing the structure of UT Bridge is shown in Figure 6.1. The pre-processor was developed in Visual Basic.

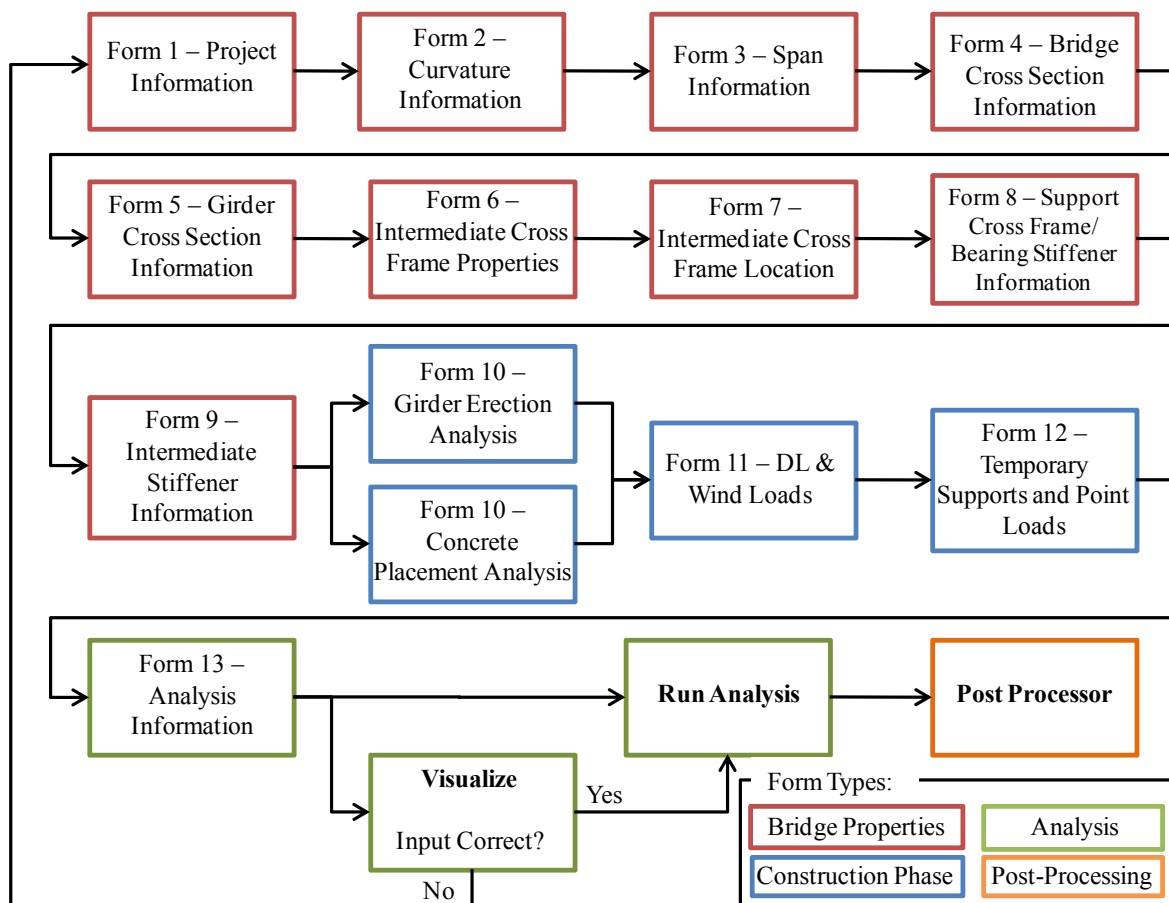


Figure 6.1: Flow Chart of UT Bridge

6.1.2 Processor

The processor within UT Bridge is a FORTRAN program that assembles the user defined input from the preprocessor and develops the geometric model of the bridge. The model is defined by the nodes and elements necessary for the three-dimensional finite element analysis. The global stiffness matrix is formulated by combining the individual stiffness matrices for the shell elements, beam elements, truss elements, and spring elements that make up the full model. The output is provided so that the post-processor (UT Viewer) can display the information.

The processor will always perform a linear elastic analysis for each analytical case specified by the user. The eigenvalue buckling analysis will only be performed if it is specified by the user. The linear elastic analysis assumes small displacement theory and thus for each erection sequence stage the global stiffness matrix is formulated and solved assuming that elastic redistribution of deflections and stresses will occur from the previous analysis case. The concrete placement analysis has a time dependent component in which the concrete material properties vary from analysis case to analysis case. Thus the concrete placement analysis is a linear incremental analysis that calculates the deflections and stresses of each analysis based only on newly applied loads and utilizing the current system global stiffness. The total deflections and stresses are calculated by summing the cumulative effects of all the previous analyses. Thus adding an intermediate shore tower during a concrete placement analysis will not result in zero displacement at the shore tower location, but rather only zero incremental displacement for the analysis case during which the shore tower exists.

6.1.3 Post-Processor

The post-processor for UT Bridge is called UT Viewer and was developed using C++. UT Viewer has the capabilities to show the user a full three-dimensional view of the user defined bridge as well as display the results from the specified analysis. After UT Bridge has completed a full analysis, the user can display two-D graphs of the stresses, displacements, and rotations of the bridge at tenth points along each span. UT Viewer also provides the cross frame forces and support reactions for each analysis case. Additionally, the numerical data is available in tabular form in case the user wishes to further manipulate the data in a program of their choice, such as Microsoft Excel.

6.2 Preprocessor

The UT Bridge preprocessor is a series of fourteen forms that allow the engineer to take information readily available from typical engineering plans and enter the necessary input in order to perform a robust 3-D finite element analysis. This philosophy was central to the development of UT Bridge with the ultimate goal of providing a tool that an engineer could quickly analyze complex systems accurately. Prior to the development of UT Bridge, these types of analyses were only completed for specialized cases at great expense. However, to fully utilize the capabilities of the program the assumptions implicit in the development need to be understood.

The program has some basic limitations and is based upon some predefined assumptions that bound the problem and provide simplifications to the input process. It is critical for the user to understand these assumptions to ensure the modeled bridge is accurate. Most bridge engineers place the bridge along a predefined profile grade line (PGL) provided by the transportation engineer. This location varies from roadway project to roadway project. The PGL can be the

center of the roadway, the edge of a line, or the center of a divided highway, which for a bridge may not lie on the bridge. Thus a standard PGL was established for all bridges in the UT Bridge program and it is set at the centerline of girder 1. Girder 1 is the left most girder on a cross sectional view looking ahead station. Figure 6.2 is a schematic of a typical bridge cross section with the girders numbered and the coordinate axis shown at the profile grade line. UT Bridge will analyze both straight and curved girder bridges. The program assumes a positive radius of curvature is a bridge curving left looking ahead station and a right curving bridge is a negative radius of curvature. Figure 6.3 is a schematic of a pair of bridges with different signs for the radius of curvatures indicating the direction of curvature consistent with the program.

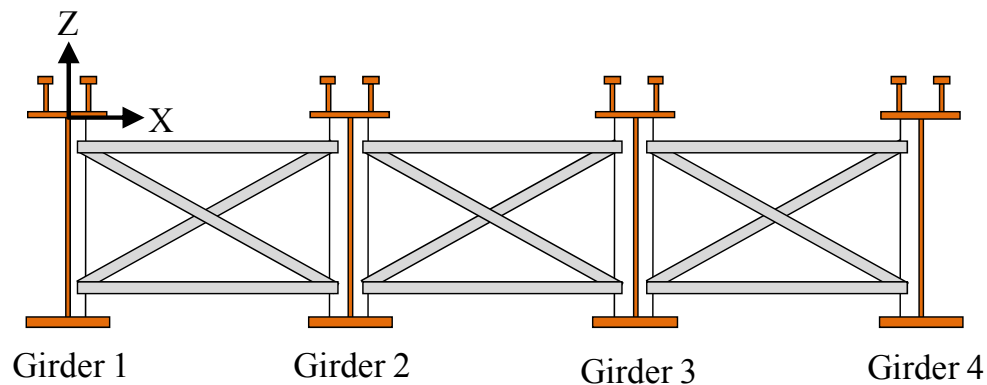


Figure 6.2: Typical Bridge Cross Section Looking Ahead Station

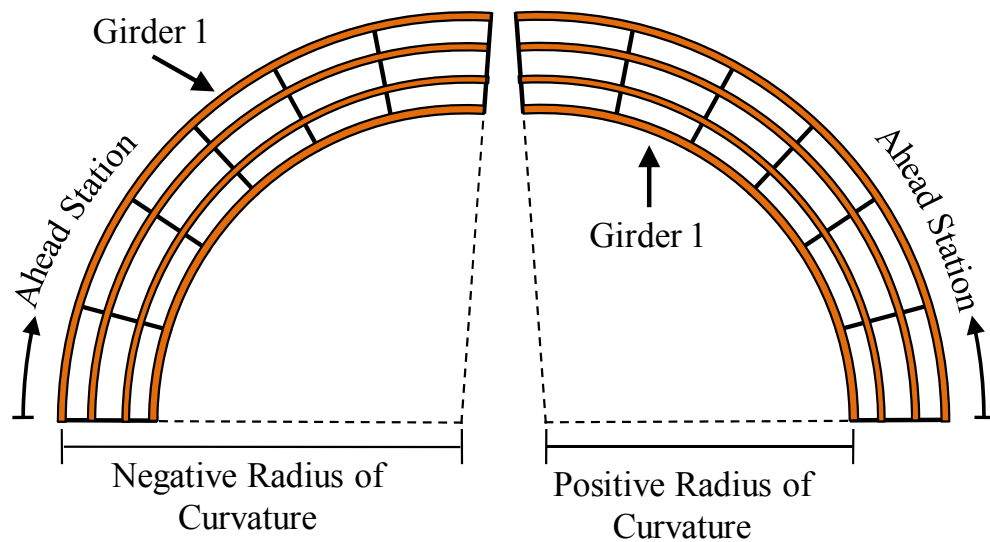


Figure 6.3: Sign Convention for Curved Bridges

UT Bridge allows for any number of girders and any number of spans; however, very large systems may have issues with the problem size (this will be discussed in more detail later in the chapter). Additionally, the program allows for substructure skew. The sign convention used within UT Bridge is arbitrarily chosen such that a right forward skew is a positive skew angle. While a left forward skew is a negative skew angle. Figure 6.4 is a schematic of a bridge

where the first abutment's skew angle (θ_1) is negative, because it is a left forward skew. The bridge's middle pier is at no skew ($\theta_2 = 0$) or perpendicular to Girder 1 and the end abutment's skew angle (θ_3) is positive or a right forward skew.

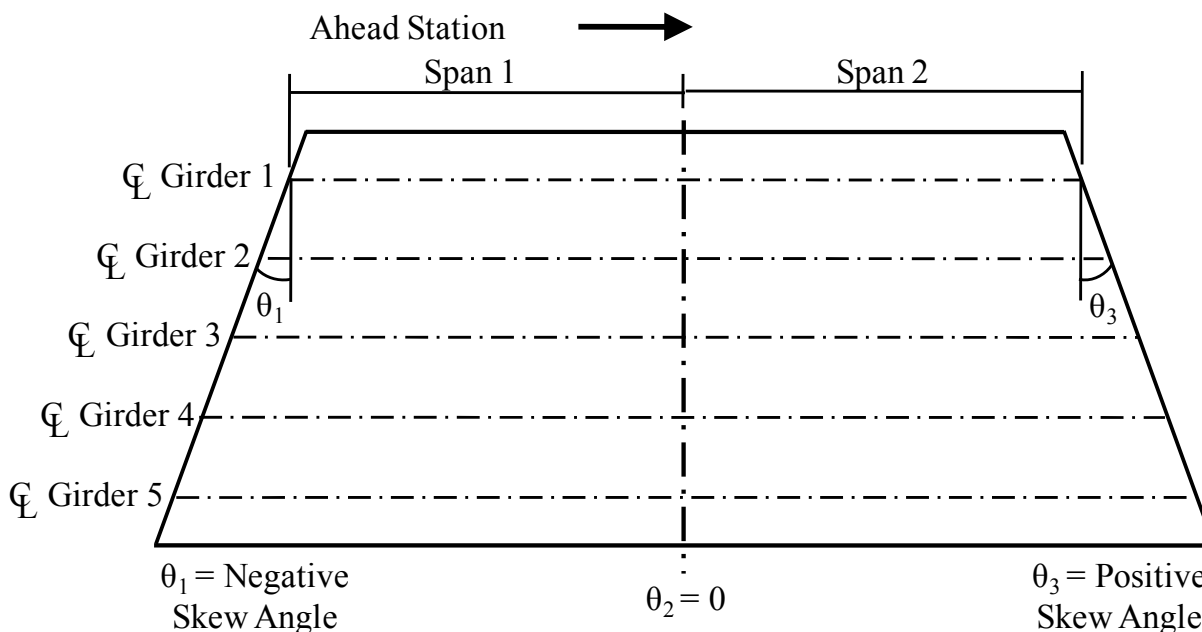


Figure 6.4: Skew Angle Sign Convention

The program assumes that all cross frames are an X-type cross frame. This cross frame type is the specified standard for curved I-girder bridges in the state of Texas and is therefore used in the program. For the purposes of cross frame stiffness, the diagonal chords are assumed to be comprised of tension only members, which is a conservative assumption with regard to the X-type cross frames. This results in the cross frames behaving as if there is a single tension diagonal and the reported output is given as such with one diagonal having zero force and the other diagonal having a tensile force. Cross frames are assumed to be attached to girders by stiffener plates and thus all girders have stiffeners located at the cross frame location. Additional intermediate stiffeners are allowed and can be specified in the preprocessor to stiffen the web and prevent web buckling in regions of high shear. Support cross frame and bearing stiffeners are assumed to exist at each substructure unit. For some curved bridges with highly skewed supports, cross frames are placed radially and do not exist along interior supports. UT Bridge will include these in the model, but their contribution to the system stiffness can be negated if the user specifies a small cross sectional area for these members. Another important assumption regarding bearing stiffeners is that the program assumes they will exist on both sides of the girder. Thus when specified by the user they only need to specify one bearing stiffener and the program will automatically place one on the other side. Figure 6.5 is a typical X-type cross frame with the individual chords labeled. The necessary input for each chord is the cross sectional area of the chord.

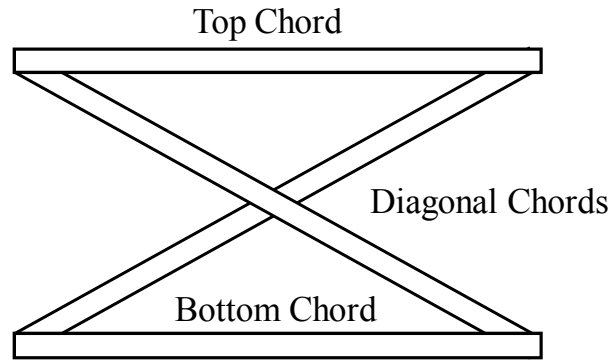


Figure 6.5: Typical X-Type Cross Frame

One of the most powerful features of the UT Bridge program is the ability to fully analyze bridge erection sequence. The program allows for each step in the erection to be analyzed individually to determine deflections, stresses, and rotation of each girder. The bridge model is assumed to be erected from one end of the bridge toward the other. This can be completed ahead station or back station. Thus a bridge built from each end and completed with a central drop-in section cannot be modeled explicitly. The program treats each set of lifted girders as an analysis case. This can be a single girder or multiple girders depending on the lifting sequence used by the erector. Typically, the first girder lifted will control the design as the unbraced length is maximized for the bridge. Subsequent intermediate construction phases may be less critical and the analysis can be performed or the engineer can choose to spend their time specifying the next potentially critical stage. This flexibility provides the erection engineer with the options previously unavailable by current bridge analysis software. Figure 6.6–6.8 are a set of screen shots from the UT Bridge post-processor, UT Viewer, showing a model of a bridge with associated pictures of the erection process being modeled.

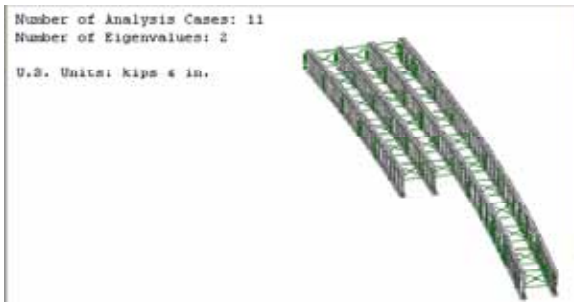


Figure 6.6: Bridge Erection Sequence with Associated UT Bridge Model

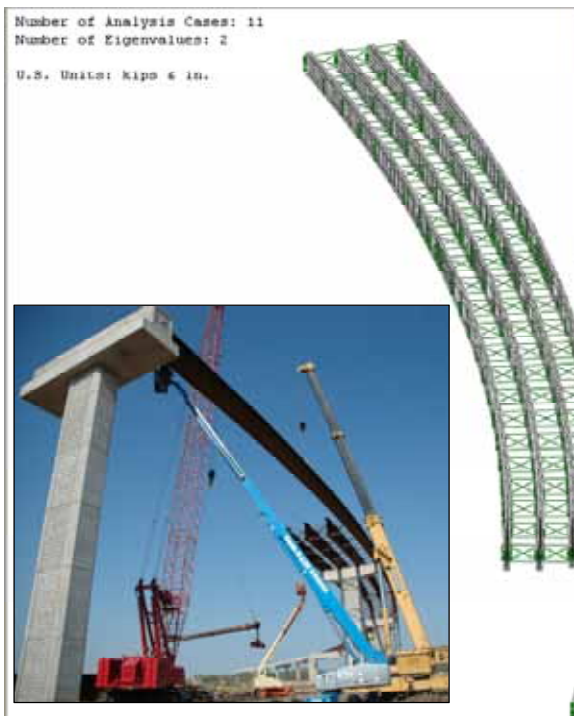
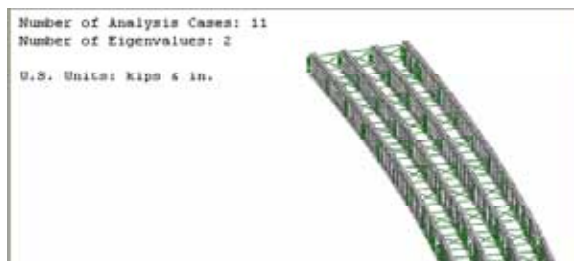


Figure 6.7: Bridge Erection Sequence with Associated UT Bridge Model

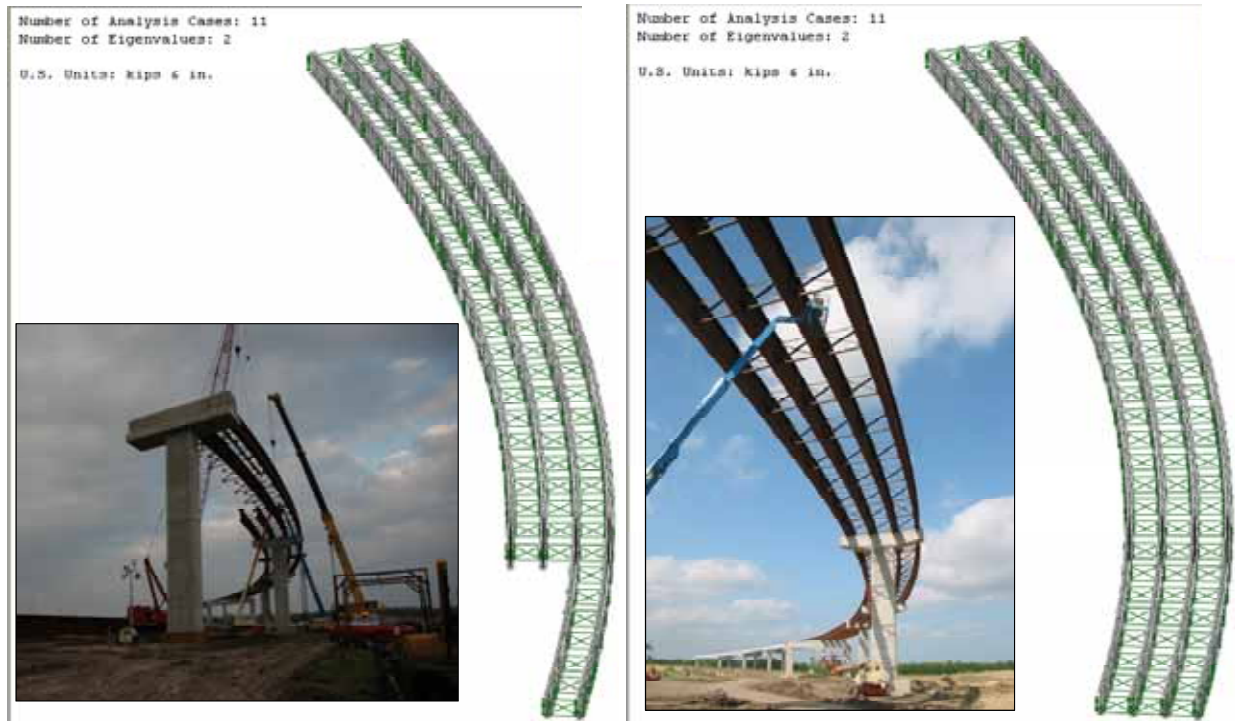


Figure 6.8: Bridge Erection Sequence with Associated UT Bridge Model

The other option for analysis is the ability to model the concrete bridge deck placement. The user can specify the sequence of the deck placement and analyze the state of stress for each stage of the concrete placement. This requires the early age concrete to be modeled in a time dependent nature. Thus a linear incremental analysis technique was used in which the loads in the present analysis case are applied to the current system stiffness. This increment of displacement and stresses is then summed with all previous analyses to obtain the current state of stress. The modeling of early age concrete and specifically the interaction of the shear studs and the early age concrete has not generally been studied extensively. The recommended method of analysis the bridge is to allow UT Bridge to interpolate the modulus of elasticity of the concrete and the shear stud spring stiffness using results from research conducted at the University of Texas at Austin by Topkaya (2002). The research included a series of push-out tests with shear studs in early-aged concrete. The concrete used was a Class-S type concrete commonly used in bridge decks in the state of Texas. The requirements for Class-S concrete include:

- Minimum 28 day Compressive Strength: 4000 psi
- Minimum 7 day Flexural Strength: 570 psi
- Maximum Water/Cement Ratio: 0.47
- Desired Slump: 3 inches (4 inches maximum)

The shear studs used were 3/4 inch diameter and with a 5 inch height. Figure 6.9 is a schematic of the deformation pattern commonly encountered during the push-out test. Figure 6.10 is a schematic of the push-out test setup and Figure 6.11 is an actual picture of the test setup.

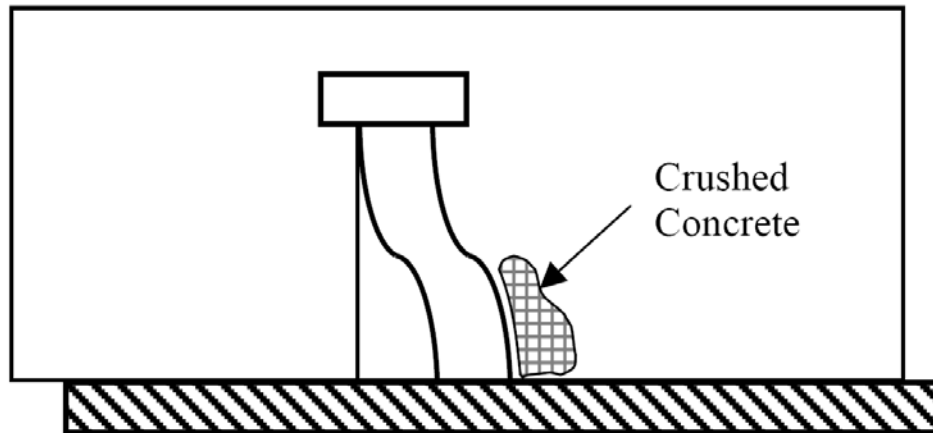


Figure 6.9: Deformation Pattern for Shear Studs in Concrete Deck (Topkaya 2002)

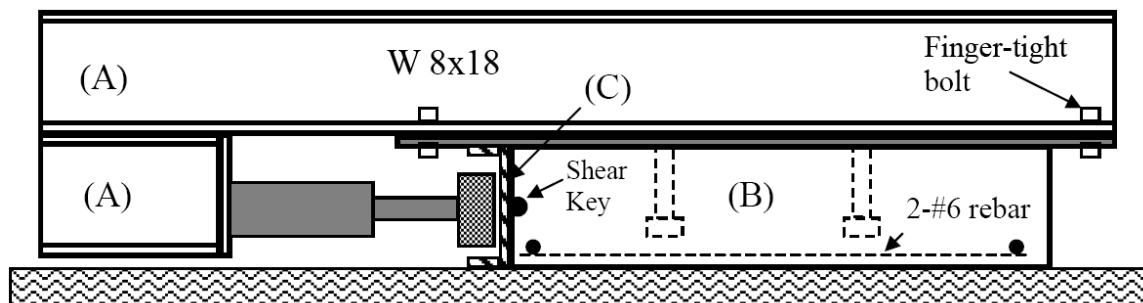


Figure 6.10: Schematic View of Push-out Test (Topkaya 2002)



Figure 6.11: Picture of Push-out Test Setup (Topkaya 2002)

A typical load displacement curve for the push-out test is shown in Figure 6.12. It was decided that the design strength of the shear stud would be at a slip of 0.03 inches. These displacement values along with the design loads give in Table 6.1 provide the shear stud spring stiffness interpolation for UT Bridge. In addition to the push-out test compressive strength and modulus test were performed simultaneously providing the interpolation for the early age concrete modulus used in UT Bridge.

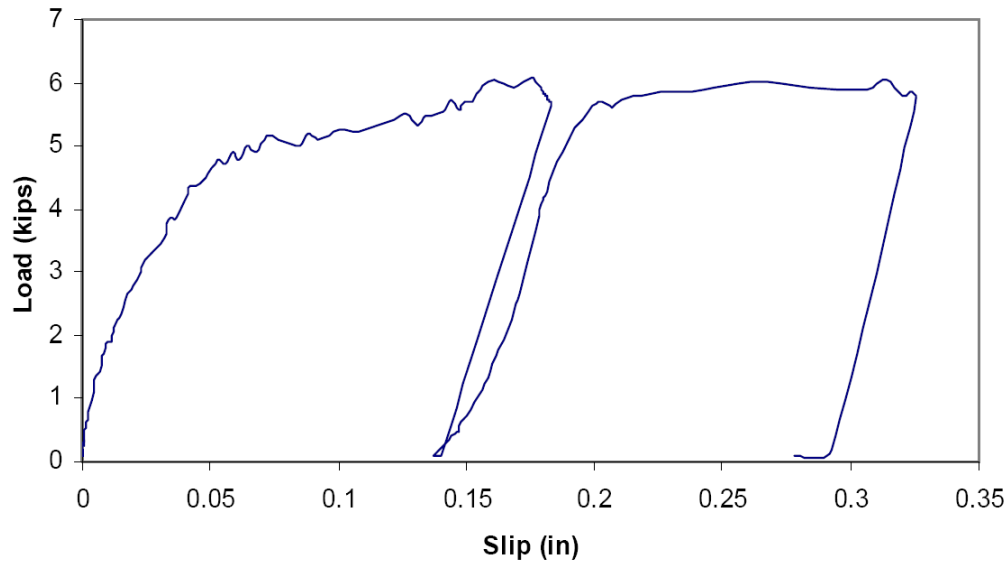


Figure 6.12: Typical Load Displacement Graph (4 hr Concrete) (Topkaya 2002)

Table 6.1: Push-out Test Results (Topkaya 2002)

| Time | Stud Design Strength, Q_d (kips) | | | | Stud Maximum Strength, Q_{max} (kips) | | | |
|--------|------------------------------------|------|------|-------------|---|------|------|-------------|
| | Specimen Number | | | Average | Specimen Number | | | Average |
| | 1 | 2 | 3 | | 1 | 2 | 3 | |
| 4 hr | 3.6 | 4.4 | 3.7 | 3.9 | 6.0 | 6.2 | 6.1 | 6.1 |
| 8 hr | 8.1 | 6.3 | 6.9 | 7.1 | 10.2 | 8.85 | 10.0 | 9.6 |
| 13 hr | 10.1 | 7.7 | 9.00 | 8.9 | 13.5 | 10.1 | 14.7 | 12.7 |
| 22 hr | 11.9 | 13.0 | 11.5 | 12.1 | 17.5 | 17.6 | 17.5 | 17.5 |
| 3 day | 13.8 | 14.5 | 13.0 | 13.7 | 17.5 | 19.4 | 19.1 | 18.7 |
| 7 day | 14.9 | 15.0 | 14.9 | 14.9 | 18.4 | 20.2 | 19.8 | 19.4 |
| 14 day | 15.3 | 16.0 | xxx | 15.6 | 19.2 | 20.1 | 21.2 | 20.2 |
| 28 day | 18.3 | 16.4 | 17.0 | 17.2 | 21.0 | 21.0 | 21.0 | 21.0 |

The program also permits the user to independently input the modulus of elasticity of the concrete and the shear stud spring stiffness used in the program. However, the user is cautioned that such input should be based upon a clear understanding of the actual properties that should be based upon independent tests.

UT Bridge discretizes the bridge into nodes and elements required for a 3-D finite element analysis. The most accurate element is a square element with a width to length (aspect ratio) of 1.0. However, because the geometry of bridge girders varies widely, the developers set the cross section such that two elements represent the flanges and four elements represent the web of each girder. The deck has two elements representing each overhang, two elements over each flange, and three elements representing the deck between the girders. The element length was set by attempting to minimize the aspect ratio for a range of typical girders.

It should be noted that within finite element theory the finer meshes will generally tend to provide improved accuracy in the solution. However, due to computational limitations (both hardware limitation and solution time) a reasonable mesh is a required balance. The normal mesh has been assessed to be reasonable for a typical bridge. However, it has been noted that for very large problems (several girders and long bridge lengths) the number of nodes and thus the number of degrees of freedom requires more memory to solve than that available on a typical workstation. Thus an option to reduce the problem size and provide the capacity to model large bridge systems is available.

Mesh density options include Coarse Mesh, Normal Mesh, and Fine Mesh. The default mesh density is Normal Mesh. A Normal Mesh density places an element at approximately every two feet for U.S. Units and approximately every 700 mm for SI Units. For a Coarse Mesh, the mesh is multiplied by a factor of two and for a Fine Mesh, the mesh is divided by a factor of two. An example of Coarse Mesh can be seen in Figure 6.13, and example of Normal Mesh can be seen in Figure 6.14, and an example of Fine Mesh can be seen in Figure 6.15.

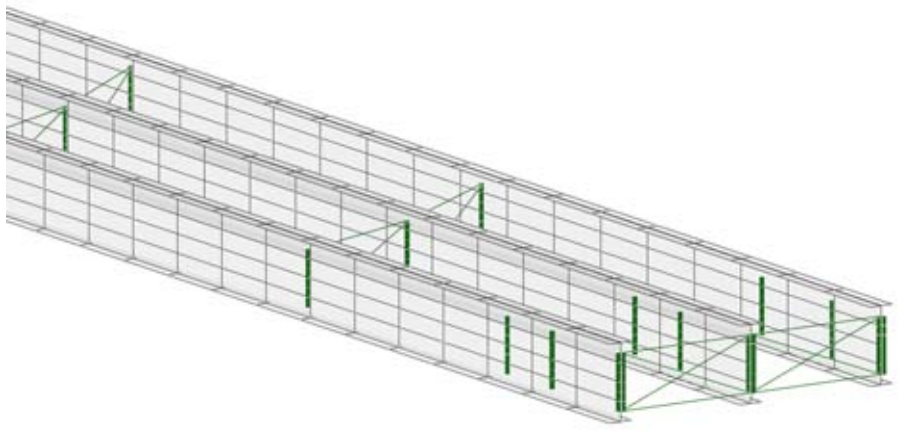


Figure 6.13: Coarse Mesh Density

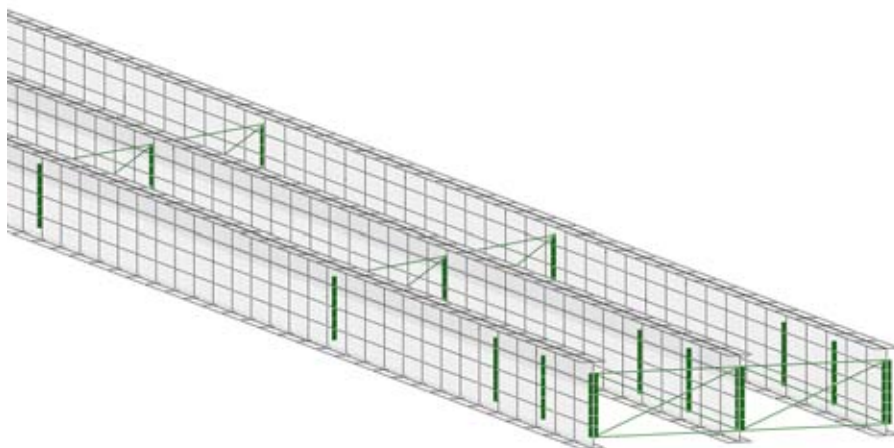


Figure 6.14: Normal Mesh Density

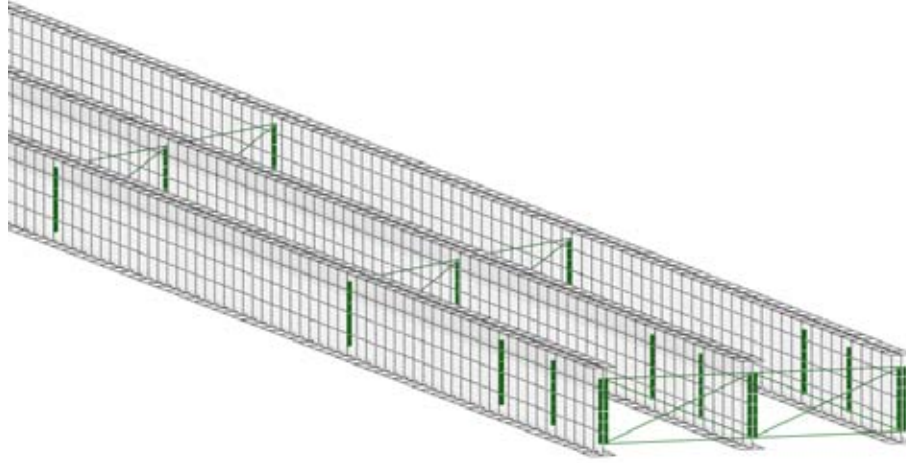


Figure 6.15: Fine Mesh Density

For a workstation with 3.50 GB of RAM the approximate capacity is 100,000 nodes. The eigenvalue solver takes more memory than the linear solver and the node capacity utilizing the linear solver only is slightly higher, but this number provides a good approximation. The approximate number of nodes can be calculated by the following equations. The expression in (4.30) is used for erection analysis and (6.2) is used for the deck placement analysis.

$$\# \text{ Nodes} = (17 * \text{Number of Girders}) * \frac{\text{Length}}{\text{Unit Factor}} * \text{Mesh Density} \quad (6.1)$$

$$\# \text{ Nodes} = (27 * \text{Number of Girders} + 3) * \frac{\text{Length}}{\text{Unit Factor}} * \text{Mesh Density} \quad (6.2)$$

Where:

| | | |
|---------------------|---|---|
| <i>Length</i> | = | Total Length of bridge in ft (U.S. Customary Units) |
| | = | Total Length of bridge in mm (SI Units) |
| <i>Unit Factor</i> | = | 1 (U.S. Customary Units) |
| | = | 350 (SI Units) |
| <i>Mesh Density</i> | = | 1 if Normal Mesh |
| | = | 2 if Fine Mesh |
| | = | 0.5 if Coarse Mesh |

6.3 UT Bridge Finite Element Computational Programming

6.3.1 Finite Element Analysis

The UT Bridge program utilizes a 3-dimensional finite element analysis. The finite element method is one of the most widely-used analysis methods available to engineers and scientist today. The flexibility and accuracy of the methods have resulted in its favorable use for a range of modern problems, specifically in structural engineering the method has been used to determine displacements of indeterminate structures. Once the displacements are known, the strain and stresses can be calculated and compared to what the code allows. The origins of the finite element method lay in mathematics by Courant (1943), but were first implemented by

engineers in the aerospace industry during the 1950s. That is when Jon Turner of Boeing Airplane Company extended the one-dimensional structural analysis to two-dimensions by discretizing a portion of an airplane wing into constant strain triangles (Turner, et al. 1956). It was a few years later that Ray Clough coined the term finite element method (Clough 1960) to describe the use of two-dimensional discretization of continuous structural surfaces to approximate the displacements over the surface and thus the stresses and strains. This was an extension of the direct stiffness method that was utilized by structural engineers for years before the development of finite element methods. To demonstrate the discretization process Figure 6.16 shows a frame discretized with beam elements as is custom for the direct stiffness method. The bridge deck in Figure 6.16 shows the discretization of the area with quadrilateral elements.

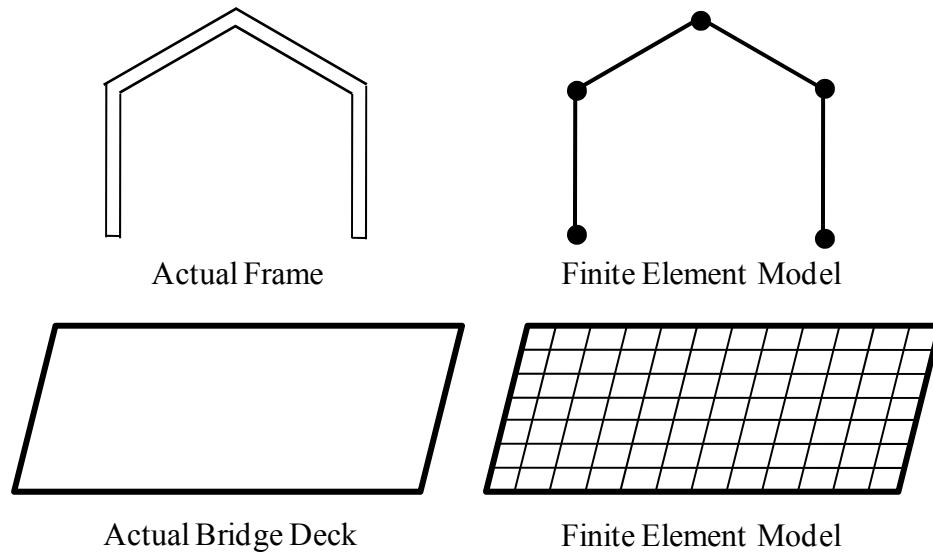


Figure 6.16: Finite Element Idealization

In both models the displacements are obtained at the node locations, the ends of the beam or the corners of the quadrilateral, and at all other locations the displacements are approximated. This is accomplished by concentrating the summation of the stiffness of the elements at the nodes of the element. The general procedure of the finite element method include discretization, generating local element stiffness, combining element stiffness into a global system, applying loads and boundary condition, solving the mathematical model, and processing the results.

The simplest form of the set of equations to be solved in the finite element process is:

$$[K]\{\Delta\} = \{P\} \quad (6.3)$$

Where:

K is the structural stiffness matrix,

Δ is the nodal displacements, and

P is the loads on the structure.

Thus the displacements can be obtained by inverting the stiffness matrix and multiplying by the loads as shown in (6.4).

$$\{\Delta\} = [K]^{-1}\{P\} \quad (6.4)$$

With this brief introduction the following sections explain the process used in the development of UT Bridge.

6.3.2 Node Numbering

This is an explanation of the node numbering approach implemented in the UT Bridge program. The program generates node locations by an algorithm developed to allow for curved or straight I-girder bridges. There is no limit on the number of girders or the number of spans. The algorithm allows for skewed substructures to be included with positive skew being defined as a right forward skew and negative skew being defined as a left forward skew. Figure 6.17 shows the node numbering schematic. There are two shell elements per flange that correspond to five flange nodes and four shell elements per web, which correspond to nine web nodes. In practice the profile grade line varies depending on the bridge. A standard was needed for the purpose of this program; the center line of the leftmost girder (or girder 1) was chosen as the standard. Therefore, the span lengths and substructure skews are designated along the center line of girder 1.

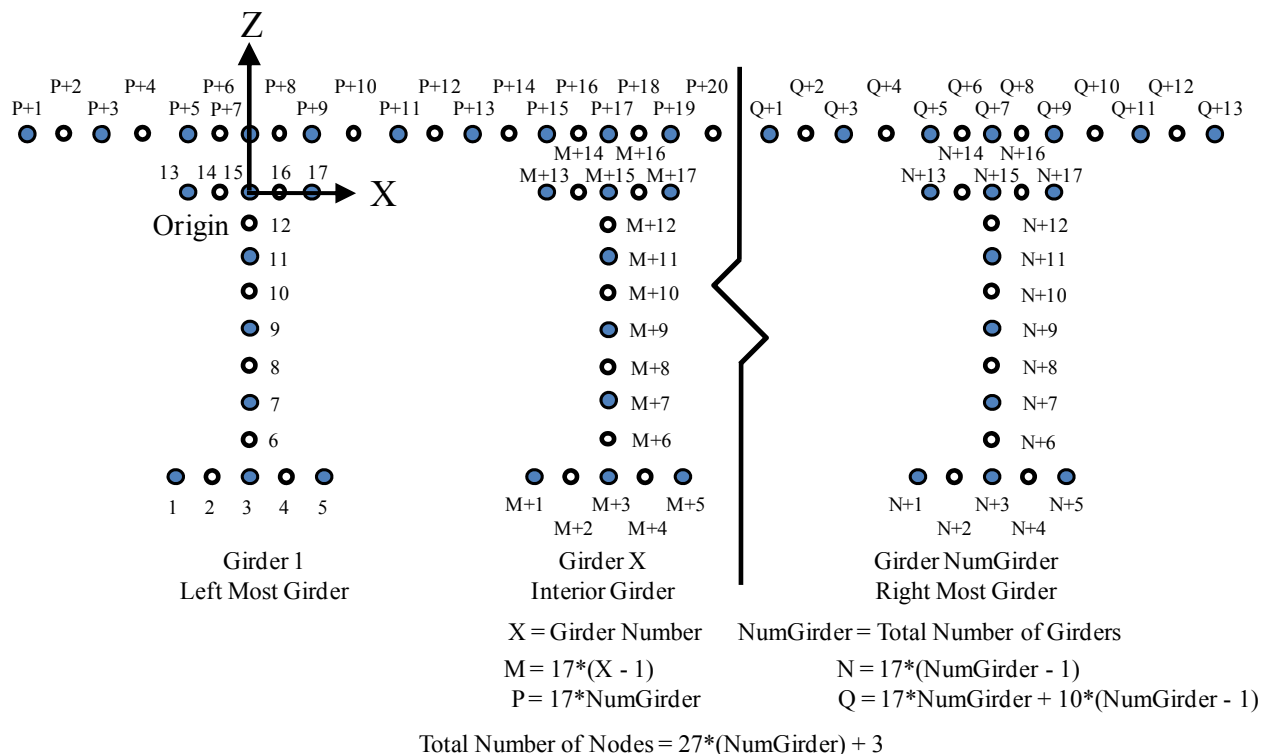


Figure 6.17: Schematic of the Node Numbering Used in UT Bridge

Element connectivity is defined relating the elements to the nodes associated with each element. Nine-node shell elements are generated for the steel plates of the girder and the concrete deck, truss elements are generated for the cross-frames, beam elements are generated for the stiffeners, and springs elements are generated for the shear studs. To ensure a regular element layout for the deck it was decided that all girders would consist of an equal number of elements. To ensure this the centerline length of each span is calculated from the skew, girder spacing, and Girder 1 information. The length is then divided into the number of segments that result in

approximately two-foot elements. By utilizing the nine-node shell elements the resulting nodal cross sections are at approximately one foot intervals along the length of the bridge. For spans with skewed substructures the element length will be larger on one side of the bridge centerline and smaller on the other side. This works well for most typical bridges, but may have trouble for short span bridges with a large skew differential from one support unit to the next as this situation will result in very small element lengths on one side of the bridge and long element lengths on the other. Figure 6.18 is a schematic of the nodal cross section layout of a skew bridge.

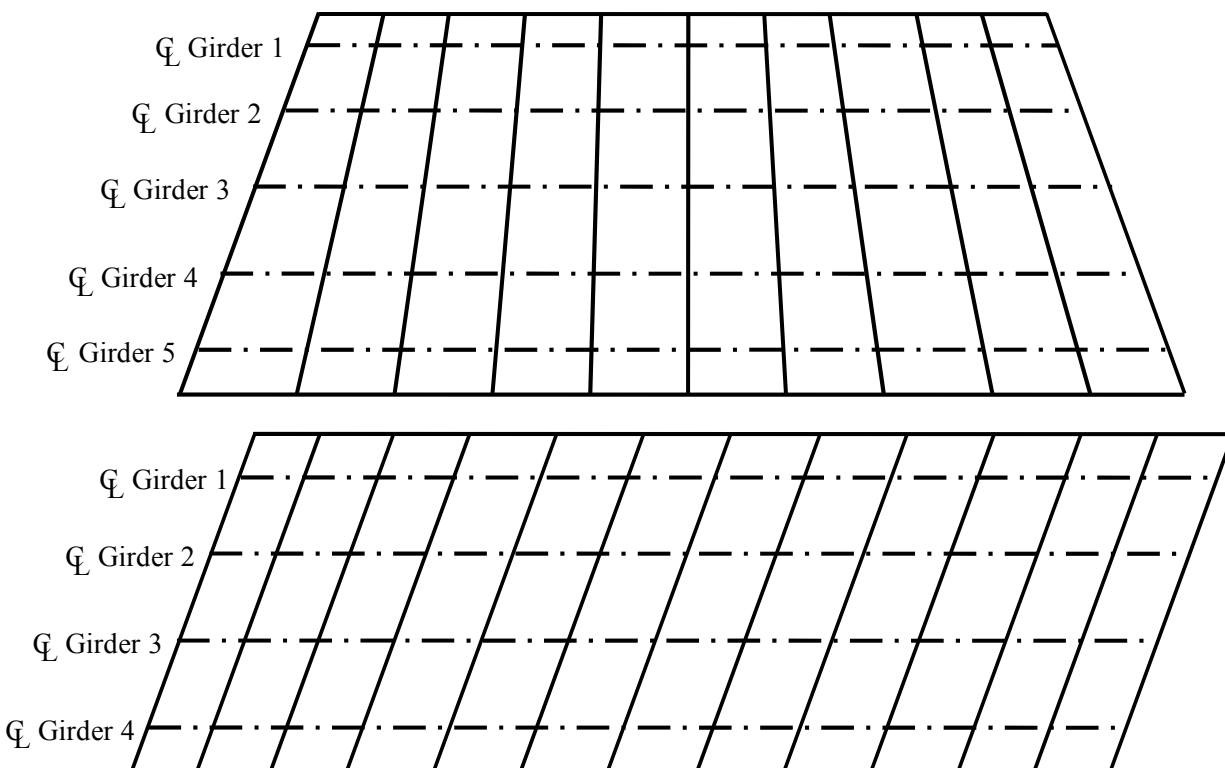


Figure 6.18: Skewed Bridge Nodal Cross Section Schematic

The element length (approximately two foot) was chosen to give acceptable element aspect ratios for typical steel plate girder bridges. The aspect ratio for a shell element is a ratio of the element's length to width. For a square the aspect ratio is one and it varies for all other quadrilaterals. During the assembly of the global stiffness matrix for the finite element analysis each individual shell element is transformed to a square master element and the stiffness is calculated following the algorithm discussed later in this chapter. The transformation to the master element introduces computational error inherent in finite element analysis, but this error can be minimized by maintaining an aspect ratio as close to one as possible. Considering the typical depth of the plate girder and flange widths it was deemed appropriate to use approximately two foot elements without a significant error. A similar aspect ratio was used in the development of U-TrAp (Toykaya 2002), which is software for analyzing trapezoidal box girders.

Another issue related to the aspect ratio is the skew of the individual elements. The element skew will also introduce a certain amount of numerical error as it is transformed to the

master element. U-TrAp 2.0 does not have the capability to allow for skewed substructure supports and thus this issue was not addressed previously, but was studied during this research and found that for typical bridges the effect is negligible.

6.3.3 Element Elastic Stiffness Formulations

Shell Element Elastic Stiffness Formulations

The first finite elements developed to model thin plates in bending were shells based on Kirchhoff plate theory which neglects shear deformations. These relatively simple shell element formulations superimposed a plate bending stiffness and a plane stress membrane stiffness. The result is a flat shell element that can be used to model flat components or used to model general curved shells as an assemblage of flat elements. The use of flat elements to represent a curved structure requires a relatively large number of elements to be used to represent the geometry to sufficient accuracy. Additionally, the use of this theory presented difficulties in satisfying the interelement continuity on the displacements and edge rotations, because the rotations are calculated from the transverse displacements (Bathe 1996). The Kirchhoff plate theory is analogous to Bernoulli-Euler Beam theory for beam elements. The more general shell element formulation used in UT Bridge separates the displacements and rotations of the surface normal vector into independent variables and allows the interelement continuity to be satisfied directly.

The model utilizes a nine-node isoparametric displacement-based shell element (Figure 6.19) originally developed by Ahmad, Irons, and Zienkiewicz (1970) and modified to prevent shear and membrane locking (Bathe 1996) to model the steel plates of the girders and the concrete decks as shown in Figure 6.20. Some details of the formulation are given in varying degrees in Bathe (1996), Topkaya (2002), and Popp (2004). An isoparametric element uses the same shape functions to define the geometry and the displacements. Displacement-based finite element procedures means the finite element solution is obtained by directly applying the variational principle in the finite element space which discretizes the space of admissible displacements for the structure (Chapelle & Bathe 2003). A functional is constructed that includes all the intrinsic features of the problem, such as the governing equations, boundary condition, and constraints, and for a structural or solids problem the functional represents the total energy of the system. Direct variational principles make use of methods such as the principles of virtual work and the principle of minimum total potential energy to determine approximate solutions to various problems (Reddy 2006). The space of admissible displacements corresponds to the smooth space of functional without discontinuities that violate the physics of the problem.

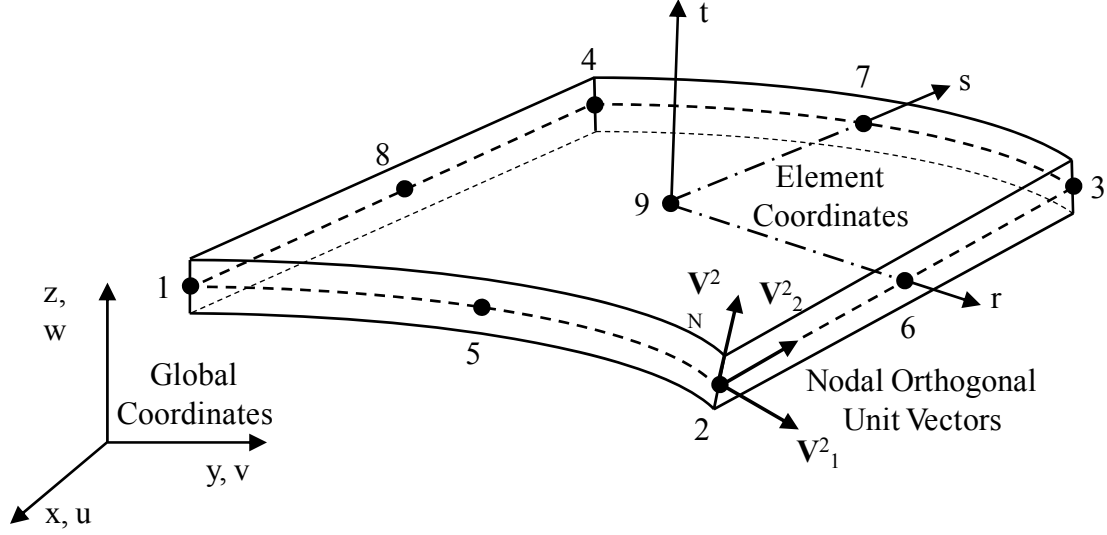


Figure 6.19: Nine-Node Shell Element Schematic

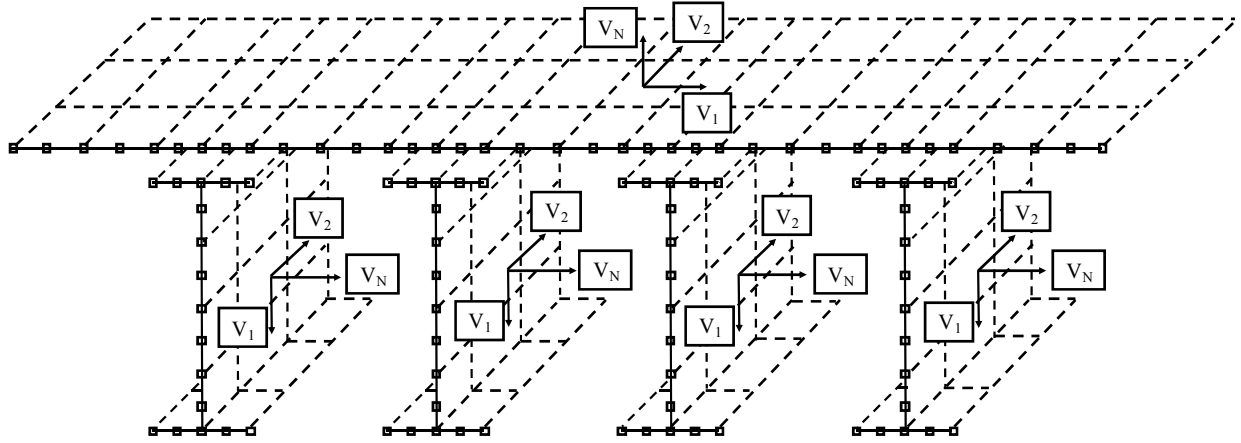
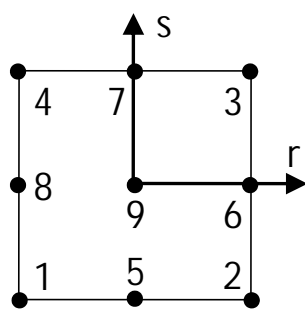


Figure 6.20: Schematic of Bridge Shell Elements

At each node a set of nodal mutually orthogonal unit vectors are defined with \mathbf{V}_N^i specifying the direction normal to the shell surface at each node location. In general, \mathbf{V}_2^i is defined along the length of the bridge, \mathbf{V}_N^i is always defined through the thickness, and \mathbf{V}_1^i is orthogonal to \mathbf{V}_2^i and \mathbf{V}_N^i . The element is mapped from global (x, y, z) coordinates to natural element coordinates (r, s, t) utilizing the following equation:

$$\mathbf{x}(r, s, t) = \sum_{i=1}^9 \left[\left(\mathbf{x}_i + t \frac{h}{2} \mathbf{V}_N^i \right) N_i(r, s) \right] \quad (6.5)$$

Where \mathbf{x} are the Cartesian coordinates of any point in the element, \mathbf{x}_i are the Cartesian coordinates of node point i , h is the thickness of the shell in the t direction at node point i , \mathbf{V}_N^i is the components of the unit normal vector at node point i , and N_i are the Lagrangian interpolation function (See Figure 6.21).



$$\begin{aligned}
 N_1(r, s) &= \frac{1}{4}(r^2 - r)(s^2 - s) & N_5(r, s) &= \frac{1}{2}(1 - r^2)(s^2 - s) \\
 N_2(r, s) &= \frac{1}{4}(r^2 + r)(s^2 - s) & N_6(r, s) &= \frac{1}{2}(r^2 + r)(1 - s^2) \\
 N_3(r, s) &= \frac{1}{4}(r^2 + r)(s^2 + s) & N_7(r, s) &= \frac{1}{2}(1 - r^2)(s^2 + s) \\
 N_4(r, s) &= \frac{1}{4}(r^2 - r)(s^2 + s) & N_8(r, s) &= \frac{1}{2}(r^2 - r)(1 - s^2) \\
 N_9(r, s) &= (1 - r^2)(1 - s^2)
 \end{aligned}$$

Figure 6.21: Figure 6.1: Natural Coordinate System and Lagrangian Shape Functions

As noted previously this is an isoparametric shell element formulation that uses the same shape functions to define the geometry and the displacements. Therefore, the form of (6.5) is used when the displacements of the element u , v , and w are mapped from global (x, y, z) coordinates to natural element coordinates (r, s, t) utilizing the following equation:

$$\mathbf{u}(r, s, t) = \sum_{i=1}^9 \left[\left(\mathbf{u}_i + t \frac{h}{2} \mathbf{V}_N^i \right) N_i(r, s) \right] \quad (6.6)$$

Where \mathbf{u} are the displacements of any point in the element, \mathbf{u}_i are the displacements of node point i , and the remainder similarly defined in (6.5). In addition to the displacements, two rotations are defined for each node (α and β) corresponding to the rotation of \mathbf{V}_N^i about the previously mentioned nodal orthogonal unit vectors \mathbf{V}_1^i and \mathbf{V}_2^i respectively. Because α and β are assumed to be small angles and the rotation of an infinitely-thin straight material line can be defined by the rotation of the vectors normal to that line, it can be shown that:

$$\mathbf{V}_N^i = -\mathbf{V}_2^i \alpha + \mathbf{V}_1^i \beta \quad (6.7)$$

which when combined with (6.6) results in the element displacements \mathbf{u} being defined as follows:

$$\mathbf{u}(r, s, t) = \sum_{i=1}^9 \left[\left(\mathbf{u}_i + t \frac{h}{2} (-\mathbf{V}_2^i \alpha_i + \mathbf{V}_1^i \beta_i) \right) N_i(r, s) \right] \quad (6.8)$$

It should be noted that this shell formulation has five degrees of freedom at each node corresponding to the displacement degrees of freedom u , v , and w and the rotational degrees of freedom α and β . The shell element does not have the sixth, “drilling,” degree of freedom corresponding to a rotation about the \mathbf{V}_N^i vector. This is keeping with the Reissner-Mindlin kinematical assumptions, which pertains to the admissible displacement profile through the shell thickness (Chapelle & Bathe 2003). The Reissner-Mindlin shell theory assumes that a straight line normal to the undeformed mid-surface of the shell will remain straight during deformation, not necessarily normal to the deformed mid-surface (Bathe 1996). This is analogous to the Timoshenko beam used in one-dimensional problems. Additionally, this “drilling” rotation,

being in the plane of the element, is small and stores relatively little strain energy. Accordingly, they can be disregarded without sacrificing accuracy in the solution (Popp 2004). Another result of this is that the model is defined to have five degrees of freedom per node except at the web flange intersection nodes. These nodes will have six degrees of freedom as the drilling degree of freedom of one shell corresponds to a rotation degree of freedom of the other and vice versa.

To evaluate the element stiffness matrix of the shell, the strain-displacement matrix (**B**) is needed. This matrix relates the element strains in terms of the derivatives of the element displacements with respect to the global coordinates to the element displacements.

This shell formulation is a degenerated brick element which utilizes the 3-D generalized stress-strain matrix for an isotropic material. In keeping with the normal shell assumption the stress normal to the surface of the shell (σ_z) is assumed to be zero. The constitutive relationship ($\mathbf{C}^{\text{local}}$), the mathematical representation of the behavior of a material to applied forces, in natural coordinates is defined as follows:

$$\begin{Bmatrix} \sigma_x \\ \sigma_y \\ \sigma_z \\ \sigma_{xy} \\ \sigma_{zx} \\ \sigma_{yz} \end{Bmatrix} = \frac{E}{1-\nu^2} \begin{bmatrix} 1 & \nu & 0 & 0 & 0 & 0 \\ & 1 & 0 & 0 & 0 & 0 \\ & & 0 & 0 & 0 & 0 \\ & & & \frac{1-\nu}{2} & 0 & 0 \\ \text{Sym.} & & & & k\frac{1-\nu}{2} & 0 \\ & & & & & k\frac{1-\nu}{2} \end{bmatrix} \begin{Bmatrix} \epsilon_x \\ \epsilon_y \\ \epsilon_z \\ \epsilon_{xy} \\ \epsilon_{zx} \\ \epsilon_{yz} \end{Bmatrix} \quad (6.9)$$

Where E and ν are the Young's modulus and Poisson's ratio of the material respectively, and k is the shear correction factor. To transform the constitutive matrix from natural coordinates to global coordinates a rotation matrix **R** is formed from the direction cosines of a local orthogonal coordinate axes consisting of unit vectors \mathbf{t}_1 , \mathbf{t}_2 , and \mathbf{t}_3 at the Gauss integration points.

The global rigidity matrix is calculated as follows:

$$\mathbf{D} = \mathbf{R}^T \mathbf{C}^{\text{local}} \mathbf{R} \quad (6.10)$$

With all the necessary components the elastic stiffness matrix is defined as:

$$\mathbf{K}_{\text{Shell}} = \int_V \mathbf{B}^T \mathbf{D} \mathbf{B} dV = \iiint_V \mathbf{B}^T \mathbf{D} \mathbf{B} \det \mathbf{J} dr ds dt \quad (6.11)$$

This integration is done numerically using Gaussian quadrature with three integration points in the r - and s -directions and with two integration points in the t -direction. The result is (6.12):

$$\mathbf{K}_{Shell} = \sum_i^{18} \mathbf{B}^T \mathbf{D} \mathbf{B} \det(\mathbf{J}) w(i) \quad (6.12)$$

Where $\det(\mathbf{J})$ is the determinant of the Jacobian matrix and $w(i)$ is the weighting factors at the integration point.

To verify the accuracy of the shell a preliminary patch test was performed to ensure the shell exhibited basic behavior necessary for accurate modeling of the bridge. Typically the strong axis bending dominates the behavior of a bridge resulting in longitudinal stresses and strains in the shell. The patch test was performed to ensure the shell would exhibit a constant strain behavior if placed under a uniform loading. This was verified for a single shell and for multiple shells connected in an orientation similar to a girder flange.

Truss Element Elastic Stiffness Formulations

The UT Bridge program uses truss elements to model the cross-frames. This is legitimized by Alfred G. Bishara and Wassef E. Elmir (1990) when they assigned beam elements to the cross-frame members of a 3D finite element analysis of a multibeam composite steel bridge, and the analysis resulted in all six internal forces. According to Bishara and Elmir the analysis results clearly showed that the axial forces are the most significant and the other internal forces are of no real significance for design purpose.

The cross frame elements are assembled into a “superelement” from four 3-dimension 2-node truss elements. The cross frame element has four nodes and twelve degrees of freedom with local element number defined by Figure 6.22 looking ahead station.

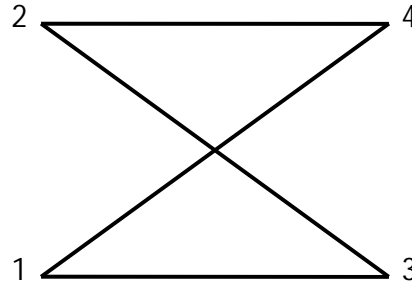


Figure 6.22: Cross Frame Schematic

The truss element used is a standard 2-node truss element formulation found in many texts including Kassimali (1999) with a local stiffness matrix.

$$\mathbf{k} = \frac{EA}{L} \begin{bmatrix} 1 & -1 \\ -1 & 1 \end{bmatrix} \quad (6.13)$$

Where E , A , and L are the Young's modulus of the material, the cross sectional area and length of the cross frame chords, respectively. The matrix is converted to global coordinates by:

$$\mathbf{K} = \mathbf{T}^T \mathbf{k} \mathbf{T} \quad (6.14)$$

Where:

$$\mathbf{T} = \begin{bmatrix} \cos \theta_x & \cos \theta_y & \cos \theta_z & 0 & 0 & 0 \\ 0 & 0 & 0 & \cos \theta_x & \cos \theta_y & \cos \theta_z \end{bmatrix} \quad (6.15)$$

Where:

$$\cos \theta_x = \frac{(X_e - X_b)}{L} \quad \cos \theta_y = \frac{(Y_e - Y_b)}{L} \quad \cos \theta_z = \frac{(Z_e - Z_b)}{L}$$

X_b and X_e are the global x-coordinates of the beginning and ending node of the truss, Y_b and Y_e are the global y-coordinates of the beginning and ending node of the truss, and Z_b and Z_e are the global z-coordinates of the beginning and ending node of the truss. Then the truss element is combined into a cross frame element as follows:

$$\mathbf{K}_{X-Frame} = \begin{bmatrix} \mathbf{K}_{13} & \mathbf{K}_{14} \\ \mathbf{K}_{23} & \mathbf{K}_{24} \end{bmatrix} \quad (6.16)$$

Where \mathbf{K}_{13} is the truss element stiffness matrix for the bottom chord of the cross frame or the truss element from node 1 to node 3 and similarly for the other submatrices.

Beam Element Elastic Stiffness Formulations

The UT Bridge program uses beam elements to model stiffeners. The stiffener elements are assembled into a “superelement” from seven 3-dimension 2-node beam elements. The beam element used is a standard 2-node beam element that has been formulated in many texts including Kassimali (1999) with a local stiffness matrix.

$$\mathbf{k} = \begin{bmatrix} \frac{EA}{L} & 0 & 0 & 0 & 0 & 0 & -\frac{EA}{L} & 0 & 0 & 0 & 0 & 0 \\ 0 & \frac{12EI_y}{L^3} & 0 & 0 & \frac{6EI_y}{L^2} & 0 & 0 & -\frac{12EI_y}{L^3} & 0 & 0 & \frac{6EI_y}{L^2} & 0 \\ 0 & 0 & \frac{12EI_z}{L^3} & 0 & 0 & -\frac{6EI_z}{L^2} & 0 & 0 & -\frac{12EI_z}{L^3} & 0 & 0 & -\frac{6EI_z}{L^2} \\ 0 & 0 & 0 & \frac{GJ}{L} & 0 & 0 & 0 & 0 & 0 & -\frac{GJ}{L} & 0 & 0 \\ 0 & \frac{6EI_y}{L^2} & 0 & 0 & \frac{4EI_y}{L} & 0 & 0 & -\frac{6EI_y}{L^2} & 0 & 0 & \frac{2EI_y}{L} & 0 \\ 0 & 0 & -\frac{6EI_z}{L^2} & 0 & 0 & \frac{4EI_z}{L} & 0 & 0 & \frac{6EI_z}{L^2} & 0 & 0 & \frac{2EI_z}{L} \\ -\frac{EA}{L} & 0 & 0 & 0 & 0 & 0 & \frac{EA}{L} & 0 & 0 & 0 & 0 & 0 \\ 0 & -\frac{12EI_y}{L^3} & 0 & 0 & -\frac{6EI_y}{L^2} & 0 & 0 & \frac{12EI_y}{L^3} & 0 & 0 & -\frac{6EI_y}{L^2} & 0 \\ 0 & 0 & -\frac{12EI_z}{L^3} & 0 & 0 & \frac{6EI_z}{L^2} & 0 & 0 & \frac{12EI_z}{L^3} & 0 & 0 & \frac{6EI_z}{L^2} \\ 0 & 0 & 0 & -\frac{GJ}{L} & 0 & 0 & 0 & 0 & 0 & \frac{GJ}{L} & 0 & 0 \\ 0 & \frac{6EI_y}{L^2} & 0 & 0 & \frac{2EI_y}{L} & 0 & 0 & -\frac{6EI_y}{L^2} & 0 & 0 & \frac{4EI_y}{L} & 0 \\ 0 & 0 & -\frac{6EI_z}{L^2} & 0 & 0 & \frac{2EI_z}{L} & 0 & 0 & \frac{6EI_z}{L^2} & 0 & 0 & \frac{4EI_z}{L} \end{bmatrix} \quad (6.17)$$

Where E , G , A , L , I_y , I_z , and J are the Young's and shear moduli of the material, the cross sectional area, length, moment of inertia about the local y-axis, the moment of inertia about the local z-axis, and the torsion constant of the stiffener, respectively. The degree of freedom

associated with the drilling degree of freedom of the web shell elements is condensed out of the element formulation.

Shear Stud Beam Element Elastic Stiffness Formulations

Shear studs welded to the top flange of steel girders, are used in modern steel bridge design to allow the concrete deck to act compositely with the steel girder. Composite action occurs when two or more components behave as a single structural element. The result is an increase in the bridge stiffness and strength. A schematic drawing of the difference between a beam with and without composite action is depicted in Figure 6.23.

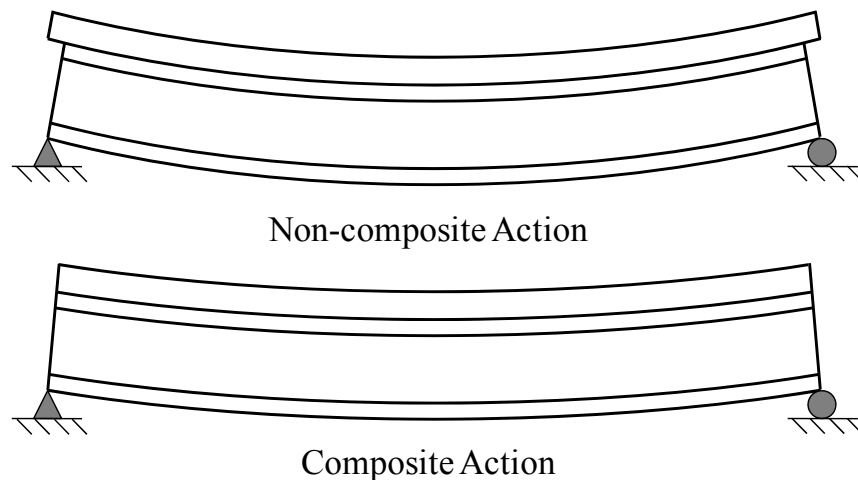


Figure 6.23: Schematic Effect of Composite Action

Within the UT Bridge program shear studs accounted for the relative horizontal movement of the deck with respect to the top flange of the girders. Significant work was completed by Topkaya at the University of Texas at Austin on the shear stud strength in early-aged concrete (Topkaya 2002, Topkaya et al., 2004). A major feature of the program was deck placement stability and understanding the shear stud behavior with recently placed concrete that generally gains stiffness quicker than the strength gain. The ability to model the recently placed concrete allows for an accurate model to be created during all stages of construction. A summary of this work was presented previously in this chapter. UT Bridge utilizes this experimental data allowing the user to specify the age of the concrete and assume a similar concrete and shear stud type as Topkaya. The program linearly interpolates for a specific age concrete or alternatively the user can provide the concrete modulus and shear stud stiffness.

U-TrAp 2.0 utilizes a standard three-dimensional two node spring to represent the shear studs. However, this approach requires the top flange and deck nodes to be coincident. In looking to improve this model by allowing the height of the haunch to be included, a variation on the beam element similar to (6.17) was created to represent the shear studs. This accounts for the variation in the deck height as a function of the deck thickness and the haunch and is shown in (6.18).

$$\mathbf{k} = \begin{bmatrix}
K_1 & 0 & 0 & 0 & \frac{K_1 L}{2} & -K_1 & 0 & 0 & 0 & \frac{K_1 L}{2} \\
& K_2 & 0 & -\frac{K_2 L}{2} & 0 & 0 & -K_2 & 0 & -\frac{K_2 L}{2} & 0 \\
& & K_3 & 0 & 0 & 0 & 0 & -K_3 & 0 & 0 \\
& & & \frac{K_2 L^2}{3} & 0 & 0 & \frac{K_2 L}{2} & 0 & \frac{K_2 L^2}{6} & 0 \\
& & & & \frac{K_1 L^2}{3} & -\frac{K_1 L}{2} & 0 & 0 & 0 & \frac{K_1 L^2}{6} \\
& & & & & K_1 & 0 & 0 & 0 & -\frac{K_1 L}{2} \\
& & & & & & K_2 & 0 & \frac{K_2 L}{2} & 0 \\
& & Sym & & & & & K_3 & 0 & 0 \\
& & & & & & & & \frac{K_2 L^2}{3} & 0 \\
& & & & & & & & & \frac{K_1 L^2}{3}
\end{bmatrix} \quad (6.18)$$

6.3.4 Element Geometric Stiffness Formulations:

Shell Element Geometric Stiffness Formulations:

To accomplish the stability analysis the geometric stiffness matrix must be formulated for the shell element. Details of the formulation are given in Popp (2004). The general three-dimensional strain vector can be divided into infinitesimal and large displacement components:

$$\boldsymbol{\varepsilon} = \boldsymbol{\varepsilon}_0 + \boldsymbol{\varepsilon}_L \quad (6.19)$$

Where the infinitesimal strain is $\boldsymbol{\varepsilon}_0$. The large displacement component is the first higher order term of the strain equation and the nonlinear strain terms can be written. Thus it can be shown that the geometric stiffness matrix is defined as follows:

$$\mathbf{K}_G = \int_V \mathbf{B}_{NL}^T \mathbf{M} \mathbf{B}_{NL} dV = \iiint_V \mathbf{B}_{NL}^T \mathbf{M} \mathbf{B}_{NL} \det \mathbf{J} dr ds dt \quad (6.20)$$

This integration is done numerically using Gaussian quadrature with three integration points in the r- and s-directions and with two integration points in the t-direction. The result is (6.21):

$$\mathbf{K}_G = \sum_i^{18} \mathbf{B}_{NL}^T \mathbf{M} \mathbf{B}_{NL} \det(\mathbf{J}) w(i) \quad (6.21)$$

Where $\det(\mathbf{J})$ is the determinant of the Jacobian matrix and $w(i)$ is the weighting factors at the integration point.

Truss Element Geometric Stiffness Formulations

The geometric stiffness matrix is formulated similarly to the elastic stiffness matrix with four truss elements assembled into a “superelement.” The formulation of the three-dimensional two-node geometric stiffness matrix is explained in great detail in Popp (2004) and given as:

$$\mathbf{k}_G = \frac{F_x}{L} \begin{bmatrix} 1 & 0 & 0 & -1 & 0 & 0 \\ 0 & 1 & 0 & 0 & -1 & 0 \\ 0 & 0 & 1 & 0 & 0 & 0 \\ -1 & 0 & 0 & 1 & 0 & -1 \\ 0 & -1 & 0 & 0 & 1 & 0 \\ 0 & 0 & -1 & 0 & 0 & 1 \end{bmatrix} \quad (6.22)$$

Where F_x is the member end axial force in the truss element from the linear elastic analysis and is calculated as follows:

$$F_x = \frac{EA}{L} * (\mathbf{T}_x^T \mathbf{\Delta})$$

$$\mathbf{T}_x = \langle \cos \theta_x \quad \cos \theta_y \quad \cos \theta_z \rangle^T \quad \mathbf{\Delta} = \langle \delta_x \quad \delta_y \quad \delta_z \rangle^T \quad (6.23)$$

$$\delta_x = \delta_{xe} - \delta_{xb} \quad \delta_y = \delta_{ye} - \delta_{yb} \quad \delta_z = \delta_{ze} - \delta_{zb}$$

\mathbf{T}_x are the direction cosines of the local x-axis about the global axis and defined in (6.15). $\mathbf{\Delta}$ are the relative nodal displacements in the three global directions. δ_{xe} and δ_{xb} are the global x-axis nodal displacement of the ending and beginning node of the truss.

The local geometric stiffness matrix is converted to global coordinates by:

$$\mathbf{K}_G = \mathbf{T}^T \mathbf{k}_G \mathbf{T} \quad (6.24)$$

Where:

$$\mathbf{T} = \begin{bmatrix} \mathbf{T}_x & \mathbf{T}_y & \mathbf{T}_z & 0 & 0 & 0 \\ 0 & 0 & 0 & \mathbf{T}_x & \mathbf{T}_y & \mathbf{T}_z \end{bmatrix} \quad (6.25)$$

Truss elements do not have an explicit y- or z-axis and are chosen arbitrarily as follows:

$$\mathbf{T}_y = \mathbf{e}_z \times \mathbf{T}_x = \langle -\cos \theta_y \quad \cos \theta_x \quad 0 \rangle^T \quad (6.26)$$

$$\mathbf{T}_z = \mathbf{T}_x \times \mathbf{T}_y \quad (6.27)$$

$$\mathbf{T}_z = \begin{Bmatrix} -\cos \theta_x \cos \theta_z \\ -\cos \theta_y \cos \theta_z \\ \cos^2 \theta_x + \cos^2 \theta_y \end{Bmatrix}$$

The four truss elements are combined similarly to (6.16).

Beam Element Geometric Stiffness Formulations

The geometric stiffness matrix is formulated in a similar fashion to the elastic stiffness matrix with seven beam elements assembled into a “superelement.” The full geometric stiffness matrix of the three-dimensional beam element is formulated by combining bending-axial force interaction, torsion-axial force interaction, and torsion-bending interaction into (6.28). This formulation is explained in detail in McGuire, Gallagher, and Ziemian (2000) and given as follows:

$$\mathbf{k}_G = \begin{bmatrix} \frac{F_{x2}}{L} & 0 & 0 & 0 & 0 & 0 & -\frac{F_{x2}}{L} & 0 & 0 & 0 & 0 & 0 \\ 0 & \frac{6F_{x2}}{5L} & 0 & \frac{M_{y1}}{L} & \frac{M_{x2}}{L} & \frac{F_{x2}}{10} & 0 & -\frac{6F_{x2}}{5L} & 0 & \frac{M_{y2}}{L} & -\frac{M_{x2}}{L} & \frac{F_{x2}}{10} \\ 0 & 0 & \frac{6F_{x2}}{5L} & \frac{M_{z1}}{L} & -\frac{F_{x2}}{10} & \frac{M_{x2}}{L} & 0 & 0 & -\frac{6F_{x2}}{5L} & \frac{M_{zy2}}{L} & -\frac{F_{x2}}{10} & -\frac{M_{x2}}{L} \\ 0 & \frac{F_{x2}I_p}{AL} & -\frac{2M_{z1} - M_{z2}}{6} & \frac{2M_{y1} - M_{y2}}{6} & 0 & -\frac{M_{y1}}{L} & -\frac{M_{z1}}{L} & -\frac{F_{x2}I_p}{AL} & -\frac{M_{z1} + M_{z2}}{6} & \frac{M_{y1} + M_{y2}}{6} & -\frac{M_{x2}}{L} & -\frac{F_{x2}}{30} \\ 0 & -\frac{2F_{x2}L}{15} & 0 & 0 & 0 & -\frac{M_{x2}}{L} & \frac{F_{x2}}{10} & -\frac{M_{z1} + M_{z2}}{6} & -\frac{F_{x2}}{30} & -\frac{M_{x2}}{L} & -\frac{F_{x2}}{30} & -\frac{M_{x2}}{L} \\ 0 & 0 & \frac{2F_{x2}L}{15} & 0 & 0 & -\frac{F_{x2}}{10} & -\frac{M_{x2}}{L} & \frac{M_{y1} + M_{y2}}{6} & -\frac{M_{x2}}{2} & -\frac{F_{x2}}{30} & -\frac{F_{x2}}{30} & -\frac{F_{x2}}{30} \\ 0 & 0 & 0 & \frac{F_{x2}}{L} & 0 & 0 & 0 & 0 & 0 & 0 & 0 & 0 \\ 0 & 0 & 0 & 0 & \frac{6F_{x2}}{5L} & 0 & -\frac{M_{y2}}{L} & \frac{M_{x2}}{L} & -\frac{F_{x2}}{10} & \frac{M_{y2}}{L} & -\frac{F_{x2}}{10} & -\frac{F_{x2}}{10} \\ 0 & 0 & 0 & 0 & 0 & \frac{6F_{x2}}{5L} & -\frac{M_{z2}}{L} & \frac{F_{x2}}{10} & \frac{M_{x2}}{L} & \frac{F_{x2}}{10} & \frac{M_{x2}}{L} & \frac{M_{x2}}{L} \\ 0 & 0 & 0 & 0 & 0 & 0 & \frac{F_{x2}I_p}{AL} & \frac{M_{z1} - 2M_{z2}}{6} & -\frac{M_{y1} - 2M_{y2}}{6} & \frac{M_{z1} - 2M_{z2}}{6} & -\frac{M_{y1} - 2M_{y2}}{6} & -\frac{M_{x2}}{L} \\ 0 & 0 & 0 & 0 & 0 & 0 & 0 & \frac{2F_{x2}L}{15} & 0 & 0 & 0 & 0 \\ 0 & 0 & 0 & 0 & 0 & 0 & 0 & 0 & \frac{2F_{x2}L}{15} & 0 & 0 & 0 \\ 0 & 0 & 0 & 0 & 0 & 0 & 0 & 0 & 0 & \frac{2F_{x2}L}{15} & 0 & 0 \\ 0 & 0 & 0 & 0 & 0 & 0 & 0 & 0 & 0 & 0 & \frac{2F_{x2}L}{15} & 0 \\ 0 & 0 & 0 & 0 & 0 & 0 & 0 & 0 & 0 & 0 & 0 & \frac{2F_{x2}L}{15} \end{bmatrix} \quad (6.28)$$

Where A and L are defined as in (6.17) and I_p is the polar moment of inertia ($I_y + I_z$). F_{x2} , M_{x2} , M_{y1} , M_{y2} , M_{z1} , and M_{z2} are the member end forces corresponding to the axial force, torsional moment, moment about the y-axis at the beginning node, moment about the y-axis at the ending node, moment about the z-axis at the beginning node, and moment about the z-axis at the ending node, respectively. These member end forces are not straightforward due to the fact that the rotation about the z-axis is not a free degree of freedom for the web nodes and thus M_z is not directly to determine. The dependent displacements are determined and then with the element

stiffness matrix all member end forces are determined and geometric stiffness matrix of the stiffeners is calculated.

6.3.5 Solvers

UT Bridge utilizes a highly optimized linear sparse solver developed at Compaq and included in Compaq's extended math library. The direct sparse solver requires that the global stiffness matrix be given in a specifically formatted set of vectors. The vectors contain only the nonzero elements of the stiffness matrix which is a huge computational savings because the vast majority of the elements of the global stiffness matrix are zero, thus a sparse matrix, and unnecessary to store. The locations of the nonzero elements are provided by the set of vectors and the large set of linear equations is solved efficiently.

The eigenvalue solver was developed at Rice University and utilizes parts of the direct sparse solver used in the linear elastic analysis with additional subroutines to solve the eigenproblem using a direct inverse approach. This approach is utilized because it requires the inversion of the global elastic stiffness matrix which can always be solved for properly constraint systems, but only requires the multiplication of the geometric stiffness matrix which may or may not be invertible. General information about the eigensolver is provided by Lehoucq (1998).

6.3.6 Post-Processing within UT Bridge

Nodal Stress Recovery

The displacement based finite element analysis approach used in this program results in the numeric approximation of the nodal displacements, which are the primary variables. The calculation of the nodal stresses is a derived or secondary variable that must be calculated after the program calculates the displacements. This final step in the finite element analysis is referred to as post-processing. It should be noted that the numeric approximation of these secondary variables results in a lower accuracy level than the primary variable. For example, if the accuracy level of the primary variable is 1% then the level of accuracy of the secondary variable may be in a range of 10%–15% (Felippa 2004).

The calculation of element stresses has been previously calculated in the formulation of the shell element geometric stiffness. However, the solution of the strain displacement matrix **B** is calculated at the 3 x 3 Gauss integration points which results in the stresses calculations at these locations. It is generally useful to report the stresses at the same locations as the displacements namely the nodal coordinates. This dilemma lends itself to two possible solutions.

1. Directly apply the nodal natural coordinates into the shape functions in the formulation of **B** and directly obtain the nodal stresses.
2. Evaluate the stresses at the Gauss points as has been discussed previously using the element stiffness integration rules and then extrapolate the element stress to the node points.

According to Felippa (2004) the second approach generally delivers better stress values of quadrilateral elements whose geometry departs substantially from the rectangular shape. This conclusion is validated by "superconvergence" results in finite element approximation theory. For rectangular elements there is no difference, but within UT Bridge this situation would be present. For highly skewed bridges the deck and flange elements will be oriented along the

bridge skew angle in a parallelogram shape. Therefore the second approach was implemented into UT Bridge.

The extrapolation from the gauss points to the node points is completed using a biquadratic extrapolation. This is an extension of a quadratic interpolation used in one-dimensional analysis (Lagrange interpolation of displacements in a three-noded finite element truss) to a two-dimensional surface. To explain the extrapolation process consider the region bounded by the Gauss points as a “Gauss element” (e') shown in Figure 6.24 and shaded blue.

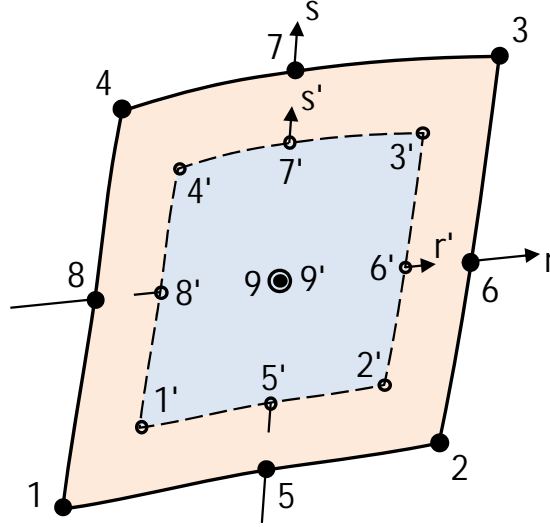


Figure 6.24: Extrapolation from 3 x 3 "Gauss Element" (e') to 9-Noded Shell Element

The stresses are calculated at the Gauss points designated as 1', 2', 3', 4', 5', 6', 7', 8', and 9' on element specified by nodes numbered 1-9. The nodes and Gauss points are located at their natural coordinates (r, s) given by the master element and show in Table 6.2. The “Gauss element” has a similar scaled coordinate system (r', s') with the Gauss points located as shown in Table 6.2 and the node locations calculated for the Gauss element coordinate system by the simple relationship given in (6.29).

$$r = \sqrt{5/3} r', \quad s = \sqrt{5/3} s', \quad r' = \sqrt{3/5} r, \quad s' = \sqrt{3/5} s \quad (6.29)$$

Table 6.2: Natural Coordinates and Gauss Element Coordinates of 9-Node Shell Element

| Nodes Number | Natural Coordinates | | Gauss Element Coordinates | |
|-----------------|------------------------|----|------------------------------|---------------|
| | R | S | r' | s' |
| 1 | -1 | -1 | $-\sqrt{5/3}$ | $-\sqrt{5/3}$ |
| 2 | 1 | -1 | $\sqrt{5/3}$ | $-\sqrt{5/3}$ |
| 3 | 1 | 1 | $\sqrt{5/3}$ | $\sqrt{5/3}$ |
| 4 | -1 | 1 | $-\sqrt{5/3}$ | $\sqrt{5/3}$ |
| 5 | 0 | -1 | 0 | $-\sqrt{5/3}$ |
| 6 | 1 | 0 | $\sqrt{5/3}$ | 0 |
| 7 | 0 | 1 | 0 | $\sqrt{5/3}$ |
| 8 | -1 | 0 | $-\sqrt{5/3}$ | 0 |
| 9 | 0 | 0 | 0 | 0 |

| Gauss Number | Natural Coordinates | | Gauss Element Coordinates | |
|-----------------|------------------------|---------------|------------------------------|----|
| | r | s | r' | s' |
| 1' | $-\sqrt{3/5}$ | $-\sqrt{3/5}$ | -1 | -1 |
| 2' | $\sqrt{3/5}$ | $-\sqrt{3/5}$ | 1 | -1 |
| 3' | $\sqrt{3/5}$ | $\sqrt{3/5}$ | 1 | 1 |
| 4' | $-\sqrt{3/5}$ | $\sqrt{3/5}$ | -1 | 1 |
| 5' | 0 | $-\sqrt{3/5}$ | 0 | -1 |
| 6' | $\sqrt{3/5}$ | 0 | 1 | 0 |
| 7' | 0 | $\sqrt{3/5}$ | 0 | 1 |
| 8' | $-\sqrt{3/5}$ | 0 | -1 | 0 |
| 9' | 0 | 0 | 0 | 0 |

Now the stresses σ whose values σ'_i at the Gauss points are known can be extrapolated through the biquadratic shape functions now expressed in terms of r' and s' . Expanding this for stresses at each node point i results in (6.30).

$$\begin{bmatrix} \sigma_1(r', s') \\ \sigma_2(r', s') \\ \vdots \\ \sigma_9(r', s') \end{bmatrix} = \begin{bmatrix} N_1^{(e')}(r'_1, s'_1) & N_2^{(e')}(r'_1, s'_1) & \dots & N_9^{(e')}(r'_1, s'_1) \\ N_1^{(e')}(r'_2, s'_2) & N_2^{(e')}(r'_2, s'_2) & \dots & N_9^{(e')}(r'_2, s'_2) \\ \vdots & \vdots & \ddots & \vdots \\ N_1^{(e')}(r'_9, s'_9) & N_2^{(e')}(r'_9, s'_9) & \dots & N_9^{(e')}(r'_9, s'_9) \end{bmatrix} \begin{bmatrix} \sigma'_1 \\ \sigma'_2 \\ \vdots \\ \sigma'_9 \end{bmatrix} \quad (6.30)$$

Interelement Averaging

The stress calculated by the previously discussed method is on an element by element basis. The result of using a nine-node shell element and quadratic displacement shape functions results in a linear approximation of the stress. However, unlike the displacements that have continuity enforced at the interelement boundaries, the stresses have no such requirement and in general are not continuous. Thus for convenience of the end user a single stress value is computed for cases in which multiple elements are connected to a single node. The most common approach is an unweighted average of all elements connected to the node. The other option is to perform a weighted average where a weighting is assigned to the elements connected to a node.

For the shell elements used in UT Bridge the stresses were calculated at the 3 x 3 integration points in the plane of the shell, but also two layers through the thickness of the shell. This is shown schematically in Figure 6.25.

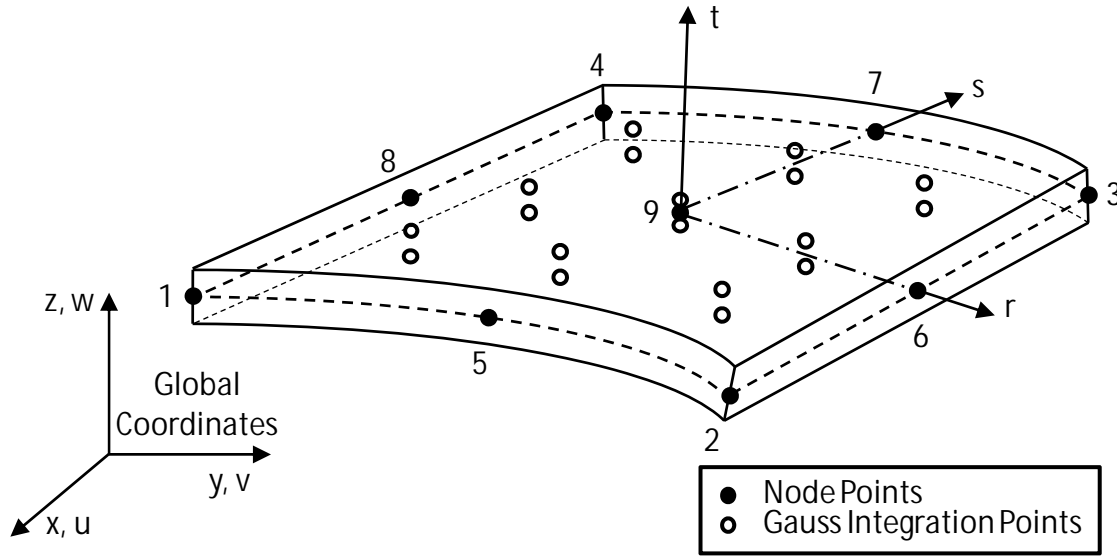


Figure 6.25: 18 Gauss Points of the 3 x 3 x 2 Integration

Assuming a linear variation through the thickness of the element (Figure 6.26) allows for the stress at the top, middle, and bottom of the shell element to be calculated by (6.31)–(6.33).

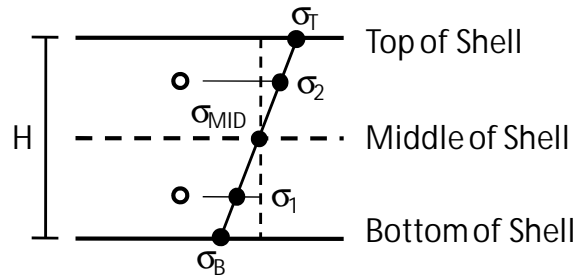


Figure 6.26: Through Thickness Stress Variation

Where:

H = The shell thickness

σ_1 = Stress at the Gauss integration point layer located $-H/2\sqrt{3}$ from the middle of the shell

σ_2 = Stress at the Gauss integration point layer located $H/2\sqrt{3}$ from the middle of the shell

$$\sigma_T = \frac{1}{2}(\sigma_1 + \sigma_2) - \frac{\sqrt{3}}{2}(\sigma_1 - \sigma_2) \quad (6.31)$$

$$\sigma_{MID} = \frac{1}{2}(\sigma_1 + \sigma_2) \quad (6.32)$$

$$\sigma_T = \frac{1}{2}(\sigma_1 + \sigma_2) + \frac{\sqrt{3}}{2}(\sigma_1 - \sigma_2) \quad (6.33)$$

When performing stress checks in an analysis the extreme fibers of the cross section will yield the maximum and minimum stress. Therefore it was desirable to report the stresses at the bottom of the bottom flange, the midsurface of the web, and the top of the top flange and deck. This approach was taken in UT Bridge. When averaging the nodal stresses for nodes at certain locations, such as the web flange interface, a simple unweighted average does not accurately give the extreme fiber stress in strong axis bending. Thus the stresses were weighted such that the web elements were 1% of the weighting of a flange element. With this approach the web flange interfaces give a stress for the extreme fibers in strong axis bending.

Calculating Reactions:

The reactions are locations at the permanent supports where the displacements have been defined as zero. In order to recover the reactions for these supports the full global stiffness matrix is partitioned to separate the free degrees of freedom and the restrained degrees of freedom as shown in (6.34).

$$\begin{bmatrix} K_{FF} & | & K_{FR} \\ - - & - + - & - - \\ K_{RF} & | & K_{RR} \end{bmatrix} \begin{Bmatrix} \Delta_F \\ - - - \\ \Delta_R = 0 \end{Bmatrix} = \begin{Bmatrix} F_F \\ - \\ R \end{Bmatrix} \quad (6.34)$$

Where:

$$\begin{bmatrix} K_{FF} & | & K_{FR} \\ - - & - + - & - - \\ K_{RF} & | & K_{RR} \end{bmatrix} = \text{the partitioned global stiffness matrix}$$

Δ_F = the free degrees of freedom.

F_F = the nodal forces.

R = the reactions at the restrained degrees of freedom.

$$R = K_{RF} * \Delta_F \quad (6.35)$$

Due to the efficient storage technique of the global stiffness matrix in UT Bridge the terms associated with the restrained degrees of freedom are not stored prior to calculating the reactions. To recover the K_{RF} matrix the element stiffness matrix of all elements connected to the reaction node are calculated and multiplied by the corresponding displacements resulting in the calculation of R .

6.4 Post –Processor, UT Viewer

UT Viewer is the post-processor for the UT Bridge program and was created to help the user easily view and analyze the results from a set of bridge analyses. After the user loads the results file, they are then able to view in 3-dimensions the bridge geometry, bridge displacements, and bridge stresses. Additionally, UT Viewer can also display numerous XY plots showing the displacements, rotations, and stresses at 10th points along the length of the bridge. The information used to generate the XY plots is also available in a tabular form. This allows the user to easily copy and paste the information to another program such as Microsoft Excel for further analysis. Additionally, cross frame forces and reactions are given graphically or in tabular form to export.

The three-dimensional graphics available in UT Viewer provide the engineer an invaluable tool to ensure the bridge intended to be modeled was properly input and key structural elements are located as indicated on the bridge plans. A *Visualization* option is provided in the preprocessor that quickly develops the bridge geometry, but does not actually perform an analysis. This allows for a check of the input prior to the analysis. Figure 6.27 is screen shot of a bridge rendered in UT Viewer.

In addition to geometric accuracy UT Viewer will display the displaced shape of the bridge for each analysis case. A 3-D contour plot of the stresses is also available to determine the maximum and minimum stress and the locations of high stress regions. The cross frame forces are given for each of the members, but it is assumed that the diagonal member is a tension only member and thus one diagonal will report zero force. The reactions for both permanent and temporary supports are given.

UT Viewer also provides a range of two-dimensional graphs. The graphs display displacements, stresses, and rotations at tenth points along each span for each girder. This provides a graphical indication of the relative displacement of the girders or location of maximum rotation as examples. The data from the graphs is also give in a tabular form to be cut and pasted into another program for future data manipulations. Figure 6.28 is a screen shot of the graph of the vertical displacement of a three-span bridge with four girders.

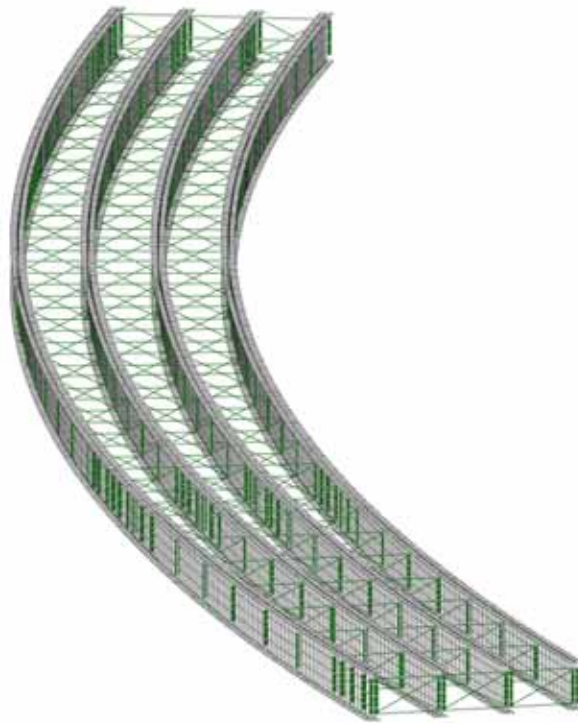


Figure 6.27: UT Viewer Screen Shot of a Bridge

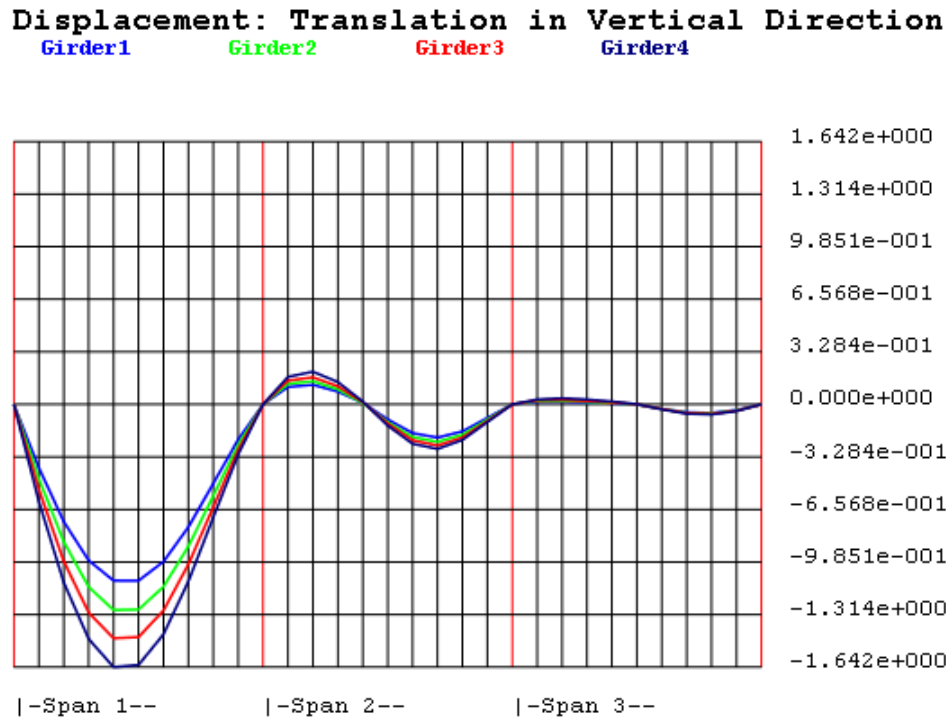


Figure 6.28: Screen Shot of UT Bridge XY Plot

6.5 Verifications

Verification of UT Bridge was a continuous process throughout development. From individual element verification to multi-element verification to entire bridge models, the program has continuously been checked for a variety of cases. However, as with all programs with the complexity of UT Bridge every possible scenario has not been checked and thus it is recommended that the design engineer perform independent checks to ensure the accuracy of the program for their specific bridge geometry. The details of the element and girder verification process will not be presented here. However, two examples of actual bridges will be given with independent verification from field data, commercially available two-dimensional grillage models, and full three-dimensional finite element analyses.

Bridge 88 was discussed previously in Chapter 3. The details of the collected field data was presented with additional details in Farris (2008). The displacement data was collected during the concrete deck placement. The deck was placed continuously starting from span 16 continuing back station toward span 15 and finally over span 14. The displacement measurements occurred in span 14 at $1/8^{\text{th}}$ points from the beginning of the span to midspan on girders 3 and 4. The displacements were measured with equipment with a $1/16^{\text{th}}$ of an inch resolution and thus each graph has set of lines representing $\pm 1/8^{\text{th}}$ inch from the measured data to provide the graph with scale. A pair of graphs that compare the field data with the predicted deflection values for Bridge 88 are presented in Figure 6.29 for the case when the deck was completely placed on span 16. The two graphs in Figure 6.29 represent the field data and UT Bridge (a) for Girder 3 and (b) for Girder 4. Figure 6.30 is another pair of graphs with similar data, but representing the time at which the first two spans were placed, span 15 and span 16. Figure 6.31 and Figure 6.32 compare UT Bridge to not only the field data, but also the results of

two separate commercially available grillage software programs, MDX and DESCUS, as well as a full three-dimensional finite element model developed in ANSYS.

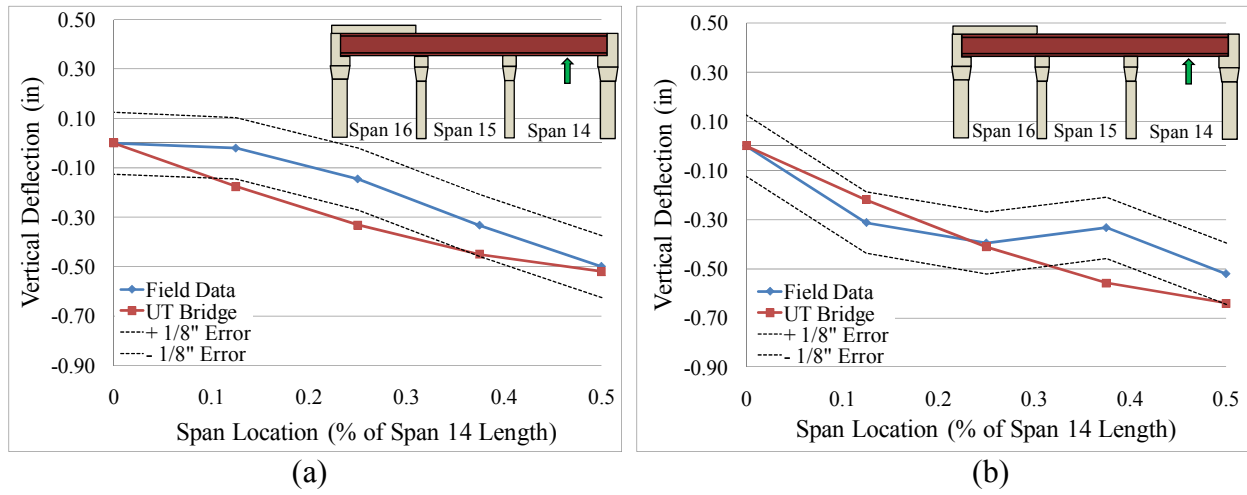


Figure 6.29: UT Bridge Field Data Comparison for Girder 3 (a) and Girder 4 (b)

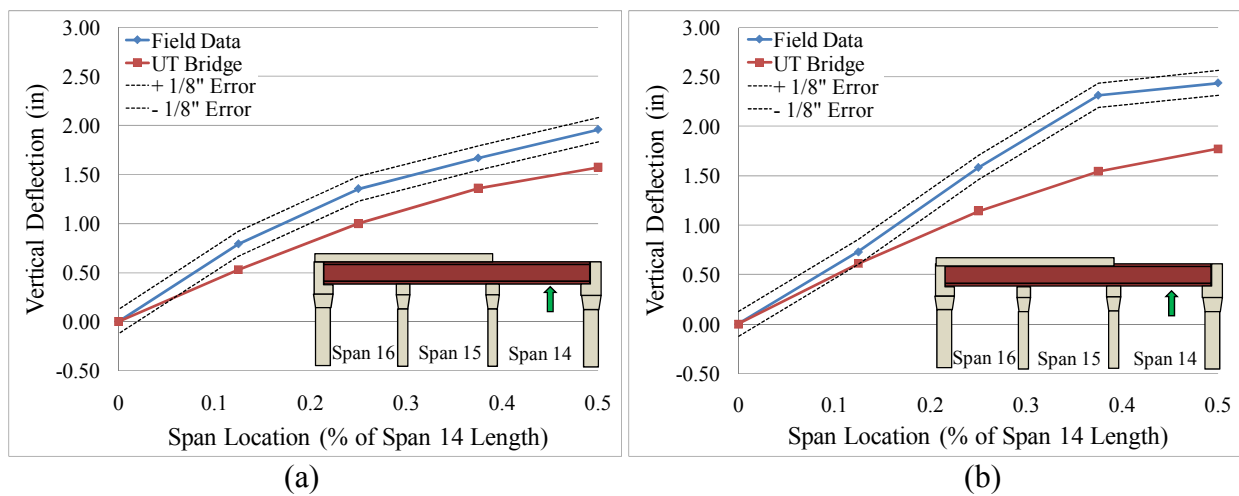


Figure 6.30: UT Bridge Field Data Comparison for Girder 3 (a) and Girder 4 (b)

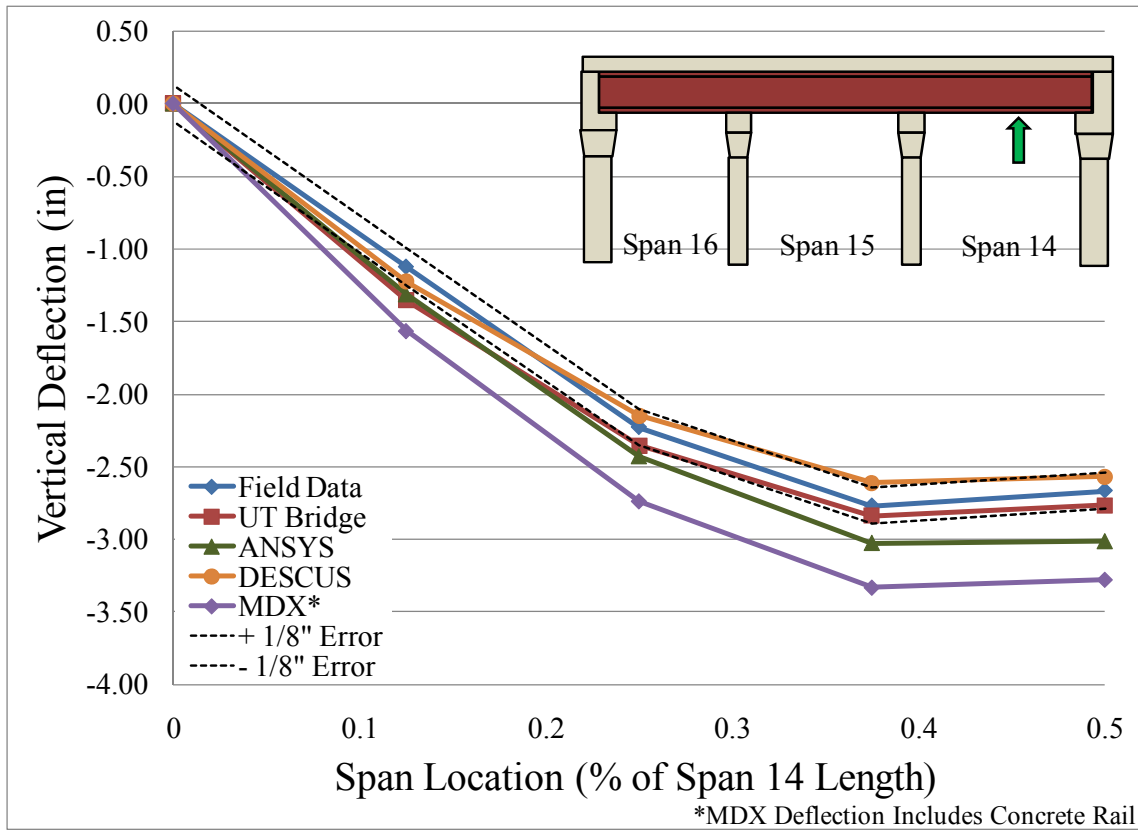


Figure 6.31: Girder 3 UT Bridge Comparison to Field Data and Commercial Programs

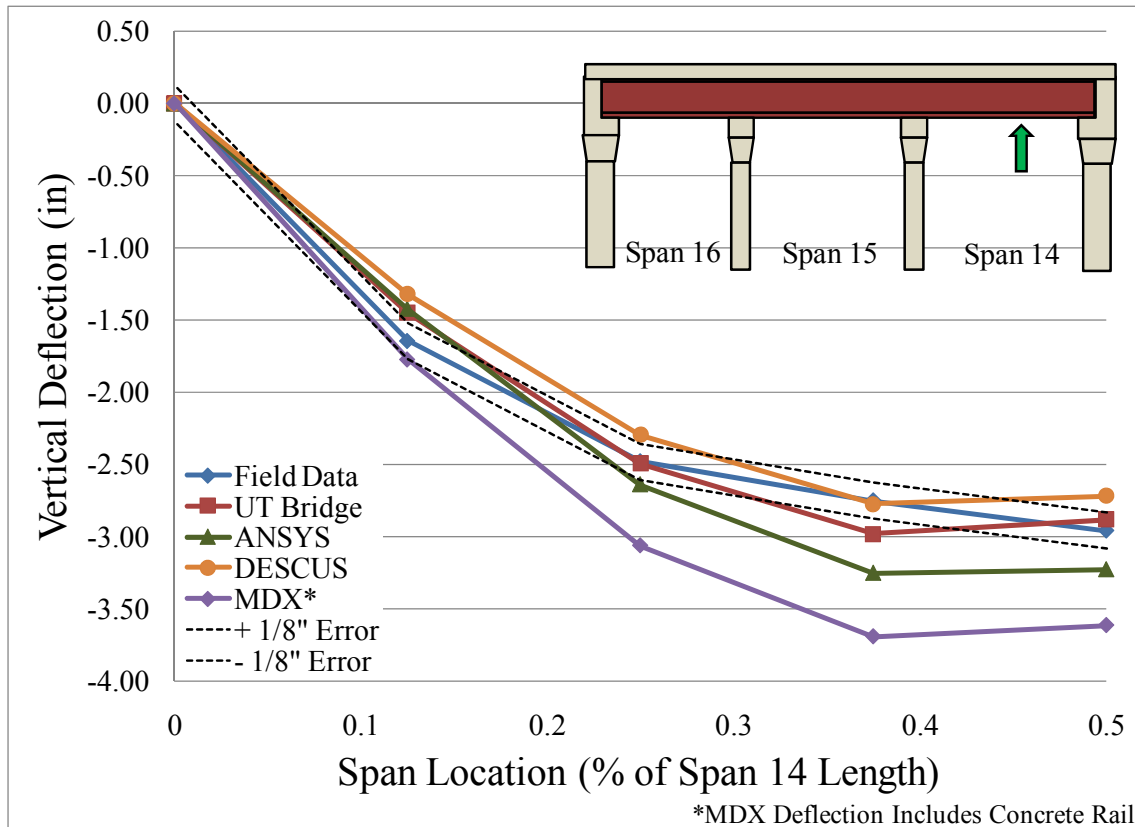


Figure 6.32: Girder 4 UT Bridge Comparison to Field Data and Commercial Programs

The second verification bridge presented here was built in Wichita Falls, Texas and analyzed independently by Dr. Quan Chen utilizing an three-dimensional finite element model in ANSYS. The Texas Department of Transportation also modeled the bridge as part of the design utilizing DESCUS. The results of both of these models were compared to UT Bridge with favorable results. There was a slight modification made to the UT Bridge program to account for the fact that the actual bridge had a point of tangency near the end of the bridge resulting in a slightly different span arrangement than a constant curvature modeled in UT Bridge. The last substructure unit was skewed 6 degrees to ensure the span lengths of all the girders matched the as-built condition in the field. Figure 6.33–6.37 are the comparisons for all five girders in the cross section along the length of the bridge for the steel dead load only. While Figure 6.38–6.42 are similar comparisons the vertical deflection for the bridge with the entire concrete deck placed.

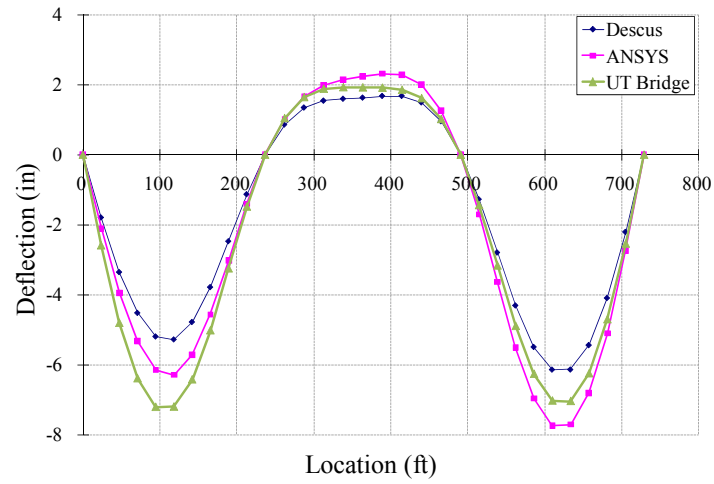


Figure 6.33: Girder 1 Comparison for Steel Dead Load Only

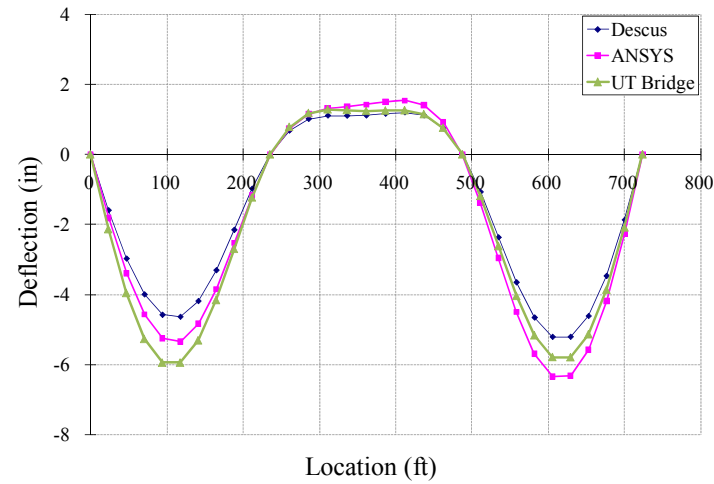


Figure 6.34: Girder 2 Comparison for Steel Dead Load Only

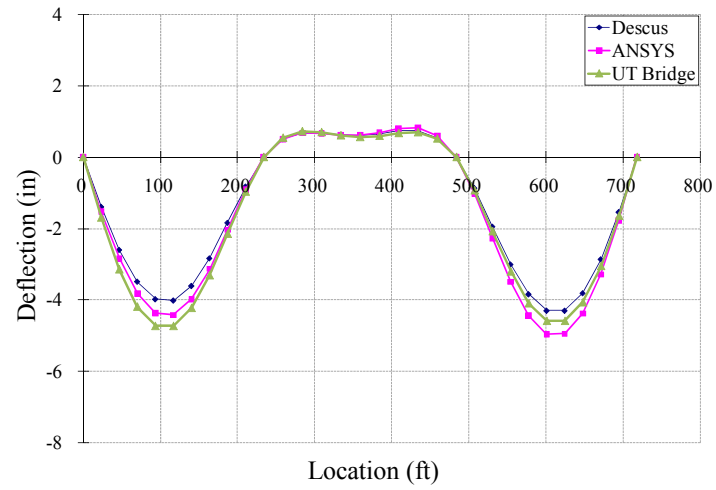


Figure 6.35: Girder 3 Comparison for Steel Dead Load Only

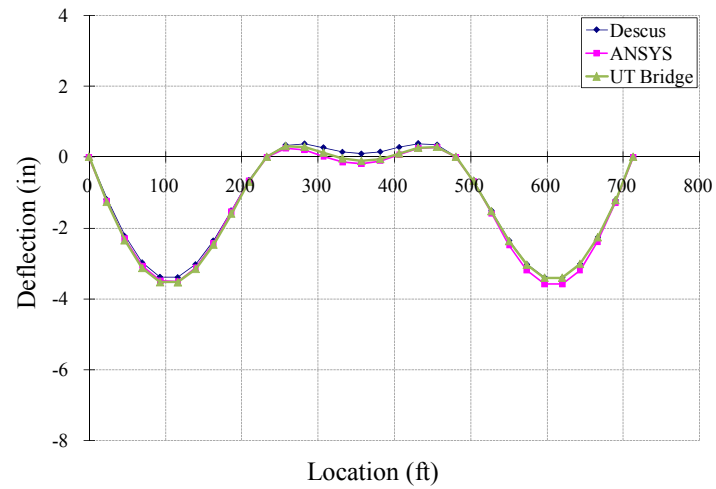


Figure 6.36: Girder 4 Comparison for Steel Dead Load Only

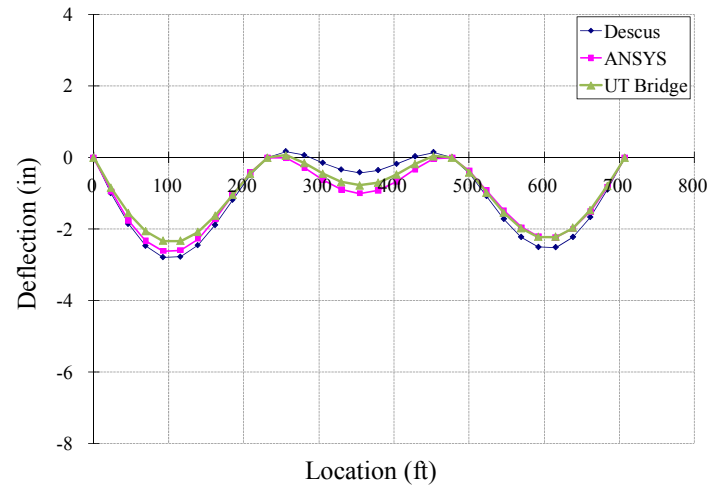


Figure 6.37: Girder 5 Comparison for Steel Dead Load Only

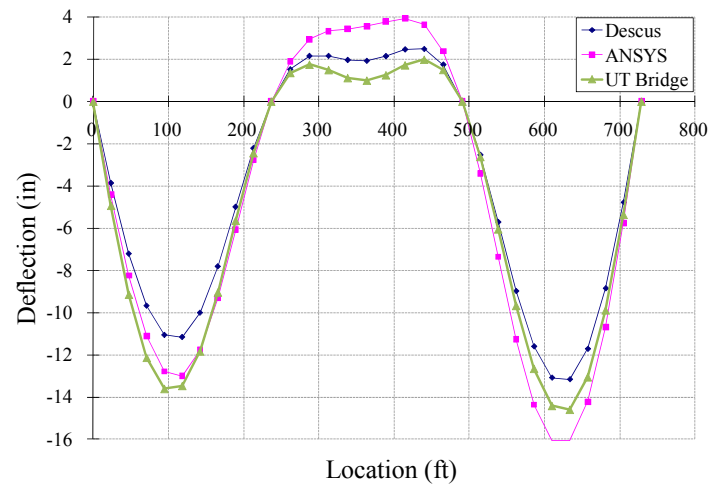


Figure 6.38: Girder 1 Comparison for Steel and Concrete Slab Loading

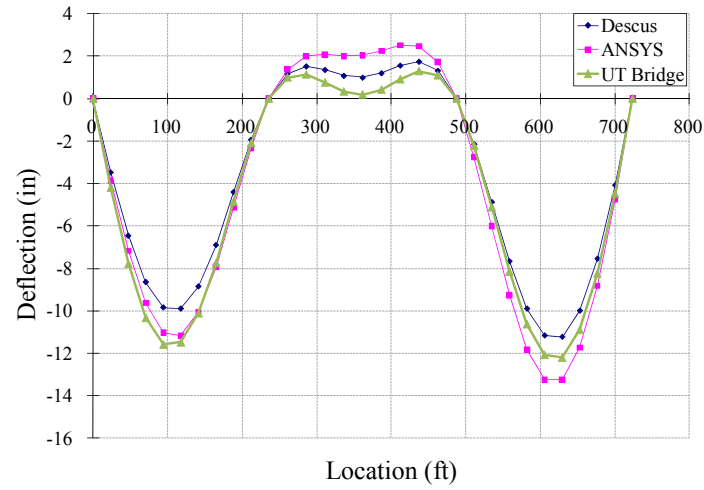


Figure 6.39: Girder 2 Comparison for Steel and Concrete Slab Loading

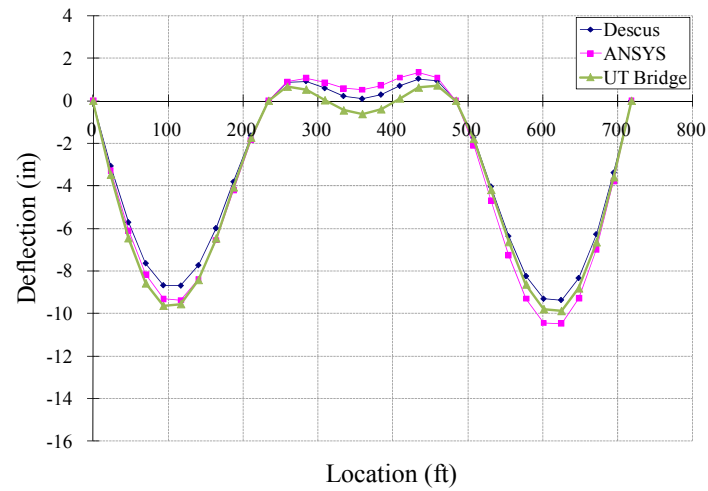


Figure 6.40: Girder 3 Comparison for Steel and Concrete Slab Loading

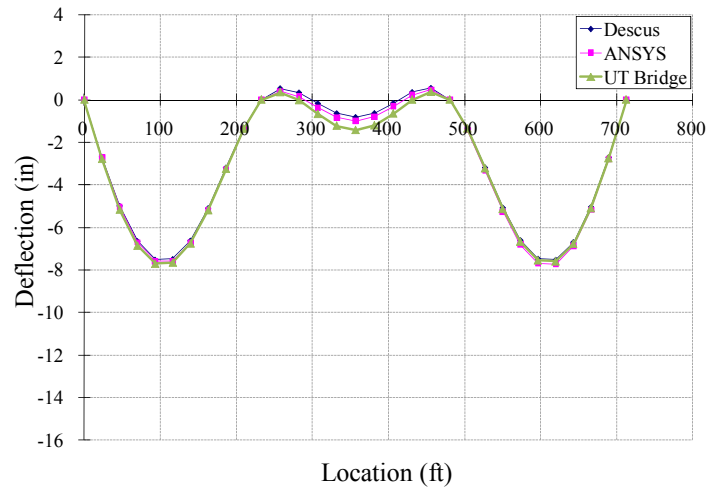


Figure 6.41: Girder 4 Comparison for Steel and Concrete Slab Loading

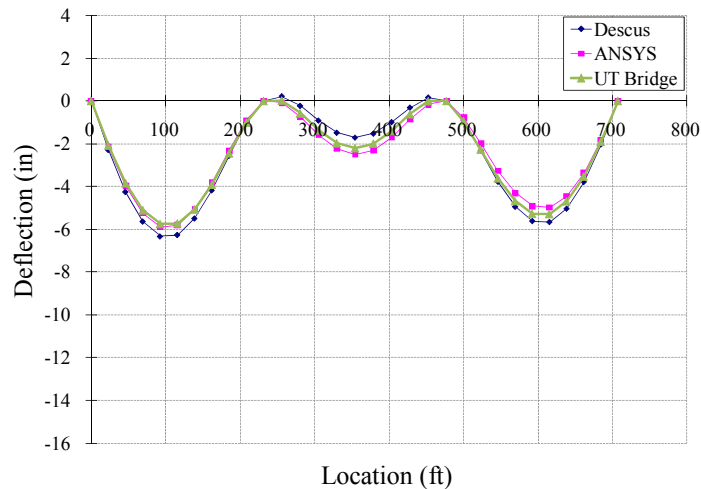


Figure 6.42: Girder 5 Comparison for Steel and Concrete Slab Loading

6.6 UT Bridge Conclusions

The UT Bridge program is a PC based three-dimensional finite element software that has a set of user-friendly preprocessor input forms. The processor is a robust finite element program that quickly discretizes the bridge, assembles the element stiffness matrices, and solves the subsequent set of linear equations. The program allows for both curved and straight I-girder bridges with any number of girders or spans. Skewed supports are allowed. Various loading types are allowed including self weight, wind, and point loads as wells additional temporary supports. A linear elastic or eigenvalue buckling analysis can be performed. The post processor, UT Viewer, provides a 3-D graphical output that ensures correct geometry was modeled as well as providing displacement, stresses, and rotations. Separate two-dimensional graphs are available for displacements, stresses, and rotations evaluated at the tenth points of each span. The output data can be given in tabular form that can be copied to other programs. Cross frame forces and reactions are also provided graphically or in tabular form. The program has been verified

throughout the development at element level, girder level, and system level. A set of actual bridges were used to demonstrate the verification comparing field data, commercially available grillage programs, and full three-dimensional finite element models in ANSYS. The availability of UT Bridge to engineers should provide a powerful tool for the evaluation of I-girder bridges during construction offering a sector of the engineering community with an analysis tool that more reasonably models the existing conditions.

Chapter 7. Design Guidelines

7.1 Purpose

The purpose of this set of guidelines is to summarize recommendations from work completed as part of the Texas Department of Transportation (TxDOT) Research Project 0-5574 entitled “Curved Plate Girder Design for Safe and Economic Construction.” The research included field tests, three-dimensional finite element parametric studies, and software development. The full report for the study will be submitted by October 31, 2009 and includes a more detailed explanation of the recommendations given within this document.

The development of general guidelines to ensure girder stability during lifting, erection, and early stages of construction is complicated by the wide range of variables that impact the behavior of the girder system. These variables include girder proportioning, partially installed bracing, crane positioning, the use and positioning of temporary supports, as well as several other factors. To aide in assuring girder stability, two analytical tools were developed as part of this research project. The analytical tools consist of a spreadsheet program (UT Lift) for evaluating girder behavior during lifting, and a finite element program (UT Bridge) for analyzing the behavior of I-girder bridges at various stages of erection and during construction of the concrete bridge deck. While the guidelines presented herein have been developed to assist in producing a stable system, the reader is encouraged to use the analytical tools, UT Lift and UT Bridge, or other suitable analytical packages, to evaluate bridge girder systems during construction.

7.2 Cross Sectional Proportioning

One of the major topics studied in the research investigation was the effect of cross sectional proportioning on the stability of curved girders during construction. Several parameters were identified including flange width to depth (b_f/D), length to depth (L/D), and radius of curvature (R). One of the catalysts for the research study was differences in the limiting b_f/D ratios commonly applied by TxDOT and the AASHTO Guidelines. According to the *AASHTO LRFD Bridge Specifications 4th Edition* (2007) the minimum b_f/D ratio is one-sixth (Eq. 6.10.2.2-2). However, TxDOT’s *Preferred Practices for Steel Bridge Design, Fabrication, and Erection* (2007) states that “for curved girders, flange width should be approximately one-third the web depth and no less than 30 percent of the web depth. The extra width for curved girders enhances handling stability and helps keep lateral bending stresses within reason.” Although the AASHTO minimum limit of one-sixth for b_f/D is relatively slender, there is no research justification for the TxDOT recommendation of twice the AASHTO value. The limit of one-third the web depth is twice as wide as the one-sixth limit specified by AASHTO.

Torsional loads have a significant contribution to the behavior of curved girders. Therefore, ensuring that girders have sufficient torsional stiffness and strength is an important consideration in proportioning the girders. For open cross sections, such as I-shaped girders, the warping stiffness has a considerable contribution to the torsional stiffness. The most significant contribution to the warping stiffness of the section is the width of the flanges (b_f). Thus, lower values of the b_f/D ratio significantly reduce the warping stiffness of girder cross sections.

For improved economy, engineers may choose to reduce the width of girder flanges because the completed bridge will have a number of cross frames and a hardened deck to brace the girders. However, during the construction process, many of the braces are not connected,

which leaves the bridge vulnerable to stability-related issues without proper analytical checks. Analytical studies bounded by the typical bridge configuration utilizing by TxDOT and measured by L/D and R that considered the impact of the b_f/D ratio showed that while the TxDOT recommended minimum value of $1/3$ was generally conservative, values close to the AASHTO limit of $1/6$ often resulted in excessive torsional flexibility that can lead to problems during construction. The studies showed that reducing the minimum b_f/D value to $1/4$ often resulted in reasonable behavior throughout the construction process. Designers are also encouraged to make use of analytical tools such as UT Lift and UT Bridge to evaluate the behavior during the construction process.

7.3 Lifting of Curved I-Girders

7.3.1 Lifting Options

The lifting of curved I-girders is an important stage of the construction process and significant progress was made in Project 0-5574 in understanding and predicting the behavior of girders during lifting. There are several options available to contractors when deciding how to lift the I-girders into place. They include:

- A) Single crane with a single lift point
- B) Single crane with two lift points and spreader bar
- C) Two cranes with two lift points
- D) Two cranes with four lift points and two spreader bars
- E) Three or more cranes

The least desirable of the above options is Case A with the single lift point as there is little control of the girder deformations, and it is recommended that it not be used for any sizable bridge girder. The scenarios in Cases B and C that use either a single crane with a lifting beam (spreader bar) or two cranes with two lift points is a reasonable option and was the focus of much of the research. The research also included a survey of erectors to determine commonly used lifting practices, and Case B was the most widely used method for lifting girders. Although the geometry of the curved girders results in torsion on the girder system, the two points of support can be positioned to provide a stable system during lifting. However, because the erector does not generally have the spreader beam with the ideal length to prevent rigid body rotation of the girder segment being lifted, the effects of rotations due to both rigid body motion and torsional deformations should be considered when evaluating the lifting behavior. Lifting the girders with the Case D scenario that makes use of two cranes and four lift points results in improved stability compared to Cases B and C due to the larger number of lift points as well as a more favorable distribution of bending moment. The four lift points provide better resistance to girder twist compared two lift points, and the four lifting reactions also lead to a reduction in the maximum bending moment. While the use of two lifting cranes can improve the girder stability, this option is often reserved for relatively long girder segments due to the cost of the extra crane, but the cost can sometimes be overcome if two cranes can complete the work more efficiently than one. Similarly, the use of three or more cranes is uncommon due to the added equipment costs, difficulty in coordinating crane movement, and variations of crane forces during the lift. The source of the variable lifting force when using more than two cranes results from the lifted girder

being an indeterminate system. With all lifting options, two limit states should be checked to ensure safety of the girders and the workers during the lifting process: a strength limit state and a serviceability limit state, both of which are discussed in the following sections.

7.3.2 Strength Limit State

Maximum stresses occurring during construction should be limited so as to preclude yielding on the cross section. Premature yielding on the cross section is affected not only by the stresses induced from applied loading but also due to the presence of residual stresses on the cross section. Depending whether Allowable Stress Design (ASD) or Load and Resistance Factor Design (LRFD) methodologies are used the following limits should be checked:

- ASD: Service Loads with an Allowable Stress of $F_y/1.67$.
- LRFD: Use Factored Loads (Load Factor of 1.5) with a stress limit of ϕF_y ($\phi = 0.9$).

For the ASD approach, the service loads will typically be the self weight of the girder and any attached cross frames. For the LRFD approach, these service loads are multiplied by the Load Factor, as indicated above.

7.3.3 Serviceability Limit State

A serviceability limit state that limits the total girder rotation to less than 1.5 degrees is recommended to prevent excessive deformation of girders during erection. The rotational limit is used to facilitate the lifting process and to aid in the aerial girder field splice connection. Additionally, excessive deformations provide an indication of a general lack of sufficient stiffness and can also indicate an impending problem with girder stability. The limit of 1.5 degrees was recommended based on information obtained from a nationwide survey of contractors, engineers, and fabricators (Farris 2008). A rotational limit larger or smaller than 1.5 degrees can be selected by the engineer; however, for larger values, the engineer should consider the complications on connection fit-up. For rotations significantly smaller than 1.5 degrees the contractor may find it practically difficult to achieve.

7.3.4 Stability of Girder during Lifting

The number of lifting points and their location is the most important factor to consider when designing the lifting plans for curved girders. If two lifting points are used, then there is a specific location where the defined line of support will pass through the center of gravity of the girder resulting in zero rigid body rotation. However, stability of the girder is maximized by lifting in the vicinity of the quarter points of the girder where the moment gradient of the girder is greatest. Schuh (2008) and Farris (2008) recommended C_b factors that can be applied to the buckling solutions derived for uniform moment loading utilizing the entire length of the girder segment for the unbraced length, L_b . The C_b expressions are applicable to girders lifted at two locations. It is conservatively recommended that for nonprismatic girders the cross sectional variables (I_y , J , C_w) should be calculated for each cross section and the resulting minimum M_{cr} should be used for design. For doubly-symmetric sections, making use of Timoshenko's (1961) buckling solution results in the following expression:

$$M_{max} < \phi M_{cr} = \phi C_b \frac{\pi}{L_b} \sqrt{EI_y GJ + E^2 I_y C_w \left(\frac{\pi^2}{L_b^2} \right)} \quad (7.1)$$

Where:

M_{max} = Factored Maximum Moment From Static Analysis

M_{cr} = Critical Buckling Moment

ϕ = Reduction Factor = 0.9

C_b = Lift Adjustment Factor

L_b = Unbraced Length = L

E = Modulus of Elasticity (ksi)

I_y = Weak Axis Moment of Inertia (in^4)

G = Shear Modulus (ksi)

J = Torsional Constant (in^4) = $\sum \frac{bt^3}{3}$

C_w = Warping Constant (in^6) = $\frac{I_y h^2}{4}$

The C_b factor that was developed based upon the work of Schuh (2008) and Farris (2008) is given in the following expressions:

$$\begin{aligned} C_b &= 2.0 \text{ for } \frac{L_{\overline{Lift}}}{L} \leq 0.225 \\ C_b &= 6.0 \text{ for } 0.225 < \frac{L_{\overline{Lift}}}{L} < 0.3 \\ C_b &= 4.0 \text{ for } \frac{L_{\overline{Lift}}}{L} \geq 0.3 \end{aligned} \quad (7.2)$$

Where:

$L_{\overline{Lift}}$ = Average Length from the Lift Points to the Ends of the Girder

The equations above provide a reasonable estimate of the buckling capacity for straight girders and for curved girders with a relatively large radius of curvature (central angle subtended by the girder length (L/R) is less than 3 degrees). Where L is the total length of the girder and R is the radius of curvature of the girder. For most curved girders, however, the equations overestimate the buckling capacity. Although the buckling solution in Eqs. 7.1 and 7.2 tends to overestimate the capacity for horizontally curved girders, computational studies showed that girders for which buckling was a problem were typically controlled by torsional deformations. In these cases, applying the 1.5 degree rotational limit discussed in the last section usually governed the lifting behavior. When this limit was enforced, buckling was not a problem.

7.3.5 UT Lift

As mentioned earlier in this document, the program UT Lift is an Excel spreadsheet for evaluating the behavior of curved I-girders during lifting. The spreadsheet provides an analytical tool to determine girder rotation and to give information to an engineer when deciding the safety of a horizontally curved steel I-girder during lifting with two lift points. The spreadsheet input that is required consists of basic information readily available to the engineer such as the thicknesses and lengths of the girder plates that make up the cross section, as well as the weight and spacing of the cross frames. The center of gravity and optimum lift locations for minimizing rigid body rotation are calculated in the spreadsheet. For a given lifting scheme, the spreadsheet will calculate the total rotation of the girder being analyzed including both the rigid body rotation and the cross-sectional twist. A stability check and several graphs are also provided for additional information that can be used to assess girder performance.

7.3.6 Recommendations

Various lifting options are available for the erection of curved girders, but it is advisable to use the maximum number of lift points possible due to the increased stability and the decreased deformations that accompany such lifting configurations. However, economic considerations require a minimum number of cranes to be utilized most of time. Applying the strength and stiffness limits described earlier will generally result in a safe system that avoids problematic deformations during lifting. Although straight girders will not generally be limited by the 1.5 degree rotational limit presented earlier, the buckling solutions from Schuh (2008) and Farris (2008) had good correlation with three-dimensional finite element solutions. The optimum location to lift a girder is between the point at which the line of support passes through the center of gravity and the girder's quarter points. For a horizontally curved segment with a prismatic cross section, lifting at the quarter points will maximize the buckling capacity, while lifting at a distance 21% of the segment length from the ends will result in no rigid body rotation, thereby minimizing the torsional deformations.

7.4 Partially Constructed Bridges

7.4.1 Critical Stages of Bridge Constructions

The critical stage for girder stability generally occurs during construction. The most critical situations to check include:

- The case where a single girder segment has been erected.
- The girder system after a holding crane or shore tower is removed.
- The first concrete placement stage on a span.

Typically, the first girder lifted at a particular cross-sectional location will have a significantly longer unbraced length than the final configuration and can exhibit stability problems. Once the next girder is constructed and cross frames are attached, the stability of the combined system is significantly improved. However, if a holding crane was used during the first stage of erection and then removed, the new configuration should be checked. Any change in the bracing or support conditions can present potential problems for bridges as can stages where the temporary supports are removed. Accordingly, if any of these conditions occur, stability of the system

should be checked. Once the concrete has cured, it provides considerable bracing for the girder system, but during the first concrete placement stage, a large load is added to the bridge without adding bracing. Any time concrete is placed on a span without previously hardened concrete, the entire system should be checked for stability and excessive deformations.

7.4.2 Shore Towers

Shore towers are primarily used to control deformations and stresses as well as provide bracing for the girders during erection. The location of a shore tower affects the behavior of the girders as well as required design forces on the shore tower. The specific location where a shore tower can be placed, however, is affected by many nonstructural restrictions such as site access, construction methodology, and girder stiffness variations. Nonetheless, it is recommended that shore towers be placed at locations where the maximum positive bending moment occurs between permanent supports. This positioning will have the greatest effect on minimizing the total deflections, and in general, it places a tower near the position where it will be required to support the least load of any position along the girder. It should be noted that adding a shore tower results in a large concentrated force and it is thus advisable to place the shore tower under a stiffener location, or alternatively, to check local yielding and stability of the girder web at the shore tower location.

A final issue on the use of shore towers is the load height effect associated with their use. A shore tower supports the girder from the bottom flange which is below the girder's center of gravity. If the girder is not properly braced and the girder is allowed to rotate, the reaction force of the shore tower results in a disturbing force. This disturbing force causes secondary moments on the cross section and increases the deflections predicted by a linear structural analysis. This lack of conservatism should be known to the designers and erectors that use a linear analysis to predict the behavior of curved girders during construction. The previous assessment neglects the tipping restraint that is often present in actual structures which provides stability and reduces the disturbing force. Tipping restraint is the beneficial effect that happens when cross-sectional twist is restricted by stiff contact surfaces between the girder and a load/reaction point. Although load position on the cross section can have dramatic impacts on the buckling capacity, the girder must be able to rotate at the load or reaction point (no bracing) for load position to have any effect. Consequently, problems associated with the disturbing force of the shore tower can be eliminated by properly bracing the girder against rotation at its support on the shore tower.

7.4.3 Holding Cranes

In lieu of a shoring tower, temporary holding cranes also provide a valuable method of supporting curved I-girders during erection. Although cranes represent expensive equipment on the job site, there are a number of benefits to using holding cranes. There are many situations where traffic demands below the bridge may not permit the use of a shore tower that will often remain standing for lengthy periods of time. The benefit of the holding crane is that the equipment is often only required during lifting of the first few girder segments. The location of a holding crane will affect the recommended load and the effectiveness of the crane to perform its primary function of controlling the deformations and the stresses of the girders it is supporting. The specific location of the holding crane can be affected by many constraints such as site access, construction methodology, and girder stiffness variations, but the recommended location is the same as the shore tower; the location of maximum positive intermediate bending moment (i.e., between the permanent supports). Additionally, the lifting load held by a holding crane

significantly affects the behavior of the girder it is supporting. It is recommended that the crane hold a load that would be equivalent to a rigid support directly under the girder. This load will maintain the vertical web and minimize deformations for ease of construction fit-up. A lifting load that varies from this recommended load will result in the girder rotating and could induce unintended stresses. Parametric finite element analyses conducted on TxDOT Project 0-5574 showed that changing the location of the holding crane from the optimum position generally has a less detrimental effect on predicted displacements and stresses than a variation of the lifting load. Small deviations in the lifting force applied by the holding crane can significantly affect a girder's displacements and stresses.

Unlike shore towers, a holding crane will normally be attached to the girder's top flange and will provide an upward force above the girder's center of gravity. Therefore, if the girder rotates, a component of the crane force acts as a restoring force causing a secondary moment that decreases the deflections predicted by a linear structural analysis. This phenomenon is conservative and should be known to the designers and to the erectors that use a linear analysis to predict girder behavior. The detrimental aspect of using a holding crane is that it does not brace the girder laterally or torsionally as a shore tower can and thus a structural analysis should be performed to ensure significant lateral deflections does not occur when using a holding crane.

7.4.4 UT Bridge

UT Bridge is a comprehensive three-dimensional finite element analysis software package with a user-friendly graphical user interface (GUI) to input girder geometry and analysis cases. The program has a graphical post-processor that allows an engineer to visualize the construction process and to identify potential problems before field work begins. The program allows for two kinds of construction analyses: girder erection sequence analysis and a concrete deck placement analysis. A linear analysis is performed for each case and if desired, an eigenvalue buckling analysis can also be performed. It should be noted that an eigenvalue buckling analysis approximates the load at which a structure will lose stability by providing a multiplier of the applied loads (factor of safety) known as the eigenvalue. This analysis assumes small deflections of the girder prior to buckling and provides a reasonable approximation for straight bridges. However, the approach over-predicts the buckling capacity of curved bridges that exhibit significant deformations prior to buckling. Consequently, eigenvalue buckling analysis can give unconservative buckling predictions for these types of structures.

While the software was developed as an analysis tool, a designer can utilize its capabilities to design and to check a bridge for a variety of load cases. This would include but is not limited to determining:

- The optimum location of shore towers,
- the design load of shore towers,
- the necessary erection stages for using holding cranes,
- when a holding crane can be released,
- the effects on displacement and stresses of a concrete placement sequence, and
- whether a girder will experience uplift at the bearing.

7.4.5 Recommendations

The critical stage for stability and safety of many steel bridge systems often occurs during construction. All erection stages should be analyzed for excessive deformations, stresses, and buckling considerations. The concrete deck placement produces a large load on the bridge before full composite action can be accounted for and the stabilizing effects of the hardened deck can be achieved. Thus, each concrete stage should be analyzed for excessive deformations, stresses, and buckling considerations. Both shore towers and holding cranes can be used to reduce the deformations and redistribute stresses. Shore towers can be used to brace girders laterally and torsionally if the bracing is adequately strong and stiff. The optimum location for shore towers or holding cranes is the location of maximum positive bending moment between permanent supports. UT Bridge is a user-friendly 3-D finite element program that can be used to analyze partially constructed bridges and to provide valuable information to engineers and contractors in the assessment of the safety of a bridge at various construction phases. Additionally, UT Bridge can be used to locate the optimum location of shore towers and provide the design loads of the shore towers.

7.5 Erection and Construction Calculation Recommendations

The design and construction of curved I-girder bridges can be complicated. Therefore, it is important for design submittals to be standardized to ensure safety during construction. The AASHTO/NSBA Steel Bridge Collaboration produced the *Steel Bridge Erection Guide Specification*, which provides guidance for the minimum submittal that should be provided by the contractor prior to the beginning of construction. These recommendations have been included below with some modifications as a recommendation for TxDOT's standard construction submittal for horizontally curved steel I-girder bridges.

7.5.1 Drawings

- 1) A plan of the work area including permanent substructure units, roads, railroad tracks, waterways, overhead and underground utilities, and other information pertinent to erection.
- 2) The erection sequence for all members (girders, cross frames, diaphragms, etc.). The location of any temporary support condition, such as holding cranes or shore towers, should be noted along with the design load for the shore towers and/or the prescribed lifting force of the holding cranes. Member reference marked on the erection drawings should be the same as those used on the shop detail drawings.
- 3) The primary member (girder) delivery location and orientation.
- 4) The location of each crane for each primary member pick, showing radius and crane support (barges, mats, etc.).
- 5) The capacity chart for each crane configuration and boom length used in the work.
- 6) Details, weight, capacity, and arrangement of all rigging for primary member picks.
- 7) The lifting weight of the primary member picks, including all rigging and pre-attached elements to correspond to erection sequence.

- 8) Details of any temporary lifting devices to be bolted or welded to permanent members, including method and time (shop or field) of attachment, the capacity, and the method, time, and responsibility for removal.
- 9) Lifting and handling procedure for each primary member including the center of gravity, the method of lifting (single crane, multiple crane, etc.), and the number and location of lifting apparatus.
- 10) Blocking or bracing details for girders at permanent supports before cross frame members are attached at temporary supports.
- 11) Shoring tower (or falsework) design details, including the tower structure, footings, top beams, tower bracing, and all connections between erected girders and top beams and another major portions of the tower.
- 12) Safety measures detailed for special event such as “Hurricane Season,” if applicable for projects in effected regions.

7.5.2 Calculations

- 1) Design calculations indicating the rotational deformations and the maximum stress of all primary girders during lifting procedures. This information should include rigid body rotation and cross-sectional twist for the rotational deformations. The maximum stress should include strong-axis bending, weak-axis bending, and warping normal stresses.
- 2) Design calculations indicating the load capacity and stability of temporary supports (shore towers and cranes) for each pick and release. Considerations for the wind load effects on temporary supports should be included.
- 3) Calculations to substantiate the structural adequacy and stability of girders for each step of bridge assembly and concrete deck placement.
- 4) Calculations to verify adequate capacity of contractor-fabricated rigging such as lifting beams, welded lugs, spreader beams, beam clamps, etc. Submit manufacturers’ certification or catalog cuts for pre-engineered devices.
- 5) Calculations indicating structural integrity of any partially bolted primary splices after release of external support system
- 6) Calculations to substantiate structural integrity of abutments and retaining walls affected by surcharge from crane.

Appendix A. Curved I-Girder Erection Questionnaire

This appendix provides a copy of the questionnaire used to survey various steel curved I-girder erection contractors, inspectors, and engineers. The questionnaire focuses on the common practice for lifting curved I-girders, including spreader beam length, number of cranes, lift points, shore towers, and length of girder segments lifted. Refer to Chapter 6 for the discussion of the responses to the questions.

Questionnaire Erecting Curved Plate I-Girders

Company: _____
Name: _____
Phone: _____
Date: _____

1. What is the typical lifting scenario?

- a. 1 girder segment lifted, then spliced in the air. What is the range of the segment lengths lifted?
- b. Multiple girder segments spliced on the ground, then lifted. What is the range of the lengths lifted?

2. Are spreader beams used? Before a girder is delivered to the site, do you know the size of spreader beam(s) that will be used? Or do you wait until the girder arrives and then choose from various spreader beams that you have on hand? What are the typical spreader beam lengths that you use?

3. When lifting a girder, is it typical to use one crane or two cranes? If you use two cranes do you employ spreader beams for each crane?

- 4. Is tilting of the girder a concern when lifting curved girders? When lifting a curved girder, what is your typical rotation tolerance?**
- 5. How do you determine where to lift the girder and the number of lifting points?**
- 6. What problems or concerns do you have about lifting curved plate girder segments that you would like to be considered in this research?**

Appendix B. Bibliography

- AASHTO/NSBA Steel Bridge Collaboration (2007) *Steel Bridge Erection Guide Specification*, Washington, D.C.
- American Association of State Highway and Transportation Officials (AASHTO). (1980). *Guide specifications for horizontally curved bridges*, Washington, D.C.
- American Association of State Highway and Transportation Officials (AASHTO). (1993). *Guide specifications for horizontally curved bridges*, Washington, D.C.
- American Association of State Highway and Transportation Officials (AASHTO). (2003). *Guide specifications for horizontally curved bridges*, Washington, D.C.
- American Association of State Highway and Transportation Officials (AASHTO). (2007) *AASHTO LRFD Bridge Specifications*, 4th Edition, Washington, D.C.
- American Association of State Highway and Transportation Officials (AASHTO). (2008) *AASHTO LRFD Bridge Construction Specifications*, 2nd Edition, 2008 Interim Revisions, Washington, D.C.
- American Institute of Steel Construction (AISC). (2005) *Steel Construction Manual*, 13th Edition.
- ANSYS, Finite element program users' manual, Version 11.0. (2007). ANSYS, Inc.
- Bathe, Klaus- Jürgen (1996). Finite Element Procedures Prentice-Hall, Englewood Cliffs, NJ, 1996.
- Beal, D. B., and Kissane, R. J. (1971). *First Interim Report on Research Project 42-1*, New York State Department of Transportation, Engineering Research and Development Bureau, Albany, New York.
- Beal, D. B., and Kissane, R. J. (1971). *Second Interim Report on Research Project 42-1*, New York State Department of Transportation, Engineering Research and Development Bureau, Albany, New York.
- Beal, D. B., and Kissane, R. J. (1972). *Third Interim Report on Research Project 42-1*, New York State Department of Transportation, Engineering Research and Development Bureau, Albany, New York.
- Bell, Bradley J. (2004). *Effects of Erection Procedures on the Response of a Horizontally Curved I-girder Bridge*. Master's Thesis, The University of Pennsylvania State University, University Park, PA.
- Bishara, Alfred G. and Elmir, Wassef E. (1990). "Interaction Between Cross Frames and Girders," *Journal of Structural Engineering*, Vol. 116, No. 5, May Pg 1319-1333.

- Brennan, P.J. (1970). "Horizontally curved bridges first annual report: Analysis of horizontally curved bridges through three-dimensional mathematical model and small scale structural testing." *Syracuse Univ., First Annual Rep., Research Project HPR-2(111)*, Syracuse, N.Y.
- Brennan, P.J. (1971). "Horizontally curved bridges second annual report: Analysis of Seekonk River Bridge small scale structure through three-dimensional mathematical model and small scale structural testing." *Syracuse Univ., Second Annual Rep., Research Project HPR-2(111)*, Syracuse, N.Y.
- Brennan, P.J. (1974). "Analysis and structural testing of a multiple configuration small scale horizontally curved highway bridge." *Syracuse Univ., Research Project HPR-2(111)*, Syracuse, N.Y.
- Brogan, D. K. (1974). "Bending behavior of cylindrical web panels." M.Sc. Thesis, Carnegie Mellon University, Pittsburgh, PA.
- Canadian Institute of Steel Construction (CISC), (2002). Torsional Sections Properties of Steel Sections.
- Chapelle, Dominique & Bathe, Klaus-Jürgen (2003). The Finite Element Analysis of Shells: Fundamentals 1st Edition, Springer.
- "Chapter 1: V-load analysis, an approximate procedure, simplified and extended for determining moments and shears in designing horizontally-curved open-frame highway bridges." (1984). *U.S.S. highway structures design handbook*, Vol. 1, United States Steel Corp., Pittsburgh, Pa.
- Chavel, Brandon William (2008). *Construction and Detailing Methods of Horizontally Curved Steel I-girder Bridges*, PhD Dissertation, University of Pittsburgh, Pittsburgh, PA.
- Chavel, B. W., and Earls, C. J. (2006). "Construction of a horizontally curved steel I-girder bridge: Erection sequence." *Journal of Bridge Engineering*, Vol. 11, No. 1, pp. 81-90.
- Chavel, B. W., and Earls, C. J. (2006). "Construction of a horizontally curved steel I-girder bridge: Inconsistent detailing." *Journal of Bridge Engineering*, Vol. 11, No. 1, pp. 91-98.
- Chen, Q. (2008). *Effects of Thermal Loads on Texas Steel Bridges*. PhD dissertation, University of Texas.
- Clough, R. W., (1960). "The Finite Element Method in Plane Stress Analysis," Proc. 2nd ASCE Conf. On Electronic Computation, Pittsburg, Pa. Sept. 1960.
- Coletti, Domenic and Yadlosky, John (2008). "Analysis of Steel Girder Bridges New Challenges." *Transportation Research Record: Journal of the Transportation Research Board*, No. 2050, Transportation Research Board of the National Academies, Washington, D.C., 2008, pp. 67-77.

- Consortium of University Research Teams (1975). "Tentative design specifications for horizontally curved highway bridges." *Part of Final Rep., Research Project HPR2-(111)*.
- Courant, R. (1943). "Variational Methods for the Solutions of Problems of Equilibrium and Vibrations," *Bull. Am. Math. Soc.*, Vol. 49, pp. 1–23.
- Culver, C. G. (1972). "Design recommendations for curved highway bridges." *Final Rep. for Research Project 68-32*, Pennsylvania Department of Transportation, Harrisburg, Pa.
- Culver, C. G., and Frampton, R. E. (1970). "Local instability of horizontally curved members." *Journal of the Structural Division, ASCE*, Vol. 96, No. 2, pp. 245-265.
- Culver, C. G., and Nasir, N. (1971). "Inelastic flange buckling of curved plate girders." *Journal of the Structural Division, ASCE*, Vol. 97, No. 4, pp.1239-1257.
- Culver, C. G., Dym, C. L., and Brogan, D. K. (1972). "Bending behavior of cylindrical web panels." *Journal of the Structural Division, ASCE*, Vol. 98, No. 10, pp. 2291–2308.
- Culver, C. G., Dym, C. L., and Uddin, T. (1973). "Web slenderness requirements for curved girders." *Journal of the Structural Division, ASCE*, Vol. 99, No. 3, pp. 417–430.
- Davidson, J. S., and Yoo, C. H. (1996). "Local buckling of curved I-girder flanges." *Journal of Structural Engineering, ASCE*, Vol. 122, No. 8, pp. 936-947.
- Davidson, J. S., and Yoo, C. H. (2000). "Evaluation of strength formulations for horizontally curved flexural members." *Journal of Bridge Engineering*, Vol. 5, No. 3, pp. 200-207.
- Davidson, J. S., Keller, M. A., and Yoo, C. H. (1996). "Cross-frame spacing and parametric effects in horizontally curved I-girder bridges." *Journal of Structural Engineering, ASCE*, Vol. 122, No. 9, pp. 1089-1096.
- Fan, Z. (1999). *Field and Computational Studies of Steel Trapezoidal Box Girder Bridges*. PhD dissertation, University of Houston.
- Farris, Jamie F. (2008) *Behavior of Horizontally Curved Steel I-girders During Construction* Master's Thesis, University of Texas at Austin, Austin, TX.
- Fasl, J. D. (2008). *The Influence of Overhang Construction on Girder Design*. Thesis, University of Texas.
- Felippa, Carlos A. "Introduction to Finite Element Methods," Textbook for Introduction to Finite Element Methods (ASEN 5007), University of Colorado at Boulder, 2004. Web accessed June 5, 2009. <http://www.colorado.edu/engineering/CAS/courses.d/IFEM.d/>
- Fiechtl, A. L., Fenves, G. L., and Frank, K. H. (1987). "Approximate analysis of horizontally curved girder bridges." *Final Rep. No. FHWA-TX-91-360-2F*, Center for Transportation Research, University of Texas at Austin, Austin, TX.

- Galambos, T. V., Hajjar, J. F., Huang, W., Pulver, B. E., Leon, R. T., and Rudie, B. J. (2000). "Comparison of measured and computed stresses in a steel curved girder bridge." *Journal of Bridge Engineering*, Vol. 5, No. 3, pp. 191-199.
- Guide to Stability Design Criteria for Metal Structures*, 5th Ed. (1998) T. V. Galambos, ed., John Wiley & Sons, Inc., New York, N.Y.
- Hartmann, Joseph L. (2005) *An Experimental Investigation of the Flexural Resistance of Horizontally Curved Steel I-Girder Systems*, PhD Dissertation, University of Maryland, College Park, MD.
- Heins, C. P. (1972). "Design data for curved bridges." *Rep. No. 47*, summary report for Maryland Department of Transportation and Federal Highway Administration, Washington, D.C.
- Helwig, Todd A., Frank, Karl H., Yura, Joseph A. (1997). "Lateral-torsional buckling of singly symmetric I-beams." *Journal of Structural Engineering*, Vol. 123, No.9, pp. 1172-1179.
- Huang, W. H. (1996). *Curved I-girder systems* PhD Dissertation, Department of Civil Engineering, University of Minnesota.
- Jung, S., and White, D. (2005). "Shear strength of horizontally curved steel I-girders – finite element analysis studies." *Journal of Constructional Steel Research*, 62, pp. 329-342.
- Kassimali, Aslam (1999). *Matrix Analysis of Structures* Brooks/Cole, Pacific Grove, CA.
- Kuo, J. T. C. and Heins Jr., C. P. (1971). "Behavior of Composite Beams Subjected to Torsion," University of Maryland Civil Engineering Research Report #39. College Park, MD.
- KWH Constructors. (n.d.). *Project Galleries-Bridge Construction-William R Bennett Bridge*. Retrieved October 26, 2009, from KWH Constructors:
http://www.kwhconstructors.com/img/gallery/williamr.bennettbridge/wrb_bridge5.JPG
- Lehoucq, R.B., Sorensen, D.C., and Yang, C. (1998). *ARPACK User's Guide Solution of Large Scale Eigenvalue Problems with Implicitly Restarted Arnoldi Method*. SIAM, Philadelphia.
- Linzell, D. G. (1999). "Studies of a Full-Scale Horizontally Curved Steel I-Girder Bridge System Under Self-Weight", PhD Dissertation, Georgia Institute of Technology, July 1999.
- Linzell, D., Leon, R. T., and Zureick, A. (2004). "Experimental and analytical studies of horizontally curved steel I-girder bridge during erection." *Journal Bridge Engineering*, Vol. 9, No. 6, pp. 521-530.
- Mast, Robert F. (1989) "Lateral Stability of Long Prestressed Concrete Beams Part 1" *PCI Journal*, Vol. 34, No. 1, pp 34-53.

- McManus, P.F., Nasir, G.A., and Culver, C.G. (1969) “Horizontally curved girders – state of the art.” *Journal of the Structural Division*, ASCE, Vol. 97, No. 10, pp. 2459-2580.
- McManus, P.F. (1971). *Lateral buckling of curved plate girders*, Ph.D. Dissertation, Carnegie-Mellon University, Pittsburgh, PA.
- Mondkar, D. P., and Powell, G. H. (1974). “CURVBRG—A computer program for analysis of curved open girder bridges.” *UC-SESM Rep. No. 74-17*, Univ. of California, College of Engineering, Berkeley, Calif.
- Mozer, J., and Culver, C. (1970). “Horizontally curved highway bridges – stability of curved plate girders.” *Rep. No. P1, Research Project HPR-2(111)*, Carnegie Mellon University, Pittsburgh.
- Mozer, J., Ohlson, R., and Culver, C. (1971). “Horizontally curved highway bridges – stability of curved plate girders.” *Rep. No. P2, Research Project HPR-2(111)*, Carnegie Mellon University, Pittsburgh.
- Mozer, J., Cook, J., and Culver, C. (1973). “Horizontally curved highway bridges – stability of curved plate girders.” *Rep. No. P3, Research Project HPR-2(111)*, Carnegie Mellon University, Pittsburgh.
- Nakai, H., Kitada, T., and Ohminami, R. (1985). “Proposition for Designing Intermediate Transverse Stiffeners in Web Plate of Horizontally Curved Girders.” *JSCE*, no. 362/I-4 October, pp. 249-257 (in Japanese).
- Nakai, H., Kitada, T., Ohminami, R. and Kawai, T. (1986). “A study on Analysis and Design of Web Plate in Curved Girder Bridges Subjected to Bending.” *JSCE*, No. 368/I-5 April, pp. 235-244 (in Japanese)
- Nasir, G. A. (1970). *Buckling of stiffened and unstiffened curved plate elements*, Ph.D. Dissertation, Carnegie-Mellon Univ., Pittsburgh.
- Nevling, D., Linzell, D., and Laman, J. (2006). “Examination of Analysis Accuracy for Curved I-Girder Bridges through Comparisons to Field Data.” *Journal of Bridge Engineering*, Vol. 11 No. 2, March 1, pp. 160-168.
- NCHRP Synthesis 345. (2005) *Steel Bridge Erection Practices, A Synthesis of Highway Practice*, Transportation Research Board of the National Academies, Washington, D.C.
- “Numerical Differentiation,” http://en.wikipedia.org/wiki/Numerical_differentiation, Access December 18, 2008.
- Ozgur, Cagri, White, Donald W. and Leon, Robert T. (2009) “Behavior of Curved and Skewed I-girder Bridge Systems During Construction and Recommendations for Practice.” Structural Stability Research Council Annual Stability Conference Proceedings, Phoenix, AZ, April 1-4, pp. 431-450.

- “Point Line Distance,” <http://mathworld.wolfram.com/Point-LineDistance2-Dimensional.html>, Access February 9, 2009.
- Popp, Daniel (2004). *U-TrAp 2.0: Linearized Buckling Analysis of Steel Trapezoidal Girders*, Master’s Thesis, The University of Texas at Austin, Austin, TX.
- Reddy, J.N. (2006). An Introduction to the Finite Element Method 3rd Edition, McGraw-Hill, New York, NY.
- Richardson, Gordon, and Associates, Consulting Engineers (1963). “Analysis and Design of Horizontally Curved Steel Bridge Girders,” United States Steel Structural Report, ADUSS 88-600301.
- Saint-Venant, B (1843). “Memoire sur le calcul de la resistance et de la flexion des pieces solides a simple ou a double courbure, en prenant simultanement en consideration les divers efforts auxquels elles peuvent entre soumises dans tous les sens.” *Compt-Rendus*, Vol. 27, l’Academic des Sciences de Paris, Paris, France 942, 1020-1031 (in French).
- Schelling, D. Namini, Ahmad H., and Fu, Chung C. (1989). “Construction Effects on Bracing on Curved I-Girders,” *ASCE Journal of Structural Engineering*, Vol. 115, No. 9, September, pp. 2145-2165.
- Schuh, Andrew C. (2008) *Behavior of Horizontally Curved Steel I-girders During Lifting* Master’s Thesis, University of Texas at Austin, Austin, TX.
- Stegmann, T. H., and Galambos, T. V. (1976). “Load factor design criteria for curved steel girders of open cross section.” *Washington Univ. Research Rep. No. 43*, Washington Univ., St. Louis.
- Stith, Jason C. (2010) *The Behavior of Curved I-girder Bridges during Construction* PhD Dissertation, University of Texas at Austin, Austin, TX (in progress).
- Structural Stability Research Council (SSRC) Task Group 14. (1991). “A look to the future.” *Rep. of workshop on horizontally curved girders*, Chicago, 1-18.
- Texas Steel Quality Council. (2007) *Preferred Practices for Steel Bridge Design, Fabrication, and Erection*, Texas Department of Transportation, Austin, TX.
- Timoshenko, Stephen P. and Woinowsky-Krieger, S. (1959). Theory of Plates and Shells 2nd Edition, McGraw-Hill College.
- Timoshenko, Stephen P. and Gere, J. (1961). Theory of Elastic Stability 2nd Edition, McGraw-Hill College, New York, NY.
- Topkaya, Cem. (2002). *Behavior of Curved Steel Trapezoidal Box Girders During Construction*, Ph.D. Dissertation, University of Texas at Austin, Austin, TX, August.

- Topkaya, Cem, Yura, Joseph A., and Williamson, Eric B. (2004). "Composite Shear Stud Strength at Early Concrete Ages" *Journal of Structural Engineering* June, pg. 952-960.
- Tung, David H. and Fountain, Richard S. (1970) "Approximate Torsional Analysis of Curved Box Girders by the M/R-Method." *Engineering Journal*, American Institute of Steel Construction, Volume 7, No. 3, July, pp. 65-74.
- Turner, M. J., Clough, R. W., Martin, H. C. and Topp, L. J. (1956). "Stiffness and Deflection Analysis of Complex Structures," *J. Aeronautical Science* 23 (9), Sept. pp. 805-823.
- Yoo, C. H. and Carbine, R. L. (1985). "Experimental Investigation of Horizontally Curved Steel Wide Flange Beams Analysis." *Proc., Structural Stability Research Council Annual Technical Session: Stability Aspects of Industrial Buildings*, 183-191.
- Yoo, C. H. and Choi, B. H. (2000). "Literature Search–Horizontally Curved Steel Girder Bridges," NCHRP 12-52 Quarterly Report, submitted to the Transportation Research Board, Washington, D.C., March 2000.
- Yoo, C. H. and Davidson, J. S. (1997). "Yield interaction equations for nominal bending strength of curved I-girders." *Journal of Bridge Engineering*, Vol. 2 No. 2, pp. 37-44.
- Yoo, C. H. and Littrell, P. C. (1986). "Cross-Bracing effects in Curved Stringer Bridges." *ASCE, Journal of Structural Engineering*, Vol. 112, No. 9, September, pp. 2127-2140.
- Zienkiewicz, O.C. (1977). *The Finite Element Method* 3rd Edition. McGraw-Hill, London.
- Zureick, A., and Naquib, R. (1999). "Horizontally curved steel I-girders state-of-the-art analysis methods." *Journal of Bridge Engineering*, Vol. 4, No. 1, pp. 38-47.
- Zureick, A., Linzell, D., Leon, R. T., and Burrell, J. (2000). "Curved steel I-girder bridges: experimental and analytical studies." *Engineering Structures*, Vol. 22, No. 2, pp. 180-190.
- Zureick, A., Naquib, R., and Yadlosky, J. M. (1994). "Curved steel bridge research project. Interim report I: Synthesis." *Rep. No. FHWA-RD-93-129*, FHWA, McLean, VA, December 1994.